JUSTUS LIEBIG UNIVERSITÄT GIEßEN, AG THORMANN

The phosphodiesterase PdeB regulates the colonization behavior of *Shewanella putrefaciens* CN-32 and localizes at the cell pole with its GGDEF domain

Dissertation zum Erlangen des Titels Dr. rer. Nat.

Tim Rick

26.10.2021

Diese Arbeit wurde an der Justus Liebig Universität Gießen am Institut für Mikro- und Molekularbiologie in der Arbeitsgruppe Thormann angefertigt.

1.	Gutachter (Molekularbiologie):	Prof. Kai Thormann
2.	Gutachter (Naturstoffforschung):	Prof. Till Schäberle
3.	Prüfer (Mikrobiologie):	Prof. Gabriele Klug
4.	Prüfer (Genetik):	Prof. Reinhard Dammann

I. Selbstständigkeitserklärung

Hiermit versichere ich, die vorgelegte Dissertation selbständig und ohne unerlaubte fremde Hilfe und nur mit den Hilfen angefertigt zu haben, die ich in der Dissertation angegeben habe. Alle Textstellen, die wörtlich oder sinngemäß aus veröffentlichten Schriften entnommen sind, und alle Angaben, die auf mündlichen Auskünften beruhen, sind als solche kenntlich gemacht. Bei den von mir durchgeführten und in der Dissertation erwähnten Untersuchungen habe ich die Grundsätze guter wissenschaftlicher Praxis, wie sie in der „Satzung der Justus-Liebig-Universität Gießen zur Sicherung guter wissenschaftlicher Praxis“ niedergelegt sind, eingehalten.

_____

Tim Rick

Diese Arbeit ist Stefanie Schulze gewidmet.

Publications

Accepted

Rossmann, F. M.*, **Rick, T.***, Mrusek, D., Sprankel, L., Dörrich, A. K., Leonhard, T., Bubendorfer, S., Kaever, V., Bange, G., & Thormann, K. M. (2019). The GGDEF domain of the phosphodiesterase PdeB in Shewanella putrefaciens mediates recruitment by the polar landmark protein HubP. Journal of Bacteriology, 201(7). https://doi.org/10.1128/JB.00534-18

This publication includes results of my bachelor´s and master's thesis

Pecina, A., Schwan, M., Blagotinsek, V., **Rick, T.**, Klüber, P., Leonhard, T., Bange, G., & Thormann, K. M. (2021). The Stand-Alone PilZ-Domain Protein MotL Specifically Regulates the Activity of the Secondary Lateral Flagellar System in Shewanella putrefaciens. Frontiers in Microbiology, 12. https://doi.org/10.3389/fmicb.2021.668892

Grützner, J., Billenkamp, F., Spanka, D. T., **Rick, T.,** Monzon, V., Förstner, K. U., & Klug, G. (2021). The small DUF1127 protein CcaF1 from *Rhodobacter sphaeroides* is an RNA-binding protein involved in sRNA maturation and RNA turnover. Nucleic Acids Research, 49(6), 3003–3019. https://doi.org/10.1093/nar/gkab146

In revision

Tim Rick*#, Vanessa Kreiling*, Alexander Höing, Svenja Fiedler, Timo Glatter, Wieland Steinchen, Georg Hochberg, Heike Bähre, Roland Seifert, Gert Bange, Shirley K. Knauer, Peter L. Graumann, Kai M. Thormann#. A GGDEF domain serves as a spatial on-switch for a phosphodiesterase by direct interaction with a polar landmark protein. NPJ Biofilms and Microbiomes https://doi.org/10.1101/2021.08.12.456111

*: Contributed equally (first author)

#: Contributed equally (corresponding author)

Abstract

The nucleotide messenger cyclic diguanylate (c-di-GMP) regulates numerous cellular processes in gram-negative bacteria, such as motility, biofilm formation, virulence and cell cycle. The production of this messenger is catalyzed by diguanylate cyclases (DGCs) which harbor a GGDEF domain, while c-di-GMP specific phosphodiesterases (PDEs) mediate its degradation with their EAL- or HD-GYP domains. Most bacteria encode a plethora of enzymes that can potentially affect the production or degradation of this messenger. The model organism that was used in this study, *Shewanella putrefaciens* CN-32, encodes 52 proteins that harbor such domains. The sheer amount of these enzymes demands a strict spatial and temporal organization of c-di-GMP signaling. This work provides novel insights into the spatiotemporal control of c-di-GMP signaling and illuminates the mechanism of a novel function of the inhibitory site of GGDEF-domains in GGDEF-EAL proteins.

The c-di-GMP-degrading enzyme PdeB harbors a GGDEF and an EAL domain in its cytoplasmic portion. Additionally, it has a HAMP/PAS module and two transmembrane domains that flank a long periplasmic region. It was found that the GGDEF domain is enzymatically inactive but obtained a novel function by localizing the protein to the cell pole. This process is mediated by a direct protein-protein interaction with the polar landmark protein HubP. Here, we identified that the inhibitory site of the GGDEF domain interacts with the far C-terminal region of the landmark protein HubP and suspect that this interaction alters the aggregation state of HubP. These results provide further insights into the complex mechanisms of the landmark protein-mediated polar localization of proteins, which is of great interest since homologues of HubP are present in numerous pathogenic bacteria. The interaction with HubP is required for full PDE activity of PdeB. We observed that PdeB affects bacterial motility by regulating the lateral flagella on a transcriptional and post translational level. Additionally, PdeB affects the assembly of MSHA-pili by regulating the activity of the extension ATPase MshE. This protein binds c-di-GMP directly with its N-terminal domain, while the second type IV pilus system is not affected. PdeB was also found to negatively regulate the production of Bpf surface adhesion proteins by repressing their transcription. We found that the PDE activity of PdeB is regulated by multiple signals. The GGDEF domain needs to interact with the landmark protein HubP and binds GTP to its active site to fully induce the PDE activity of the EAL domain. We suspect that both processes rearrange the hinge-helix that connects both domains. Additionally, the results indicate that the periplasmic region of PdeB binds an unknown extracellular ligand. Accordingly, we found that the periplasmic region of PdeB is also required for full PDE activity.

Combining the results of the polar localization of PdeB and the influence on motility and biofilm factors we postulate that the polar localization generates heterogeneity in the population and governs an efficient colonization strategy of new environments, similar to the previously proposed “touch-seed-and-go” model.

Zusammenfassung

Der sekundäre Botenstoff zyklisches Diguanylatmonophosphat (c-di-GMP) reguliert eine Reihe von Prozessen in gram-negativen Bakterien, wie Motilität, Biofilmproduktion, Virulenz und den Zellzyklus. Der Botenstoff wird durch so genannte Diguanylatzyklasen (DGCs) aufgebaut, welche eine charakteristische GGDEF Domäne besitzen, während der Abbau durch c-di-GMP spezifische Phosphodiesterasen (PDEs) vermittelt wird, die eine EAL oder HD-GYP Domäne aufweisen. Die meisten Bakterien besitzen eine Vielzahl von Enzymen, die potentiell die Produktion oder den Abbau dieses Botenstoffs beeinflussen können. Der Modellorganismus *Shewanella putrefaciens* CN-32 beispielsweise besitzt 52 Proteine, die potentiell Einfluss auf den c-di-GMP Spiegel haben könnten. Die bloße Menge dieser Enzyme erfordert eine strikte räumliche und zeitliche Organisation dieses Netzwerks. Diese Arbeit bietet neue Einblicke in die räumliche und zeitliche Organisation von c-di-GMP vermittelter Regulation und beleuchtet eine neue Funktion der *inhibitory sites* (i-sites) von GGDEF-Domänen in GGDEF-EAL Proteinen.

Das c-di-GMP abbauende Enzym PdeB besitzt eine GGDEF- und eine EAL-Domäne. Zusätzlich besitzt es ein HAMP/PAS-Modul und zwei Transmembranhelices, die einen langen periplasmatischen Bereich flankieren. Die GGDEF Domäne ist enzymatisch inaktiv aber hat im Laufe der Evolution eine neue Funktion erworben, nämlich die Lokalisierung von PdeB zum Zellpol. Dieser Prozess wird durch eine direkte Protein-Protein-Interaktion mit dem zellulären Lokalisierungsmarker-Protein (*landmark protein*) HubP vermittelt. In dieser Studie wurde identifiziert, dass die *i-site* der GGDEF-Domäne mit dem C-terminalen Bereich von HubP interagiert und die biochemischen Experimente legen nahe, dass sich der Aggregationszustand von HubP durch die Interaktion verändert. Dies ist von besonderem Interesse, da Homologe von HubP in einer Vielzahl von Pathogenen vorkommen. Die Interaktion mit HubP wird außerdem für die Aktivierung der PDE Aktivität von PdeB benötigt. Es wurde beobachtet, dass PdeB die bakterielle Bewegung reguliert und das laterale Flagellensystem beeinflusst. Außerdem kontrolliert PdeB den Aufbau der MSHA-Pili, indem es die Aktivität der ATPase MshE reguliert. Dieses Protein bindet c-di-GMP mit seiner N-terminalen Domäne. Im Gegensatz dazu wurde identifiziert, dass das zweite Typ-IV-Pilussystem nicht von PdeB beeinflusst wird. Zusätzlich wurde gezeigt, dass PdeB die Produktion von Bpf Oberflächenadhäsions-Proteinen beeinflusst. Die GGDEF-Domäne von PdeB benötigt die Interaktion mit HubP und die Bindung von GTP, um die PDE Aktivität der EAL-Domäne zu aktivieren. Wir vermuten, dass dieser Prozess eine Helix arrangiert, die die GGDEF mit der EAL Domäne verbindet. Zusätzlich legen die Ergebnisse nahe, dass PdeB einen extrazellulären Liganden mit seiner periplasmatischen Domäne bindet. Dies ist ebenfalls nötig um die volle PDE Aktivität zu induzieren.

Die Ergebnisse zur polaren Lokalisation von PdeB und seinem Einfluss auf Motilität und Biofilmbildung führen zu dem Schluss, dass die polare Lokalisation zu Heterogenität der Population führt und dass dies eine effiziente Kolonisierungsstrategie steuert. Diese ist ähnlich zu dem zuvor postulierten „*touch-seed-and-go“*-Modell.

List of Abbreviations

Name	Abbreviation
Amino acid	AA
Active site	A-site
Adenosine triphosphate	ATP
Bacterial-2-hybrid	B2H
Biolayer interference	BLI
Cyclic adenosine monophosphate	cAMP
Cyclic diguanylate mono phosphate	c-di-GMP
Crosslinking mass spectrometry	CL-MS
Column volumes	CV
Deoxyribonucleic acid	DNA
Diguanylate cyclase	DGC
Dimethyl sulfoxide	DMSO
Systematic Radial Capillary Action of Ligand Assays	DRaCALA
Disuccinimidyl Dibutyric Urea	DSBU
Extracellular polysaccharides	EPS
Flavin adenine dinucleotide	FAD
Figure	fig.
Flavinmononucleotid	FMN
Fluorescence recovery after photo bleaching	FRAP
Guanosine triphosphate	GTP
Hydrogen deuterium exchange mass spectrometry	HDX-MS
Isopropyl-β-D-thiogalactopyranosid	IPTG
Inhibitory site	I-site
Isothermal titration calorimetry	ITC
N'-Methylanthraniloyl	MANT
Mannose-sensitive hemagglutinin pilus	MSHA pilus
Normalized	norm.
Optical density at 600 nm	OD_{600}
Phosphodiesterase	PDE
Guanosin-3',5'-bispyrophosphat	ppGpp
Ribonucleic acid	RNA
Size exclusion chromatography	SEC
***Shewanella oneidensis* MR-1**	So
***Shewanella putrefaciens* CN-32**	Sp
Supplemental figure	sup. fig.
Type 1 secretion system	T1SS
Transmembrane	TM
5-Brom-4-chlor-3-indoxyl-β-D-galactopyranosid	X-Gal

Inhalt

List of figures

List of tables

1. Introduction

1. 1 Introduction to nucleotide messengers

Bacteria are often exposed to rapidly changing environmental conditions, like fluctuations of the pH value, osmotic concentration, nutrient availability and exposure to metabolic products. To cope with these changes, bacteria developed numerous regulatory pathways and mechanisms that ensure the survival of the population (Veening et al., 2008). Several of these mechanisms are tightly controlled by nucleotide second messengers, as for example the extensively studied molecule cAMP. In the γ-proteobacterium *Escherichia coli,* cAMP is used as hunger signal and activates transcription of the *lac*-operon by binding to the catabolite activator protein CAP/CRP (Busby & Ebright, 1999). Another example for nucleotide-based second messenger is ppGpp. This molecule gets rapidly produced under amino acid starvation conditions (Traxler et al., 2008). It was found that, in *E. coli,* the protein RelA can sense binding of uncharged tRNAs to the ribosome and produces ppGpp in response to that (Traxler et al., 2008).

The main focus of this work however will be on cyclic diguanylate (c-di-GMP). This messenger is used primarily by Gram-negative bacteria, but can also be found in Gram-positive bacteria such as *Bacillus subtilis* (Kunz et al., 2020). It was first discovered in 1987 as regulator of the cellulose synthase of *Gluconacetobacter xylinus* and was extensively studied since then (Ross et al., 1987). It was found to regulate several crucial cellular processes like the cell cycle, virulence, motility and biofilm formation (Chao 2013; Hall & Lee, 2018; Rotem et al., 2016). The molecule is almost completely twofold symmetric, caused by only minor variations in the dihedral angles (Schirmer, 2016). In solution it is mainly present as monomer, but it can also self-intercalate, resulting in the formation of dimers. This can be exploited to measure PDE activity by CD-spectroscopy but also plays an important role in nature, as for example during the c-di-GMP-dependent inhibition of diguanylate cyclases (Schirmer, 2016; Stelitano et al., 2013). The degradation of c-di-GMP is catalyzed by so called c-di-GMP dependent phosphodiesterases (PDE), and produced by diguanylate cyclases (DGC) (Römling et al., 2013).

1.2 Synthesis of c-di-GMP

Proteins that catalyze the production of c-di-GMP, diguanylate cyclases, harbor a characteristic GG[D/E]EF sequence in the active center. Ausmees *et al* found that GGDEF domains are present in numerous prokaryotic bacteria and are often combined with several

sensory domains. In this work the authors also suggested for the first time that these domains possess DGC activity (Ausmees et al., 2001). Pei and Grishin then predicted that GGDEF domains are structurally similar to adenylate cyclases, which was later confirmed by several X-ray crystallography studies, as for example by Vorobiev and colleagues (Pei & Grishin, 2001; Schirmer, 2016; Vorobiev et al., 2012). It was found that both domains have a characteristic (βααββαβ)-fold as common core, while the N-terminus differs between diguanylate and adenylate cyclases (Schirmer, 2016). These findings make an evolutionary link between diguanylate and adenylate cyclases very likely (Pei & Grishin, 2001; Schirmer, 2016).

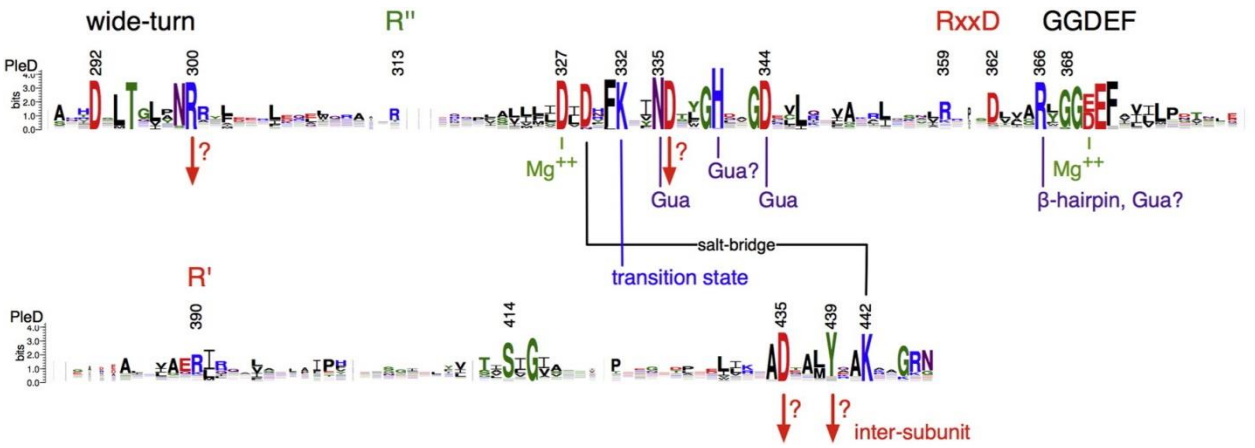

Figure 1.1) Sequence conservation of GGDEF domains. The sequence logo was published by Tillmann Schirmer and consists of 37 sequences of GGDEF domains with cyclase activity found in the Pfam data base. Crucial residues are annotated with known or predicted function : Mg^{++}, magnesium coordination; Gua, guanine binding and residues that may be part of the subunit interface are indicated with red arrows (Schirmer, 2016)**.**

As shown in the sequence logo published by Tillmann Schirmer (**fig. 1.1**), a characteristic wide turn is found at the N-terminus of GGDEF domains. In the central part, several conserved amino acids are found that bind and coordinate the substrate guanosine triphosphate (GTP) and the cofactor magnesium. Importantly, a conserved aspartic acid was found to connect the central region with the C-terminal part of GGDEF domains by forming a highly conserved salt bridge with a lysine. The already mentioned RxGG[D/E]EF motif is found in the central part of the domain and is crucial for magnesium binding and enzymatic activity. This region is structurally remarkable, since it connects the chains β2 and β3 with a non-canonical β-hairpin that forms a sharp kink of the polypeptide chain, which is necessary to provide the required space for the intermolecular reaction. This hairpin is also a crucial structural difference to adenylate cyclases that form a canonical β-hairpin at this position (Schirmer, 2016).

The GTP gets bound to the active center by interaction of the β-, γ-phosphate with the P-loop/N-cap. The specificity for the guanine base is obtained by an asparagine and an aspartic acid of helix α1/α2. GGDEF domains that contain serine or threonine instead of aspartic acid have relaxed substrate specificity and can also bind ATP. These enzymes are called hypr GGDEF domains and are able to synthesize multiple cyclic dinucleotides like cGAMP and c-di-GMP. The discovery was made very recently and 30 years after GGDEF domain-containing enzymes were first discovered (Hallberg et al., 2016; Schirmer, 2016).

The substrate for canonical GGDEF domains is GTP and c-di-GMP is synthesized by cyclization of two nucleotides. Since each GGDEF protomer only binds one GTP, active cyclases need to oligomerize. To this end, the loaded GGDEF protomers dimerize, resulting in an antiparallel orientation of the two GTP molecules. A model for this has been proposed by Zähringer and colleagues for the DGC DgcZ of *E. coli* (Schirmer, 2016; Zähringer et al., 2013). They propose that catalysis of both GTP molecules results in a conformational change where the newly synthesized c-di-GMP molecule bridges both protomers and induces the postcatalytic state (Zähringer et al., 2013).

1.3 Regulation of diguanylate cyclases

The DGC activity of GGDEF-domains can be inhibited by multiple mechanisms (**fig. 1.2**). When Chan and colleagues solved the crystal structure of PleD, they found that c-di-GMP can not only bind to the active site of GGDEF domains but that the protein was also binding an additional c-di-GMP dimer. They suggested that this binding may result in a noncompetitive allosteric product inhibition (Chan et al., 2004). GGDEF domains harbor two inhibitory sites (i-sites) at three different regions of the primary sequence. The first i-site consists of the RxxD motif directly N-terminal of the GGDEF motif and the ER (R') motif, which is located C-terminal of the active site (see **fig. 1.1**). The second i-site is located close to the N-terminus and C-terminal of the wide turn (R'' in **fig. 1.1**) (Schirmer, 2016). It was found that c-di-GMP binding to both i-sites is necessary to induce full inhibition, while binding to only one i-site only has minor effects. This can be explained by the available structural data (e.g. PDB code 1W25): The inhibition is induced by immobilizing the GGDEF protomers, where the conserved arginine (R'') of the second i-site binds the c-di-GMP molecule that is bound by the other GGDEF protomer (Wassmann et al., 2007). This results in crosslinking of the protein and therefore immobilization, which in turn also explains why the inhibition overrules all input-mediated signals (Schirmer, 2016).

Another mechanism to inhibit the DGC activity of GGDEF domains is inhibition by signal transduction. GGDEF proteins almost always occur with additional sensor and signal transduction domains: A Pfam search for GGDEF proteins resulted in more than 4000 different domain organizations. These additional domains often have regulatory functions and can either activate or inhibit DGC activity. According to the literature and the Pfam database, domains that occur very frequently are REC-, PAS-, GAF-, or HAMP-domains (exemplary uniprot IDs: Q0MYT4, O87377, Q8VRN4, Q3KK31), but also other, such as heme- and zinc-binding, domains are often present (Sawai et al., 2010; Schirmer, 2016; Zähringer et al., 2013). These additional domains either lead to oligomerization of the protein or rearrange an already existing oligomer to induce a competent state (Schirmer, 2016). An example for the first mechanism is the protein PleD of *Caulobacter crescentus*, which harbors a Rec-domain upstream of the GGDEF domain. The respective protein remains mostly in a monomeric state when no divalent ions are present. However, Wassmann and colleagues found that the protein dimerizes when Mg^{++} or Mn^{++} or BeF_3^- is added to the protein solution. This dimerization then activates the enzymatic activity of the GGDEF domain. When they solved the crystal structure of the active state of the protein they found that addition of BeF_3^- causes a rearrangement of the adaptor protein und leads to the formation of a competent dimer of the preloaded GGDEF protomers (Wassmann et al., 2007). An example for the second mechanism, where the sensor domain leads to a rearrangement of the already formed dimer, is the protein DgcZ. As mentioned above, the GGDEF domain of DgcZ is a constitutive dimer and has a regulatory chemoreceptor zinc-binding (CZB) domain N-terminal of the GGDEF domain. However, Zn^{++} binding to the CZB domain results in non-productive arrangement of the GGDEF domain. Zähringer and colleagues solved the crystal structure of this protein. Unfortunately, the resolution of the X-ray crystallography was not high enough to observe the aforementioned process in detail, but they proposed a model for this mechanism. They claim that the condensation reaction is not possible when Zn^{++} is bound because “the γ-torsion angle (O5′-C5′-C4′-C3′) is −60° as opposed to +60° in the c-di-GMP product” (Zähringer et al., 2013).

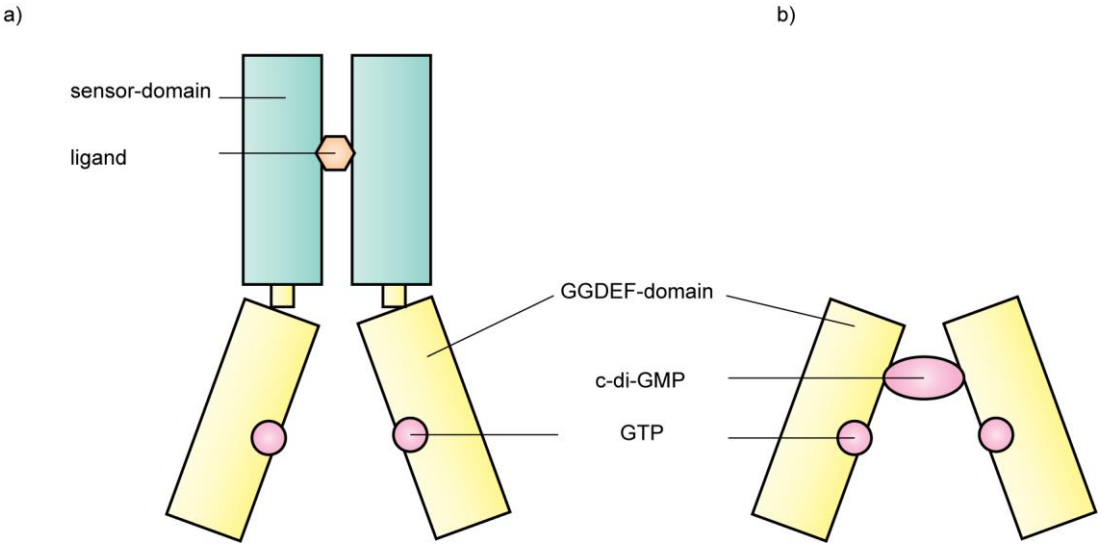

Figure 1.2) Model for the inhibition of DGCs. a) The enzymatic activity of DGCs can be inhibited by sensor domains. The binding of the ligand induces a conformational change in the structure of the protein that prevents formation of a competent dimer. **b)** Another common mechanism for the inhibition of DGC activity is binding of c-di-GMP to the i-site of the GGDEF domain. This crosslinks the protein domains and results in immobilization.

1.4 Degradation of c-di-GMP

Enzymes that degrade c-di-GMP are called phosphodiesterases (PDEs) and can be divided into two different classes: HD-GYP- and EAL-domain proteins. Both domains are named after their characteristic sequence motif in the active center of the protein (Römling et al., 2013). The HD-GYP domain proteins were first described by Slater and colleagues in 2002, were they identified a two-component system that regulates the synthesis of extracellular polysaccharides (EPS) by transposon mutagenesis. In their study the transposon integrated into the gene *rpfG*, leading to reduced virulence and DSF ("diffuse signal factor") production. They then conducted a SMART analysis and found that the protein has a C-terminal HD-domain. Surprisingly, they observed that the protein also has a highly conserved GYP signature motif (Slater et al., 2002). However, the mechanism remained unclear until the group of Maxwell Dow postulated that HD-GYP domains are involved in c-di-GMP turnover. In their study the authors purified the HD-GYP domain of RpfG and conducted *in vitro* HPLC based c-di-GMP degradation assays. They found that the purified protein domain degrades c-di-GMP into two GMP molecules (Ryan et al., 2006). When Bellini and colleagues solved the crystal structure of the HD-GYP domain protein PmgH, they found that these enzymes form a trinuclear binding site and that an iron cofactor is essential for full PDE activity (Bellini et al., 2014).

While HD-GYP domains degrade c-di-GMP into two GTPs, EAL domains linearize their substrate into pGpG. This was stated in 2005 by the group of Mark Gomelsky in a study were they purified the EAL-domain protein YahA of *E. coli* and did HPLC based c-di-GMP degradation assays. In contrast to GGDEF domains, oligomerization is not essential for enzymatic activity. They also found that the cations Mg^{++} or Mn^{++} are required for enzymatic activity, while Ca^{++} strongly inhibits this process (Schmidt et al., 2005). The required divalent cations coordinate two H_2O molecules in the active center of the protein. Besides the conserved EAL motif, these domains also encode a conserved DDFG(T/A)GYSS-motif that is located on loop 6 and is essential for enzymatic activity (**fig. 1.3**). This region is structurally important and mutating a conserved aspartic acid resolves in stabilization of loop 6, resulting in full inhibition of enzymatic activity (Rao et al., 2008). Since oligomerization is not essential for enzymatic activity, several of these enzymes are found as stand-alone EAL-domain proteins, such as PdeH from *E. coli* that has been extensively studied by the group of Regine Hengge (Povolotsky & Hengge, 2016; Reinders et al., 2016). However, accessory signaling domains are common for most EAL-domain proteins: A Pfam database search resulted in more than 2700 different domain architectures.

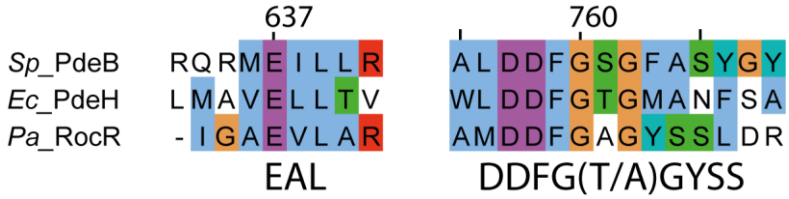

Figure 1.3) Conserved amino acid sequences of EAL domains. The figure 1.3 shows an alignment of the active PDEs PdeB (*S. putrefaciens*), PdeH (*E. coli*) and RocR (*P. aeruginosa*). The numbers are corresponding to the primary sequence of PdeB.

1.5 Hybrid GGDEF-EAL proteins – regulatory and other functions of GGDEF domains

Surprisingly, EAL-domains are often found together with GGDEF domains in a single protein. It long remained unclear if, in these proteins, both domains can be active or if one domain lost enzymatic activity and obtained a new, regulatory function. Over the last years, research showed that both mechanisms occur in nature (Cole & Lee, 2016; Feirer et al., 2015; Chong Liu et al., 2018). Since the catalyzed reactions of GGDEF and EAL domains are opposing each other, simultaneous activity may be disadvantageous for the organism since it would distort the signal and waste energy. This would lead to evolutionary conflict and loss of the enzymatic activity of one of these protein domains. Therefore, DGC and PDE activity of hybrid GGDEF-EAL proteins must be strictly regulated.

Proteins with DGC and PDE activity are rarely reported. One example for these proteins is DcpA that was characterized in *Agrobacterium tumefaciens* by the group of Clay Fuqua. Since c-di-GMP regulates the biofilm formation in this organism, they constructed mutants with inactivated GGDEF and/or EAL domains and used the biofilm formation as read-out for the enzymatic activity. As expected for PDEs, inactivation of the EAL domain led to strongly increased biofilm formation. However, inactivation of the GGDEF domain only leads to minor decreases in the biofilm formation. They suggested that the DGC activity of DcpA gets negatively regulated by host proteins and continued by expressing the protein in the heterologous host *E. coli*. Here they were able to show that DcpA is in fact a *bona fide* bifunctional DGC-PDE protein. They were also able to show that the required regulation of these two functions is Pterin-mediated (Feirer et al., 2015).

However, most GGDEF domains in GGDEF-EAL proteins obtained a new function as regulatory domain. In these proteins it is often found that the GGDEF-domain is located N-terminally of the EAL-domain. The structural basis for the GGDEF-mediated PDE regulation has just recently been elucidated by Liu and colleagues using the Protein RbdA from *P. aeruginosa* as model. RbdA is a PAS-GGDEF-EAL protein with two transmembrane domains and a periplasmic region. It exhibits strong PDE and weak DGC activity. It was also found that the presence of GTP strongly increases the PDE activity of RbdA. The group was able to purify the protein as PAS-GGDEF-EAL truncation and solved the crystal structure in the active and inactive form by adding GMPPNP instead of GTP to the protein solution, which can be bound by the GGDEF domain but is not converted into c-di-GMP. They found that RbdA forms a dimer and that the PAS domain is connected to the GGDEF domain by a helix structure which they called S-helix. Additionally, they observed that the GGDEF domain is connected to the EAL domain by another long helix (“hinge-helix”). Using their obtained crystal structures, they found that, when no GTP is bound to the GGDEF domain, the protein is rather flexible. This state corresponds to low PDE activity. When GTP gets bound to the GGDEF domain, the protein undergoes a conformational change (**fig. 1.4**) and becomes more compact. They claim that residues 361 to 365, which build the S-helix upstream of the GGDEF domain, are crucial for this process and lock the EAL domain in a non-canonical configuration. Additionally, the hinge-helix, which connects the GGDEF to the EAL domain, undergoes a conformational change. These changes lead to the formation of the competent EAL-dimer when GTP is bound to the GGDEF domain. This in turn then results in activation of full PDE activity of the EAL domain (Chong Liu et al., 2018).

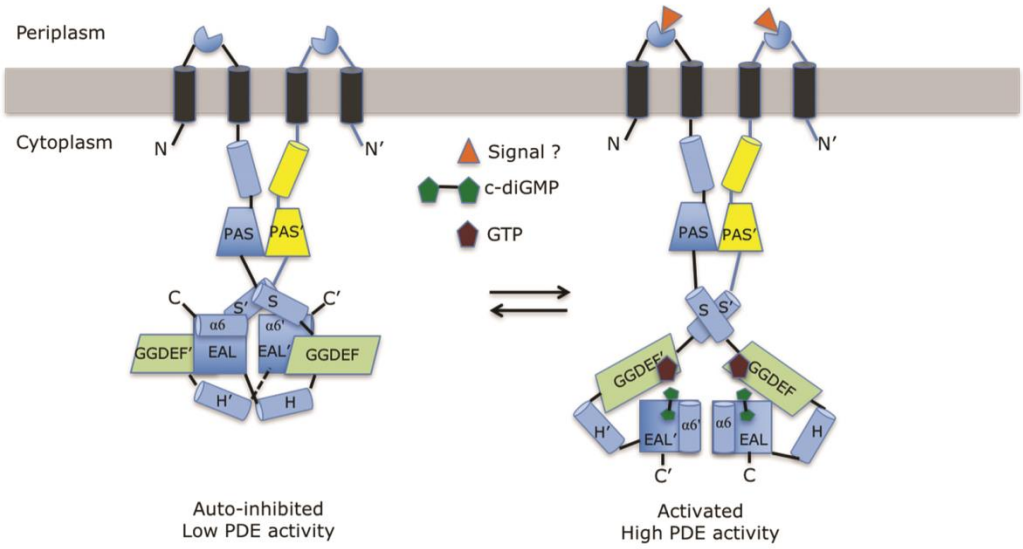

Figure 1.4) Model for the GGDEF-dependent regulation of PDE activity as published by Liu and colleagues. The authors purified the protein RbdA in the inactive (left) and active state (right) using GMPPNP. They found that binding of GTP to the GGDEF domain leads to conformational changes in the S- and Hinge-Helix that leads to the formation of the competent EAL dimer and full PDE activity (Chong Liu et al., 2018)**.**

1.6 c-di-GMP signal perception

While c-di-GMP gets produced by GGDEF-proteins and is degraded by EAL- or HD-GYP-domains, the receptors for this messenger are quite diverse. One class of c-di-GMP binding molecules has already been described in the previous chapters, where the i-site of GGDEF-domains acts as c-di-GMP receptor and regulates the DGC activity. But also enzymatically inactive GGDEF domains have been found to act as c-di-GMP receptors. (Römling et al., 2013). For a summary of c-di-GMP receptors see **fig. 1.5**.

Historically, PilZ-domain proteins were the first to be predicted and later experimentally verified proteins to act as c-di-GMP specific receptors (Amikam et al., 2006; Ryjenkov et al., 2006; Römling et al., 2013). The group of Mark Gomelsky was able to purify the two PilZ proteins *Ec*YcgR and *Gx*BcsA and found that both proteins bind c-di-GMP with a high affinity. The group further verified the *in vitro* experiments by introducing mutations into conserved residues of the PilZ domain of YcgR and found that the protein regulates flagellum-mediated motility in a c-di-GMP dependent manner (Ryjenkov et al., 2006). As summarized in the review by Römling and colleagues, soon after Ryjenkov and co-workers published their study on YcgR, many PilZ domain proteins were experimentally proved to act as c-di-GMP receptors, such as DgrA from *C. crescentus* (Christen et al., 2007) and PlzC and PlzD from *V. cholerae* (Pratt et al., 2007; Römling et al., 2013). It was also found that PilZ domains can have different binding modes of c-di-GMP, as elucidated by Ko and colleagues. They found

that some PilZ domains can not only bind monomeric, but also dimeric c-di-GMP. They also state that PilZ domains react differently to c-di-GMP binding regarding their aggregation state: PP4397 was found to undergo a dimer-to-monomer transition upon c-di-GMP binding (Ko et al., 2010). A conserved consensus sequence required for c-di-GMP was identified consisting of the sequence RxxxRx20–30(D/N)x(S/A)xxG (Römling et al., 2013).

As summarized in the review by Römling, not only PilZ domains can act as c-di-GMP receptors, but also enzymatically inactive EAL and HD-GYP domains. These proteins lost their enzymatic activity but are still able to bind c-di-GMP. One example for such a protein is FimX (Römling et al., 2013). The group of Holger Sondermann was able to solve the crystal structure of *Pa*FimX, which is involved in regulating twitching motility. Their study provides the structural basis for c-di-GMP sensing by degenerated PDEs, and they used isothermal titration calorimetry (ITC) to prove that FimX acts as c-di-GMP binding receptor. They suggest that the dimerization of the EAL domain may be important for this process (Navarro et al., 2009). Another well-studied example for these kind of c-di-GMP receptors is the protein LapD, which also can bind c-di-GMP with its degenerated EAL domain (Römling et al., 2013). However, this protein will be covered in detail in later chapters.

Recently, c-di-GMP binding riboswitches were discovered, such as Bc3, Bc4 and Bc5 from *Bacillus thuringensis* (H. Zhou et al., 2016). Riboswitches are structured RNA elements that are located in the 5'-untranslated region (UTR) of a gene. The three c-di-GMP-binding riboswitches Bc345 were found in the 5'-UTR of *csp*ABCDE by Zhou and colleagues. These receptors allowed the construction of a plasmid-based dual-fluorescence reporter system, where the authors of the mentioned study integrated the riboswitch between *amcyan* and *turborfp*. This system allows monitoring the relative *in vivo* c-di-GMP level of individual cells or populations (H. Zhou et al., 2016). This method was also used in this study; for further information see material and methods and results.

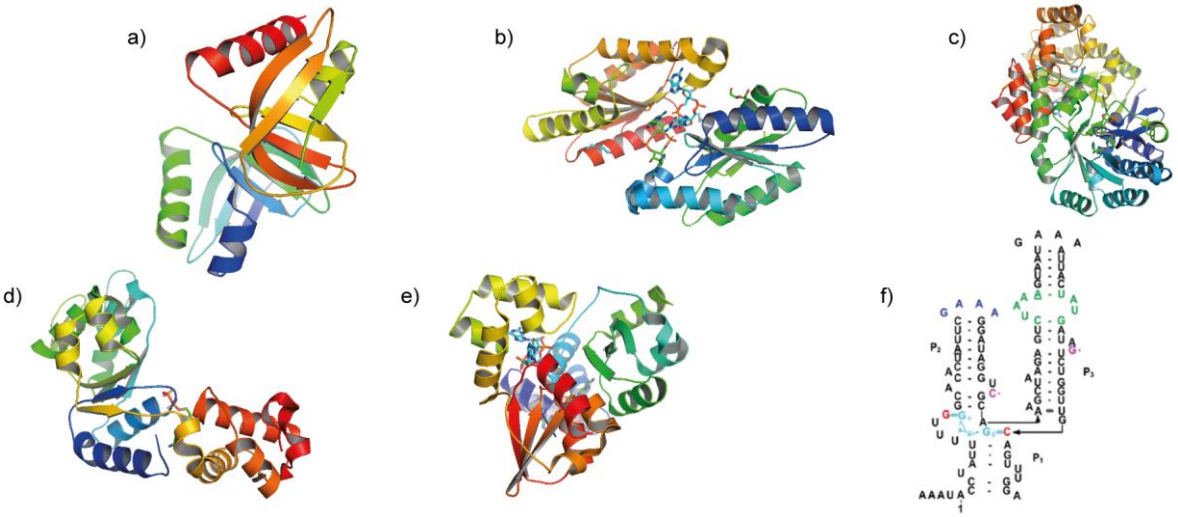

Figure 1.5) Diversity of c-di-GMP receptors. a) Structure of PilZ from *X. axonopodis* (PDB: 3CNR). **b)** Structure of a GGDEF domain of *X. campestris* with bound c-di-GMP to the i-site (PDB: 3QYY). **c)** Structure of an EAL domain of *E. coli* with bound c-di-GMP (PDB: 4LJ3). **d)** Structure of the transcriptional master regulator FleQ from *P. aeruginosa* (PDB: 5EXT). **e)** Structure of the extension ATPase MshE from *V. cholera* with bound c-di-GMP (PDB: 5HTL). **f)** Secondary structure of the c-di-GMP binding riboswitch Bc3 from *B. thuringensis* (Zhou et al., 2016, modified).

Another common high-affinity c-di-GMP receptor was just recently identified in 2015 by the group of Fitnat Yildiz, using a systematic Radial Capillary Action of Ligand Assay (DRaCALA) and is called MshEN-domain (Roelofs et al., 2015). In their study they tested *V. cholerae* ORFs for c-di-GMP binding and heterologously expressed them in *E. coli* and using the binding of ^{32}P-c-di-GMP as read-out. They found that the Extension ATPase of the mannose-sensitive hemagglutinin pilus (MSHA), MshE, bound ^{32}P-c-di-GMP in their screening (Roelofs et al., 2015) and verified the binding with ITC experiments where the measured KD values were in the low micromolar range (Wang et al., 2016). Subsequently, they solved the crystal structure of the N-terminal domain of *Vc*MshE (MshEN-domain) and found two highly conserved binding motifs, that each bind half of the c-di-GMP molecule. Remarkably, this is the longest nucleotide binding motif reported so far and consists of a RLGxx(*L/V/I)(L/V/I*)xx*G*(*L/V/I)(L/V/I*)xxxxLxxxLxxQ sequence motif. Another interesting aspect is that several highly conserved leucines are crucial for c-di-GMP binding in these domains and that binding is primarily mediated by hydrophobic interactions. Wang and co-workers state that MshEN domains are ubiquitous regulatory domains and identified more than 10,000 proteins containing them. In their study they tested several MshEN domains from different organisms and found KD values ranging from 0.5 µM to 14 nM. They also found low binding affinity to the nucleotide messenger cGAMP, but further research is needed to elucidate if this binding plays a role in nature (Wang et al., 2016).

In their screening they also found several known c-di-GMP-binding proteins, such VpsT and VpsR (Roelofs et al., 2015). These proteins are transcriptional regulators, which is another class of c-di-GMP receptors. To this end, Srivastava and colleagues conducted a study in which they linked c-di-GMP signaling to quorum sensing. AphA is an activator of virulence gene expression and involved in the regulation of the quorum sensing pathway. VpsT acts as transcriptional activator of biofilm formation genes. They found that activation of both proteins requires the transcriptional activator VpsR which binds c-di-GMP (Srivastava et al., 2011). However, c-di-GMP-binding transcriptional regulators are diverse and hard to identify *in silico*. Another subclass of these sensors are AAA+ ATPases, like the transcriptional regulator FleQ (Matsuyama et al., 2016). This protein has regulatory roles in flagellar and EPS biosynthesis operons. Binding of c-di-GMP reduces the ATPase activity of FleQ, which results in down-regulation of flagellar gene expression (Claudine & Harwood, 2013; Hickman & Harwood, 2008; Matsuyama et al., 2016). The group of Holger Sondermann was able to solve the crystal structure of FleQ in the active and inactive state and found that binding of c-di-GMP results in destabilization of the hexameric ring, which in turn leads to the described c-di-GMP dependent phenotype (Matsuyama et al., 2016). While the mentioned studies on FleQ were conducted in *P. aeruginosa*, several functional orthologs are present in other organisms, such as FlrA from *S. putrefaciens* CN-32 (Blagotinsek et al., 2020).

1.7 c-di-GMP regulates bacterial motility and virulence

Over the last decades, researchers found that c-di-GMP regulates numerous cellular processes, such as virulence, cell cycle, motility and biofilm formation. One of the earliest findings regarding virulence regulation was in *V. cholerae* by Tischer and Camilli (Tischler & Camilli, 2005). Virulent strains of *V. cholerae* utilize the cholera toxin, which is encoded by the *ctxAB* genes, in acute infections. They found that the c-di-GMP dependent PDE VieA positively regulates the expression of these genes (Tischler & Camilli, 2005). It was also found that high c-di-GMP levels led to inhibition of acute infections of the pathogenic bacteria *Yersinia pestis* and *Borellia burgdorferi*, likely by affecting the expression of extracellular matrix components (Bobrov et al., 2011; Römling et al., 2013; Sultan et al., 2011).

One virulence factor of tremendous importance is bacterial motility. Over the course of evolutionary time bacteria developed several mechanisms to move, such as flagella mediated motility, twitching, swarming, gliding and screw thread motility (Harshey, 2003; Macnab & Aizawa, 1984; Kühn et al., 2018). While not all pathogenic bacteria are motile (e.g. *Mycobacterium tuberculoses*), many other rely on motility to infect their host (Sultan et al., 2013). Therefore, the human immune system did not only evolve toll-like receptors that can

sense motility factors such as flagella, but recently it was also shown that motility itself is linked to host-cell-induced expression of immune regulators (Felgner et al., 2020).

In this study, the main focus regarding motility is on flagellar mediated movement. Flagella are thin helically shaped structures that rotate to propell the cell forward. The structure of flagella is shown in **fig. 1.6**. The number and positioning of flagella can be diverse and are characteristic for the bacterial species. The proteobacterium *E. coli* for example is peritrichously flagellated, hence posesses several flagella distributed over the cell body (Sim et al., 2017). Other bacteria only harbor one or more polar flagella (e. g. *P. aeruginosa*) or subpolar flagella, like *Rhodobacter sphaeroides* (Cai et al., 2016; Kobayashi et al., 2003). The current state of reasearch regarding flagella-driven motility in bacteria is summarized in the review by Nakamura and Minamino (Nakamura & Minamino, 2019). The flagellum is composed of the flagella filament, hook and rod, the export apparatus and the basal body rings (see **fig. 1.6**). The filament is formed by around 30,000 copies of the flagellin protein (Nakamura & Minamino, 2019). In some bacteria, like *S. putrefaciens* CN-32, the flagellum is built of different flagellin proteins (FlaA and FlaB) (Kühn et al., 2018). The use of different flagellins improves motility in numerous environmental conditions and play an important role in scew-like motility, as shown by Marco Kühn using the model organism *S. putrefaciens* CN-32 (Kühn et al., 2018). The filament is connected to the hook filament, a universal joint, which consists of several hundred copies of the hook protein (Nakamura & Minamino, 2019). In a study by Spöring and colleagues the authors found that the hook length is crucial for optimal stability of the flagellar bundle in *Salmnonella enterica*. They performed several experiments regarding different hook lengths and found that too short hook structures may buckle and create an instability of the flagellar bundle of the peritrichously flagellated model organism (Spöring et al., 2018). But the hook also plays an important role in monotrichous flagellated bacteria. Xie and collegues found that monotrichous flagellated bacteria utilize a run-reverse-flick mechanism for changing the direction of movement and the group of Stocker found that the flexibility of the hook plays a crucial role in reorientating, by exploiting flagellar buckling instability to change direction (Son et al., 2013; Xie et al., 2011). In contrast to MSHA pili (see later chapters), the flagellar structure grows at the distal end of the filament, starting with the rod (Minamino, 2014). The export apparatus is a type III secretion system and embedded into the cell membrane. It consists of an export gate and a soluble ATPase ring that act as specific chaperone. The export itself however does not use ATP but an ion gradient as power source (Minamino, 2014). The basal body consists of several ring structures, called the L ring, P ring, MS ring and C ring. The L and P rings are only present in gram-negative bacteria and are both located in the outer membrane and the peptidoglycan

layer and act as bearing for the rod. Meanwhile the C ring is crucial for torque generation and switching the direction of motor rotation. (Nakamura & Minamino, 2019)

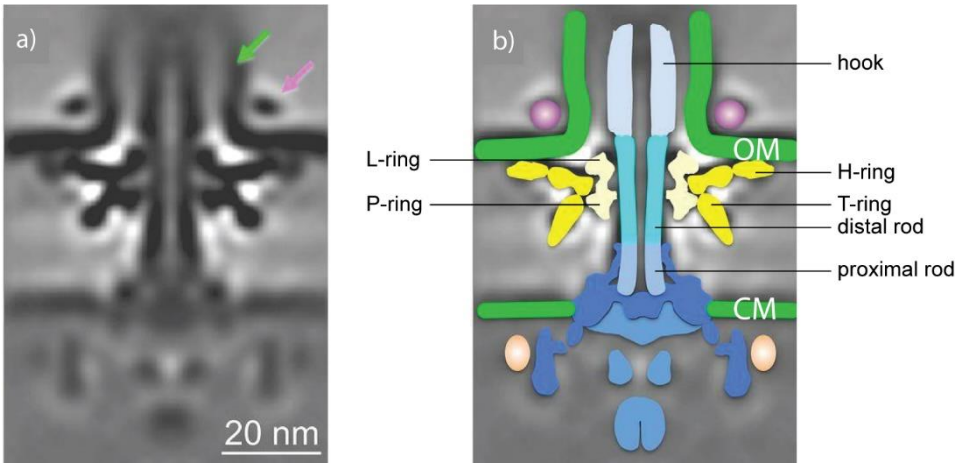

Figure 1.6) Structure of Flagella. a) Electron tomography image of the sheather flagellum from the Gram-negative bacterium *V. alginolyticus*. **b)** Schematic model overlaid on the cryo-ET picture that is shown in a. (Zhu et al., 2017, modified)

Most bacteria, such as *E. coli*, can react to environmental cues and move directed towards an attractant or away from a repellent. This process is controlled by a so-called chemotaxis system that utilizes specific transmembrane chemoreceptors to sense important molecules (Briegel et al., 2009; Nakamura & Minamino, 2019). CheA acts as a central protein of this system and undergoes autophosphorylation when ligands bind to the methyl-accepting chemotaxis proteins. The phosphate is then transferred from CheA to the response regulator CheY. CheY binds in its phosphorylated form to FliM and FliN and induces conformational changes of the C ring. This process leads to a switch of the direction of flagellar motor rotation (Cluzel et al., 2000; Nakamura & Minamino, 2019).

The second messenger c-di-GMP can regulate flagella mediated motility via numerous ways. In general, high intracellular c-di-GMP level are correlated with low motility and high biofilm formation (Römling et al., 2013). One particulary interesting example for this process was found by the group of G. O'Toole in the pathogenic bacterium *P. aeruginosa*. These bacteria can utilize their flagella to swarm over surfaces. They also encode two different stator complexes in their genome (*motAB* and *motCD*). The authors found that under high c-di-GMP levels the stator composition is altered, excluding the MotCD complex from the stator complex. Since MotAB does not generate enough torque for swarming motility, the absence of MotCD results in strongly decreased swarming motility (Kuchma et al., 2015). Interestingly, the same group found in a later study that not only c-di-GMP can affect the stator composition, but also that the stator MotC can interact with the transmembrane region

of a DGC called SadC. They propose that this interaction stimulates the c-di-GMP production by SadC, generating a positive-feedback loop that disengages MotAB from the stator complex (Baker et al., 2019). In a third publication they found that the displacement of MotC is mediated by a PilZ-domain protein, FlgZ, that can specifically bind c-di-GMP. When the messenger is bound to FlgZ, the protein interacts with the stator protein MotC and induces the delocalization of MotC from the motor complex (Baker et al., 2016). This regulatory pathway can be seen as example how c-di-GMP can manipulate the activity of flagella. Another example for PilZ domain proteins that can act as molecular brake for flagella is YcgR (Paul et al., 2010). This protein interacts with the switch-complex proteins FliG and FliM under high c-di-GMP conditions and reduces torque generation (Paul et al., 2010). An additional example is the protein DgrA from *B. subtilis* which acts as molecular clutch on the flagellar stator protein (Subramanian et al., 2017). It was also found that c-di-GMP can regulate motility by repressing the export of flagellins in *P. fluorescens* by binding to the export AAA+ ATPase FliI (Trampari et al., 2015).

But c-di-GMP can also inferfere with the chemotaxis response, as shown by Nesper and colleagues. In their study using *C. crescentus* as model, the authors found a novel class of CheY-like regulators that are able to bind c-di-GMP, named Cle proteins. These proteins interact with the flagellar switch to control motor activity. When they deleted all five Cle proteins that the model organism encodes, they found a 400% increased spreading radius on semisolid agar plates. They state that this effect is caused by an altered chemotaxis response and observed differences in directional changes (Nesper et al., 2017). A second example for the c-di-GMP dependent regulation of chemotaxis is the protein MapZ (Zhu et al., 2017). The group of Gu solved the structural basis for this project and found that binding of MapZ to the methyltransferase CheR blocks the SAH/SAM binding pocket and therefore inhibits the activity of CheR (Zhu et al., 2017).

The named examples showed that c-di-GMP can regulate motility on a posttranslational level. However, c-di-GMP can also regulate motility by affecting transcription. One example for this is the transcriptional master regulator FleQ. This transcription factor controls, together with another ATPase called FleN, the expression of flagellar genes in *P. putida*. FleQ is able to bind c-di-GMP, which leads to destabilization of its hexameric ring structure. These changes in the aggregation state inactivate the transcription factor and prevents the expression of the flagellar gene cascade, leading to reduced flagellar mediated motility (Matsuyama et al., 2016).

1.8 The motile to sessile transition is controlled by c-di-GMP

Bacteria need to adhere to surfaces to colonize new habitats. This process is correlated with biofilm formation and inversely correlated to motility. The transition from a motile to sessile lifestyle is strongly controled by c-di-GMP (Römling et al., 2013).

Several studies were published about the role of c-di-GMP in this process over the last decades (Floyd et al., 2020; Laventie et al., 2019; Römling et al., 2013). The surface of many Gram-negative bacteria is covered with different types of pili. One type that is crucial for bacterial attachment is the MSHA pilus system, which is classified as Type4a pilus system (Mattick, 2015). These pili allow the cell to adhere to biotic and abiotic surfaces and play a major role in virulence and biofilm formation. One example for this is the pathogenic bacterium *V. cholerae*, which has been found to adhere to zooplankton using their MSHA pili; making the system crucial for its environmental persistence in aquatic habitats (Chiavelli et al., 2001). The system can also be used to directly adhere to human cells, as was shown for *V. parahaemolyticus.* This bacterium causes acute inflammatory gastroenteritis and utilizes MSHA pili to adhere to human intestinal epithelial cells (O'Boyle et al, 2013).

Type IV pili are multiprotein complexes, consisting of the pilus filament, a cytoplasmic extension ATPase, a platform protein and an outer membrane secretin. Some systems also contain a retraction ATPase that allows twitching motility by retracting the pilus and pulling the cell forward. The filament is built of an alpha-helical arrangement of pilin proteins that are shuttled as monomers out of the cytoplasm by utilizing ATP as energy source. In contrast to flagella, the filament is extended from the surface, starting with a priming complex of minor pilins (Mattick, 2015).

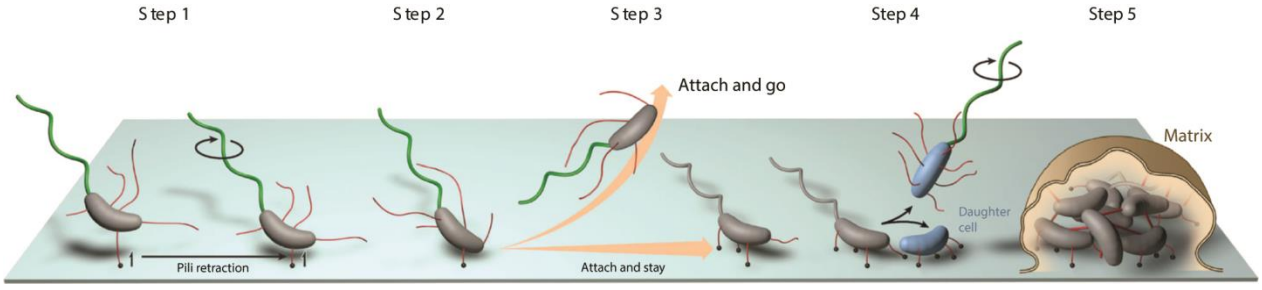

Figure 1.7) MSHA-induced attachement. The Figure 1.7 shows a model how bacteria attach to surfaces by the utilization of the MSHA-pilus system. As first step, the bacteria adhere to the surface by a single MSHA-pilus. The cell is then pulled towards the surface by pilus retraction. The cell then either detaches ("attach and go") or utilizes other systems, like the Lap-system, to extensify the adherence. The cell then starts dividing, and production of a matrix is induced. Additionally, some swarmer cells are created by heterogeneity (Floyd et al., 2020)**.**

The role of c-di-GMP in regulating MSHA pili was extensively studied in *V. cholerae* (Floyd et al., 2020; Jones et al., 2015; Roelofs et al., 2015). The group of Fitnat Yildiz states in their

study that the first step of adherence to surfaces is mediated by MSHA pili (**fig. 1.7**). The extension of this pilus is mediated by the c-di-GMP binding extension ATPase MshE. They found that the ATPase activity is correlated with c-di-GMP binding (Floyd et al., 2020). Once adherence occurs, the swimming behaviour changes drastically and the cells start to rotate around the point of attachement (Jones et al., 2015). The authors call this orbitting; in contrast to the unadhered roaming behaviour. At this point, adherence is still reversible but a subpopulation of these cells utilizes their retraction ATPase to pull the cell to the surface were additional systems, like the Lap-system, can mediated irreversible attachment (Floyd et al., 2020).

The Lap-system is another machinery that mediates attachment and is controlled by c-di-GMP. It is classified as a type I secretion system (T1SS) and can transport large cargo of more than 500 amino acid proteins out of the cell (Smith et al., 2018). These secretion systems consist of three main components: An ABC transporter that is located in the inner membrane, a membrane fusion protein and an outer membrane factor. The cargo can be bound and transported by the ABC transporter, which uses ATP as energy source. The membrane fusion protein is embedded in the inner membrane and connects the system to the outer membrane factor, which forms a pore that allows transport of the cargo out of the cell (Smith et al., 2018). The Lap system, which is also called Bpf-system in some bacteria, encodes an RTX-toxin named LapA. This protein gets recognized and bound at the C-terminus by the ATPase LapB (**fig. 1.8**). Due to the large size of this RTX-toxin, LapA needs to remain unfolded to fit into the space of the pores. It is then transported to the inner membrane and bound by the outer membrane factor LapE. At this point, the N-terminus of LapA remains in the periplasmic space, while the C-terminus is presented on the cell surface. In contrast to other T1SS, the Lap-system contains two additional factors called LapD and LapG. The latter has protease activity and gets bound and inactivated by a competent dimer of LapD at its PAS-domain. LapD is a GGDEF-EAL protein that acts as c-di-GMP receptor and can bind the messenger with its degenerated EAL domain (Smith et al., 2018). Binding of c-di-GMP to LapD results in sequestering of LapG and therefore presentation of LapA on the cell surface. LapA can bind to surfaces and mediate irreversible attachement (Floyd et al., 2020; Smith et al., 2018). Recent studies determined the Kd value for c-di-GMP binding of LapD to around 15 µM (Newell et al., 2009). This can be seen as relatively weak binding compared to other c-di-GMP receptors, such as MshE, and means that under relatively low c-di-GMP concentrations most LapD molecules are present in their ligand free state. This results in release of the protease LapG, which in turn cleaves the N-terminal region of LapA. The RTX-toxin is then released into the extracellular space and not presented on the surface anymore, resulting in decreased adherence (see **fig. 1.8**) (Smith et

al., 2018). All genes of the Lap-system are located in the same operon and controlled by the master regulator FleQ/FlrA. Since this master regulator is also controlled by c-di-GMP, this adds another layer of c-di-GMP dependent regulation to this system (Smith et al., 2018; Schirmer, 2016).

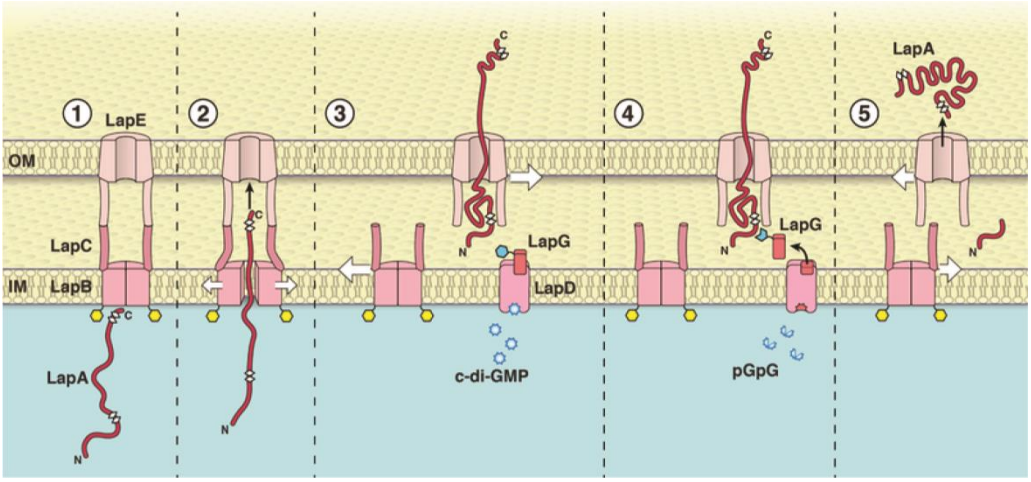

Figure 1.8) Schematic structure of the Lap-system. The Lap-system spans the inner and outer membrane.The RTX-toxin LapA is transported by LapB through the inner membrane (1) to LapE (2). Under high c-di-GMP conditions LapD binds and inactivates the protease LapG and LapA is presented on the surface (3). When LapD has no c-di-GMP bound, LapG autocleaves itself and gets released (4). LapG then cleaves LapA and the RTX-toxin is released (5). (Smith et al., 2018)

After the cells adhered to the surface, the last step for biofilm formation is the production and secretion of extracellular substances, such as as cellulose, alginate and poly-N-acetylglocosamine, that form the biofilm matrix (Smith et al., 2018; Morgan et al., 2014). As previously stated, it was one of the first findings in c-di-GMP research that the cellulose synthase of *Gluconacetobacter xylinus* is regulated by c-di-GMP. However, the process is not exclusive to this specific organism but occurs in several others, such as *Rhodobacter sphaeroides* (Morgan et al., 2014). Morgan and colleagues managed to unravel the structural basis for this process. In their study, the crystal structure of the cellulose synthase, consisting of BcsA and BcsB, in complex with c-di-GMP has been solved. They found that, when no c-di-GMP is bound, the cellulose synthase complex is present in an autoinhibited state where a salt bridge tethers the gating loop, which controls access to the active site of the complex. However, when c-di-GMP gets bound, this salt bridge is disrupted, resulting in substrate coordination at the active site and synthase activity (Morgan et al., 2014).

Another extracellular substance that is crucial for biofilm formation in many bacterial species is alginate. The secretion of this molecule is also controlled by c-di-GMP and the structural basis for this process was solved using *P. aeruginosa* as model organism. Biofilm formation of this organism plays a crucial role in patients with cystic fibrosis and chronic pulmonary

diesease, underlining the importance of c-di-GMP research. The authors were able to solve the crystal structure of Alg44 in complex with c-di-GMP. The protein is located in the inner membrane and can produce alginate enzymatically. They found that Alg44 binds a self-intercalated dimer of c-di-GMP and itself is also present as dimer. They were able to identify two critical arginine residues that are crucial for binding and state that Alg44 adopts a PilZ domain fold with a novel dimerization mode (Whitney et al., 2015).

Summarizing this, elevated c-di-GMP concentrations induce the switch from a motile to sessile lifestyle and increase biofilm formation. The increased biofilm formation was verified multiple times, one example for this is the study of DosD, which is an enzymatically active DGC that is present in *S. putrefaciens* CN-32. In a study conducted by Chao Wu and colleagues the authors found that deletion of *dosD* leads to decreased cellular c-di-GMP concentrations, indicating DGC activity of DosD. They then conducted biofilm assays and found that deletion of *dosD* resulted in decreased biofilm formation. They state that the activity of DosD is regulated by oxygen and that the protein regulates the transcription of the *bpf* operon (Wu et al., 2013).

Another example where the effect of c-di-GMP on the biofilm formation was shown is the study by Tischler and Camilli, where they used *V. cholerae* as model. The authors studied the effects of the EAL protein VieA and showed that it acts as an active PDE. Using biofilm assays and microscopy they were able to show that deletion of *vieA* leads to increased biofilm formation. They attributed this to the increased c-di-GMP level and found that this regulates the transcription of the *vps* genes, which play a crucial role in the exopolysaccharide synthesis in *V. cholerae* (Tischler & Camilli, 2004).

1.9 Spatiotemporal organization and motility

Bacteria are highly structured organisms that obtain a strict spatial and temporal organization of cellular factors. This is especially important during cell division, but also for motility, colonization and pathogenicity (Govindarajan et al., 2012). When cells divide, the DNA needs to become equally distributed between the mother and daughter cells; when cells colonize new habitats they need to construct motility and biofilm factors and localize them at the desired cellular compartment. As previously stated, the positioning and number of flagella are characteristic for the respective species. The γ-proteobacterium *S. putrefaciens* CN-32 for example constructs one single polar flagellum that is located close to the chemotaxis system at the cell pole (Rossmann et al., 2015).

But how is spatiotemporal organization achieved? The current understanding of polarity relies strongly on so-called “landmark” proteins. These are factors that recruit several other proteins to their designated position. Regarding the positioning of the polar flagellum and the chemotaxis system in *S. putrefaciens* CN-32, two landmark proteins called FlhF and HubP are crucial. Rossmann and colleagues were able to show that the SRP-like GTPase FlhF is essential for polar recruitment of the polar flagellar system. When they deleted *flhF*, they found that the polar flagellum is still constructed but delocalized. To distinguish delocalized flagella of the polar system between flagella of the lateral system they specifically labeled the polar flagellins with a fluorescent dye. Remarkably, despite flagella are still being produced, the spreading radius on motility plates is dramatically reduced compared to the wild type; underlining the importance of spatiotemporal organization. On the other hand, the chemotaxis system was still polarly localized upon deletion of *flhF*. The authors found that the model organism encodes a functional ortholog of FimV, HubP, that is encoded by the gene *sputcn32_2442.* This gene is essential for polar localization of the chemotaxis system. When they deleted the gene they found that the position of chemotaxis factor CheA is not limited to the cell pole anymore, while the primary flagellum is still positioned at the pole. Using motility assays they found that delocalization of the chemotaxis system results in dramatic loss of spreading in complex environments; again underlining the importance of spatiotemporal organization in bacteria (Rossmann et al., 2015).

Summarizing this, the example of FlhF and HubP shows that spatiotemporal organization can be obtained by the interaction of landmark proteins with their clients. This is not only the case for motility but also for other fundamental processes, such as cell division. In the case of HubP, the previous study also shows that this protein is involved in the localization of the *oriC*, underlining the importance of HubP in spatiotemporal organization (Rossmann et al., 2015). The protein is anchored in the cell wall with its C-terminal LysM domain. This domain is also responsible for the polar localization of HubP: When the LysM-domain is fused to a fluorescent protein and produced ectopically, fluorescent clusters are visible at the cell pole (Rossmann et al., 2015). However, the exact mechanism how HubP reaches the cell pole is still not clear. Possibly the cell wall and cell membrane have special characteristics at the cell pole that allow interaction with HubP but further research is needed to answer this question sufficiently. In addition to the LysM domain, HubP is also anchored in the cytoplasma membrane with a transmembrane helix. The cytoplasmic portion consists of ten imperfect TPR-repeats, followed by a C-terminal FimVc-domain (Rossmann et al., 2015). Since orthologs of HubP are not only present in *Shewanella* species but also in other γ-proteobacteria, the protein has been researched by several groups (Nicastro et al., 2020; Rossmann et al., 2015; F. M. Rossmann et al., 2019; Semmler et al., 2000; Yamaichi et al.,

2012). It has first been discovered by Semmler and colleagues in 2000, were they found a novel gene that is involved in twitching motility in *P. aeruginosa*. Due to that function they named the gene *fimV*. They state that *fimV* homologues are found in several genomes of type IV-fimbriated bacteria but not in species that lack this system (Semmler et al., 2000). The group of Burrows did bioinformatical analysis regarding distribution and similarity of HubP homologues and constructed a phylogenetic tree (**fig. 1.9a**). The structure of the C-terminal region of *Pseudomonas aeruginosa* FimV (PDB: 4MBQ) is shown in **fig. 1.9b,c**.

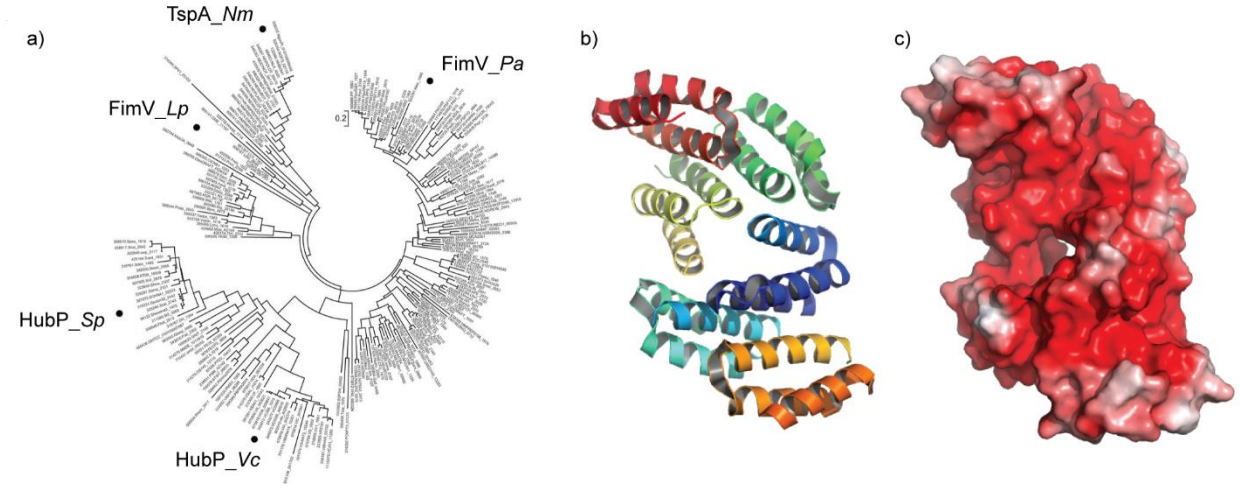

Figure 1.9) Phylogenetic tree and structure of HubP. a) The polar landmark protein HubP is present in many Gram-negative species, such as *Neisseria*, *Legionella*, *Shewanella*, *Vibrio* and *Pseudomonas*. Buensuceso and colleagues analyzed this by creating a phylogenetic tree. The protein is called TspA in *Neisseria*, FimV in *Pseudomonas* and *Legionella* and HubP in *Shewanella* and *Vibrio* (Buensuceso et al., 2016, modified)**. b)** Structure of the C-terminal region of FimV (PDB: 4MBQ). **c)** The electrostatic potential of the FimVc-domain was calculated by APBS electrostatic. The protein shows an overall negative surface charge.

They found that HubP is present in several *Shewanella* and *Vibrio* species. The name rose from its function as "Hub of the Pole" (Yamaichi et al., 2012).

1.10 Spatiotemporal organisation of c-di-GMP signaling

Since many organisms encode a plethora of c-di-GMP regulating proteins, the sheer number of factors require a strict spatiotemporal organization of c-di-GMP signaling. The simplest way for temporal regulation is the use of sensor domains that modulate enzymatic activity as reaction to a signal. Several examples are described in the previous chapters, such as the oxygen dependent DGC activity of DosD in *S. putrefaciens* (Wu et al., 2013). However, mechanisms that are more complex are known, such as the use of trigger PDEs. These proteins are multifunctional: They can degrade c-di-GMP but also interact directly with macromolecular targets, such as transcription factors. They have been first described by the

group of Regine Hengge using *E. coli* as model organism. They state that the enzymatically active PDEs, PdeR and PdeL, are such trigger PDEs (Hengge, 2016).The protein PdeR can bind and degrade c-di-GMP but also inhibits DgcM and the transcription factor CsgD by direct protein-protein interaction, which regulates the transcription of the *csg* operon. On the other hand, PdeL activates its own expression under low c-di-GMP levels. This results in a positive feedback loop, were low c-di-GMP levels result in stronger expression of PdeL, which in turn lowers the cellular c-di-GMP level even more. This allows the fast switch between high- and low-c-di-GMP level conditions in the cell (Hengge, 2016).

These are examples for the temporal control of c-di-GMP signaling. However, the spatial regulation was also found to be crucial in c-di-GMP signaling. One example for this is localization behavior of the PDE Pch. Kulasekara and colleagues found that Pch localizes at the cell pole by getting recruited by the chemotaxis machinery. The activity of Pch is then regulated by the sensor kinase CheA: The authors found that the phosphorylated form of CheA activates the PDE activity of Pch. It still remains to be elucidated if local gradients of c-di-GMP exist in *P. aeruginosa*, but the authors state that the polar localization is crucial to create heterogeneity in the population (**fig. 1.10**). To show this, they developed a FRET-based c-di-GMP sensor. Using fluorescence microscopy, they were able to show that cells in wild-type populations are heterogeneous regarding their c-di-GMP levels (50 – 700 nM), while cells in populations that lack *pch* cluster exclusively between 600 nM – 700 nM c-di-GMP. They state that the polar localization of Pch leads to asymmetric cell division, were only the mother- but not the daughter-cell inherit Pch (Kulasekara et al., 2013).

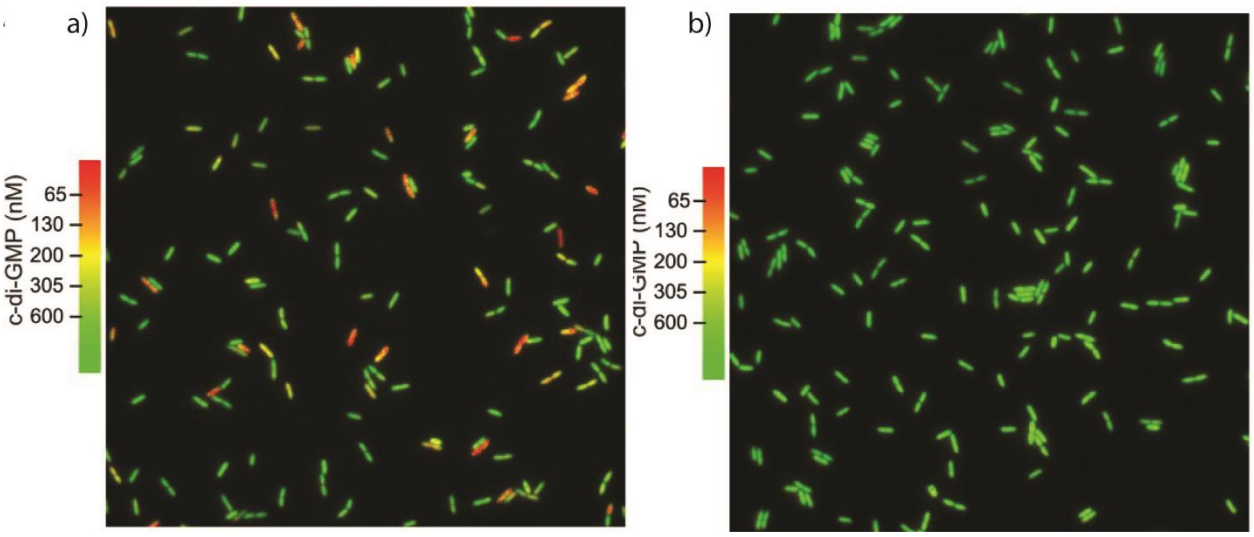

Figure 1.10) Heterogeneity of c-di-GMP in bacterial populations. a) The c-di-GMP level of single cells was analyzed by Kulasekara and colleagues by using a FRET-based reporter system. Cells that are colored in red have low c-di-GMP levels around 65 nM and cells that are colored in green have high c-di-GMP level of up to 600 nM. In the wild-type cells the population is very heterogeneous. **b)** The c-di-GMP level of single cells was also

analyzed in a strain that lacks the polar localizing PDE Pch. Absence of Pch leads to a population with homogenously high c-di-GMP levels. (Kulasekara et al., 2013, modified)

A more recent study was conducted by the lab of Urs Jenal and links the spatiotemporal regulation of c-di-GMP to motility and pathogenicity (**fig. 1.11**) (Laventie et al., 2019). Similar to the study of Kulasekara *et al*., they used the opportunistic pathogen *P. aeruginosa* as model organism. During infection, these bacteria colonize the host epithelia using pili as adhesins. They found that cells can sense surface contact in a flagellar motor-dependent manner and that this signal results in rapid change of the cellular c-di-GMP level within few seconds. The cell-surface contact increases the c-di-GMP level, which activates the c-di-GMP receptor FimW, which in turn promotes pilus assembly. However, since the previously described PDE Pch localizes at the cell pole, the attached cell undergoes asymmetric cell division where only one cell inherits Pch. This PDE leads to decreased c-di-GMP levels in one cell. Since low c-di-GMP levels lead to increased motility and decreased adherence, the cell with low cellular c-di-GMP concentration detaches and uses flagella mediated motility to further colonize the area. The authors named this mechanism “touch-seed-and-go” and claim that the cellular asymmetry leads to the formation of a motile spreader and a sessile striker cell. This is of great importance, since they also state that this heterogeneity boosts infection spreading and tissue damage (Laventie et al., 2019).

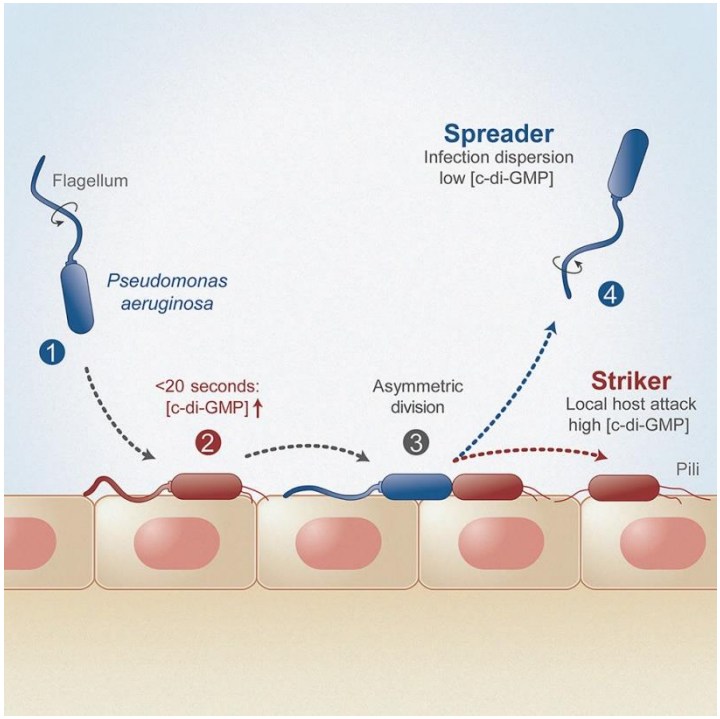

Figure 1.11) Model for the “touch-seed-and-go” mechanism. The motile bacterial cell (1) comes in contact with the host cells. This contact triggers the production of c-di-GMP and the cellular level increases strongly in less than 20 seconds (2). When the adhered cell divides, the polar localizing PDE Pch leads to asymmetric cell

division. Thus, the daughter cell has low c-di-GMP levels and produces motility factors, while the mother cell attacks the host and has high c-di-GMP levels (4). (Laventie et al., 2019)

Another model organism that is frequently used as model for spatiotemporal regulation is *C. crescentus*. This bacterium switches from a flagellated motile cell to a sessile stalked cell. This process is regulated by asymmetrical distribution of c-di-GMP during cell division. One major contributor to the asymmetry is the DGC PleD. Before the cells undergo cell division, *Caulobacter* cells have equivalent c-di-GMP levels. But as soon as septation occurs, the c-di-GMP level of the flagellated swarmer cells decreases drastically. This process is mediated by the polar localization of PleD, which leads to asymmetric cell division where only the sessile stalked cell inherits PleD. The activity of PleD is further regulated by PleC, which acts as negative regulator. It was found that PleC is also crucial for asymmetrical distribution of c-di-GMP during cell division (Christen et al., 2010).

1.11 Model organisms and goals of this work

The main model organism that was used in this work is the γ-proteobacterium *S. putrefaciens* CN-32. This bacterium has a primary flagellar system that produces a single flagellum at the cell pole and a secondary flagellar system that produces up to six lateral flagella. Both systems are independently regulated, making it an ideal model organism for spatiotemporal organization. Furthermore, the species is able to sense attractants and repellents with a polarly localized chemotaxis system that regulates the rotation of the polar flagellum. As described above, the two key landmark proteins FlhF and HubP determine the position of the primary flagellar system and the chemotaxis system. Another crucial factor in this process is the protein FlhG, which causes that only one flagellum is assembled by the primary system. Both flagellar systems are not only independently regulated but also use different energy sources: The polar flagellum is powered by an efflux of sodium ions, while the secondary system utilizes the proton gradient. Besides that, *S. putrefaciens* CN-32 is known for its respiratory diversity and can utilize several different carbon and energy sources, such as lactate and arabinose and amino acids. It is classified as facultative anaerobic species and can use multiple electron acceptors such as oxygen, nitrate and DMSO (Hau & Gralnick, 2007; Cong Liu et al., 2017). The organism is ideal for c-di-GMP related research, since it encodes a plethora of different proteins that can influence the c-di-GMP level (see results). It was found that this messenger is involved in the regulation of several crucial cellular processes, such as motility, biofilm formation and metabolism (Cong

Liu et al., 2017; Wu et al., 2013). Since high levels of c-di-GMP lead to decreased spreading on motility plates, this method can be used as fast read-out for the c-di-GMP level.

The second model organism of this study is the closely related species *S. oneidensis* MR-1. It is mostly known for its ability of extracellular electron transfer and is able to reduce toxic metals (Dundas et al., 2018). Similar to *S. putrefaciens* CN-32 it is metabolically diverse and uses c-di-GMP to regulate motility and biofilm formation (Chao et al., 2013; Wu et al., 2013). In contrast to *S. putrefaciens* CN-32, it only encodes one flagellar system. Both organisms however utilize two independently regulated type IV pilus systems, called Pil and MSHA.

This study focuses on the spatiotemporal organization of c-di-GMP signaling and unravels the molecular mechanism of GGDEF-domain mediated polar targeting. The protein that was analyzed is called PdeB and was first encountered by our group during a transposon mutagenesis screening in *S. putrefaciens* CN-32 that selected phenotypes with reduced spreading on motility plates. The protein was first described by the group of Alfred Spormann in *S. oneidensis* (Chao et al., 2013). The protein has two transmembrane domains with a long periplasmic region that has no homology to any known domain. An overview of the domain architecture is shown in **figure 3.1** and **figure 3.2a**. Close to the second transmembrane domain, PdeB has a PAS-domain. These domains can mediate multimerization, can be posttranslationally modified and bind small ligands. However, sequence analysis and color of purified protein make binding of a flavin or hem cofactors to the PAS-domain very unlikely. A GGDEF and an EAL domain are located at the C-terminus of PdeB. In *S. oneidensis*, the purified cytoplasmic region of PdeB showed PDE activity *in vitro*, while no DGC activity was found. The authors of this study were indifferent why no c-di-GMP product was formed, since they claimed that the GGDEF domain harbors all residues required for enzymatic activity (Chao et al., 2013).

In this study we not only found why the GGDEF-domain of PdeB is enzymatically inactive, but that it evolved a new function that recruits PdeB to the cell pole. Following this finding, we wanted to identify the molecular basis for this unusual function and analyze the consequences on the single-cell and population level. We aimed to study the spatiotemporal organization of PdeB by using several fluorescence microscopy techniques. To investigate the molecular basis of the polar localization we used *in silico* analysis and performed several *in vitro* experiments to characterize the interaction of PdeB with its interaction partner. Additionally, we aimed to study how PdeB and c-di-GMP affect motility and biofilm formation by using a combination of *in vivo* and *in vitro* approaches.

2. Methods

2.1 Growth conditions

The model organisms *S. putrefaciens* CN-32 and *S. oneidensis* MR-1 were used in this study. Both were grown in lysogeny broth (LB) medium (Sigma Aldrich; **table 2.1**) at 30°C. Alternatively, the mineral medium 4M (**table 2.2**) was used in some motility experiments for *S. putrefaciens* CN-32.

Additionally, the *E. coli* strains DH5α λpir, WM3064 and BL21 STAR DE3 were grown at 37°C in LB medium. The *E. coli* strain B2H was grown at 30°C.

Table 2.1) Composition of Luria-Miller LB medium.

Reagent	Concentration
Yeast extract	5 g/l
Tryptone	10 g/l
NaCl	10 g/l

Table 2.2) Composition of 4M medium.

Reagent	Concentration
Lactate (85%)	5.13 ml/l
HEPES	250 µM
NaCl	1.5 mM
K_2HPO_4	12.7 mM
KH_2HPO_4	7.3 µM
$(NH_4)_2SO_4$	90 µM
$MgSO_4$	0.5 µM
$CaCl_2$ x 2 H_2O	0.485 µM
Na_2EDTA x 2 H_2O	72 µM
$MnSO_4$	1.3 µM
$FeCl_2$ x 4 H_2O	5.4 µM
$CoCl_2$ x 6 H_2O	5 µM
$ZnSo_4$ x 5 H_2O	1 µM
$CuSO_4$ x 5 H_2O	0.2 µM
H_3BO_3	56.6 µM
Na_2MO_4 x 2 H_2O	3.9 µM
$NiCl_2$ x 6 H_2O	5 µM
Na_2SeO_4	1.5 µM

pH = 7.4

2.2 Polymerase chain reaction

The polymerase chain reaction (PCR) was used to amplify DNA fragments required for cloning and verification of genomic mutations. The starter oligonucleotides (primer) were designed with an R-script that searches for DNA regions with 50% GC-content, 58°C melting temperature, and more than 18 base pairs in length. The DNA was then synthesized by Sigma-Aldrich (Taufkirchen, Germany).

The Phusion polymerase was used to amplify DNA fragments for cloning, since this method requires a polymerase with proof reading activity. The HF-buffer (Thermo Scientific) was used for samples that have around 50% GC content, while the GC-buffer (Thermo Scientific) was used for samples with higher GC content. To verify genomic mutations the Taq-polymerase (in house produced) was used. For difficult samples with strong secondary structures DMSO was added to a final concentration of 2.5% to linearize the DNA.

In general, PCRs can be divided into three steps: Melting of DNA fragments, annealing of primer and elongation. This procedure gets repeated 32 – 40 times; doubling the amount of target DNA in each cycle. The exact program for each polymerase is described in **tables 2.3 - 2.4**:

Table 2.3) Program used for Phusion-PCR

Step	Temperature [°C]	Time [s]	cycles
Initial melting	98	420	1
Melting	98	15	
Annealing	56	15	32
Elongation	72	30 / 1000 bp	
Final elongation	72	420	1

Table 2.4) Program used for colony PCR

Step	Temperature [°C]	Time [s]	cycles
Initial melting	98	420	1
Melting	98	30	
Annealing	56	30	40
Elongation	72	60 / 1000 bp	
Final elongation	72	420	1

Consecutively, the PCR product was analyzed in agarose gels and purified either with the DNA probe purification kit (Omega Biotek, Norcross) or gel extraction kit (Omega Biotek, Norcross). The procedure was done according to manufacturer information.

2.3 *In vitro* digestion of DNA

Plasmids required for cloning were cleaved by using endonuclease restriction enzymes. The fast digest enzymes and the green buffer by Thermo Scientific were used for these reactions and the procedure was done according to manufacturer information with the exception that the reaction time was elevated to 1 hour. The reaction mix is described in **table 2.5**:

Table 2.5) Recipe for *in vitro* digestion of extracted plasmid DNA

Reagent	
Nuclease	1 µl
10x reaction buffer	2.5 µl
Plasmid	1 µg
H_2O	*ad*. 25 µl

Cleavage was verified by analysis in 1% agarose gels stained with ethidiumbromide and the specific product was purified by a gel extraction kit (Omega Biotek, Norcross). The procedure was done according to manufacturer information.

2.4 Isothermal assembly

To assemble DNA fragments, the isothermal Gibson assembly method was used. This method allows the single-step assembly of multiple overlapping DNA molecules (Gibson et al., 2009). The primers were designed with at least 20 overlapping nucleotides to the target region.

The reaction mix consists of a 5'-exonuclease (Thermo Scientific), a DNA polymerase with proof reading activity (Phusion polymerase, Thermo Scientific) and a DNA ligase (Thermo Scientific). The DNA fragments generated by PCR were mixed in equimolar concentrations and were added in 10-fold excess to the linearized plasmid. Following, the reaction mix was incubated for 1 hour at 50°C and the reaction was stopped by placing it on ice. The product can be stored at -20°C until the next day or immediately transformed into the *E. coli* strain DH5α λpir. The plasmid was further verified by DNA sequencing (Microsynth Seqlab, Göttingen).

2.5 DNA transformation

The plasmids from the isothermal assembly were transformed into the chemically competent *E. coli* strain DH5α λpir. To this end, the reaction mix was added without further purification to 50 µl of competent cells. The sample was then incubated for 5 – 30 minutes on ice.

Following, the sample was subjected to a heat shock by placing the tube for 45 seconds at 42°C and cooling down in an ice bath afterwards. LB medium (500 µl) was added and cells were incubated for at least 45 minutes at 37°C under vigorous shaking to allow production of antibiotic resistance proteins, which are encoded on the transformed plasmid. Afterwards, cells were plated onto LB-medium agar plates supplemented with the appropriate antibiotic to select for successful transformation.

The transformation into other *E. coli* strains was done using the sample protocol with the exception that not assembly mix but 1 µl of purified plasmid was added to the competent cells.

2.6 Strain construction

To modify the genome of *Shewanella* species, the suicide vector pNPTS was used (Lassak et al., 2010). This plasmid encodes a gene that mediates kanamycin resistance and the suicide gene *sacB*. The *sacB* gene encodes levansucrase which is an enzyme that catalyzes the reaction of sucrose to levan. This product is toxic for the used *Shewanella* species and therefore allows selection for cells which lost the plasmid. Additionally, the plasmids were constructed with 500 basepairs homologous regions to the target sequence, thus allowing sequential homologous recombination.

The *E. coli* strain wm3064 was used to conjugate the appropriate plasmid into *S. putrefaciens* CN-32 or *S. oneidensis* MR1. The cells were grown in LB medium with the appropriate supplements overnight and were harvested on the next day by centrifugation. They were washed with LB medium to remove the antibiotic, and the *E. coli* cells were added to the recipient *Shewanella* strain in a final volume of 200 µl. The suspension was pipetted onto a LB plate supplemented with DAP, which was incubated overnight at 30°C. The used *Shewanella* strains are not able to amplify the pNPTS plasmid but due to the homologous regions the plasmid integrates into the genome by homologous recombination. The next day, cells were washed off by adding 2 ml LB medium onto the plate and the suspension was transferred into a new microcentrifuge tube. The sample was washed at least three times with LB medium to remove the DAP. Following, the cells were plated on a LB agar plate supplemented with 50 µg/ml kanamycin. Since the used *E. coli* strain wm3064 is DAP-auxotroph and the plate contains kanamycin, only *Shewanella* cells that integrated the plasmid into their genome grew on the plate. On the next day 10 colonies were first transferred to a LB plate supplemented with sucrose and second onto a LB plate supplemented with kanamycin. After incubation overnight, three colonies that grew on

kanamycin plates but not on sucrose plates were used to start a liquid culture in LB medium. Cells were grown for several hours into exponential phase and then plated on a LB agar plate supplemented with sucrose. This allows the selection for cells that accomplished the second homologous recombination. Following, the plate was incubated over night at 30°C and the next day 32 colonies were first transferred onto a plate supplemented with kanamycin and then onto a plate supplemented with sucrose. Cells that grew on sucrose but not on kanamycin were tested by colony PCR for the desired mutation.

2.7 Soft-agar motility assays

To analyze effects on the motility in complex environments, soft-agar motility assays were used. The cells were grown in an overnight culture and a new culture was inoculated to a final OD_{600} of 0.02 on the next day. The culture was incubated until the exponential phase was reached. Meanwhile, around 70 ml of 0.25% select agar (Thermo Scientific) in LB medium was poured into a squared plate and left to cool down. Subsequently, 3 µl of each culture was dropped onto the plate and the sample was incubated overnight. These experiments were done in triplikates. The next day, each plate was scanned and the spreading radius was measured using Fiji (Schindelin et al., 2012). The obtained values were normalized by dividing the spreading radius of the mutant by the radius of the positive control. The result was then visualized by bar plots or dot plots.

2.8 Determination of swimming velocity

To quantify the swimming velocity of a population, cells were grown in liquid culture overnight and then transferred into a new Erlenmeyer flask with fresh medium. They were grown until exponential phase was reached and 20 µl were transferred onto a glass covered slide. A microscope (Leica DMI 6000 B inverse microscope; Leica, Wetzlar, Germany) was used to obtain a 10-second-long time lapse video of swimming cells. The data was analyzed with Fiji (Schindelin et al., 2012) and a cut off was set to 2 µm/s swimming speed to remove artifacts of brownian movement. Following, the mean swimming speed was calculated of at least 300 cells.

2.9 SDS PAGE

The strains of interest were grown to exponential phase before cells with an OD_{600} of 10 in 100 µl were collected by centrifugation. The supernatant was discarded and cells were resuspended in 100 µl sample buffer (**table 2.6**). Afterwards, the samples were heated for 7 minutes at 95°C and cooled down on ice before 10 µl of each sample was loaded on a SDS gel (7.5% - 15% acrylamid concentration; depending on protein size). The SDS-gel consists of a running gel and a stacking gel to create sharp bands. The lower gel was created by using the lower gel buffer (**table 2.7**), while the upper gel was made with the upper gel buffer (**table 2.8**). The prestained protein marker (Thermo Scientific) was used to evaluate the molecular weight of protein bands. The running buffer is described in **table 2.9**.

Table 2.6) Sample buffer. The buffer was used to solubilize and linearize proteins.

Reagent	Concentration
Glycerol	200 ml/L
SDS	40 g/L
β-mercapto ethanol	100 ml/L
Bromphenol blue	0.2 g/L
Tris-HCl	125 mM

pH = 6.8

Table 2.7) 4x SDS-gel running gel buffer.

Reagent	Concentration
Tris-HCl	181.7 g/L
SDS	4 g/L

pH = 8.8

Table 2.8) 4x SDS-gel stacking gel buffer.

Reagent	Concentration
Tris-HCl	60.6 g/L
SDS	4 g/L

pH = 6.8

Table 2.9) Running buffer for SDS-PAGE.

Reagent	Concentration
Tris	25 mM
Glycine	192 mM

pH = 8.3

The proteins were separated by using electrical current (150 mA) for one to three hours. The proteins were then stained with Coomassie solution (**table 2.10**) before fixing solution was added (**table 2.11**).

Table 2.10) Coomassie solution.

Reagent	Concentration
Coomassie brilliant blue G250	1 g/l
Methanol	50 %
Acetic acid	10 %

Table 2.11) Fixing solution.

Reagent	Concentration
Acetic acid	5 %
Ethanol	25 %
H_2O	75 %

2.10 Western blot

The PVDF membrane was activated by placing it for 15 seconds in methanol. After activation, the membrane was washed for 3 minutes in H_2O and 5 minutes in western transfer buffer (**table 2.12**). The membrane was placed on three layers of Whatman papers soaked with western transfer buffer before the gel was brought onto the membrane. The gel was then covered with three layers of Whatman papers and protein transfer was induced by the use of an electrical current (120 mA / membrane) for 50 minutes.

The membrane was washed with PBS-T (**table 2.13**) after the protein transfer. After washing, the membrane was blocked by using PBS-T supplemented with 5% milk powder. After 1h incubation at room temperature the membrane was washed one time with PBS-T.

Table 2.12) Western transfer buffer.

Reagent	Concentration
Tris	25 mM
Glycine	192 mM
Methanol	10%

pH = 8.6

Table 2.13) PBS-T. The buffer was used for antibodies, MBP-GGDEF and FimVc proteins.

Reagent	Concentration
NaCl	8 g/L
KCl	0.2 g/L
Na_2HPO_4 x 2 H_2O	1.78 g/L
KH_2PO_4	0.24 g/L
Tween20	0.01 %

pH = 7.4

The corresponding antibodies were added to the membrane, followed by 1 h incubation at room temperature. The membrane was washed three times with PBS-T and, if required, the second antibody was brought onto the membrane with the same method.

When the used antibodies were coupled to alkaline phosphatase, the membrane was incubated for 5 minutes in detection buffer (**table 2.14**). Then, the luminescence was induced by adding 1 ml of a mixture of detection buffer with CDP star working solution (Roche, 1 CDP star : 100 detection buffer).

Table 2.14) Detection buffer.

Reagent	Concentration
Tris-HCl	100 mM
NaCl	100 mM

pH = 9.5

For antibodies which are coupled to horseradish peroxidase, 1 ml of Chemoluminescence working solution (PerkinElmer Western lightning Chemoluminescence Reagent Plus Kit; 1 Enhanced luminol reagent 1 oxidizing reagent) was added to the membrane to induce the luminescence.

2.11 Fluorescent staining of flagellar hooks

To visualize and quantify flagellar hooks, cysteine mutations were integrated into the genes that encode the flagellar hooks (Schuhmacher et al., 2015). This method was required, because these proteins form long extracellular oligomers and are therefore not suitable for translational fusions with fluorescent proteins. The induced mutations exchange a surface exposed serine or threonine to cysteine, which can then be attacked by the used maleimide dyes.

Prior to staining, cells were grown in an overnight culture that was used to inoculate a new liquid culture with a final OD_{600} of 0.02 the next day. Afterwards, cells were grown to OD_{600} 0.5 and 500 µl were harvested by centrifugation for 5 minutes at 5000 x g. Then, cells were resuspended in 50 µl PBS supplemented with 1 µl Alexa Fluor 488-maleimide (Molecular Probes, Life Technologies). The cells were incubated without light exposure for 20 minutes at room temperature. Subsequently, the staining solution was removed by centrifugation for 5 minutes at 5000 x g and cells were resuspended in 500 µl PBS. Following, 3 µl of each sample was brought onto an agar slide for microscopy.

2.12 MSHA pili quantification

To quantify the number of extended MSHA pili we introduced a mutation into the pilin (MshA) that allows the staining with fluorescent malemeid dyes. This technique was developed by the lab of Fitnat Yildiz for the pilin of *V. cholearae* (Floyd et al., 2020). An alignment with the pilin of *S. putrefaciens* CN-32 was conducted to identify the corresponding residue. The pili were stained with a similar protocol that was used for the flagella stain (see previous chapter).

2.13 Fluorescence microscopy

Overnight cultures of *Shewanella* cells containing the corresponding mutations or plasmids were transferred to fresh medium with a final OD_{600} of 0.02. The cells were grown to exponential phase (OD_{600} of 0.3 – 0.5) before 3 µl were transferred onto an agar slide. The sample was analyzed by using a Leica DMI 6000 B inverse microscope (Leica, Wetzlar, Germany) equipped with an sCMOS camera and an HCX PL APO 100×/1.4-numerical-aperture objective. Pictures in the DIC or phase contrast channel were taken with 100% intensity and 50 ms exposure time, while 500 ms exposure time was used for the fluorescence channels. The obtained data were analyzed with Fiji (Schindelin et al., 2012) and BacStalk (Hartmann et al., 2020).

To quantify the localization pattern of fluorescence clusters two different methods were used. One was to simply count the number of fluorescence clusters and cells and then divide both values to obtain the quotient of fluorescence clusters divided by cells. For this method, at least 300 cells were counted for each strain. The second method involved the use of BacStalk and R. The microscopy data were analyzed with BacStalk to obtain following parameters: Cell length, intensity of strongest fluorescence signal, distance of strongest

fluorescence signal to cell center and mean cellular fluorescence. Here, exactly 500 cells were analyzed for each sample. The obtained data were analyzed with the programming environment R, using the program Rstudio (RStudio PBC) to generate 3d scatterplots. To show the position of the strongest fluorescence cluster we developed a formula that creates a new parameter called “normalized distance to center”. A “normalized distance to center” value of 0 means that the strongest signal is at the cell center and a value of 1 means that it is at the cell pole. The formula is as follows:

$$norm.distance\ to\ center = abs(\frac{\text{distance of strongest fluorescence signal to cell center}}{(\frac{cell\ length}{2})})$$

The cluster intensity is shown as “normalized intensity” parameter. This value is created by subtracting the mean cellular fluorescence of the intensity of the strongest fluorescence signal.

To visualize the localization pattern, the normalized distance to center was plotted against the normalized intensity and the cell length is shown by coloring.

2.14 Protein production and purification

The pET24c plasmid encoding the gene of interest was transformed into *E. coli* BL21 STAR DE3 and cells were grown overnight at 37°C on an agar plates supplemented with 50 µg/ml kanamycin. Multiple colonies were used to inoculate a 50 ml liquid culture and the culture was incubated under vigorous shaking overnight. The preculture was transferred the next day into a new Erlenmeyer flask containing 1 l LB medium supplemented with 50 µg/ml kanamycin and cells were grown under vigorous shaking at 37°C until OD_{600} 0.5 – 1 was reached. Subsequently, the culture was chilled in an ice bath for 10 minutes before the protein expression was induced by addition of 1.25% lactose. Protein expression continued for 12 – 24 hours under vigorous shaking at 16°C before the cells were harvested by centrifugation for 10 minutes at 5000 rpm. The resulting cell pellet was flash frozen in liquid nitrogen and stored at -20°C until use.

The pellet was resuspended in its corresponding protein buffer (**tables 2.15 – 2.18**), supplemented with 20 mM imidazole, and cells were lysed by sonification (Sono plus, Bandelin) for at least 3 times for 45 seconds. The sample was centrifuged for 20 minutes at 20,000 rpm to remove cell debris and unlysed cells. Following, the supernatant was extracted and clarified by filtering through a 0.4 µm syringe filter. Further, an affinity chromatography column was connected to the ÄKTA PURE25 system (GE healthcare), as

well as a 150 ml superloop (GE healthcare), filled with protein buffer. The sample was injected into the superloop by the use of an external peristaltic pump and the run was started. The program begins by washing the column with 5 column volumes (CV) of water (5 ml/min), followed by equilibration with 5 CV of protein buffer, supplemented with 20 mM imidazole (5 ml/min). The sample was applied with a slower rate (1 ml/min) to assure binding of the protein of interest to the NiNTA column (HisTrapHP 5 ml, GE Healthcare). After this step is finished, the unspecific proteins are removed by washing with 10 CV with 5 ml/min of protein buffer, supplemented with 10% of elution buffer. The elution buffer consists of the corresponding protein buffer supplemented with 600 mM imidazole.

The proteins were eluted with 3 CV of a linear gradient of lysis buffer with 10% elution buffer to 100% elution buffer (3 ml/min). This step was followed by 3 CV of 100% elution buffer, to assure removal of proteins. Following this, the column was washed with 5 CV of water (5 ml/min) and 5 CV of 20% ethanol (5 ml/min). Depending on the downstream method, the protein buffer was exchanged by using a ZebaSpin 7 kDa filter (Thermo-Fisher, Waltham) and proteins were stored at -20°C after snap freezing in liquid nitrogen or they were immediately further purified by using size exclusion chromatography (SEC).

For SEC, four different columns were used depending on the sample volume and protein size. The Superdex 200 (GE Healthcare) and Superdex200 increase (GE Healthcare) columns were used for volumes up to 500 µl and 600 kDa; the Superdex200 PG column (GE Healthcare) was used for volumes up to 2 ml and 600 kDa and the Superpose 6 column (GE Healthcare) was used for volumes up to 2 ml and 5000 kDa.

Prior to purification, the column and a sample loop were connected to the ÄKTA PURE25 system. Then, the column was washed with water for at least 1.5 CV at maximum flow rate, followed by equilibration with protein buffer for at least 2 CV at maximum flow rate. The sample was then injected into a sample loop by the use of a syringe and the run was started. The SEC runs started with injecting the proteins into the column, followed by isocratic elution for 1 CV. After use, the column was washed with 1.5 CV water at maximum flow rate and 2 CV 20% ethanol before storage.

Table 2.15) HEPES protein buffer. The buffer is suitable to purify and store MBP-GGDEF and FimVc proteins from *S. putrefaciens* CN-32 and *S. oneidensis* MR-1.

Reagent	Concentration
HEPES	20 µM
NaCl	500 µM
KCl	50 µM
$MgCl_2$	5 µM

pH = 7.5

Table 2.16) Low salt HEPES protein buffer. The buffer is suitable to purify and store MBP-GGDEF and FimVc proteins from *S. putrefaciens* CN-32 and *S. oneidensis* MR1. Additionally it was used to purify and store MshE, MshE-N and PilB-N.

Reagent	Concentration
HEPES	20 µM
NaCl	50 µM
KCl	50 µM
$MgCl_2$	5 µM

pH = 7.5

Table 2.17) Tris protein buffer. The buffer is suitable to purify and store MBP-GGDEF and FimVc proteins from *S. putrefaciens* CN-32 and *S. oneidensis* MR-1. Additionally, the buffer was used to purify and store the cytoplasmic portion of PdeB as MBP-fusion protein.

Reagent	Concentration
Tris-HCl	50 µM
NaCl	500 µM
KCl	50 µM
$MgCl_2$	5 µM

pH = 8

Table 2.18) PBS protein buffer. The buffer is suitable to purify and store MBP-GGDEF and FimVc proteins from *S. putrefaciens* CN-32 and *S. oneidensis* MR-1.

Reagent	Concentration
NaCl	8 g/L
KCl	0.2 g/L
Na_2HPO_4 x 2 H_2O	1.78 g/L
KH_2PO_4	0.24 g/L

2.15 Analytical SEC

The SEC method was not only used for protein purification but also for analysis of the aggregation state. For this, proteins were first purified by affinity chromatography and SEC as described above. Following, the superdex 200 increase column (GE healthcare) was used for analysis. We used the high molecular weight calibration kit (GE healthcare) to obtain a calibration curve. This kit consists of blue dextran to determine the void volume of the column and several globular proteins for calibration. The used flow rate was 200 µl/min and the sample size was 200 µl, which is according to manufacturer information for analytical runs. The obtained elution volumes were used to create a calibration curve by plotting the elution volume against a logarithmic scale of the molecular weight of the calibration proteins. The proteins of interest were analyzed with SEC by using the same flow rate and sample size and the obtained formula for the calibration curve was used to calculate the molecular weight

of the eluted protein. The protein was further analyzed by SDS-PAGE to obtain data about the aggregation state.

2.16 MANT-c-di-GMP and MANT-GTP binding assay

MANT (2'-(or-3')-O-(N-Methylanthraniloyl)-labeled ligands were used to show *in vitro* binding of c-di-GMP and GTP to proteins, since this fluorophore increases its fluorescence when located in hydrophobic surroundings, such as binding sites of proteins. The proteins of interest were purified as described above. The protein concentration was measured using a nanodrop (Thermo Scientific) and samples were diluted to 1 µM. Subsequently, 25 µl of each protein and control samples were transferred into a white 96-well plate. Afterwards 25 µl of the ligand was added to a final concentration of 1 µM and the mixture was incubated for 30 minutes on a plate shaker at room temperature, until the fluorescence was measured with λ_{exc} 295 nm and λ_{em} 455 nm in triplikates. The obtained fluorescence values were plotted by using GraphPad Prism (GraphPad Software, Inc). Increased fluorescence compared to the control samples indicates ligand binding.

2.17 MANT-c-di-GMP PDE assay

The MANT-c-di-GMP degradation assay was done as described in Eli et al., 2017. The PDE RocR was used as positive control and was purified following the protocol by NiNTA affinity chromatography. Afterwards, 90 µl of each sample (50 µM) were transferred into a 96-well plate. The plate was sealed and incubated at 37 °C for 30 minutes until the ligand was added and the fluorescence was measured at 448 nm every 2 min for 30 minutes. The fluorescence was then plotted against the time in minutes.

2.18 Extraction of cellular nucleotide messengers and quantification

To quantify the cellular c-di-GMP level, we extracted the cellular nucleotides which were then quantified by Dr. Heike Bähre using MS. We also tested an influence of PdeB on cAMP and the presence of cGAMP in *S. putrefaciens* CN-32. All messenger molecules were extracted with the same protocol, published by Bähre and Kaever (Bähre & Kaever, 2017).

Bacterial cells were grown in liquid culture to exponential phase (OD_{600} of 0.5). Following, 2 ml were transferred into a new microcentrifuge tube and harvested by centrifugation for 20 min at 4°C and 2500 x g. The obtained cell pellet was washed and nucleotides were

extracted by addition of 300 µl extraction solution (2 acetonitril : 2 methanol : 1 water). This was repeated three times and the residual cell pellet was used to quantify cellular proteins with BCA assays, which is needed for normalization. The extracted nucleotides were dried by vacuum centrifugation and stored at -80°C until further use.

For MS-quantification (carried out at the medizinische Hochschule Hannover by Heike Bähre), the nucleotides were resuspended in HPLC grade water. A test mix and a set of calibrators were analyzed by HPLC and MS to obtain the specific retention times. The samples of interest were injected and tandem mass spectrometry in positive ionization mode was performed. The MS/MS data was interpreted by "calculating the ratios of the peak areas of the calibrators and samples in relation to the respective peak areas of the internal standard" (Bähre & Kaever, 2017).

2.19 BCA assay

The Pierce BCA protein assay kit (Thermo scientific, cat. No. 23225) was used to quantify precipitated proteins. The method was done according to manufacturer information.

Prior to use, the proteins were solubilized by addition of sodium hydroxide. Consecutively, 9 samples of BSA were prepared to generate a standard curve, ranging from 0 µg/ml to 2000 µg/ml. Following, 25 µl of each sample was pipetted into a 96 well plate. The protein solution was mixed with 200 µl of the reaction solution and the plate was incubated for 30 minutes at 37°C. After cooling the plate to room temperature, the absorbance at 562 nm was measured in a tecan plate reader (Tecan Infinite M200, Tecan, Switzerland). The mean absorbance of the blank standard was subtracted from the obtained values and the protein concentration was blotted against the adjusted absorbance values. The obtained function was used to calculate the protein concentration of the unknown samples. Each sample was analyzed in triplicates.

2.20 Isothermal titration calorimetry (ITC)

The ITC was done by using the MicroCal ITC2000 (Malvern Pananalytical, Kassel, Germany). The proteins were rebuffered by using a Vivaspin 6, 10000 column Sartorius, Göttingen, Germany) at 4900 x g and 4 °C and ITC buffer (**table 2.19**). Samples were then degassed by using the MicroCal ThermoVac (Malvern Pananalytical, Kassel, Germany). Then, 18 injections of 2 µl 50 µM c-di-GMP were added to 200 µl 50 µM protein solutions. Each injection step took 4 s and it was measured for 180 s between each injection at 25°C.

The air of the tip was removed by first injection 0.4 µl. Each experiment was done as ligand-to-buffer and buffer-to-protein titration to adjust the obtained values for possible heat of dilution. Data analysis was done by using the MicroCal Analysis (OriginLab). The first injection peak was removed and the values were adjusted by subtracting both controls. A non-linear fit with one set of binding sites was used to calculate the affinity and dissociation constants.

Table 2.19) ITC buffer. The buffer was used to test the binding of c-di-GMP to the proteins MshE, MshE-N and PilB-N.

Reagent	Concentration
HEPES	20 µM
NaCl	250 µM
KCl	50 µM
$MgCl_2$	5 µM

pH = 7.5

The experiment was performed by Alexander Höing he described the protocol in Rick & Kreiling *et al*., 2021.

2.21 Fluorescence polarization assay (FP)

The FP assays were done by using a FP-8300 fluorescence spectrometer (Jasco, Pfungstadt, Germany). The experiment was carried out in high precision cells (Hellma Analytics, Müllheim, Germany). The assay buffer is described in **table 2.19** and all samples were degassed by using a MicroCal ThermoVac (Malvern Pananalytical, Kassel, Germany). Since GTP and c-di-GMP cannot be used for FP experiments, we used ligands with an additional MANT group (MANT-c-di-GMP (Biolog, Hayward) and MANT-GTP (JenaBioscience, Jena)). The ligand concentration was kept constant and the protein solution was titrated to the ligand in increasing volumes (0.5 µL, 0.5 µL, 1 µL, 2 µL, 4 µL, 8 µL, 16 µL, 32 µL, 64 µL, 128 µL). For the MANT-c-di-GMP binding, we used a ligand concentration of 0.7 µM and a protein solution with a concentration of 100 µM. For MANT-GTP binding we used a ligand concentration of 1 µM and a protein solution with a concentration of 100 µM. The assays were carried out at 25°C. The samples were mixed after each injection and the changed fluorescence anisotropy was measure five times (λ_{exc} 355 nm, λ_{em} 448 nm). Then, the mean change of each replicate was calculated. Subsequently, a quadratic binding equation for one-site specific binding models was calculated by using the Graph Pad Prism 5 software (GraphPad Software, Inc):

$$r = r_0 + r_{max} * \frac{(F + x + K_D) - \sqrt{(F + x + K_D)^2 - 4 * x * F}}{2 * F}$$

R = anisotropy, r_0 = anisotropy before titration, r_{max} =maximum anisotropy, F = fluorophor concentration, x = protein concentration, K_D = dissociation constant

The experiment was performed by Alexander Höing and is described in Rick & Kreiling *et al*., 2021.

2.22 Biolayer-interference-assay (BLI)

The BLITZ system (ForteBio, Fremont) was used to determine kinetic parameters of protein-protein interactions. The used proteins were purified by affinity chromatography and SEC in PBS buffer (**table 2.18**). To biotinylate the ligand protein, equimolar amounts of NHS-PEG-biotin (Thermofisher) were added to the protein solution and the sample was incubated for 20 minutes at room temperature. The unbound biotin was removed by using a VivaSpin 7 kDa desalting column (Thermofisher, Waltham).

The sensors of the BLI system were hydrated for 10 minutes before use. Following this, an unspecific binding control without ligand was done. The run is initiated by placing the sensor for 30 seconds in buffer. Then, the sensor is placed in the ligand solution for 120 seconds. After this step, the sensor is again positioned for 30 seconds in buffer. This step is followed by another 30 seconds in buffer before the sensor is placed in the analyte solution for 300 seconds to measure the association. This step can be followed by placing the sensor in buffer for 300 seconds to measure the dissociation. Experiments that measure both, the association and dissociation, used the integrated BLITZ software (ForteBio, Fremont) to calculate the kinetic constants, while experiments that measured only the association were evaluated using GraphPad Prism (GraphPad Software, Inc).

2.23 Pull-down assays

Pull-down assays were conducted with MBP-tagged bait proteins. These were bound to amylose resins (New England Biolabs, Ipswich) and unbound proteins were removed by washing with Tris buffer (**table 2.17**). Afterwards, equimolar concentrations of prey protein solution were added to the beads and the samples were incubated for 2h at 4°C. The samples were then centrifuged for 5 min at 4000xg and the supernatant was discarded. The

beads were washed five times before the proteins were eluted by adding 50 µl of sample buffer (**table 2.6**). The eluted proteins were then analyzed by SDS-PAGE.

2.24 Hydrogen-deuterium-exchange-MS (HDX-MS)

The HDX-MS assays were done in a similar manner as described in Steinchen et al., 2015. The proteins were purified by affinity chromatography and SEC before the assay was conducted. The used buffer is described in **table 2.11**. The individual proteins and the protein complex were adjusted to a concentration of 60 µM before 5 µl of the protein solutions were mixed with 45 µl of D_2O containing SEC buffer. The sample was then incubated at 25°C and after 0.25, 0.5, 1, 2 or 10 min, 50 µl of ice-cold quench buffer was added to stop the deuterium exchange with acidic pH. The mixture was then injected into an ACQUITY UPLC M-Class System with HDX Technology (Waters). Additional samples without deuteration were obtained by using SEC buffer without D_2O.The samples were then brought onto a porxine pepsin column (Enzymate Pepsin Column, 300Å, 5 µm, 2.1 mm X 30 mm (Waters)) with a flow rate of 100 µl/min in H_2O + 0.1% (v/v) formic acid at 12 °C to digest the proteins and create peptides. These were then tapped at 0.5°C for 3 minutes on an AQUITY UPLC BEH C18 1.7 µm 2.1 x 5 mm VanGuard Pre-column (Waters). The peptides were then separated by using an ACQUITY UPLC BEH C18 1.7 µm 1.0 x 100 mm column (Waters) with a gradient of H_2O + 0.1% (v) formic acid and acetonitrile + 0.1% (v/v) formic acid with a flow rate of 30 µl/min.

The peptides were ionized as described in (Geromanos et al., 2009). The ionization was done with a capillary temperature of 250°C and a spray voltage of 3.0 kV and mass spectra over 50 – 2000 m/z were obtained on a Synapt G2-Si HDMS mass spectrometer with ion mobility separation (Waters). The undeuterated samples were run in $HDMS^E$ mode, while the deuterated samples were analyzed in the HDMS mode. Then, [Glu1]-Fibrinopeptide B standard (Waters) was used to correct the Lock mass. The pepsin column was washed three times during the separation of peptides. Each washing step used 80 µl of 4% (v/v) acetonitrile and 0.5 M guanidine hydrochloride and between each sample blank runs were done. The data was obtained in three technical replicates per incubation point. The data analysis was conducted using the ProteinLynx Global SERVER (PLGS, Waters) to identify peptide ions. The incorporation of deuterium into peptides was analyzed and quantified using DynamX 3.0 (Waters) as described in Osorio-Valeriano et al., 2019.

The experiment was performed by Wieland Steinchen and he described the procedure in Rick & Kreiling *et al*., 2021.

2.25 Crosslinking MS (CL-MS)

CL-MS was used to obtain data about the interaction surface of the PdeB-HubP complex. The proteins were purified with affinity chromatography in HEPES buffer (**table 2.15**) and the obtained proteins were separated into two samples. Both samples were further purified with SEC, where the first purification was conducted in HEPES buffer and the second in PBS (**table 2.18**). We used two different buffers to assure that the crosslinking reaction is successful and found during analysis that both buffers work well for these proteins.

The crosslinking reaction was done by adding DSBU (Thermo Scientific) in 10-fold excess, before the samples were incubated for 30 minutes at room temperature. The reaction was stopped by adding 20 µl of 20 mM Tris-HCl. Following, the proteins were digested by addition of 1 µg trypsin (Promega) at 30°C overnight. This was followed by addition of 0.5 % Sodiumdeoxycholate and Iodoacetamide to reduce the proteins. This was followed by an additional digestion step with 1 µg trypsin for 2 h. The peptide solution was rebuffered using C18 reversed phase solid phase extraction cartridges (Macherey-Nagel).

The Q-Exactive Plus mass spectrometer connected to an electrospray ion source (Thermo Scientific) was used to collect data of the cross linked and digested peptides. The peptides were separated by using an Ultimate 3000 nanoLC-system (Thermo Fisher Scientific) with a packed in-house C18 resin column (Magic C18 AQ 2.4 µm, Dr. Maisch). A preconcentration set-up was used at which the peptides are first loaded onto a C18 precolumn before they were eluted in backflush mode. This was done with a gradient from 98 % solvent A (0.15 % formic acid) and 2 % solvent B (99.85 % acetonitrile, 0.15 % formic acid) to 35 % solvent B over 60 min. A flow rate of 300 nL/min was used and the data acquisition mode for the initial LFQ study was set at a resolution of 70000 (m/z, 200, MS1) and 17500 (m/z 200, MS2) with a scanning range from 375 to 1500 m/z. This was followed by MS/MS scans of the 10 strongest ion signals. The charged state screening modus was set to exclude unassigned, singly and doubly charged ions to increase the identification efficiency. The parameter for the dynamic exclusion duration was set to 30 s, while the ion accumulation time was set to 100 ms. A value of 3×10^6 was used for the automatic gain control for MS survey scans, while this value was set to 1×10^5 for MS/MS scans. The obtained data was analyzed with MeroX (v2.0) in default settings as mfg-file.

The experiment was performed in collaboration with Timo Glatter and he described the procedure in Rick & Kreiling et al., 2021

2.26 *In silico* protein structure prediction

The structure of proteins was either predicted by using the Phyre2 tool (Kelley et al., 2015) or the swiss model tool (Waterhouse et al., 2018). The primary sequence was used as input and the data was analyzed using PyMol (DeLano Scientific LLC) and the included APBS electrostatics tool.

2.27 *In silico* sequence analysis

The amino acid sequences were aligned using the ClustalOmega tool (Sievers et al., 2011). The data was then visualized with JalView (Waterhouse et al., 2009).

To generate position based weight maps the Seq2Logo tool (Thomsen & Nielsen, 2012) was used and maps were created with the weighted Kullback-Leiber algorithm.

2.28 c-di-GMP *in vivo* reporter

A plasmid containing the c-di-GMP riboswitches Bc345 and two fluorophores was used to monitor the relative c-di-GMP level of individual cells. The riboswitches control the expression of the red fluorophore turboRFP$_{AAL}$. The AAL-tag increases the degradation to obtain higher temporal resolution. The fluorophore amcyan is constitutively expressed and allows normalization to the plasmid number. The system is described in Zhou et al., 2016.

The plasmid was conjugated into the appropriate *Shewanella* strain and cells were grown as overnight culture in LB medium at room temperature. These were then used to inoculate an overday culture and cells were grown to exponential phase (OD_{600} of 0.5) before 3 µl were placed on an agar slide. The fluorescence data was obtained by using a Leica DMI 6000 B inverse microscope (Leica, Wetzlar, Germany) equipped with an sCMOS camera and an HCX PL APO 100×/1.4-numerical-aperture objective. The data was then analyzed with BacStalk (Hartmann et al., 2020) to obtain several parameters such as cell length, mean red cellular fluorescence and mean blue fluorescence. At least 500 cells were analyzed for each strain.

The experiment was performed in collaboration with Vanessa Kreiling. She collected the data and I analyzed it.

2.29 Transcriptional Lux-reporter assay

To test if *pdeB* affects the transcription of flagellar or *bpf* genes, we introduced the LuxCDABE genes into the appropriate positions of the genome of *S. putrefaciens* CN-32 (Bubendorfer et al., 2012). The strains were grown to exponential phase before 100 µl were transferred onto a 96 well plate. Each experiment was done in biological triplicates with eight technical replicates. The absorbance at OD_{600} was measured to normalize the obtained values before the luminescence was measure in a Tecan plate reader (Tecan Infinite M200, Tecan, Switzerland). The obtained luminescence was divided by the OD_{600} for normalization.

2.30 Single molecule microscopy

The strains of interest were grown as overnight cultures before an over day culture was inoculated the next day. Then, cells were grown to exponential phase (OD_{600} of 0.5) before 5 µl were placed on an agar slide (1% agarose in LB medium). The Nikon Eclipse Ti microscope (100x oil-immersion objective, NA=1.49) was used for data collection and the cells were imaged with the central part of a 514 nm-laser (TOPTICA Beam Smart, maximum power = 100 mW). The laser used about 160 – 200 W cm^{-2} and after around 100 frames the single molecule level was reached. For each movie 2000 frames were collected using an EM-CCD camera (ImageEM X2 EM-CCD, Hamamatsu). For data analysis the first 100 frames were removed using the Fiji software. The data was further analyzed with Oufti (Paintdakhi et al., 2016) to determine the cell outlines. The trajectories were analyzed using the software UTrack 2.2.1. The SMTracker 1.5 was then used to analyze the protein dynamics. Further, a squared displacement analysis was done to obtain the diffusion constants.

The experiment was done by Svenja Fiedler and she described the procedure in Rick & Kreiling et al., 2021.

2.31 Fluorescence-based quantification of molecule number

To determine the number of PdeB-mVenus molecules per cell on a single cell level we used strains of *S. putrefaciens* that encode *pdeB-mvenus* and a strain that does not harbor any fluorophore. The negative control was required to determine the auto-fluorescence. Each

strain was analyzed on the same day and 11 movies were taken for each. In contrast to the above described single molecule microscopy the first 100 frames were not removed during analysis. The software SMTracker 2.0 was used to analyze the data. The single bleaching steps of PdeB-mVenus were measured and divided by the initial fluorescence to obtain data about the number of fluorophores in the individual cell.

The experiment was done by Svenja Fiedler and she described the procedure in Rick & Kreiling et al., 2021.

2.32 Microscopy based heterogeneity assay

Shewanella strains with fluorescently labeled PdeB were grown over night in liquid culture at 30°C with LB medium. A new culture was inoculated the next day and cells were grown to exponential phase before 3 µl were transferred onto a microscopy slide. The division of cells was then observed by microscopy. The data was analyzed with Fiji (Schindelin et al., 2012) and GraphPad Prism (GraphPad Software, Inc). Exactly 250 cell divisions were observed for each strain.

The experiment was done by Vanessa Kreiling.

2.33 iSCAM assay

The $GGDEF_{PdeB}$ and $FimVc_{HubP}$ proteins were purified in low salt HEPES buffer (**table 2.16**). The assay was conducted by using a Refeyn OneMP mass photomoeter (Refeyn, UK) to obtain the mass spectra. The Native Mark standards (ThermoFisher) were used to calibrate the device and all measurements were done at room temperature. The samples were diluted to 1 µM before the protein solutions were brought onto a high precision glass coverslip (24x50 mm2, No. 1.5H, Marienfeld, Germany) with a self-adhesive CultureWellTM gasket (Grace Bio-Labs). An 18 µl drop of buffer was added to obtain the correct focus for the instrument. Following, 2 µl of the protein solution was added and mixed with the buffer before the measurement was conducted. We collected 6000 frames for each measurement and the obtained data was analyzed by using the DiscoverMP software (Refeyn, UK).

The experiment was performed in collaboration with Dr. Georg Hochberg.

2.34 Bacterial-adenylate-cyclse-2-hybrid-assay (B2H)

B2H-assays are a simple and fast method to screen for protein-protein interactions (Karimova et al., 1998). The genes of the two proteins of interest were cloned into the vectors pUT18, pUT18C, pKT25 and pKNT25 (Euromedex). Then, all possible combinations of plasmids were co-transformed into the *E. coli* BTH strain (Euromedex). The empty plasmids and a leucine zipper were used as controls. The cells were grown over night at 30°C in LB medium supplemented with kanamycin (50 µg/ml) and ampicillin (100 µg/ml) before they were used to inoculate a new culture. These cultures were then grown to exponential phase before 5 µl of culture was transferred onto a LB plate supplemented with X-gal, IPTG and the appropriate antibiotics. The plate was then incubated at 30°C overnight. Coloring of the colonies was observed the next day. Each experiment was done in triplicates.

3. Results

Flagella-mediated motility allows bacteria to colonize new habitats, move towards attractants or away from repellents and plays a crucial role in infections. However, production of flagella and rotation of the filament consume huge amounts of energy and therefore need to be strictly regulated. This is not only true at the single cell level but also for bacterial populations: Colonization of new habitats require motility but also attachment and biofilm formation. Previous studies showed that individual cells inside the populations of *S. putrefaciens* CN-32 are phenotypically diverse, were some cells exhibit high motility by production of multiple flagella and other are non-motile and produce biofilm factors (Bubendorfer et al., 2014). But how is this heterogeneity achieved? The nucleotide based second messenger c-di-GMP plays a major role in this process.

The results are published in Rossmann & Rick et al., 2019 and Rick & Kreiling et al., 2021 (submitted).

3.1 In silico analysis of c-di-GMP signaling in *S. putrefaciens* CN-32

We started our study by generally characterizing the c-di-GMP signaling network of *S. putrefaciens* CN-32. To gain a first insight, we evaluated how many and which proteins may be involved in c-di-GMP signaling. For this, we accessed the Pfam database (Bateman et al., 2014) and used the BLAST algorithm to identify proteins that are potentially involved in the production (GGDEF-domain proteins) or in the degradation (EAL- and HD-GYP-domain proteins) of this messenger. We identified 51 proteins that harbor one of such domains. Only five of these proteins have a HD-GYP domain, while 46 proteins have a GGDEF or EAL domain. In this study we are only focusing on GGDEF- and EAL-domain proteins. Following, we further characterized them by separating them into cytoplasmic and transmembrane proteins by using the TMHMM tool (Krogh et al., 2001) and SMART (Letunic et al., 2021), see **table 3.1**.

Table 3.1) Summary of GGDEF and EAL proteins in *S. putrefaciens* CN-32. The sequences were obtained by accessing multiple data bases and the prediction of transmembrane regions was done with the TMHMM and SMART tool.

	EAL	GGDEF	GGDEF/EAL
Total	4	21	21
Cytoplasmic	3	13	11
Transmembrane	1	8	10

We then followed this up by obtaining the amino acid sequence of each GGDEF and EAL protein and predicted the protein organization by using the SMART tool offered by the EMBL

Heidelberg (Letunic et al., 2021). The domain organization of all GGDEF and EAL proteins of *S. putrefaciens* CN-32 is shown in **sup. table 9**. Interestingly, while we found that 20 proteins have a GGDEF-EAL module, the SMART tool only predicted one protein, Sputcn32_3319, to have an EAL-GGDEF module. In this protein, the GGDEF domain was only recognized as Pfam domain with a low confidence. Thus, we performed amino acid sequence alignments with the sequences of all GGDEF domains and found that the predicted GGDEF domain of Sputcn32_3319 was falsely predicted as GGDEF domain. While Sputcn32_3319 contains a "GGDEF" amino acid sequence, these five amino acids were the only ones that aligned while no other characteristic sequential feature was present. In conclusion, *S. putrefaciens* CN-32 only contains GGDEF-EAL but no EAL-GGDEF proteins. As described in the introduction, GGDEF-domains in these dual proteins can often regulate its EAL domain. The fact that only GGDEF-EAL modules were found points towards the hypothesis that the order of these domains is crucial for the structural basis of this process.

Another theory that occurred during this *in silico* analysis is that most of these proteins may have evolved by gene duplication. It was noticeable that many of these proteins show very similar domain architectures, as demonstrated in **fig. 3.1**.

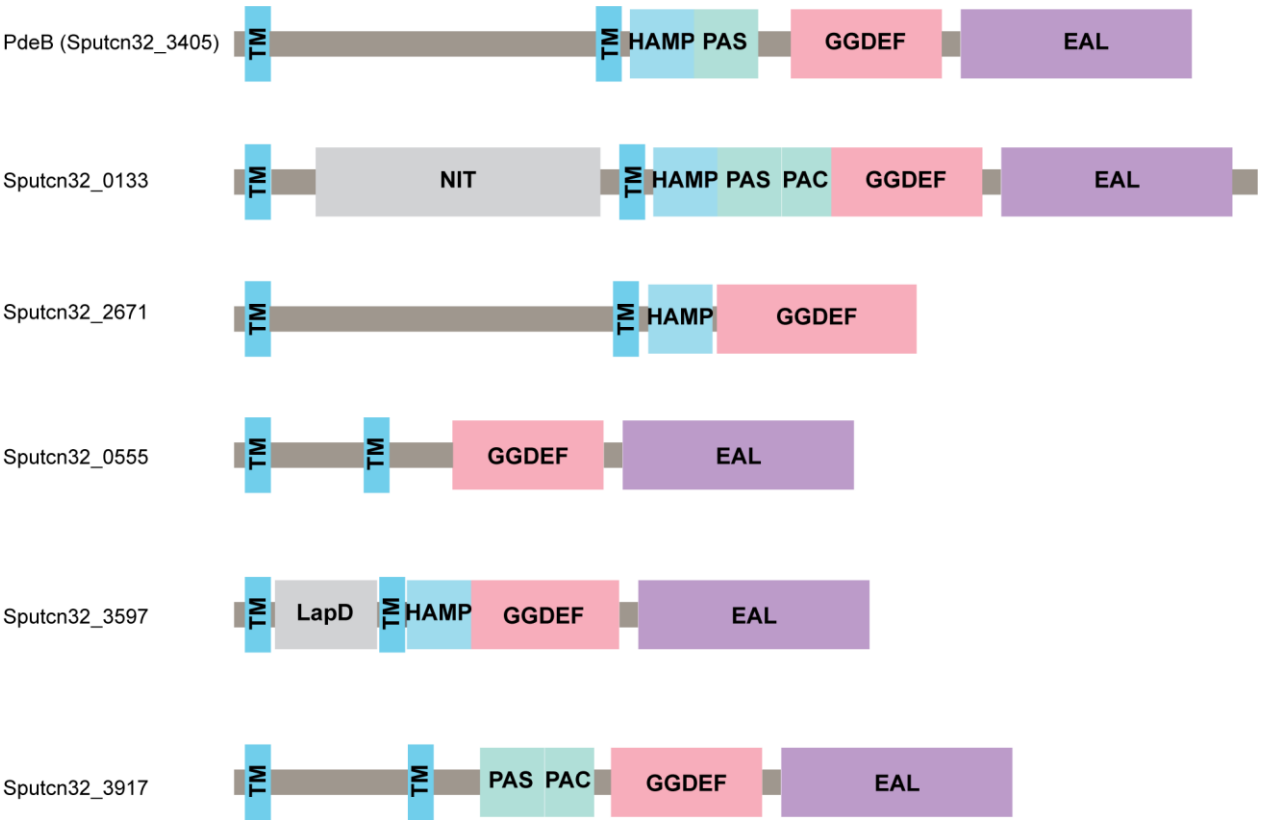

Figure 3.1) Common domain architectures of GGDEF-proteins of *S. putrefraciens* CN-32. The sequences were obtained by BLAST and domain analysis was done by using the SMART tool offered from the EMBL Heidelberg. The domain organizations of GGDEF proteins are very similar to each other, indicating that they may have evolved by gene duplication. The common architecture is a periplasmic domain that is flanked by two transmembrane helices and a sensor domain followed by a GGDEF and sometimes an EAL domain.

This is especially true for the transmembrane proteins, which often have two transmembrane domains with a long periplasmic region followed by a HAMP and other sensor module and a GGDEF domain. However, these proteins frequently have specific sequences in the periplasmic region that don't match the ones of the other. The protein Sputcn32_0133 for example was found to possess a NIT domain in the periplasmic region, while according to BLAST the periplasmic domain of PdeB doesn't share homology to any known sequence. The diversity of these periplasmic regions may play a role in orchestration of the complex c-di-GMP signaling.

3.2 PdeB regulates motility in *S. putrefaciens* CN-32 by affecting the c-di-GMP level

PdeB is a multidomain protein and SMART analysis predicted it to harbor two transmembrane domains, which flank a long periplasmic region. In the cytoplasmic portion, SMART predicted a HAMP/PAS module followed by a GGDEF and an EAL domain (**fig. 3.2a**). Genomic in-frame deletion of *pdeB* led to drastically reduced spreading on soft-agar motility plates when using LB medium. When grown in mineral medium, however, the Δ*pdeB* strain did not show a significant difference with respect to spreading. The protein was identified to be a homologue of *S. oneidensis* PdeB using the BLAST algorithm.

Since Chao *et. al.* showed that *So*PdeB is not a diguanylate cyclase (DGC) but has phosphodiesterase (PDE) activity (Chao et al., 2013) we tested the PDE activity of *Sp*PdeB by mutating a residue in the active center of the EAL domain and then performed soft-agar motility assays (**fig. 3.2b**). The $pdeB_{AAL}$ strain showed the same phenotype as the Δ*pdeB* strain, indicating that *Sp*PdeB also acts as PDE.

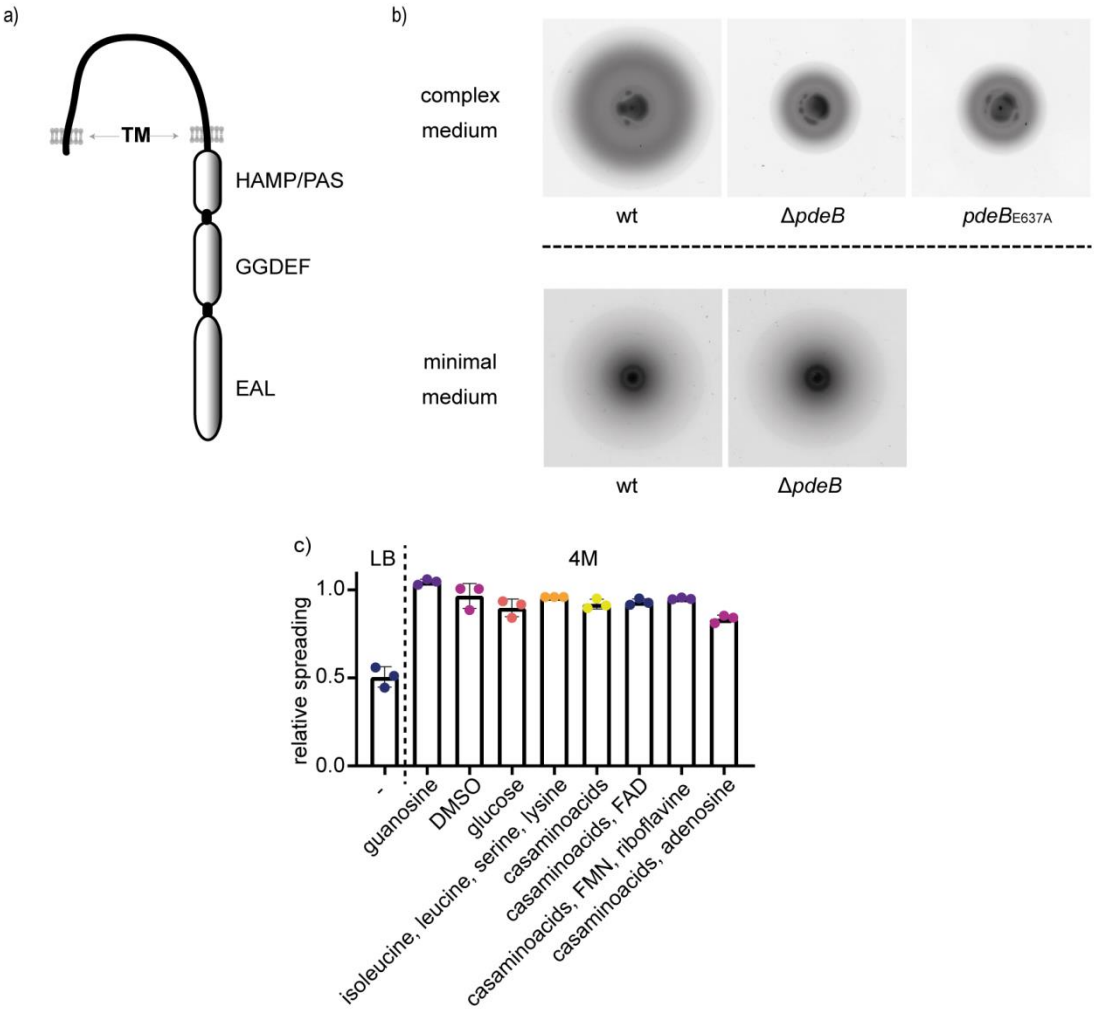

Figure 3.2) Spreading phenotype of PdeB. a) The domain organization of PdeB was predicted using the SMART tool and TMHMM. The protein consists of two transmembrane helices that flank a long periplasmic region. The periplasmic region does not show any homology to known domains or sequences. A HAMP/PAS module is located in the cytoplasm, which is followed by a GGDEF and an EAL domain. **b)** The phenotype of PdeB in complex medium (LB medium) is shown in the top part and the phenotype in mineral medium (4M medium) on the bottom part. The deletion of *pdeB* decreases the spreading radius in complex medium, but not in mineral medium. Additionally, we found that mutating one amino acid residue in the active center of the EAL domain lead to the same phenotype as deletion of the whole gene. This indicated that PdeB acts as PDE. This experiment was performed by Florian Rossmann. **c)** Several guesses about the potential ligand for PdeB were tested in motility assays. Neither guanosine, DMSO, glucose, amino acids, FAD, FMN, riboflavin or adenosine activated the PDE activity of PdeB. Each dot represents an individual motility plate. The experiment was conducted with a Δ*pdeB* mutant that was normalized to a wild-type strain. A relative spreading of 1 indicates no difference between the wild type and the Δ*pdeB* mutant (Rossmann & Rick et al., 2019; modified)

We made several educated guesses about the potential activator of PdeB: We conducted motility assays in 4M medium with different additives like carbon sources, energy sources and cofactors (**fig. 3.2c**). However, neither addition of DMSO, glucose, amino acids, FAD, FMN, riboflavin nor adenosine resulted in decreased spreading of the Δ*pdeB* mutant compared to the wild type.

We also investigated if the phenotype of the *pdeB* deletion can be complemented by ectopically producing another PDE, called PdeH. We found that ectopically producing PdeH fully complements the Δ*pdeB* phenotype (**sup. fig. 1a**). To compare the enzymatic activity of PdeB to other c-di-GMP producing enzymes we deleted several DGCs in a strain lacking *pdeB*. The spreading radius of these strains was then observed on motility plates (**sup. fig. 1b**). We observed that deletion of these DGCs is not sufficient to fully complement the phenotype of the *pdeB* deletion.

3.3 PdeB regulates the lateral flagellar system and adhesion factors

S. putrefaciens CN-32 possess two independently regulated flagellar systems. The single polar flagellum determines the swimming speed and can be controlled by a chemotaxis system. The lateral system however does not increase the swimming speed but increases the spreading on motility plates by increasing the directional persistence of swimming (Bubendorfer et al., 2014). We suspected that the reduced spreading on motility plates of the *pdeB* mutant may be caused by reduced flagella activity. Therefore, we observed the swimming speed in liquid environments using microscopy. Briefly, cells were grown to exponential growth phase before they were transferred onto an agar slide. The swimming was then recorded in 10 second long time lapses and the swimming speed was calculated using Fiji (Schindelin et al., 2012). Surprisingly, we could not find a significant difference between the swimming speed of cells with or without *pdeB* (about 40 $\mu m \cdot s^{-1}$). We found that the motility phenotype of cells lacking *pdeB* does not occur in liquid, but only in structured environments. On motility plates, cells need to navigate through narrow passages and dead ends. Since this navigation is mainly controlled by the chemotaxis system, we hypothesized that *pdeB* could act by influencing this system. To this end we analyzed the swimming tracks and quantified the number of turn events. However, no difference in turns was found between cells with or without *pdeB* (about 0.24 turns per track). Summarizing this, the results suggest that the motility phenotype of *pdeB* predominantly occurs in structured environments and is not caused by reduced swimming speed or altered taxis.

Since the absence of *pdeB* results in reduced spreading on motility plates and *S. putrefaciens* CN-32 encodes two independently regulated flagella systems, we further analyzed the phenotype by observing the effect on each system individually. To this end, we used strains that lack the genes for the polar or lateral flagellins and observed the spreading behavior on motility plates in presence and absence of PdeB (**fig. 3.3a,b**). We found that absence of *pdeB* significantly reduced the spreading radius of cells that harbor either the polar or lateral flagellar system. However, the effect was more pronounced in cells that only

possess the lateral system. Therefore, we concluded that either both systems are affected or that *pdeB* acts on additional factors. We then tested if *pdeB* may influence the synthesis of flagella. To this end, we inserted genomic mutations that allowed us to fluorescently label the extracellular hook proteins of living cells by using a fluorescent dye that binds to extracellular cysteins. The number of polar and lateral hooks was then quantified using fluorescence microscopy (**fig. 3.3c**). We found that in presence and absence of *pdeB* around 55% of the cells had polar hooks and no significant difference was found. However, when we quantified the number of lateral hooks, we found that absence of *pdeB* leads to significantly reduced lateral hooks per cell. We found that around 26% of WT cells had a signal for lateral hooks, while only 13% had a signal in the Δ*pdeB* mutant. To further understand this process, we investigated if this regulation happens at the transcriptional level. As previously stated both flagellar systems are individually regulated (Bubendorfer et al., 2012). Hence, we constructed strains that harbor a transcriptional Lux reporter system for either the polar or lateral flagellin genes. The cells were then grown to the exponential phase and the luminescence was measured in presence or absence of *pdeB* (**fig. 3.3d**). We found that transcription of the polar system was not altered in absence of *pdeB*. However, the transcription of the lateral flagellins was significantly reduced when *pdeB* was not present. Together these results indicate that *pdeB* acts as regulator of the transcription of the lateral, but not the polar flagellar system. In contrast to that, we found that absence of *pdeB* reduces the spreading radius on motility plates of cells that can only synthesize the polar system, leading to the conclusion that PdeB affects an additional factor that influences motility.

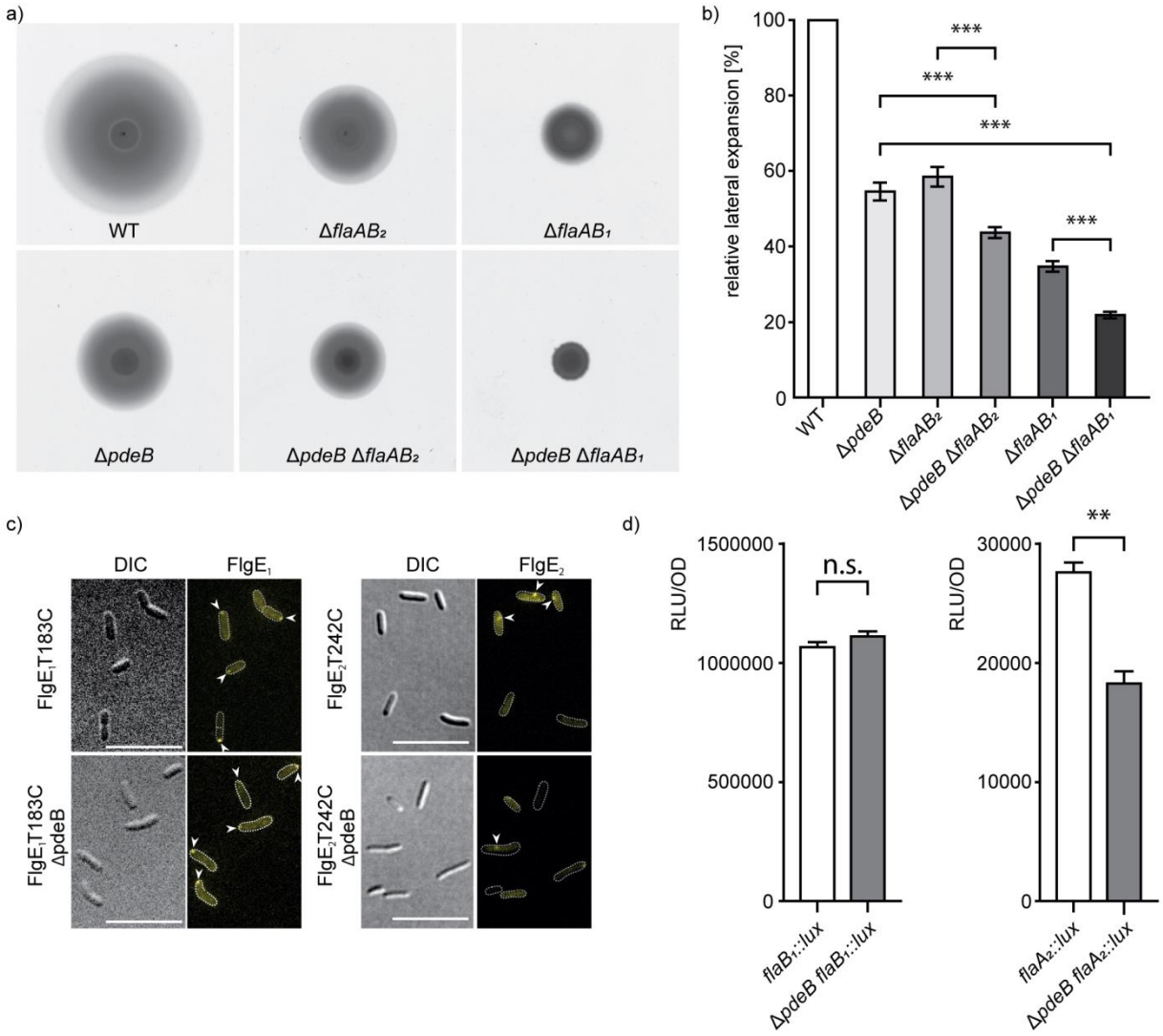

Figure 3.3) Effect of *pdeB* on the flagellar systems. a) The effect of PdeB was observed by motility assays in strains that cannot produce the lateral (middle) or polar (right) flagellar systems. **b)** The spreading radius was quantified and normalized to that of the wild type. All strains show significantly reduced spreading in absence of *pdeB*. **c)** The construction of the flagellar systems was quantified in presence and absence of *pdeB* by integrating a mutation into the hook protein FlgE that allows to fluorescently label the hook structure. The hooks were then quantified, and it was found that deletion of *pdeB* led to reduced construction of the lateral, but not the polar flagellar system. **d)** An effect on the transcription of the flagellar system was tested by integrating a Lux-reporter system into the genome of *S. putrefaciens* CN-32. Absence of *pdeB* had no effect on the signal intensity for the polar system (left), while it decreased the signal for the lateral system (right). (Rossmann & Rick et al., 2019; modified)

To identify the additional targets of PdeB we used transposon mutagenesis and screened for mutations that complemented the spreading phenotype on motility plates of cells that lack *pdeB*. It was found that the integration of a transposon into *mshJ*, which is part of the MSHA-pilus gene cluster, strongly complemented spreading in the absence of *pdeB*. The MSHA pilus is a type IVa pilus system that is involved in surface adhesion (Saville et al.,

2010; Young et al., 2020). All genes involved in pilus production are located in the same gene cluster.

To verify that this system impacts the spreading behavior on motility plates and to investigate the role of *pdeB,* we constructed clean in-frame deletions of *mshE,* which is essential for pilus assembly. Since we already showed an effect of *pdeB* on the lateral flagella systems, the following experiments were done in strains that can only produce the polar system (ΔL). The strain construction and data collection were done by Vanessa Kreiling. We found that the deletion of *mshE* has only minor effects when *pdeB* is present, but it strongly complements the absence of *pdeB* (**fig. 3.4a**). This data suggests that *pdeB* may regulate the MSHA pilus system.

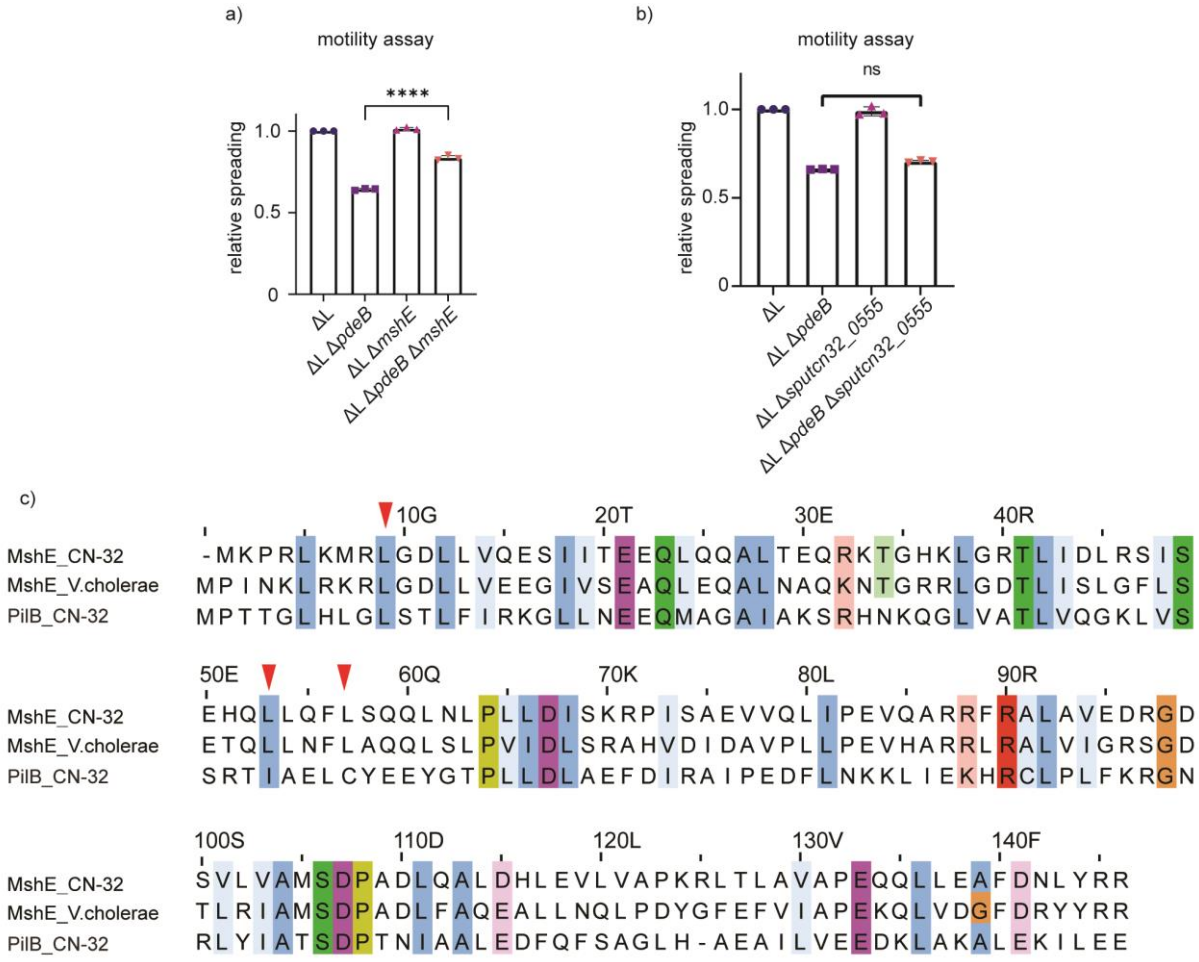

Figure 3.4) Effect of PdeB on the MSHA pilus system. a) The influence of the MSHA system on motility was tested in presence and absence of *pdeB*. **b)** The influence of *sputcn32_0555*, which is a degenerated GGDEF-EAL protein, on motility was tested by motility assays. **c)** Alignment of the protein sequence of *Sp*MshE, *Vc*MshE and *Sp*PilB. Crucial leucine residues required for c-di-GMP binding (Wang et al., 2016) are indicated by red arrows. (Rick & Kreiling et al., 2021, modified)

One possibility how *pdeB* could influence this system was the protein Sputcn32_0555, which is predicted to be a degenerated GGDEF-EAL protein that is located immediately upstream of the first MSHA-pilus biogenesis gene. Thus, we constructed in-frame deletions and again observed the spreading phenotype on motility plates (**fig. 3.4b**). However, deletion of *sputcn32_0555* had no effect on the spreading radius.

It was recently found that some extension ATPases of Type IV pili can bind c-di-GMP with its N-terminal domain (Floyd et al., 2020; Wang et al., 2016). Therefore, we conducted *in silico* sequence alignments of *Sp*MshE with *Vc*MshE and found that *Sp*MshE harbors all residues required for c-di-GMP binding (**fig. 3.4c**). *S. putrefaciens* CN-32 encodes a second, independently regulated type IV pilus system named Pil. In contrast to the MSHA system, genes involved in pilus assembly are scattered over the genome. However, it also contains an extension ATPase called PilB that is needed for pilin export. While PilB has an N-terminal MshEN domain, alignments showed that several leucine residues required for c-di-GMP binding are not present (**fig. 3.4c)**.

To test if *Sp*MshE is able to bind c-di-GMP, we heterologously produced the full-length protein and a truncated version consisting of the amino acid residues 2-145. The proteins were purified by Ni-NTA affinity chromatography followed by size exclusion chromatography (SEC) (**sup. fig. 2a-b**). Both approaches yielded sufficient amounts of protein but showed different elution behavior: While the truncated version eluted as a single sharp peak on the expected elution volume, we found that *Sp*MshE eluted earlier than calculated. The elution volume suggests that the full-length protein forms penta- and hexamers *in vitro*.

We also tried to purify the extension ATPase PilB. However, the protein precipitated after affinity chromatography. Thus, we purified the N-terminal region (residues 2-145) by affinity chromatography and SEC. Similar to the N-terminal domain of MshE, the truncated protein eluted as monomer (**sup. fig. 2c**).

Subsequently, we tested c-di-GMP binding to MshE and PilB by isothermal titration calorimetry (ITC) (**fig. 3.5a-c**) and FP (**fig 3.5d-f**). Both assays show that the truncated and the full-length MshE protein are able to bind c-di-GMP with high affinity *in vitro*. Agreeing with the *in silico* analysis, PilB is not able to bind these ligands *in vitro*.

The ATPase MshE is crucial for export of pilins and pilus elongation (Floyd et al., 2020; Jones et al., 2015; Wang et al., 2016). Therefore, we aimed to test if deletion of *pdeB* leads to increased production of elongated MSHA pili. To this end, we introduced appropriate mutations that allowed us to label extracellular pilins with a fluorescent dye. We then quantified the number of elongated MSHA pili per cell in presence and absence of *pdeB* (**fig.**

3.5g-h). The experiment shows that the absence of *pdeB* leads to a significantly increased number of elongated MSHA pili per cell, verifying that *pdeB* acts as regulator of MSHA pilus assembly by controlling MshE activity.

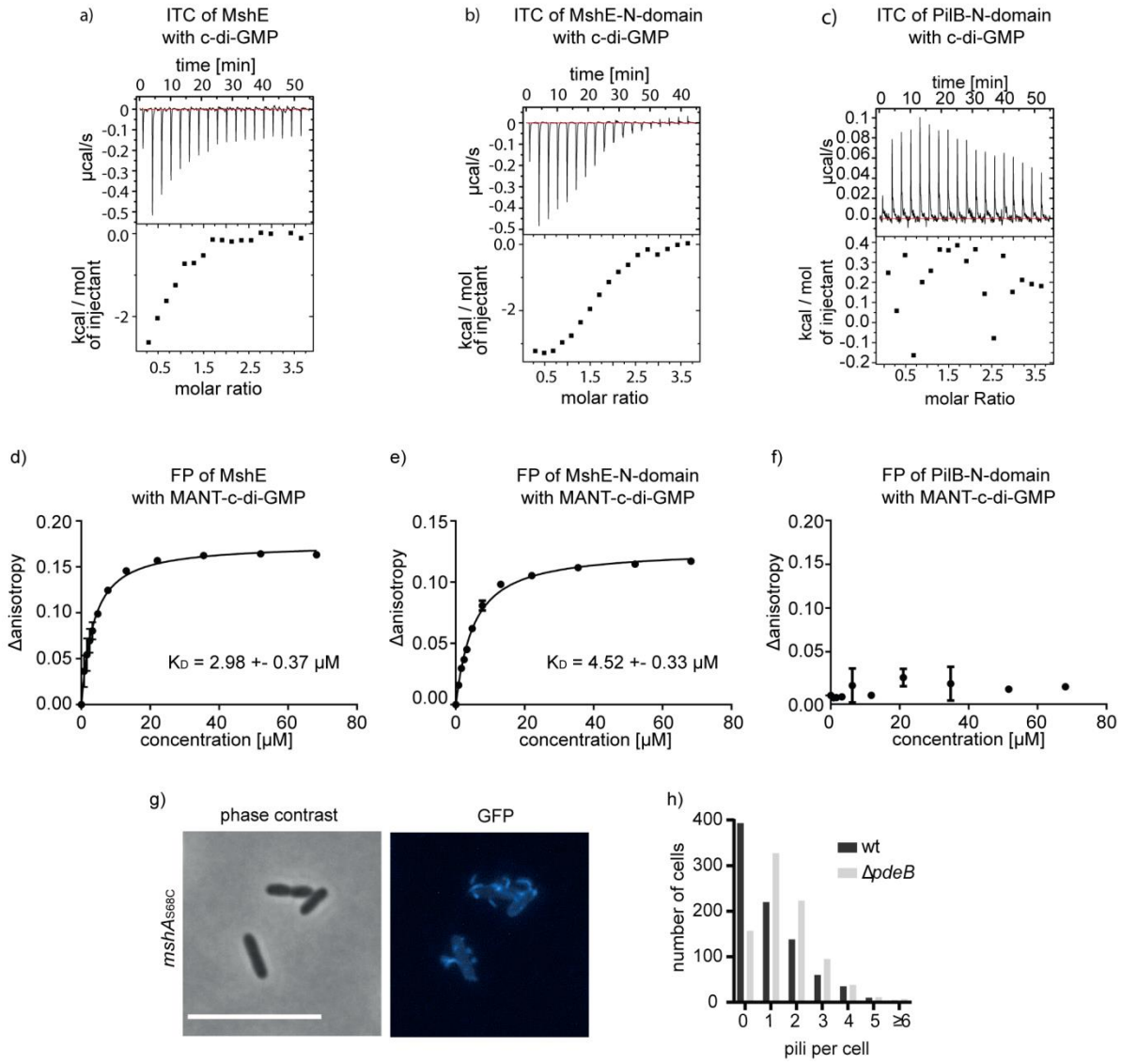

Figure 3.5 MSHA pilus assembly is regulated by c-di-GMP. a-b) The MshE protein and its N-terminal domain (residues 2 – 145) were heterologously produced and purified and ITC experiments were done with c-di-GMP as ligand. Both versions bind c-di-GMP with high affinity. **c)** The N-terminal domain (residues 2 – 145) of the extension ATPase PilB was purified and c-di-GMP binding was tested with ITC. No binding was observed. **d-e)** The binding of MshE and MshEN to c-di-GMP was verified by FP experiments with MANT-c-di-GMP as ligand**. f)** The non-binding of PilB to c-di-GMP was verified with FP experiments using MANT-c-di-GMP as ligand. **g-h)** An effect of *pdeB* on the assembly of MSHA-pili was tested by introducing appropriate mutations to fluorescently label the extracellular pili. The pili were quantified using fluorescence microscopy. Exemplary micrographs of cells with elongated pili are shown in (g); scale bar = 10 µm. The quantification is shown in (h) as histogram. Deletion of *pdeB* leads to significantly increased amounts of elongated pili. (Rick & Kreiling et al., 2021, modified)

The model organism *S. putrefaciens* CN-32 encodes another system that mediates surface attachment, called *bpf*. This can be classified as T1SS and previous studies showed that it is affected by c-di-GMP (Wu et al., 2013). All genes are organized in an operon, starting with the gene for the RTX-toxin AggA. According to transcriptional data obtained by my colleague John Hook, the operon seems to be regulated by the transcriptional master regulator FlrA (data not shown). Therefore, we hypothesized that *pdeB* may also influence the transcription of the *bpf*-operon and constructed strains that harbor a transcriptional Lux reporter system of *bpfA*. The cells were then grown to exponential phase and the luminescence in presence and absence of *pdeB* was measured in a plate reader. Deletion of *pdeB* resulted in significantly increased luminescence, indicating that *pdeB* regulates the transcription of the *bpf*-system (**fig. 3.6a**).

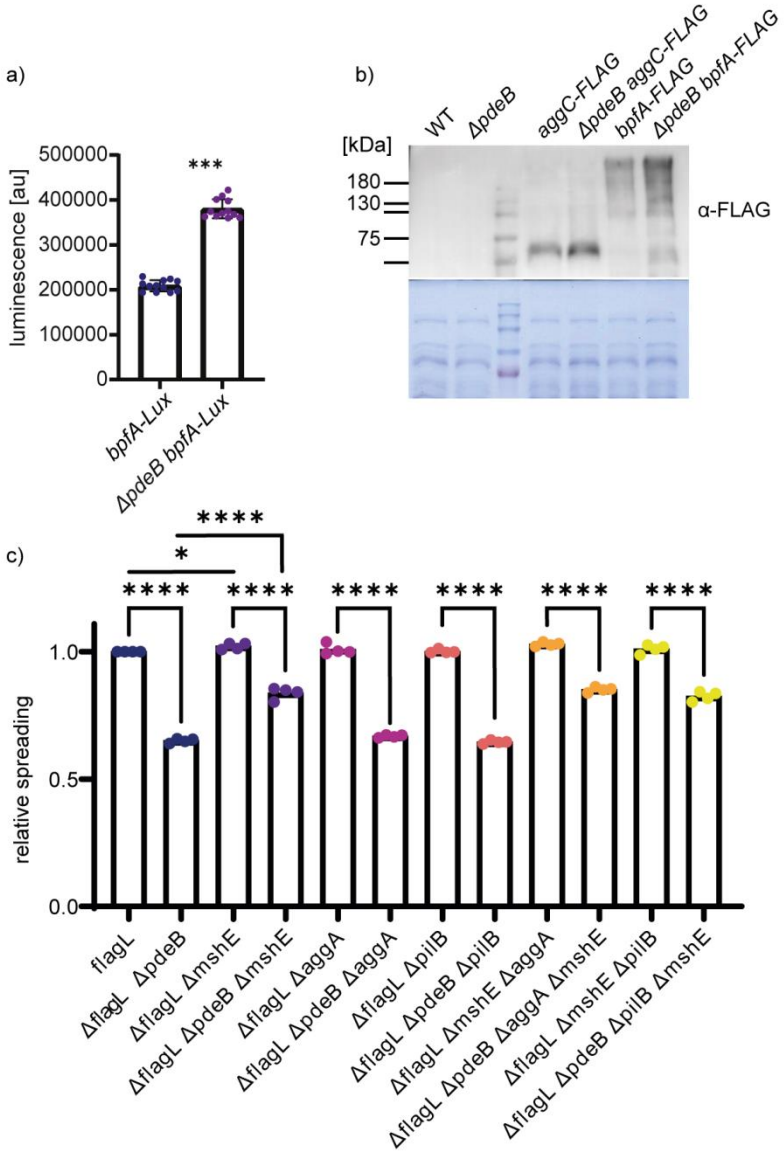

Figure 3.6) PdeB regulates the *bpf*-system. a) An effect of *pdeB* on the transcription of *bpfA* was tested by Lux-reporter assays. Deletion of *pdeB* leads to significantly increased transcription of *bpfA*. **b)** Deletion of *pdeB* leads to increased amounts of AggC and BpfA. This was tested by immunoblot analysis. **c)** The *bpf* system has no influence on the spreading phenotype of *pdeB*. This was tested by motility assays. It was also verified that the Pil-system does not contribute to the spreading phenotype of *pdeB*. (Rick & Kreiling et al., 2021, modified)

My colleague Vanessa Kreiling followed up on this experiment by showing that deletion of *pdeB* results in increased amounts of BpfA and AggC on the protein level, using immunoblot analysis (**fig. 3.6b**). We then tested if this system is involved in the spreading phenotype of the Δ*pdeB* strain by using motility assays. However, inactivation of the *bpf*-system did not complement the spreading phenotype of *pdeB* (**fig. 3.6c**). To this end we also verified that inactivation of the Pil-system does not complement the *ΔpdeB* phenotype.

3.4 Screening for additional targets of *pdeB*

To identify additional targets of *pdeB* we isolated spontaneous suppressor mutants. To do that, we incubated cells lacking *pdeB* on motility plates and incubated them for several days. After around three days, the shape of the swimming region changed and flairs of spontaneous mutants occurred. We took samples from the flairs and grew these cells overnight in liquid cultures, until we transferred them to new motility plates with the appropriate controls. Mutants that swam further than the Δ*pdeB* strain were collected and cryo cultures were made until further use. For exemplary data of such mutants see **fig. 3.7**.

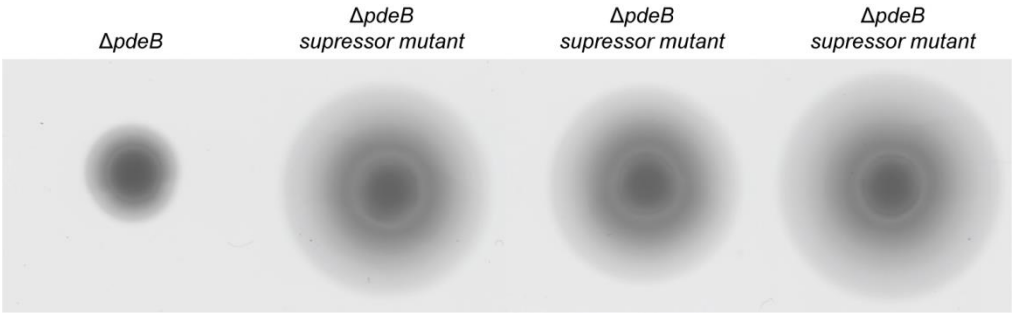

Figure 3.7) Exemplary data of spontaneous suppressor mutants. The Δ*pdeB* strain was grown for several days on motility plates until flairs of spontaneous mutants appeared. These mutants were collected and the increased spreading was verified by another motility assay, as shown in this figure. The mutants showed drastically increased spreading radii, sometimes exceeding even the radius of the wild type.

Afterwards, we again grew these mutants and extracted the genomic DNA, which was then sequenced by Dr. Kalinowski (CeBiTec, Bielefeld) to identify SNPs that may be responsible for the increased spreading radius. In total, we sequenced seven mutants of the strain Δ*pdeB* and 13 mutants of the strain Δ*pdeB* Δ*flaAB*$_2$. After removal of synonymous mutations, we identified eight genes that obtained SNPs (see **table 3.2**).

Table 3.2) Identification of SNPs. To identify additional targets of *pdeB* we isolated suppressor mutants. The genome of these were sequenced and mutations in the DNA sequence were analyzed. The table shows the genes where SNPs were found and the column "Hits" indicates in how many sequenced genomes mutations in this gene occured. In total, 20 genomes were sequenced.

Gene	Protein	Hits
sputcn32_0491	cell division protein FtsZ	1
sputcn32_0999	conserved hypothetical protein	5
Sputcn32_1968	heavy metal efflux pump, CzcA family	1
sputcn32_2053	alpha-N-arabinofuranosidase	1
sputcn32_2100	cation diffusion facilitator family transporter	2
sputcn32_2165	YD repeat protein	2
sputcn32_2555	CheB methylesterase	5
sputcn32_3807	phage integrase family protein	2

Additionally, we also found three SNPs in intergenic regions. One was located between two genes that encode the tRNA for glutamic acid and the second one was found between the gene encoding the tRNA for isoleucine and the 16s-rRNA. The third one was in the chemotaxis gene cluster between the genes *cheR* and *cheW*. Thus, a potential role of *pdeB* on chemotaxis is likely, since not only SNPs in the CheB gene, but also in the intergenic region between *cheR* and *cheW* were found. The conserved hypothetical protein Sputcn32_0999 is located in an operon with a sulfate ABC transporter, indicating that it may play a role in the sulfate metabolism. Correspondingly, we also found by *in silico* analysis that *sputcn32_2100* is located in an operon that encodes a sulfatase (*sputcn32_2097)* and a diguanylate cyclase (*sputcn32_2096*). The YD repeat protein Sputcn32_2165 has a signal peptide and is a very large protein with 1600 amino acids in length. It is predicted to be cotranscribed with a phage integrase family protein (Sputcn32_2164) but domain analysis does not hint on a potential function. This is similar to the found phage integrase family protein Sputcn32_3807, which is a 1400 amino acid long protein that is predicted to be cotranscribed with other phage integrase family proteins.

However, verification of a role of these proteins in *pdeB* mediated signaling is still pending.

3.5 GGDEF domain of PdeB mediates localization to the flagellated cell pole

C-di-GMP signaling is known for having a strict spatial and temporal control (Römling et al., 2013). Therefore, we investigated if PdeB localizes at a specific cellular compartment. To this end we constructed translational fusions of PdeB with sfGFP. The strain construction and data collection were done by Florian Rossmann. To differentiate between the flagellated and non-flagellated cell pole we introduced this mutation into a strain with *mCherry* labeled $FliM_1$, which is a protein of the primary flagellar system. The localization of PdeB-sfGFP was then analyzed using fluorescence microscopy and it was found that around 60% of cells show a polar PdeB-sfGFP signal that colocalized with $FliM_1$-mCherry at the flagellated cell pole (**fig. 3.8**). Interestingly, while no effect of *pdeB* on the polar flagella system was found, the fluorescence signal was exclusively visible at the flagellated cell pole and not the opposing pole. The stability and expression of PdeB-sfGFP was verified by Western blot analysis (**sup. fig. 3a**).

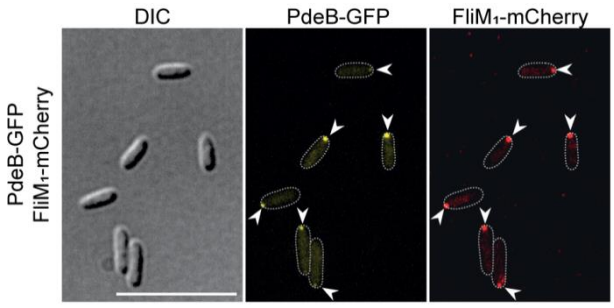

Figure 3.8) Micrographs of PdeB-sfGFP in $FliM_1$-mCherry. The localization of PdeB was observed by adding a translational GFP fusion into a strain with fluorescently labeled $FliM_1$ to identify the flagellated cell pole. We found that PdeB-sfGFP localizes exclusively to the flagellated cell pole but not to the new pole. Scale bar = 10 µm. (Rossmann & Rick et al., 2019; modified)

Since we previously demonstrated that PdeB regulates adhesion factors, we hypothesized that PdeB may be recruited to the cell pole upon surface contact. To test this, we grew the cells in liquid culture and fixed them with paraformaldehyde before they were brought onto an agar slide. The localization was determined by fluorescence microscopy (**fig. 3.9**). However, surface contact was not required for polar PdeB-sfGFP localization.

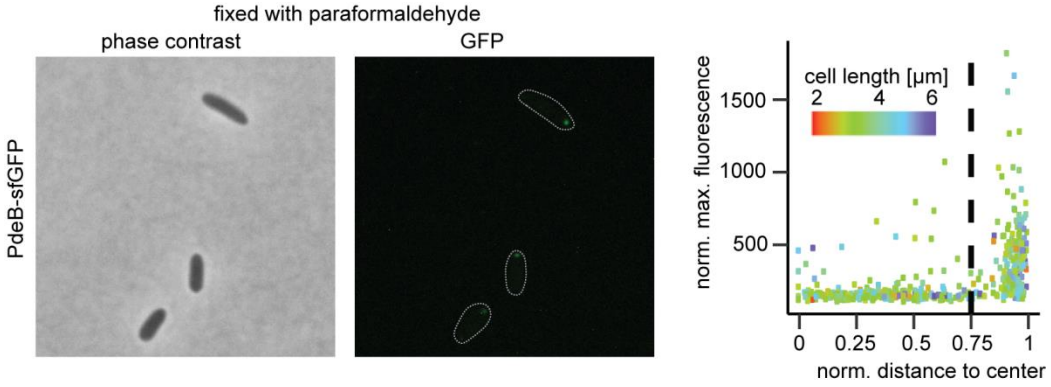

Figure 3.9) Polar localization of fixed *pdeB-sfgfp* cells. The localization pattern of fixed cells with fluorescently labeled PdeB was observed by fluorescence microscopy. Fixing did not lead to absence of polar fluorescence signals (left). The localization was quantified by 3d scatter plots (right).

The polar localization of PdeB raised the question about the mechanism. It is well known that PAS-domains can mediate direct protein-protein interactions (Hennig et al., 2009), which made it likely that the PAS-domain could mediate this process. Another possibility would be that PdeB could recognize membrane curvature with its transmembrane and periplasmic regions. To test these hypotheses, we constructed truncated versions of PdeB-sfGFP and then determined the localization pattern using fluorescence microscopy (**fig. 3.10**). The respective strains were constructed by Florian Rossmann and he collected the data. The quantification of fluorescence clusters was done by me.

Surprisingly, we found that the GGDEF domain is essential for polar localization of PdeB and is itself sufficient for polar targeting (**fig. 3.10a**). Deletion of the GGDEF-domain led to absence of polar fluorescence. When we ectopically expressed the GGDEF-domain as sfGFP fusion protein, we observed polar fluorescence clusters. This indicates that the GGDEF-domain of PdeB mediates polar localization. Neither deletion of the HAMP-, or PAS-domain or the periplasmic region did result in absence of polar localization of PdeB (**fig. 3.10b**). Removal of the EAL domain also had no impact on the localization. However, all strains that lack the GGDEF-domain of PdeB showed no polar fluorescence signal. Additionally, we also tested if the active site of the GGDEF or EAL domain is essential for localization but inserting inactivating point mutations did not result in absence of polar localization. The micro graphs are shown in **sup. fig. 4a-b** and stability and expression of each fusion protein was verified by immunoblot analysis (**sup. fig. 5a**)

It was verified that enzymatic activity of PdeB is not required for polar localization by observing the localization of PdeB-sfGFP in 4M medium. Under these growth conditions PdeB was found to be inactive in motility assays. However, the localization pattern was not altered when cells are grown in 4M medium (**fig. 3.11a**).

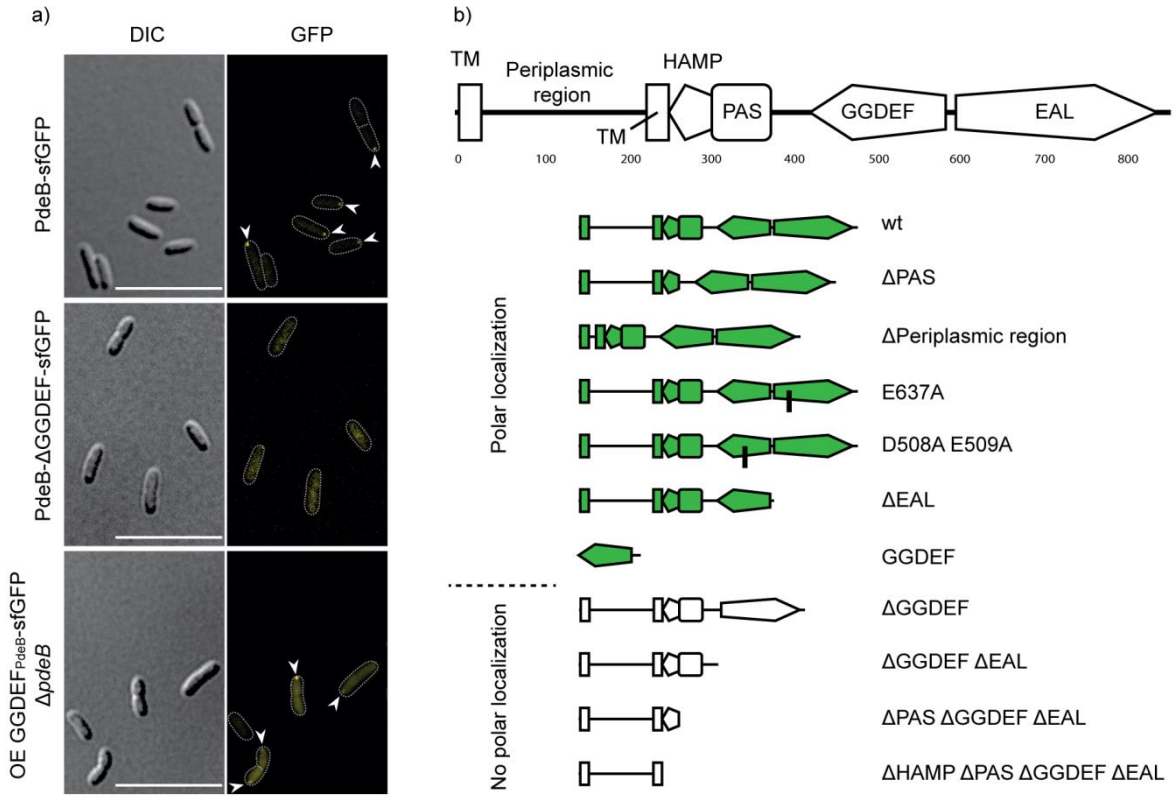

Figure 3.10) GGDEF-domain of PdeB mediates polar localization. a) The GGDEF domain of PdeB was genomically deleted in-frame in a PdeB-sfGFP background. While PdeB-sfGFP localizes to the cell pole, deletion of the GGDEF domain results in abolished polar fluorescence. Ectopic expression of the GGDEF-domain as GFP-fusion protein in a strain lacking *pdeB* is sufficient for polar localization. scale bar = 10 µm. **b)** The localization of truncated PdeB-sfGFP versions was tested by fluorescence microscopy. The domains were genomically in-frame

deleted. Deletion of the EAL-, HAMP- and PAS-domain did not lead to delocalization of the protein but strains that lack the GGDEF-domain do not show polar fluorescence. Introducing mutations into the active center of the GGDEF- and EAL-domain had no influence on the polar localization of PdeB-sfGFP (Rossmann & Rick et al., 2019; modified).

3.6 $GGDEF_{PdeB}$ directly interacts with the polar landmark protein HubP

The previous results raised the question how the GGDEF domain mediates the polar localization of PdeB. Since the protein localizes only to the flagellated, but not the opposing cell pole, it was possible that interaction with flagellar proteins mediate this process. We therefore deleted the genes of the polar flagellum and the chemotaxis gene cluster in a *pdeB-sfgfp* background and determined if this alters the localization pattern. However, none of these genes are essential for the polar localization of PdeB-sfGFP (**fig. 3.11a**).

Many γ-proteobacteria, encode a landmark protein called HubP, that recruits flagellar and chemotaxis components to the cell pole (Rossmann et al., 2015). The gene for this protein is not part of the flagellar and chemotaxis gene clusters and was still present in the previous experiments. Since HubP recruits several proteins to the cell pole we hypothesized that HubP may be involved in the polar localization of PdeB and genomically deleted the gene *hubP*. Remarkably, deletion of *hubP* resulted in full absence of polar PdeB-sfGFP clusters (**fig. 3.11b**). The data also shows that both proteins colocalize. The stability and expression of PdeB-sfGFP in the Δ*hubP* background was verified by immunoblot analysis (**sup. fig. 6a**)

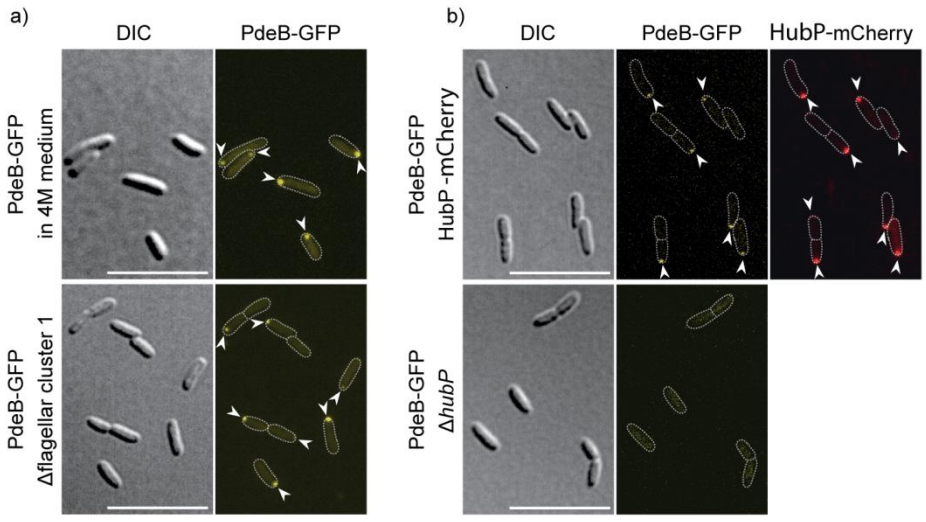

Figure 3.11) Micrographs of PdeB-sfGFP in different background strains. a) The localization of PdeB-sfGFP was observed in 4M medium (top) and LB medium in a background that lacks all genes of the polar flagellum and the chemotaxis system (bottom). While we previously showed that PdeB is not active in 4M medium, it still localized to the cell pole under these conditions. Additionally, no genes of the polar flagellar cluster or the chemotaxis system are required for the polar localization. **b)** PdeB-sfGFP colocalizes with the polar landmark protein HubP in fluorescence microscopy (top). Deletion of *hubP* also led to absence of polar PdeB-sfGFP signals. Scale bar = 10 µm. These experiments were performed together with Florian Rossman. (Rossmann & Rick et al., 2019; modified)

We continued by fluorescently co-labeling PdeB with sfGFP and HubP with mCherry and analyzing the spatiotemporal organization of both proteins by time lapse series (**fig. 3.12**). The experiment was performed together with Florian Rossmann and shows that HubP and PdeB colocalize to the flagellated cell pole. In the early stages of cell division, a second cluster of HubP appears at the new cell pole while PdeB remains tightly bound at the old pole. After cell division, only the mother cell shows polar PdeB-sfGFP localization. Most daughter cells develop polar PdeB-sfGFP clusters at later time points, but the time required for this process is very heterogeneous were some cells show polar PdeB-sfGFP fluorescence after 10 minutes and other need up to 40 minutes.

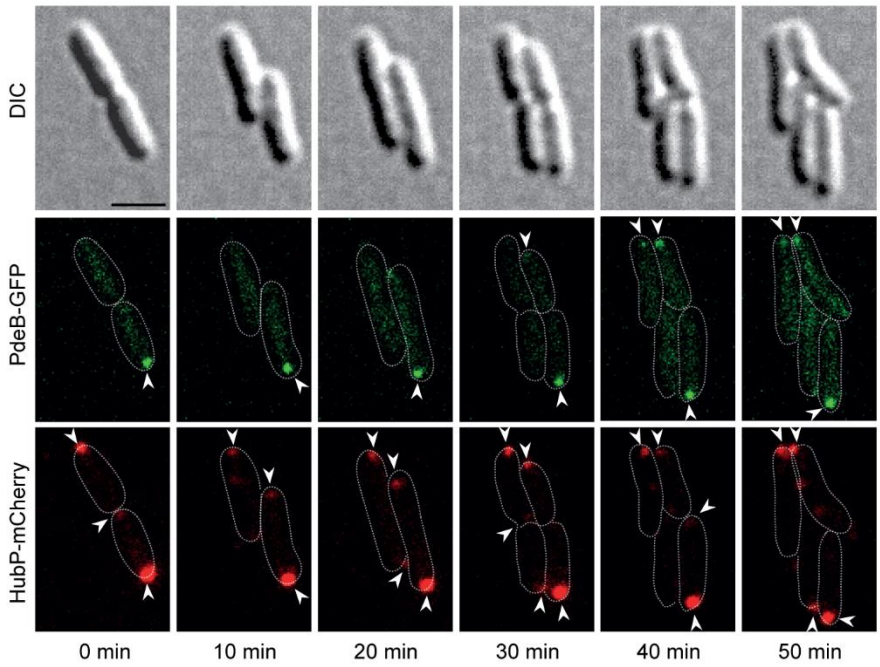

Figure 3.12) Timelapse series of PdeB-sfGFP in HubP-mCherry. The temporal organization of the localization of PdeB-sfGFP and HubP-mCherry was observed by fluorescence microscopy. The data was collected every 10 minutes in the DIC, GFP and mCherry channel. PdeB-sfGFP colocalizes with HubP-mCherry to the old pole. During cell division, a new fluorescence signal of HubP-mCherry forms at the new cell pole. However, a PdeB-sfGFP signal at the new pole occurs much later and only after cell division is completed. The time for this process varies strongly between individual cells. Scale bar = 5 µm. (Rossmann & Rick et al., 2019; modified)

Since we found that the GGDEF domain of PdeB and HubP are essential for localization of PdeB we used bacterial-2-hybrid (B2H) assays to test if both proteins directly interact with each other. Briefly, the expression of β-Gal is coupled in this experiment to a regulatory cascade depending on the interaction of the two proteins of interest. A leucine zipper was used as positive control and empty plasmids were used as negative control.

Since the GGDEF domain is localized in the cytoplasm we used multiple truncated versions of the cytoplasmic portion of HubP, consisting either of the cytoplasmic repeat domains or the far C-terminal FimVc-domain.

The experiment shows that $GGDEF_{pdeB}$ does not interact with the repeat domains of HubP (**fig. 3.13a**). In these approaches only the positive control shows blue coloring, while the negative control and all other samples remain colorless. However, when we tested the interaction of $GGDEF_{pdeB}$ with the far C-terminal FimVc-domain of HubP, we found blue coloring of colonies when the reporter fragment was fused to the N-terminus of GGDEF and the C-terminus of FimVc. This indicates that $GGDEF_{PdeB}$ directly interacts with $FimVc_{HubP}$.

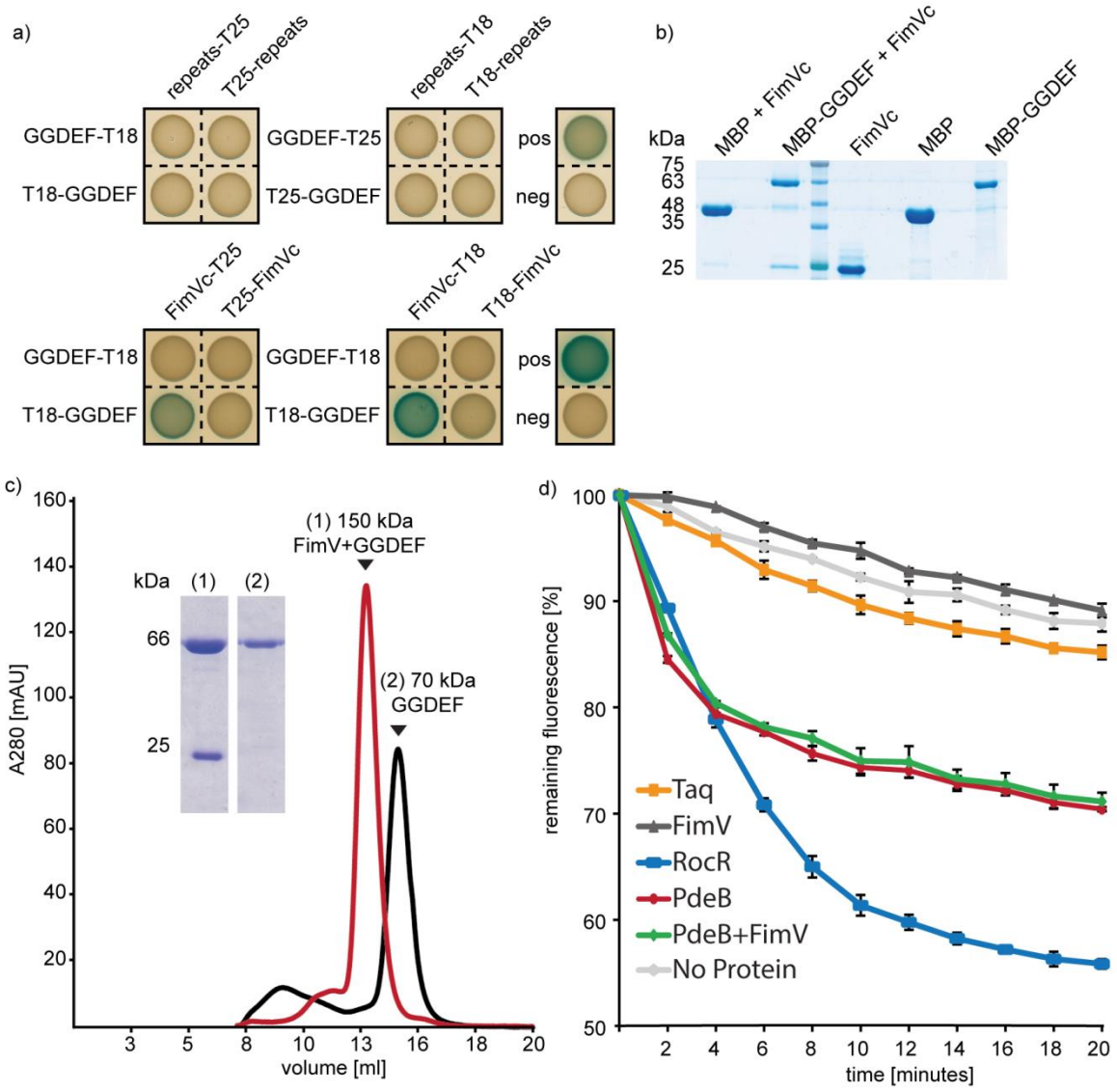

Figure 3.13) $GGDEF_{PdeB}$ interacts with $FimVc_{HubP}$. a) The interaction of $GGDEF_{PdeB}$ with the cytoplasmic regions of HubP was tested by B2H assays. Two leucine zipper-domain proteins were used as positive control and empty plasmids as negative control. $GGDEF_{PdeB}$ was found to interact with the FimVc-domain of HubP, but not with the cytoplasmic repeats. **b)** The GGDEF-domain of PdeB and the FimVc-domain of HubP were

heterologously expressed and purified and interaction was verified by pull-down assays. The two proteins coelute, indicating that both proteins interact *in vitro*. The MBP-protein was used as negative control. **c)** The interaction was further verified by SEC (Superdex200 Increase column). Both proteins coelute and the elution volume suggests a molecular weight of 150 kDa, which corresponds to a stoichiometry of 2:2. **d)** We tested if the addition of $FimVc_{HubP}$ increases the PDE activity of the cytoplasmic portion of PdeB *in vitro* by conducting MANT-c-di-GMP degradation assays. The active PDE RocR was used as positive control and Taq-polymerase and $FimVc_{HubP}$ served as negative control. Under these conditions, no influence of $FimVc_{HubP}$ to the PDE activity of PdeB was observed. These experiments were performed together with Florian Rossman. (Rossmann & Rick et al., 2019; modified).

To verify this interaction, we heterologously produced $GGDEF_{PdeB}$ and $FimVc_{HubP}$ and purified both using affinity and size exclusion chromatography. While the FimVc domain could be purified without problems, the GGDEF domain was prone to aggregation and precipitated immediately after affinity purification. To increase the solubility, we had to add a translational fusion with MBP. As the B2H data suggested, we fused the MBP-tag to the N-terminus of the GGDEF domain and obtained sufficient amounts of protein. We then continued by performing a pull-down assay with amylose resins, where MBP-GGDEF was used as bait protein (**fig. 3.13b**). The experiment showed that $FimVc_{HubP}$ remains bound to the bait protein after several washing steps. Heterologously produced und purified MBP protein was used as negative control. This result verifies the direct interaction of $GGDEF_{PdeB}$ and $FimVc_{HubP}$ that was indicated by B2H. Furthermore, we showed that both proteins interact with each other by SEC (**fig. 3.13c**). When $FimVc_{HubP}$ was present, the peak was shifted to the left, indicating a higher molecular weight. While the GGDEF-domain eluted as monomer, the elution volume of the complex indicates a stoichiometry of 2:2. To investigate if the interaction of $FimVc_{HubP}$ with $GGDEF_{PdeB}$ increases the PDE activity of PdeB, we purified the cytoplasmic portion of PdeB by affinity chromatography. The MANT-c-di-GMP degradation was then measured in a Tecan plate reader over 20 minutes and the time was plotted against the remaining fluorescence. However, no effect of $FimVc_{HubP}$ on the PDE activity was observed under these conditions (**fig. 3.13d**).

To further verify that the $GGDEF_{PdeB}$-$FimVc_{HubP}$ interaction is the driver for the polar localization of PdeB we genomically deleted the FimVc domain of HubP in a strain with fluorescently labeled PdeB and HubP. We then determined the localization pattern by fluorescence microscopy (**fig. 3.14a**) and found that deletion of the FimVc-domain of HubP strongly decreases the polar localization of PdeB. We observed that the fluorescence clusters were much weaker and fewer cells showed polar PdeB-sfGFP fluorescence. While around 73% of wild-type cells show polar fluorescence, only 38% of cells show polar localization of PdeB-sfGFP in the strain that lack the FimVc-domain.

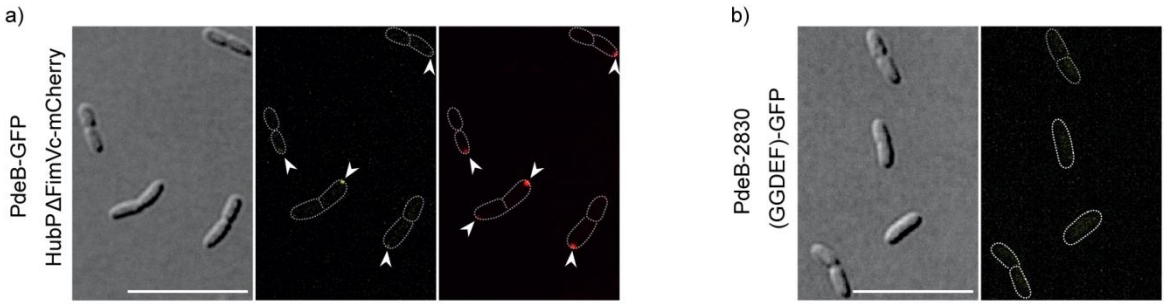

Figure 3.14) The GGDEF$_{PdeB}$-FimVc$_{HubP}$ interaction mediates polar localization of PdeB. a) The localization pattern of PdeB-sfGFP was observed in a strain that lacks the FimVc-domain of HubP. Absence of this domain leads to strongly reduced localization of PdeB-sfGFP. However, small fluorescence foci were visible, indicating that PdeB-sfGFP may also interact with other parts of HubP or another unknown interaction partner. This experiment was performed together with Florian Rossmann. **b)** The GGDEF domain of PdeB is essential for polar localization and other GGDEF domains cannot complement this function. This was shown by exchanging the GGDEF domain of PdeB with the GGDEF domain of Sputcn32_2830, which leads to absence of polar PdeB-sfGFP signals. Scale bar = 10 µm. (Rossmann & Rick et al., 2019; modified)

Finally, we verified that the polar localization is a specific feature of the GGDEF domain of PdeB by genomically exchanging the GGDEF domain of PdeB with the GGDEF domain of Sputcn32_2830. We then again determined the localization by fluorescence microscopy and found that this exchange prevents the polar localization of PdeB, since no fluorescence clusters were visible (**fig. 3.14b**). To this end, we also tested if the GGDEF-domain of Sputcn32_0099 is able to interact with FimVc$_{HubP}$ by B2H assays but no interaction was found (**sup. fig. 7a**).

3.7 The GGDEF$_{PdeB}$ - FimVc$_{HubP}$ interaction is conserved among *Shewanella* species

Since this was the first time that a GGDEF domain alone was shown to be sufficient to localize a protein to the cell pole, our goal was to study the biochemical and structural basis for this process. Our first approach was to crystalize the complex of both protein domains, but, as described above, the GGDEF domain was prone to aggregation and was not suitable for this method. Thus, we continued by exploring common features of PdeB that may give valuable information to gain insight into the molecular mechanism. While all previous experiments were done in *S. putrefaciens* CN-32, the closely related organism *S. oneidensis* MR-1 encodes a functional ortholog of PdeB that regulates motility and biofilm formation (Chao et al., 2013). However, it has not been shown yet that *So*PdeB also localizes at the flagellated cell pole. Hence, we constructed a *S. oneidensis* MR-1 strain that encodes a translational *pdeB-sfgfp* fusion to test if the polar localization may be conserved among other

Shewanella species. Fluorescence microscopy showed that *So*PdeB-sfGFP also localizes at the cell pole (**fig. 3.15a-b).** The stability and expression of *So*PdeB-sfGFP was verified by immunoblot analysis (**sup. fig. 8a**).

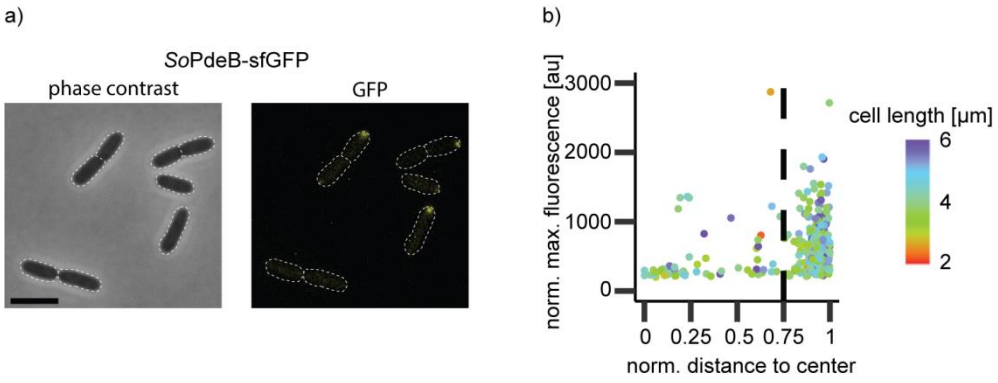

Figure 3.15) Fluorescence microscopy of *So*PdeB-sfGFP. a) The localization of *So*PdeB was tested by using translational sfGFP fusions. The obtained micrographs are shown with a scale bar of 5 µm. **b)** The localization of *So*PdeB was quantified by 3d scatter plots (Rick & Kreiling et al., 2021, modified).

We continued by testing if the $GGDEF_{PdeB}$-$FimVc_{HubP}$ interaction also occurs in *S. oneidensis* MR-1 and we expressed both proteins heterologously and purified them with affinity and size exclusion chromatography. Like the proteins of *S. putrefaciens, So*$FimVc_{HubP}$ was purified in high amounts and purity, while the truncated versions of *So*PdeB were prone to aggregate. Thus, an N-terminal translational MBP fusion was used that allowed purification of high amounts of soluble protein. Surprisingly, the *S. oneidensis* version of MBP-$GGDEF_{PdeB}$ showed around 10 times fewer aggregates compared to the *S. putrefaciens* constructs, allowing us to use sensitive methods like iSCAM assays (**fig. 3.16a**). The experiment showed that both proteins form a complex *in vitro* with a molecular weight of 145 kDa, which suggests a 2:2 stoichiometry. The method requires very low protein concentrations of 50 nM. The fact that a complex is visible under these conditions indicates a high affinity of these proteins to form a complex. To further investigate this, we conducted biolayer interference (BLI) assays monitoring the association of 15 different concentrations and then calculated the dissociation constant (**fig. 3.16b**). As expected from the iSCAM assays, the affinity is very high with a K_D value of 418 nM.

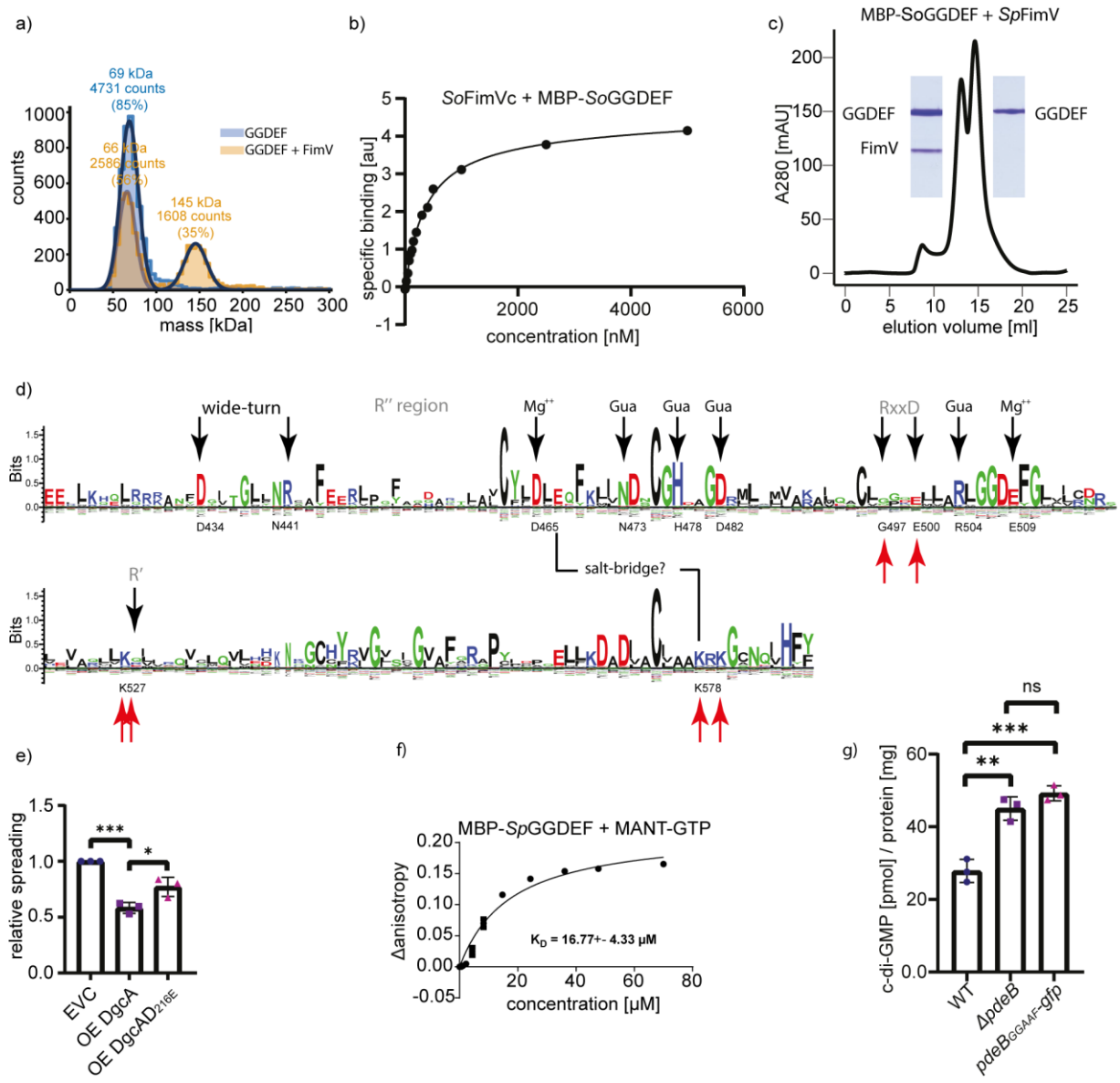

Figure 3.16) GGDEF-FimVc interaction is conserved in *Shewanella* species. a) $GGDEF_{PdeB}$ and $FimVc_{HubP}$ from *S. oneidensis* MR1 were purified and interaction was tested with iSCAM assays. A complex of both is detectable even under very low protein concentrations of 50 nM. The molecular weight was calculated to be 145 kDa, suggesting a 2:2 stoichiometry. **b)** The dissociation constant was calculated using BLI assays and monitoring the association of 15 different concentrations of $GGDEF_{PdeB}$. The K_D was calculated to be around 400 nM. **c)** The interaction of *So*$GGDEF_{PdeB}$ with *Sp*$FimVc_{HubP}$ was tested by SEC. Both proteins interact with each other, showing a cross-species interaction. **d)** A position-based weight map of the GGDEF-domain of 50 PdeB homologues from different *Shewanella* species was created by using the Seq2Logo tool. Black arrows indicate characteristic regions and residues of GGDEF domains. Gray labelling indicate that the regions are degenerated. Red arrows show the residues that are involved in the interaction with $FimVc_{HubP}$**.** The numbers correspond to the pirmary sequence of *So*PdeB **e)** The *in silico* analysis suggested that $E467_{SpPdeB}$ may be responsible for the lacking DGC activity of PdeB. This mutation was introduced into the active DGC VdcA and the wild type and mutated version were ectopically produced in *S. putrefaciens* CN-32. The spreading on motility plates was used as read-out for the DGC activity. The assay shows that mutating D216 to another negatively charged amino acid significantly reduces DGC activity. **f)** The GGDEF domain of *Sp*PdeB is still able to bind GTP. This was tested by FP assays using MANT-GTP binding as ligand. **g)** The effect of GTP binding on the PDE activity of PDE activity was tested by extracting the cellular c-di-GMP from a mutant that is not able to bind GTP anymore (Rick & Kreiling et al., 2021, modified)

Since the previous experiments showed that in both species, *S. putrefaciens* and *S. oneidensis*, $GGDEF_{PdeB}$ and $FimVc_{HubP}$ interact with each other, we wanted to know if both species use the same mechanism of interaction. Therefore, we tested by SEC if *So*$GGDEF_{PdeB}$ and *Sp*$FimVc_{HubP}$ are able to form a complex together (**fig. 3.16c**). We found that when both proteins are injected, an additional peak was present with a lower elution volume than for the single proteins. SDS-PAGE revealed that both proteins were present in the new peak. This indicates that the interaction surface of $GGDEF_{PdeB}$ and $FimVc_{HubP}$ is conserved among *Shewanella* species and allowed us to search for common sequential features that may reveal the amino acid residues involved in this interaction. To this end, we used the BLAST algorithm to obtain 50 sequences of $GGDEF_{PdeB}$ from different *Shewanella* species. The obtained data was then analyzed using the Clustal omega alignment tool and the Seq2Logo tool that creates a position-based weight map using the Kullback-Leiber algorithm (**fig. 3.16d**). The obtained results were then compared with the position-based weight map of *bona fide* digaunylate cyclases published by Tillmann Schirmer (Schirmer, 2016). We found that PdeB encodes all residues directly involved in GTP binding to the GGDEF domain. Other residues which are required for enzymatic activity, for example a lysine that stabilizes the transition state, are also present in all PdeB homologues. However, the group of Alfred Spormann showed that the purified *So*GGDEF domain exhibits no DGC activity *in vitro* (Chao et al., 2013). Hence, we continued by searching for the absence of highly conserved residues and found that the first inhibitory site, while still present, is strongly degenerated. The region for the second inhibitory site is absent in all PdeB homologous. However, the inhibitory site is not essential for DGC activity (Schirmer, 2016). We hypothesized that at least one amino acid that is crucial for enzymatic activity by affecting the structure must be altered in PdeB compared to *bona fide* cyclases. Canonical GGDEF domains possess a characteristic salt bridge that connects a lysine residue at the C-terminus of the GGDEF domain with an aspartic acid located between the first and second inhibitory site (see **fig. 1.1**). The C-terminal lysine ($K578_{SoPdeB}$) is present in all PdeB homogues. However, while the aspartic acid is not present in PdeB homologues, they possess another negatively charged amino acid, glutamic acid ($D467_{SoPdeB}$). While both amino acids are structurally very similar to each other, we doubted that they are interchangeable at this position due to role in forming the structurally important salt bridge mentioned above. To test this hypothesis, we ectopically produced an active DGC, VdcA (from *Vibrio cholerae*), in *S. putrefaciens* and introduced named mutation. Since we previously showed that a high c-di-GMP level reduces the spreading radius on motility plates we used the spreading radius as read-out for DGC activity (**fig. 3.16e**). The ectopic production of VdcA lead to strongly reduced spreading on soft-agar plates. However, introduction of the single point mutation

drastically complemented this phenotype. This shows that the found variation of $GGDEF_{PdeB}$ may be responsible for the lack of DGC activity of $GGDEF_{PdeB}$ found by the Spormann group. Nevertheless, the production of $VdcA_{D216E}$ does significantly reduce the spreading radius compared to that of the wild type, indicating that there may be additional sequential features that contribute to the lack of DGC activity of PdeB. However, the *in silico* analysis showed that $GGDEF_{PdeB}$ still harbors all residues required for GTP-binding. To test this, we used FP assays with MANT-GTP as ligand and found that the protein binds MANT-GTP with a K_D-value of around 15 µM (**fig. 3.16f**). However, the protein is not able to bind MANT-c-di-GMP (**sup. fig. 9a**). We tested if the GTP-binding to the active site of the GGDEF-domain affects the PDE activity of PdeB *in vivo* by extraction of the cellular nucleotides and quantification by MS (**fig. 3.16g**). We found that inserting a mutation into the active center of the GGDEF-domain ($PdeB_{GGAAF}$) resulted in significantly increased cellular c-di-GMP levels. The difference between the Δ*pdeB* mutant and the mutant that is unable to bind GTP was not significant.

3.8 I-site and far C-terminal region of $GGDEF_{PdeB}$ mediate interaction with $FimVc_{HubP}$

We continued by testing other GGDEF proteins for polar localization to gain more information about sequential features of GGDEF domains that mediate polar localization. Thus, we ectopically produced several GGDEF proteins that were predicted to have similar domain architectures as PdeB with translational sfGFP fusions in a background strain with mCherry labeled HubP (**fig. 3.17**).

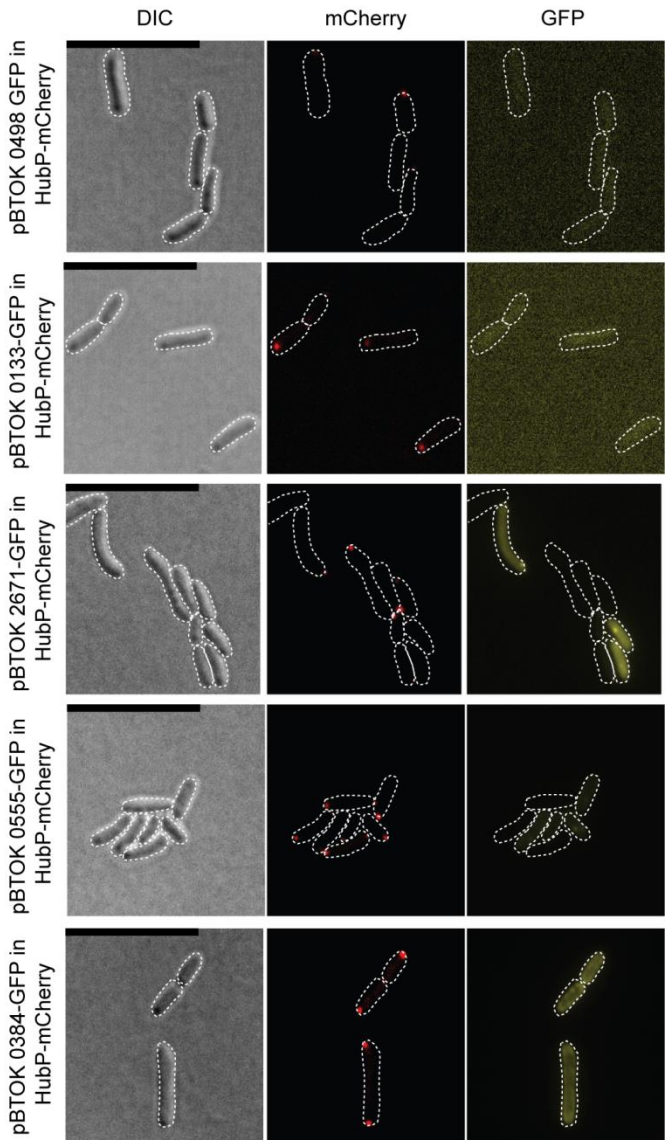

Figure 3.17) Polar localization is a specific feature of the GGDEF domain of PdeB. Five GGDEF-domain proteins were ectopically produced as sfGFP-fusion proteins and the polar localization was tested by fluorescence microscopy. HubP-mCherry was used as polar marker. None of the tested proteins localize at the flagellated cell pole. Scale bar = 10 µm

We observed in all approaches the expected polar signal of HubP-mCherry. However, none of the GGDEF proteins tested showed colocalization with HubP. The only protein displaying fluorescence clusters was Sputcn32_2671-sfGFP. The clusters were localized subpolarly. However, the expression was very uneven between individual cells and it is likely that the observed signals may be inclusion bodies.

Despite the fact that we did not identify other GGDEF domains that mediate polar localization, the fluorescence microscopy experiments with different GGDEF proteins allowed us to continue with further *in silico* analysis. We previously showed that the $GGDEF_{PdeB}$-

FimVc$_{HubP}$ interaction is conserved among *Shewanella* species. Additionally, we identified five GGDEF proteins that do not localize to the cell pole. Hence, amino acids that are involved in the polar localization of PdeB can be expected to be conserved among PdeB homologues and should be different in the non-localizing GGDEF domains. As described in the introduction, the electrostatic surface potential of FimVc domains is highly negatively charged. Thus, we predicted that the interaction surface of GGDEF$_{PdeB}$ is likely to be positively charged. Additionally, the interaction surface must be surface exposed. We therefore used an alignment of 50 PdeB homologues from different *Shewanella* species and compared it with an alignment of all GGDEF proteins from *S. putrefaciens*. We identified three regions in the primary sequence of GGDEF$_{PdeB}$ that have an unusual positively charged amino acid (R557, K490 and K527) and introduced genomic mutations into these regions. We then determined the localization pattern by fluorescence microscopy (**fig. 3.18**).

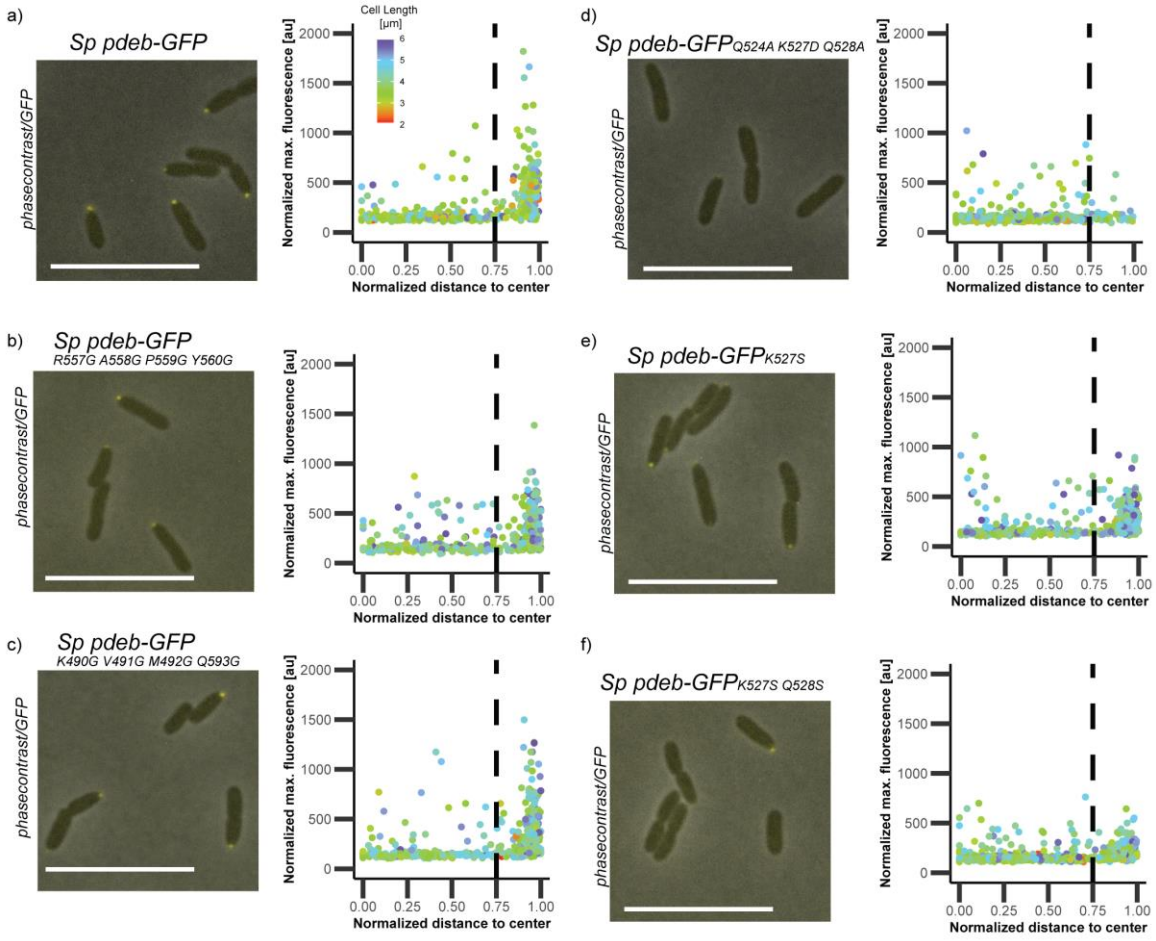

Figure 3.18) The degenerated ER motif of PdeB is needed for the polar localization of PdeB. a-d) Three different regions of PdeB were found to have unusual positively charged amino-acid residues. These were mutated in PdeB-sfGFP and the localization was tested by fluorescence microscopy. While K490$_{PdeB}$-Q593$_{PdeB}$ and R557$_{PdeB}$-Y560$_{PdeB}$ had no influence on the localization (b-c), the degenerated ER region (d) is required to form polar fluorescence clusters. **e-f)** The two crucial residues were mutated and localization was observed using fluorescence microscopy. Mutating either of the two results in significantly decreased polar localization. scale bar = 5 µm. (Rick & Kreiling et al., 2021, modified)

We found that the regions $K490_{PdeB}$-$Q593_{PdeB}$ and $R557_{PdeB}$-$Y560_{PdeB}$ only had minor effects on the localization of PdeB (**fig. 3.18a-c**). Surprisingly, when we mutated $K527_{PdeB}$ and $Q528_{PdeB}$ the polar fluorescence was drastically reduced (**fig. 3.18d-f**). These two amino acids are part of the first i-site in canonical GGDEF domains (Schirmer, 2016). The stability and expression of these PdeB-sfGFP mutants was verified by immunoblot analysis (**sup. fig. 10a**).

We continued by using multiple biochemical approaches: Hydrogen-deuterium-exchange assays allow the determination of interaction surfaces by analyzing, which residues are surface exposed. When the proteins of interest form a complex, previously surface exposed residues cannot be accessed and exchanged by deuterium anymore. Hence, we purified *Sp*$GGDEF_{PdeB}$, *Sp*$FimVc_{HubP}$ and the complex of both by affinity chromatography and SEC. Subsequently, each sample was then individually exposed to deuterium before quenching the reaction with low pH buffer, digestion and MS analysis. Due to the low pH value after the quenching reaction only acid proteases can be used for this method. Unfortunately, the GGDEF domain was found to be resistant to acid proteases. We tried to solve this problem by using different buffer conditions and acid proteases, but we found that only the MBP but not the GGDEF domain was digested and, therefore, no result was obtained for the interaction surface of *Sp*$GGDEF_{PdeB}$. However, *Sp*$FimVc_{HubP}$ was digested sufficiently, and MS analysis showed that residues 1047 – 1107 exhibited reduced deuterium exchange when the proteins are in complex (**fig. 3.19a**).

To determine the interaction surface for the GGDEF domain we continued by using a similar approach as before by chemically crosslinking the complex with DSBU followed by investigating which peptides are crosslinked by MS. This method is performed under neutral to basic conditions, allowing the use of different proteases that are able to digest not only $FimVc_{HubP}$, but also $GGDEF_{PdeB}$. SDS-PAGE was used to verify successful crosslinking (**sup. fig. 11a**). Crosslinked proteins move faster in the SDS-Gel since they cannot be fully linearized anymore. While the protein complex forms two sharp bands in SDS-PAGE, the crosslinked samples show blurred bands and additional signals with higher molecular weight, indicating that the complex was successfully crosslinked. Each sample was then digested and analyzed by MS. While we were not able to obtain data for the *Sp*GGDEF-*Sp*FimVc complex, it was found that the peptide *So*$FimVc_{HubP}$1053-1088 was crosslinked to *So*$GGDEF_{PdeB}$566-577 (**fig. 3.19b**). As shown in the alignment, this data agrees with the HDX data, identifying the same region on the $FimVc_{HubP}$ site.

To further analyze the interaction surface we predicted the structure of the FimVc-domain of *So*HubP using Swiss Model (Waterhouse et al., 2018) (**fig. 3.19c**). The region is predicted to form three alpha helices. To further gain insight into the mechanism of action we calculated the electrostatic surface potential of this region by using the APBS electrostatic tool and Pymol (**fig. 3.19d**). This revealed that the crosslinked peptide is part of a negatively charged pocket. Hence, we hypothesized again that the interaction surface of GGDEF must be positively charged and, therefore, contains more positively than negatively charged amino-acid residues. Since the identified peptide of $GGDEF_{PdeB}$ only contains two positively charged residues, $K575_{SoPdeB}$ and $K577_{SoPdeB}$, we introduced serine mutations at the appropriate locations and purified the proteins by affinity chromatography and SEC (**sup. fig. 12**) and tested if these alter the K_D value in BLI assays (**fig. 3.19f-h**). When $K577_{SoPdeB}$ was substituted we calculated a K_D value of around 2 µM, which is a 10-fold increase compared to the wild-type version. Substitution of K575 resulted in an even higher K_D value of around 20 µM, which is a 100-fold increase compared to the wild type. This data suggested that both lysines may be involved in the interaction of PdeB with HubP. To verify that the proteins are otherwise still functional we used MANT-GTP binding assays and found that both proteins bind MANT-GTP with approximately the same affinity as the wild type (**sup. fig. 11c**). These results support our hypothesis that the interaction surface of $GGDEF_{PdeB}$ has a positive surface charge and contains multiple positively charged amino-acid residues. When K527 was substituted with the small amino acid serine we found increased aggregation and the protein was therefore not suitable for sensitive methods like BLI assays (**sup. fig. 11e**). MANT-GTP binding assays showed that the protein is still functional. Thus, we tested the interaction with HubP by pull-down assays and found drastically reduced amounts of prey protein (**sup. fig. 11c,f,g**). However, K524 could be exchanged to the canonical glutamic acid without increased aggregation. When we tested the affinity of $SoGGDEF_{K527E-Q528S}$ with BLI assays we found that the protein is not able to bind $FimVc_{HubP}$ anymore, while still being able to bind MANT-GTP with roughly the same affinity as the wild type version (**fig. 3.19i / sup. fig. 11c**). The data suggests that the degenerated R` region may be involved in the polar recruitment of PdeB. The available structural data shows that the R` region is structurally in close proximity to the RxxD motif of the inhibitory site (PDB: 3QYY). We hypothesized that the degenerated RxxD region may also be involved in the interaction with HubP and proceeded by mutating G494 and E497 and purifying the proteins. Mutating these residues did not lead to increased aggregation and the proteins were still able to bind MANT-GTP with roughly the same affinity as the wild-type proteins (**sup. fig. 11c**). However, they showed decreased affinity to $FimVc_{HubP}$ in BLI assays (**fig. 3.19j-k**), suggesting that not only the R` but also the RxxD region is part of the interaction surface with HubP.

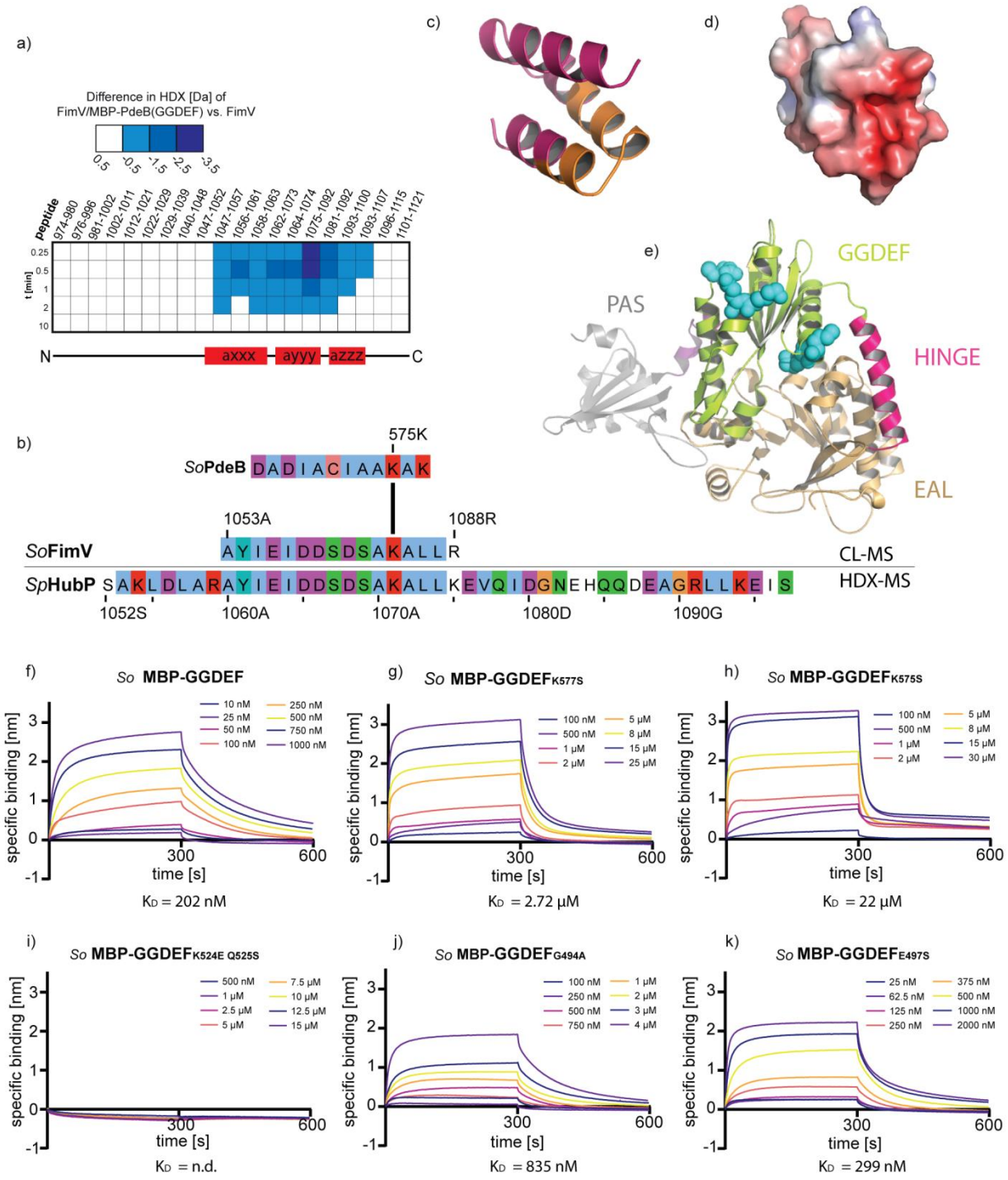

Figure 3.19) The I-site and the far C-terminal region of GGDEF$_{PdeB}$ mediate interaction with FimVc$_{HubP}$. a) The interaction surface of the *Sp*GGDEF$_{PdeB}$ - *Sp*FimVc$_{HubP}$ complex was determined by HDX-MS. No results were obtained for the GGDEF-domain due to acid protease resistance, but it was found that residues 1047 – 1107 of *Sp*HubP have reduced deuterium content when the protein is present in complex with GGDEF$_{PdeB}$. **b)** Interacting regions of the complex were identified by CL-MS. It was found that the peptide 1053 - 1088$_{SoHubP}$ was crosslinked to K575$_{SoPdeB}$. The result is shown as alignment with the interacting region that was found during HDX-MS. **c-d)** The structure of the FimVc-domain of *So*HubP was predicted by the Swiss Model tool (c) and the elctrostatic surface potential was calculated by the APBS electrostatics tool (d). The peptide that was identified by CL-MS is colored in orange. It was predicted to form a negatively charged pocket *in silico*. **e)** The structure of the PAS-GGDEF-EAL region was predicted with the Phyre2 tool. Residues that are involved in the interaction with FimVc$_{HubP}$ are shown in cyan. **f-k)** Residues of GGDEF$_{PdeB}$ that are potentially involved in the GGDEF$_{PdeB}$ – FimVc$_{HubP}$

interaction were mutated and the affinity to $FimVc_{HubP}$ was tested by monitoring the association and dissociation with BLI assays. Mutating any of these residues results in decreased affinity to $FimVc_{HubP}$. The residues K524-Q525 had the strongest effect. (Rick & Kreiling et al., 2021)

3.9 I-site and far C-terminal region of $GGDEF_{PdeB}$ mediate polar localization

We previously found that mutating lysins of the far C-terminal region and residues of the degenerated inhibitory site of *So*$GGDEF_{PdeB}$ resulted in decreased affinity to *So*$FimVc_{HubP}$ *in vitro*. To test if this also applies to *S. putrefaciens* CN-32 *in vivo,* we genomically introduced particular mutations into *pdeB-sfgfp*. Production and stability of these proteins was verified by immunoblot analysis (**sup. fig. 13a**). The localization of PdeB-sfGFP mutants was then analyzed by fluorescence microscopy and compared to that of the wild type version (**fig. 3.20a-f**). The experiment showed that all mutants have decreased localization of PdeB-sfGFP compared to the wild-type protein.

To further verify previous results, we introduced the $K527E\text{-}Q528S_{SpPdeB}$ mutation into *pdeB-mvenus* and used single molecule microscopy (**fig. 3.20g**). This method allows observing single proteins in living cells and to determine their diffusion rates. Compared to the wild-type version, $PdeB\text{-}mVenus_{K527E\text{-}Q528S}$ showed significantly increased diffusion rates *in vivo*. While for PdeB-mVenus more than 80% of the observed molecules were observed to be tightly bound to the cell pole, around 60% of the observed $PdeB\text{-}mVenus_{K527E\text{-}Q528S}$ molecules showed low diffusion rates. This verified that the inhibitory site of $GGDEF_{PdeB}$ plays a crucial role in polar recruitment of PdeB. Additionally, we also quantified the diffusion rates of PdeB-mVenus mutants that have mutations in the active site of the EAL or GGDEF domain. As suggested by our previous results, these mutations had negligible effects. The controls for the single molecule microscopy are shown in **sup. fig. 13b-e**.

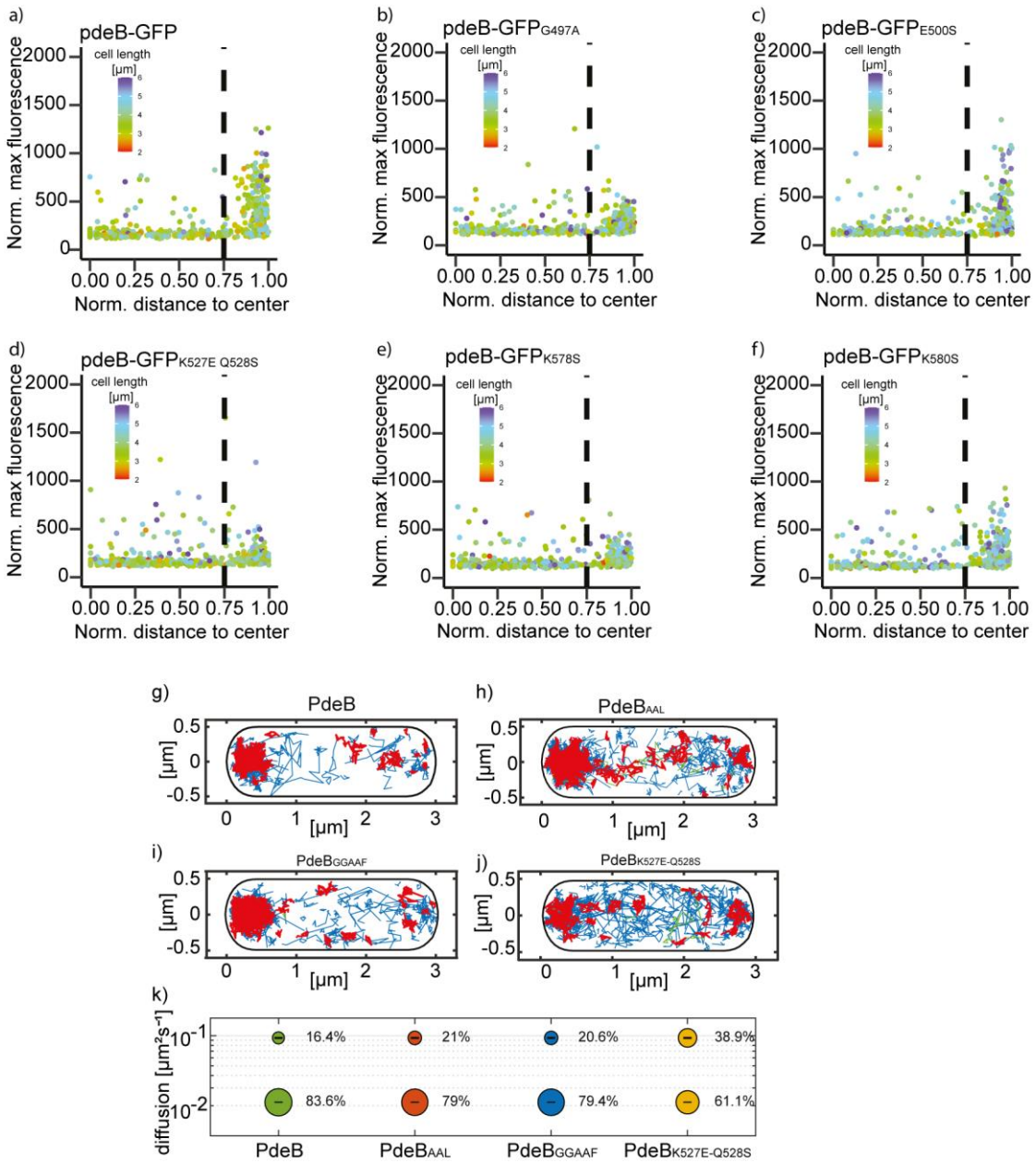

Figure 3.20) I-site and far C-terminal regions of GGDEF$_{PdeB}$ are necessary for polar localization. a-f) Residues identified to reduce the affinity to FimVc$_{HubP}$ were genomically mutated and the localization was tested by fluorescence microscopy. Mutating any of these amino acid residues resulted in decreased polar localization of PdeB. **g-j)** The localization pattern of different mutants was analyzed using single molecule microscopy. The experiments were performed with PdeB-mVenus. The wild-type version showed extraordinary strong localization with 83% of the proteins displaying low diffusion rates. Mutating the active site of the GGDEF or EAL domain had no impact on the localization pattern of PdeB, while mutating the i-site (K527E Q528E) resulted in decreased localization. **k)** Diffusion rates of PdeB-mVenus mutants obtained by single molecule tracking (Rick & Kreiling et al., 2021, modified)

3.10 Polar localization of PdeB is required for full PDE activity

The previous experiments allowed us to create strains with reduced polar PdeB localization. We used these strains to further study the consequences of the polar localization of PdeB. To test if the localization is essential for PdeB activity *in vivo* we extracted the cellular c-di-GMP from cells of strains with reduced PdeB localization, quantified the amount by MS and compared it to the those of wild-type cells (**fig. 3.21a**). We used the wild type, a *pdeB* deletion strain and a strain with an inactivating mutation in the active center of the EAL domain as controls. We found that mutants with decreased polar localization of PdeB showed significantly increased c-di-GMP levels. The only exception was the strain $pdeB_{K580S}$, where the difference was not significant. Building on these results we used a riboswitch- and plasmid-based c-di-GMP reporter system (Zhou et al., 2016) to determine the c-di-GMP levels in vivo at the single-cell level. The plasmid encodes the gene for $turborfp_{AAL}$. The expression of the latter is controlled by three consecutive c-di-GMP binding riboswitches that activate transcription when c-di-GMP is bound. Additionally, the plasmid encodes the gene for a second fluorophore, CFP, which is constitutively expressed and allows normalization to the plasmid number. The fluorescence can then be quantified by fluorescence microscopy. We used the wild type and a *pdeB*-deletion strain as controls and determined the c-di-GMP level in three mutants with decreased polar PdeB localization (**fig 3.21b**). The data was collected by Vanessa Kreiling and the analysis was done by me. We found that the strains with delocalized PdeB show a significantly increased quotient of red fluorescence divided by blue fluorescence. Therefore, the experiment verified that polar PdeB localization is required for full PDE activity of PdeB.

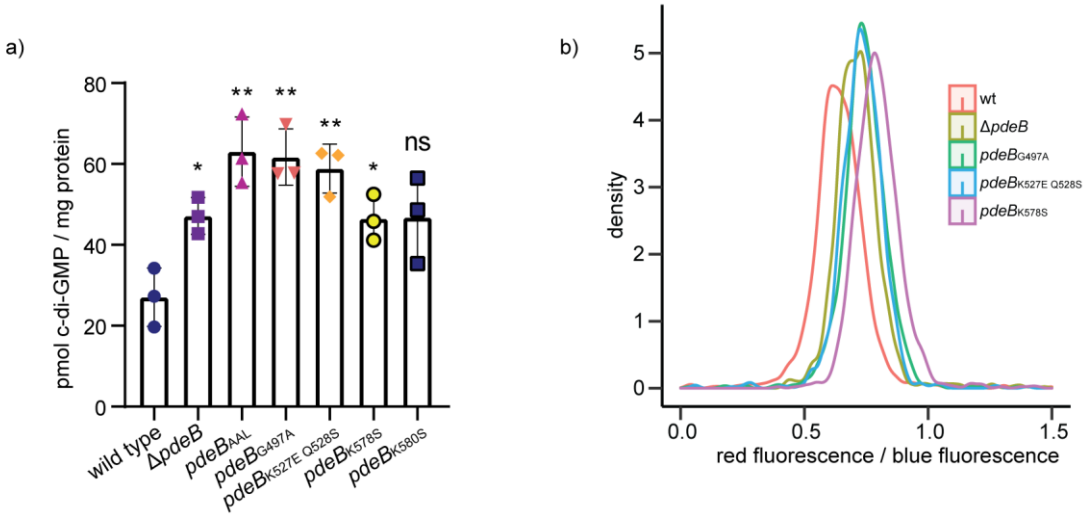

Figure 3.21) Polar localization of PdeB is required for full PDE activity. a) The cellular c-di-GMP of strains with reduced polar PdeB localization was extracted and quantified by MS. Strains with delocalized PdeB showed significantly increased c-di-GMP levels. **b)** The relative c-di-GMP level of strains with reduced PdeB localization was determined by using a plasmid-based fluorescence reporter. The quotient of red fluorescence divided by blue fluorescence indicated the c-di-GMP level. 1000 cells of each strain were analyzed and the density function of the

population was calculated. Strains with reduced PdeB localization show increased c-di-GMP levels. (Rick & Kreiling et al., 2021)

3.11 PdeB creates phenotypic heterogeneity

To obtain insights into the consequences of the polar localization of PdeB we again used the plasmid based c-di-GMP reporter assay. The previous experiment showed the density function of the relative c-di-GMP level of different strains (**fig. 3.21b**). While density functions are useful to show differences of mean concentrations, they have the disadvantage that small populations are often not visible. This is caused by the mathematical basis of density function which compares three bins to create a y-value. Thus, we repeated the experiment with the wild type and Δ*pdeB* strains of *S. putrefaciens* and *S. oneidensis* and analyzed the data using histograms and scatter plots (**fig. 3.22a-d**). When we quantified the c-di-GMP levels of *S. putrefaciens* CN-32 we found that the measured values cluster in two distinct populations (**fig. 3.22a)**. The vast majority of cells had a quotient of around 0.5 when dividing the red fluorescence by the blue fluorescence. This population showed a broad bell-shaped distribution. The second population, however, was much smaller and had a very low quotient of around 0.2 which indicated low cellular c-di-GMP concentrations. This population was not observable when *pdeB* was absent, indicating that *pdeB* may be important in creating heterogeneity and swarmer cells with low c-di-GMP levels. Additionally, we found that the median quotient of the other population is shifted to higher values in absence of PdeB.

We repeated the experiment with *S. oneidensis* MR-1 (**fig. 3.22b**). The experiment showed a similar distribution as for *S. putrefaciens* CN-32 with an additional low c-di-GMP level population that is *pdeB*-dependent. However, the population with low c-di-GMP levels was much larger than in *S. putrefaciens* CN-32 and contained the majority of cells. This population was not present when *pdeB* was deleted, and the median quotient was shifted to higher values. We also measured the cell length of each individual cell and plotted it against the relative c-di-GMP level (**fig. 3.22c-d**). We attempted to test with this experiment if the c-di-GMP level differs between cells that just divided and older cells. However, we did not find a correlation between cell length and relative c-di-GMP level. We think that the used fluorophores are too stable to obtain the required temporal resolution for such experiments. Previous attempts tried to approach this problem by using with higher turnover rate due to an AAL-tag, however the problem remains to be solved. We also tried to address the problem by using FRAP (fluorescence recovery after photobleaching), but the required sample size was too high due to the heterogeneity of the population.

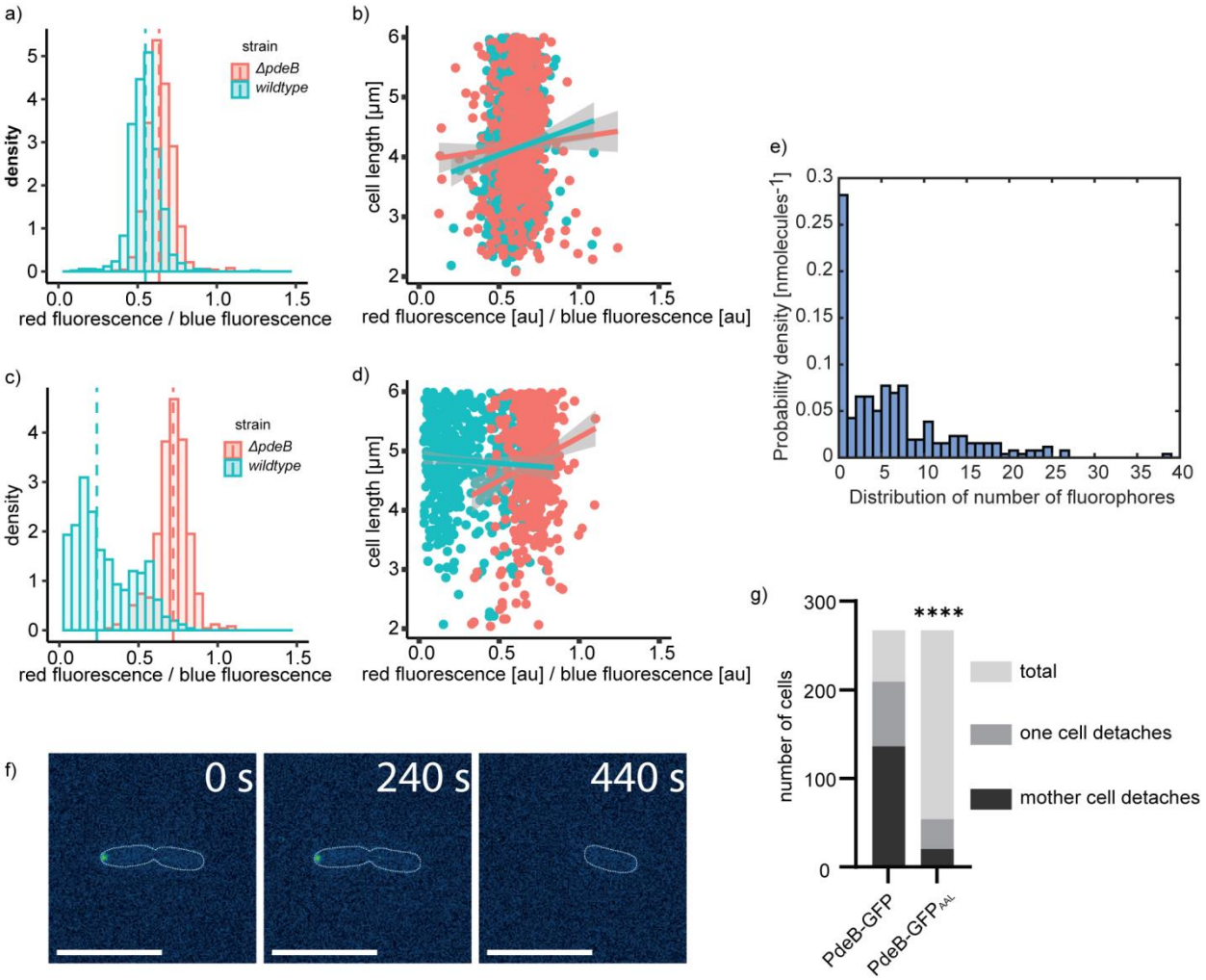

Figure 3.22) Polar localization of PdeB leads to phenotypic heterogeneity. a-b) The relative c-di-GMP level of individual *S. putrefaciens* CN-32 cells in the presence and absence of *pdeB* were analyzed using a plasmid based reporter system. The wild type showed a small subpopulation with low c-di-GMP levels and a major subpopulation with higher c-di-GMP levels (a). A correlation of the c-di-GMP level with the cell length was not found (b). Each dot represents an individual cell. **c-d**) The c-di-GMP quantification was done for *S. oneidensis*. Similar to *S. putrefaciens* CN-32, a subpopulation with low and a subpopulation with high c-di-GMP levels was visible. In contrast, the subpopulation with low c-di-GMP levels was much greater in *S. oneidensis* (c). No correlation between cell length and c-di-GMP levels was found (d). **e)** The number of PdeB molecules in individual cells was determined using single molecule microscopy. Around 25% of observed cells did not contain any PdeB molecule, while the majority had 1 – 7 molecules/cell. The rest of the population contained 8 - 25 molecules and some up to 40. **d-g)** The cell division of *S. putrefaciens* CN-32 was observed using microscopy and PdeB-sfGFP was used as marker for the mother cell. Exemplary micrographs are shown in (f), scale bar = 10 µm. It was determined how many times the mother- and daughter cells detached from the surface after cell division. In presence of active PdeB, in around half of the observed events, one of the cells detached from the surface. In virtually all events this was the mother cell. When PdeB was inactivated by genomically introducing a mutation into the active center of the EAL domain, detaching events occurred significantly less frequent. (Rick & Kreiling et al., 2021, modified)

We previously showed that PdeB localizes to the flagellated cell pole by interacting with extraordinary high affinity with the polar landmark protein HubP. We also observed an extremely low diffusion rate of PdeB molecules *in vivo*. This raised the hypothesis that the polar localization of PdeB results in asymmetric cell division, since virtually all PdeB

molecules remain bound to the cell pole of the mother cell. To visualize this asymmetric cell division we used two different approaches. The first one was to quantify the exact number of PdeB molecules *in vivo* by single molecule microscopy (**fig. 3.22e**). To this end we used translational PdeB-mVenus fusion proteins, since the fluorescence of mVenus is brighter than the fluorescence of sfGFP. The experiment showed that around 25% of the cells do not contain any PdeB molecule. This is likely attributed to the asymmetric cell division. The majority of cells however (around 35%) contain between one and seven PdeB-mVenus molecules. The other cells have 8 – 25 molecules, while some contain up to 40.

The previous results raised the hypothesis that the asymmetric cell division allows a very efficient colonization strategy. During cell division, the monopolar localization of PdeB creates two different cells, where the mother cell inherits PdeB, but the daughter cell does not. Therefore, the mother cell has low c-di-GMP levels, while the daughter cell has high levels. Thus, we suspected that the daughter cell will produce adherence factors while the mother cell remains motile. To test this hypothesis, we monitored the cell division of *S. putrefaciens* cells that produce PdeB-sfGFP under the microscope. To this end we observed 250 cell divisions of *S. putrefaciens pdeB-sfgfp* (**fig. 3.22f-g**). This experiment was done by Vanessa Kreiling. She found that that in more than 80% of the observed events one cell detaches from the surface and continues with flagella mediated motility. In around 50% of the observed events, she found that the mother cell detached, while in 30% of events it was not determinable which cell detached due to bleaching of the fluorophore. However, no event was observed were the daughter cell detached.

To gain insights into the role of PdeB during this process we repeated the experiment with a strain that lacks enzymatic activity of PdeB. We again observed 250 cell division events and found that in cells lacking enzymatic activity of PdeB the number of detaching events was drastically reduced. Here we found that in around 75% of the events both cells remained attached to the surface. In only 25% of the events one cell detached from the surface using flagella mediated motility.

Summarizing these experiments, we found that the polar localization of PdeB results in the generation of phenotypically different cells with one motile and one sessile cell. This process may allow the cells to colonize new environments very efficiently.

4. Discussion

In this study we analyzed the polar localization of PdeB and investigated a novel function of GGDEF domains. We found sequence features that mediate the interaction with the landmark protein HubP and characterized this process with several *in vitro* experiments. Additionally, we identified multiple systems that are involved in the signaling network of c-di-GMP.

4.1 PdeB affects flagella-mediated motility by degrading c-di-GMP

While the GGDEF domain of PdeB has no enzymatic activity, the EAL domain is able to degrade the second messenger c-di-GMP. This was verified by several *in vitro* and *in vivo* experiments, like riboswitch-based reporter systems (Zhou et al., 2016) and MANT-c-di-GMP degradation assays (Eli et al., 2017). This also agrees with the study conducted by Chao and colleagues about the PDE activity of *So*PdeB (Chao et al., 2013). It was found that PdeB regulates motility on multiple levels. The model organism *S. putrefaciens* CN-32 encodes two independently regulated flagella systems (Bubendorfer et al., 2014). In this study we found that PdeB primarily acts on the lateral system by positively regulating its transcription. We assume that PdeB influences the transcription of the lateral system via the transcriptional master regulator $FlrA_2$. Homologues of this protein are present in a variety of species, such as *P. aeruginosa* where it is called FleQ. This protein harbors a Walker A motif that is able to bind c-di-GMP, which results in a change of the oligomerization state of the protein (Claudine & Harwood, 2013). Thus, it is very likely that the observed effect of *pdeB* on the lateral flagella system is perceived and transmitted via this factor.

However, it remains unclear why PdeB does not affect the transcription of the polar flagellum. It is possible that the binding affinity of c-di-GMP to $FlrA_1$ is lower than to $FlrA_2$ and that the PDE activity of PdeB is not strong enough to influence the polar system. To test this, both transcriptional regulators could be purified and the binding affinity to c-di-GMP could be tested with BLI assays.

Additionally, our group found another regulator of the lateral flagella, called MotL, which regulates the activity on a post-translational level. The protein is a stand-alone PilZ domain protein that was found to bind c-di-GMP. The protein was found to regulate the activity of the lateral, but not the polar flagella in response to c-di-GMP. The authors found that MotL slows down the lateral flagella in response to high c-di-GMP levels but is also able to speed the flagella up under low c-di-GMP conditions (Pecina et al., 2021). Therefore, PdeB does not only promote the production of lateral flagella but also regulates its motor activity.

In *S. putrefaciens* CN-32, the lateral flagellum does not increase the swimming speed of the cells, but instead increases the directional persistence (Bubendorfer et al., 2014). This mechanism is advantageous to spread through complex environments and to speed up the colonization at the population level. This may explain why no decreased swimming velocity was found in microscopy experiments when *pdeB* was deleted, despite its effect on the transcription and activity of the lateral flagella system. One could also argue that PdeB may not be enzymatically active when grown in liquid medium in which the swimming velocity experiments were conducted. However, this is very unlikely since we showed by extraction and quantification of cellular nucleotides that PdeB decreased the c-di-GMP level of liquid cultures.

But why does PdeB not affect the polar flagellum? Currently we can only hypothesize, but one reason could be that the polar flagellum has more functions than only motility. It can also act as mechanosensor (Fujiu et al., 2011) and studies showed that flagella play an important role in biofilms (Wood, 2013). Thus, it may be disadvantageous to repress the production of the polar flagellum only to reduce motility. Using motility assays we found that PdeB is active in LB but not in mineral medium. Thus, it may be possible, that when the activator of PdeB is not present, the population still benefits from utilizing flagella mediated motility. However, the repression of the lateral flagella system may serve as a strategy to conserve energy under these limited conditions. To this end it would be interesting to identify the periplasmic ligand of PdeB. It is likely that it could be a molecule that can be utilized as carbon or energy source. One of such molecules would be N-acetylglucosamine; This carbohydrate can be utilized by several *Shewanella* species that harbor the *nag* genes (Rodionov et al., 2010). We tested if N-acetylglucosamine could serve as activator of PdeB, but the results were inconclusive (data not shown).

Additionally, the given results do not exclude that c-di-GMP could regulate the polar flagellum. Since *S. putrefaciens* encodes a plethora of DGCs and PDEs it may be possible that the combined activity of these enzymes is necessary to influence the transcription and construction of the polar flagellum. One way to address this would be to delete multiple PDEs simultaneously or overexpress a DGC and then quantify the number of polar flagella.

Also, it is possible that another nucleotide messenger, ppGpp, affects the polar flagellum. This molecule functions as alarmon in response to amino acid starvation (Traxler et al., 2008). When ppGpp production is induced, the cell depletes its GTP pool and, thus, slows translation of new proteins. Hence, no new proteins of the polar system are produced upon ppGpp induction. Depletion of the GTP pool also leads to inactivation of PdeB, since binding of GTP to its GGDEF domain is essential for full PDE activity. Additionally, our former Lab member Florian Rossmann found that several bacterial species, including *Shewanella*, eject

their flagellum when starved (Ferreira et al., 2019). In the means of a master's thesis, our group found indications that *S. putrefaciens* cells discard their flagella when ppGpp is induced by serine-hydroxamate. These results indicate that there may be a cross regulation of GTP, c-di-GMP and ppGpp which together affects the polar flagellum.

Another way how PdeB could influence the polar flagellum, without affecting its production or activity, could be by modifying the chemotactic response. In *S. putrefaciens* CN-32 the chemotaxis system is located at the flagellated cell pole and localizes in dependency of the landmark protein HubP (Rossmann et al., 2015). In this study we got mixed results regarding the influence on taxis: On one hand, no effect was found on the ratio of turns divided by tracks in microscopy experiments. On the other hand, multiple SNPs in chemotaxis genes were found in suppressor mutants. A cross-talk of c-di-GMP and the chemotaxis machinery is known for multiple organisms, such as *C. crescentus* and *P. aeruginosa* (Kulasekara et al., 2013; Nesper et al., 2017). In *P. aeruginosa,* the chemotaxis component CheA controls the cellular c-di-GMP level by directly interacting with the PDE Pch. This process was found to be important in generating heterogeneity among the population (Kulasekara et al., 2013). Currently we have no indications that PdeB directly interacts with CheA. When the chemotaxis gene cluster together with the primary flagella system was deleted, the localization of PdeB was not altered. Instead, the activity and localization of PdeB is controlled by the landmark protein HubP, which in turn recruits the chemotaxis system. However, PdeB could influence taxis on a similar fashion as Nesper and colleagues found in *C. crescentus*. This organism encodes several CheY-like regulators that can bind c-di-GMP and in response control motor activity. These proteins are called Cle proteins (Nesper et al., 2017). Currently it is not known if this class of proteins exists in *S. putrefaciens* CN-32. Hence this study could be followed up by *in silico* screenings to identify potential proteins and *in vitro* assays to verify c-di-GMP binding of CheY-like proteins in *S. putrefaciens* CN-32.

We found that some suppressor mutants obtained SNPs in the gene *cheB* and in the intergenic region between *cheR* and *cheW*. The proteins CheR and CheB are both involved in regulating the methylation status of MCPs, where CheR acts as constitutive methyltransferease and CheB as methylesterase. The CheR protein uses *S*-adenosylmethionine as methyl donor to mediate methylation of MCP proteins, which increases the autophosphorylation of CheA (Sampedro et al., 2015; Springer & Koshland, 1977). The activation of CheA results in increased CheY-P levels and, therefore, increased tumbling events (Sampedro et al., 2015). CheB, on the other hand, removes the methyl groups from MCPs, which in turn results in decreased phosphorylation of CheY and therefore fewer tumbling events (Sampedro et al., 2015). While *cheB* and *cheR*, were identified to repress the swimming phenotype of the Δ*pdeB* mutant, it is unlikely that they can bind c-di-

GMP. Instead, these proteins could be regulated by another c-di-GMP binding protein like MapZ (Xin et al., 2019). This protein was studied in *P. aeruginosa* and functions as an adaptor protein that is associated with the chemotaxis pathways. Xin and colleagues found that flagellar motor switching and directional reversals are regulated by c-di-GMP in a MapZ dependent manner (Xin et al., 2019). Thus, our study could be followed up by *in silico* analysis to identify homologues of MapZ in *S. putrefaciens*. Following, the protein could be purified and the c-di-GMP binding tested *in vitro* with MANT-c-di-GMP binding assays.

Since PdeB localizes to the flagellated cell pole, we first hypothesized that it could not only regulate bacterial motility via c-di-GMP, but also through direct protein-protein interaction with the polar flagellum. However, with the given result this hypothesis is quite unlikely. We tested this by genomically deleting *pdeB* and ectopically expressing the phosphodiesterase PdeH from *E. coli*. This protein has strong PDE activity and is crucial to maintain a low c-di-GMP level in its host (Reinders et al., 2016). The overexpression resulted in full complementation of the Δ*pdeB* phenotype, indicating that the phenotype of PdeB may be fully traced back to its PDE activity.

4.2 PdeB regulates surface attachment

We found that the motility phenotype of *pdeB* was extensive on motility plates, but the swimming velocity was not altered in liquid medium. While an effect on the lateral flagellum was found, there was still a discrepancy between the spreading radius of cells without the lateral flagella system in presence and absence of *pdeB*. Using the existing literature and transposon mutagenesis we predicted and showed that *pdeB* regulates the activity of the MSHA-pilus system at a post-translational level. The extension ATPase MshE was found to bind c-di-GMP directly. The group of Fitnat Yildiz studied this process extensively in the model organism *V. cholera* and was the first group to describe MshEN-domains as high affinity c-di-GMP receptors (Floyd et al., 2020; Jones et al., 2015). Using *in silico* analysis we identified that MshE harbors a fully conserved c-di-GMP-binding motif, strengthening our result that MshE binds c-di-GMP directly.

While MSHA-pili are utilized for surface attachment and not for swimming, we found that they strongly influence the spreading on motility plates. Bacterial cells need to navigate through a maze of carbohydrate fibers in such environments. A study conducted in *V. parahaemolyticus* found that MSHA pili have lectin functionality and bind to sugar molecules (O'Boyle et al., 2013). While deletion of *mshE* had no significant effect on the spreading radius in wild-type cells, it strongly complemented the absence of *pdeB*. Likely, the increased extension of MSHA-pili leads to increased attachment to the carbohydrate fibers. To this end,

the group of Fitnat Yildiz found that, when cells attach to a surface with a single MSHA-pilus, the swimming behavior changes drastically. Despite the attachment being reversible and cells still being able to swim at this point; they begin to rotate with high speed around the point of attachment (Jones et al., 2015). Hence, even when cells detach again, these orbiting events will decrease the spreading distance.

Our model organism *S. putrefaciens* CN-32 encodes a second pilus system called Pil. Similar to the MSHA pilus system, this system encodes an extension ATPase, named PilB. It would be possible that this molecular machine is also able to adjust its activity by directly binding the second messenger c-di-GMP. However, we found during *in silico* and *in vitro* experiments that this protein is not able to bind c-di-GMP. It could, however, still be possible that another factor mediates a c-di-GMP-dependent regulation of this pilus-system. One example for such a mechanism would be the c-di-GMP receptor FimX (Navarro et al., 2009). This protein was discovered in *P. aerguinosa* and belongs to the class of degenerated GGDEF-EAL proteins. It was found to govern pili-dependent twitching motility. However, a homologue of FimX is not known in *S. putrefaciens* CN-32 nor *S. oneidensis* MR-1. With the given results however, it is unlikely that the Pil system contributes to the phenotype of Δ*pdeB*, since inactivation did not affect the spreading in presence or absence of *pdeB* on motility plates. Another possibility could be that the transcription of one or both pilus systems may be affected. However, this has not been tested yet.

It was previously shown that c-di-GMP affects the Bpf-system in *S. putrefaciens* (Wu et al., 2013). Hence, we measured the transcription of the *bpf* operon in presence and absence of *pdeB* and found that deletion of *pdeB* results in increased transcription of *bpf* genes. Interestingly, the Bpf system does not contribute to the spreading phenotype of PdeB on motility plates. Since the system is crucial for cellular surface attachment (Newell et al., 2009) we think that the effect on *bpf* is another indicator that PdeB governs the transition from a motile to a sessile lifestyle. It is likely that this system is not only affected at the transcriptional but also at the post-translational level. The Bpf system was extensively studied by the group of Georg O'Toole in *P. fluorescence*. They found that the degenerated GGDEF-EAL protein LapD (BpfD in *Shewanella*) binds c-di-GMP and, in absence of its ligand, induces the release of LapG, which in turn then cleaves LapA. Presenting LapA on the cell surface leads to increased surface attachement (Smith et al., 2018). Another group studied this system in *S. oneidensis* and found that the systems functions similarly in this organism. They verified that *So*BpfD interacts with both *So*BpfA and *So*BpfG. While they did not verify the c-di-GMP binding of *So*BpfD *in vitro*, the sequence homology makes it very likely that it functions in a similar manner as in *Pseudomonas* species (Zhou et al., 2015). Hence, increased c-di-GMP levels should result in decreased cleavage of the RTX-toxin

AggA (also named BpfA) in *Shewanella*. We addressed this question by immunoblot analysis and found that deletion of *pdeB* resulted in increased amounts of Bpf proteins. The high expression of the system however prevented exact quantification of cleaved and uncleaved proteins since only blurred bands were obtained. Future studies could therefore use alternative methods like mass spectrometry to address the *pdeB* dependent posttranslational regulation of the Bpf-system. Our findings agree with the previously published literature where another c-di-GMP regulating protein, DosD, affects the Bpf system in *S. putrefaciens* (Wu et al., 2013).

Integrating the given results of the MSHA pilus assembly, the Bpf-system and the effect on flagella mediated motility into a model, we found that PdeB governs the switch from a motile to sessile lifestyle. On one hand, PdeB reduces motility by repressing the transcription and activity of the lateral flagellar system and, on the other hand, promotes surface attachment. We propose that the transition happens in a similar fashion as postulated for *V. cholerae*: The motile cell that utilizes flagella mediated motility extends their MSHA-pili and by chance adheres to the surface. Once a pilus is attached the cell switches from a roaming behavior to an orbiting behavior. By retracting the MSHA-pilus the cell is pulled to the surface and gets in close contact with it. At this point the cell either detaches or other attachment factors, such as the Bpf-System, strengthens the adherence (Floyd et al., 2020; Jones et al., 2015; Smith et al., 2018; Wang et al., 2016). A model for the regulatory c-di-GMP network is shown in **fig. 4.1**.

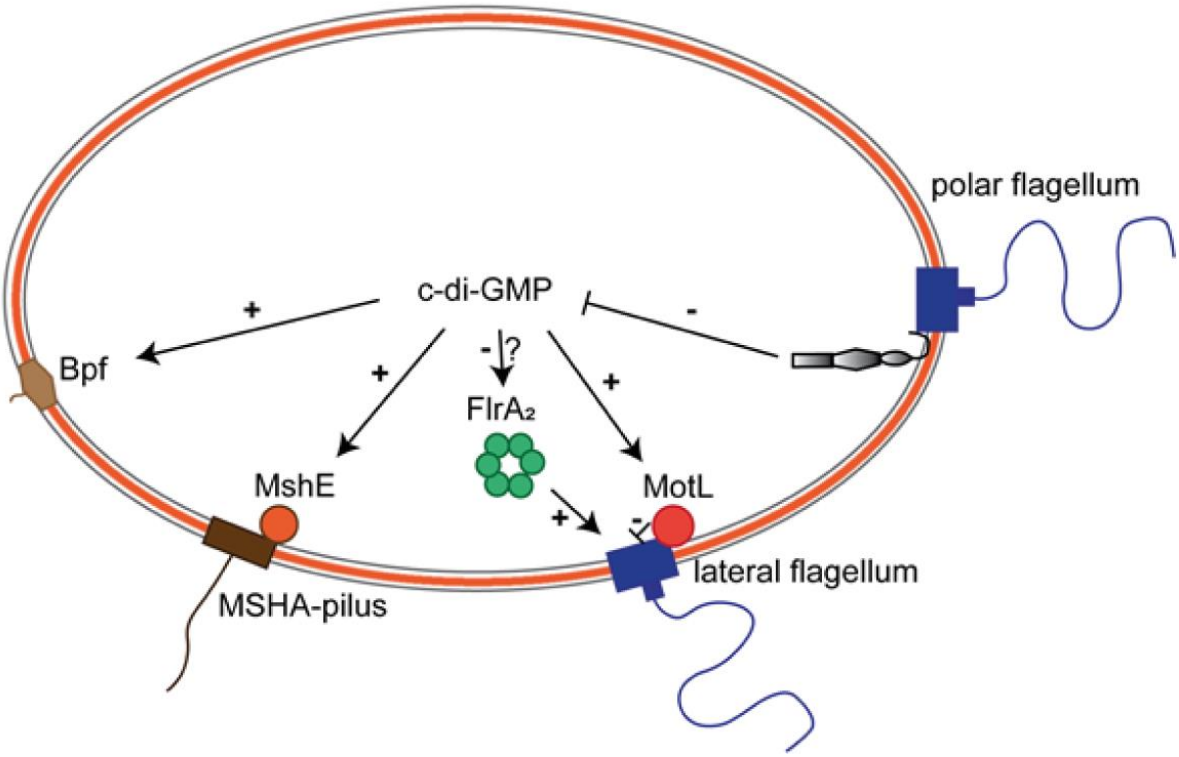

Figure 4.1) Signaling network of PdeB in *S. putrefaciens*. The protein PdeB acts as phosphodiesterase and degrades c-di-GMP. This second messenger decreases the transcription of the lateral flagellar system, likely by a $FlrA_2$-mediated mechanism. Additionally, the PilZ-domain protein MotL regulates the activity of the lateral Flagellum. c-di-GMP also increases the activity of the MSHA pilus at the post-translational level by interaction with the extension ATPase MshE. It also up-regulates the production of the Bpf-system.

While we did not use *S. putrefaciens* as model for infections, the obtained results can also be interpreted the way that PdeB regulates virulence. Human infections with *Shewanella* are rare but infections with the species *S. putrefaciens* and *S. algae* occur; most commonly in ears, skin and soft tissue (Holt et al., 2005). Motility and biofilm formation are key factors for bacterial infections (Felgner et al., 2020; Josenhans & Suerbaum, 2002). The evolutionary development of TLR-receptors that recognize bacterial flagella underline this statement: The TLR5 receptor was found to bind bacterial flagellins and induces a potent immune response (Hajam et al., 2017). More recent studies found that not only recognition of the flagella induces such a response, but also that swimming itself results in activation of the immune system (Felgner et al., 2020). In addition, biofilm formation and cellular adherence play a major role in infections. The opportunistic pathogen *Enterococcus spp.* for example forms biofilms during infections (Stępień-Pyśniak et al., 2019). Bacterial biofilms also play a major role in chronic infections and such cell formations show increased tolerance against antibiotics and phagocytosis. This makes for example the treatment of *P. aeruginosa* induced

cystic fibrosis very challenging (Høiby et al., 2010). Our study therefore serves as great example for the c-di-GMP dependent regulation of virulence factors.

4.3 PDE activity of PdeB is controlled by multiple mechanisms

We previously demonstrated that PdeB acts as c-di-GMP-specific PDE. The regulation of its enzymatic activity proved to be very complex and is dependent on multiple signals. Similar to the results obtained by the group of Alfred Sporrmann regarding *So*PdeB; *Sp*PdeB was active in LB medium, but inactive in mineral medium (Chao et al., 2013). We hypothesize that the periplasmic domain might act as sensor domain for a specific ligand. Unfortunately, *in silico* analysis did not suggest a potential ligand since the periplasmic region has no homology to any known domain. Additionally, the periplasmic region varies between different *Shewanella* species; thus, we hypothesize that the signal may be specific for the various *Shewanella* species. We were able to purify the periplasmic region of *Sp*PdeB, but the quality was, so far, not sufficient for crystallization experiments. Our collaboration partner Monica Gerth (Victoria University of Wellington) performed binding assays with the purified proteins but did not obtain a specific binding signal for any of the used ligands (data not shown). From their obtained data they suspected that the ligand was already bound to the purified protein. Therefore, further studies will aim at purifying the periplasmic region in sufficient amounts to identify the ligand by mass spectrometry techniques. The used mineral medium, called 4M medium, contains lactate as carbon source. Hence, we can exclude lactate as possible activator of PdeB. While lactate still influences the c-di-GMP level, the effect is mediated by the *lbr* operon (Sputcn32_0303 - Sputcn32_0305) which is described as three-component regulatory system (Liu et al., 2017). The used LB medium contains high amounts of yeast extract, thus we think that the activator of PdeB could be produced by yeast. We hypothesized that PdeB could sense amino acids with its periplasmic domain, but addition of these to the growth medium did not activate PdeB. Thus, so far, the external signal that is necessary for full activation of PdeB remains elusive. The group of Alfred Spormann performed RNA-sequencing experiments in *S. oneidensis* with strains that lack *pdeB* and postulated that it affects the sulfur metabolism (Chao et al., 2013). However, the group was not able to identify the ligand and it is not clear yet if this also applies to *S. putrefaciens*. In our study we generated spontaneous mutants that complement the phenotype of *ΔpdeB* and identified SNPs by full genome sequencing. Several SNPs were located in operons that are annotated to be involved in sulfur metabolism. This matches the results obtained by the group of Alfred Spormann, but further verifications are necessary. To this end, the group of Guilani published interesting results and postulated that in some

bacterial species the c-di-GMP level regulates the adherence to sulfur (Castro et al., 2015). Thus, it may be possible that PdeB could not only regulate the sulfur metabolism, but also the adherence to sulfur.

The genes *hemE* and a gene encoding a short chain dehydrogenase are located in direct genetic neighborhood of PdeB. Many c-di-GMP-related enzymes contain heme as cofactor to sense specific signals. As an example, the phosphodiesterase CdpA that was described in *V. cholerae* binds heme as cofactor to regulate its PDE activity (Heckler et al., 2020). One domain that could mediate heme binding are PAS domains (Gilles-Gonzalez et al., 2004). *In silico* analysis shows that the PAS domain of PdeB does not contain an obvious heme-binding motif. To assign a function to the PAS domain we used *in silico* analysis to search for FAD, flavin, heme A, heme B, malate and tricarboxylate binding sites, but no known binding motif was found. However, a bacterial-2-hybrid experiment conducted in a student course suggested that the PAS domain interacts with itself. Thus, we propose that the PAS domain may be required for the correct aggregation state and could mediate dimer- or multimerization. However, these experiments require confirmation. Multimerization is a common function of PAS domains and this hypothesis agrees with the existing literature (Pongratz et al., 1998). It is still unclear if this process needs a specific signal or if PdeB is constitutively present as dimer- or multimer. Future studies could try to address this question with *in vitro* experiments. We were already able to purify a truncated version of PdeB consisting of the PAS- and GGDEF-domain with an N-terminal MBP-tag. At this point it is unclear if the PAS-domain plays a role in the interaction with HubP.

Another regulatory mechanism is the GTP-dependent stimulation of phosphodiesterase (PDE) activity. The GGDEF-domain of PdeB harbors all amino acids required for GTP binding and stabilization of the transition state. This is not only true for *Sp*PdeB but was also stated by the Spormann group for *So*PdeB. Our in-depth sequence analysis of 50 homologues of PdeB from different *Shewanella* species showed that the conservation of these residues is a common feature of PdeB homologues. However, the GGDEF domain has no enzymatic activity as we showed by motility assays with the appropriate mutants. This also agrees with the existing literature about *So*PdeB, where the authors determined the diguanylate cyclase activity *in vitro* (Chao et al., 2013). So far, it was unclear why PdeB does not exhibit diguanylate cyclase (DGC) activity. We addressed this question by *in silico* analysis and found that a highly conserved aspartic acid is exchanged with a glutamic acid at position $E467_{SpPdeB}$, which usually forms a salt bridge with a C-terminal lysine at position $K578_{SpPdeB}$. This sequential feature was overlooked before, since aspartic acid and glutamic acid are both negatively charged amino acids and are sometimes interchangeable. Since this

residue connects the central part with the C-terminal part of the GGDEF domain, I hypothesized that this variation alters the structure and prevents DGC activity. The exact structural consequences are currently not solved, but since E467 $_{Sp}$PdeB is located close to the active center we think that the structure of the reaction center might be altered. This could for example prevent the nucleophilic attack onto the α-phosphorous atoms (Schirmer, 2016).

However, we found that the GGDEF domain is still able to bind GTP *in vitro*. Additionally, we observed that mutating the A-site of the GGDEF domain leads to loss of PDE activity, suggesting a regulatory function of the GGDEF domain in dependence of GTP binding. The majority of EAL domains containing PDEs encode a GGDEF domain upstream of the EAL domain. *S. putrefaciens* CN-32 for example encodes 25 EAL domain proteins out of which 21 occur as GGDEF-EAL hybrid proteins. Considering the domain organization of these proteins, most seem to have evolved by gene duplication. While the GGDEF domain of such GGDEF-EAL hybrid proteins can exhibit enzymatic activity, they mostly function as regulatory domains for the EAL domain by allosterically binding GTP (Mantoni et al., 2018). Mantoni and colleagues solved the structural basis of this process using the GGDEF-EAL protein RmcA as model. This protein has a similar domain organization as PdeB with a periplasmic region followed by a PAS-PAS-PAS-LOV region and a GGDEF-EAL module. However, in contrast to PdeB, this enzyme exhibits DGC and PDE activity. In their study the authors were able to solve the crystal structure in presence and absence of GTP and found that a helical structure (‘hinge helix’) connects the GGDEF with the EAL domain. Their model protein crystallized as dimer in which both GGDEF monomers have bound one GTP molecule. They found that GTP binding induces a conformational change of the hinge helix that results in the formation of a competent EAL dimer. This active state is stabilized by the formation of a salt bridge, where an arginine of the hinge helix interacts with an aspartic acid of the EAL domain (Mantoni et al., 2018). Thus, we predicted the structure of the PAS-GGDEF-EAL region of PdeB by using the Phyre2 tool and found that this crucial hinge helix is predicted to be present in PdeB. We propose that the GTP binding to GGDEF$_{PdeB}$ results in rearrangement of the hinge helix and induces the formation of a competent dimer. However, further structural studies are needed to verify this hypothesis. Future works should aim at solving the structure of the GGDEF-EAL region of PdeB by crystallization or Cryo-EM. The question whether the hinge helix of PdeB in fact interacts with its EAL domain could also be approached by *in silico* analysis followed by the introduction of mutations into the amino acids of interest and then using motility assays as read-out for PDE activity.

We found that the GGDEF domain of PdeB binds c-di-GMP with micromolar affinity. Since the cellular GTP level is in the milimolar range, the binding site of GGDEF$_{PdeB}$ should be

occupied under normal conditions (Chong Liu et al., 2018). However, the GTP pool can be depleted when the cell faces nutrient and amino acid starvation (Chong Liu et al., 2018; Traxler et al., 2008). Therefore, it may be possible that the activity of PdeB is limited to nutrient rich conditions. A similar conclusion was made by Chong Liu and colleagues for the protein PA0575. As described earlier, PA0575 is a hybrid GGDEF-EAL protein that can bind GTP with its GGDEF domain and the PDE activity of its EAL domain is regulated by this process. The authors hypothesyze that this may be a strategy to “promote the decrease in c-di-GMP levels only under maximal biosynthetic potential” (Chong Liu et al., 2018).

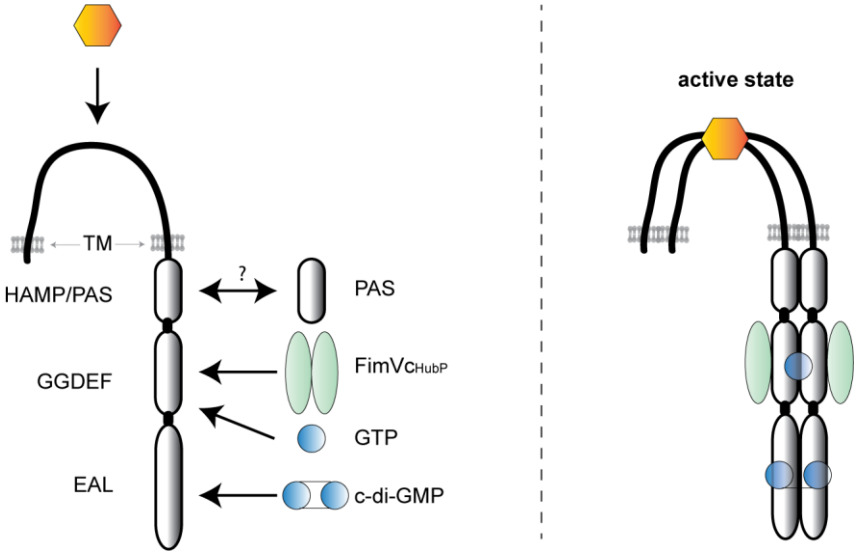

Figure 4.2) Regulation of PdeB. The PDE PdeB has two transmembrane domains that flank a long periplasmic region. We assume that this region can bind a yet unknown ligand. The PAS domain is assumed to mediate oligomerization. The GGDEF-domain can bind $FimVc_{HubP}$ and GTP and both ligands are required for full PDE activity. The EAL-domain is enzymatically active and can bind and degrade c-di-GMP.

The data that we obtained shows that the GTP binding alone is not sufficient for full induction of PDE activity. We found that the landmark protein HubP serves as on-switch for the EAL domain by interacting with the I-site and C-terminal region of $GGDEF_{PdeB}$. When we inserted mutations that prevent the interaction with HubP we found that the PDE activity was drastically reduced. Interestingly, one of the binding sites is located in direct proximity to the hinge helix that connects the GGDEF- with the EAL-domain. Thus, we think that not only GTP binding but also HubP binding is required to induce the conformational change of the hinge helix and activate full PDE activity. A model for the regulation of PdeB is shown in **fig. 4.2**.

4.4 Polar localization of PdeB is mediated by its GGDEF domain

We previously demonstrated that the GGDEF domain of PdeB recruits the protein to the flagellated cell pole. Using several methods such as HDX-MS, CL-MS and *in silico* analysis we succeeded in identifying crucial residues that are involved in this process. These amino acids are located at three different positions in the primary sequence: At the degenerated RxxD motif, the degenerated ER motif and the far C-terminal region of the GGDEF domain. These results were confirmed by fluorescence microscopy and single-molecule microscopy, where reduced polar localization was observed when these residues were mutated. While the GGDEF-domain of PdeB encodes all residues that are involved in GTP- and cofactor binding, the group of Alfred Spormann postulated that this domain lacks enzymatic activity. Using sequence analysis, we attributed this to an unusual variation in a negatively charged residue that usually forms a salt bridge with a lysine located within the C-terminal region of the domain. It is possible that this structural feature is not only the major cause of lacking DGC activity, but that it might also be crucial to allow the interaction with HubP. It was found by CL-MS that $FimVc_{HubP}$ was crosslinked to the salt-bridge forming C-terminal lysine $K575_{SoPdeB}$. When we exchanged this lysine to the small amino acid serine, we observed a 100-fold increased K_D-value. This could either be attributed to disruption of the described salt-bridge, or $K575_{SoPdeB}$ could directly interact with HubP. Since the protein is not suitable for crystallization, this question could be approached by Cryo-EM. In close proximity to this residue we found another lysine ($K577_{SoPdeB}$ / $K580_{SpPdeB}$) that influences the polar localization of PdeB and the affinity to HubP. This residue is fully conserved among PdeB homologues of *Shewanella* species, but varies in *bona fide* DGCs (Schirmer, 2016). Hence, we postulate that this lysine residue directly interacts with HubP and is involved in the polar recruitment of PdeB.

Further residues that were found to regulate the localization of PdeB and influence the affinity to HubP are located at the two different regions of the I-site of the GGDEF-domain. One common feature of interaction surfaces is that they are surface exposed. Usually, I-sites of GGDEF domains bind c-di-GMP and lead to inhibition of DGC activity by immobilizing the protomers of the GGDEF complex (Schirmer, 2016). Since the I-site already forms a surface exposed pocket, only minor changes are necessary to obtain a new function. We found that a positively charged lysine ($K524_{SoPdeB}$ / $K527_{SpPdeB}$) is present in the I-site of $GGDEF_{PdeB}$ instead of a negatively charged glutamic acid. We hypothesize that this variation changes the surface charge of the I-site and is the main driver for the interaction with HubP. Our *in silico* data shows that this lysine is fully conserved among PdeB homologues. Thus, not only the charge but also the shape of this residue may be important, since no other positively charged amino acid was found at this position. Possibly, the backbone of this lysine stabilizes the

alpha helix that is formed by this region, since exchange to the small amino acid serine led to destabilization and increased aggregation of this protein, while exchange to the larger amino acid glutamic acid did not have such an effect. However, this question is difficult to approach since it would require solving the structure of the GGDEF domain with very high resolution. Another residue is located at position $Q525_{So\text{PdeB}}$/$Q528_{Sp\text{PdeB}}$ in immediate proximity to the described lysine. In canonical GGDEF domains, this residue is a conserved arginine that directly binds the c-di-GMP molecule (Schirmer, 2016). Homologues of PdeB do not always encode an arginine at this position, but either a large hydrophilic or positively charged residue. *S. putrefaciens* CN-32 and *S. oneidensis* MR-1 both contain a glutamine at this position. We previously demonstrated that the GGDEF domain of PdeB is not able to bind c-di-GMP to its I-site. The variation at position $Q525_{So\text{PdeB}}$/$Q528_{Sp\text{PdeB}}$ is one of the reasons why this function is not present in $GGDEF_{PdeB}$. While $Q525_{So\text{PdeB}}$/$Q528_{Sp\text{PdeB}}$ and $K524_{So\text{PdeB}}$/$K527_{Sp\text{PdeB}}$ are not in close proximity to the RxxD motif on the primary sequence, studies on the structure of GGDEF domains show that they are in the tertiary structure (PDB IDs: 3QYY, 5XGB, 6ZXB). In functional I-sites, the arginine and aspartic acid of the RxxD motif are essential for c-di-GMP binding and are not interchangeable (Schirmer, 2016). In PdeB homologues, however, both residues vary between different species. For the used model organisms *S. putrefaciens* CN-32 and *S. oneidensis* MR1 the arginine is exchanged to the smallest amino acid glycine and the aspartic acid to glutamic acid. Together with the two previously described variations in the primary sequence of the I-site of $GGDEF_{PdeB}$, these are the reasons why $GGDEF_{PdeB}$ is not able to bind c-di-GMP in its I-site. Instead, our data shows that all four residues located in the I-site are directly involved in the interaction with the C-terminal region of HubP and therefore mediate the polar localization of PdeB.

Our data suggests that the main driver for the $GGDEF_{PdeB}$-$FimVc_{HubP}$ interaction may be electrostatic interactions. This is supported by our *in silico* data and the solved crystal structure of FimV of *P. aeruginosa* (PDB: 4MBQ), since this protein domain is almost completely negatively charged on the surface. However, one should be aware that our screening mainly focused on unusual positively charged residues. Thus, we expect that additional hydrophobic amino acids contribute to the $GGDEF_{PdeB}$-$FimVc_{HubP}$ interaction but were not identified by the used methods yet.

Currently there is not much known about how HubP can recruit different proteins to the cell pole. To date, only the structure of the 50 amino acid long C-terminal region of *P. aeruginosa* FimV protein (PDB: 4MBQ) was solved. The data obtained in the HDX-MS and iSCAMs experiments may give new insight into the mechanism of action: The stoichiometry of the $GGDEF_{PdeB}$-$FimVc_{HubP}$ complex was determined to be 2:2 in iSCAM experiments. However, no dimer of $FimVc_{HubP}$ was observed when the single $FimVc_{HubP}$ protein was analyzed.

Instead, we did not detect any signal corresponding to $FimVc_{HubP}$ when we analyzed the single protein. This can only be interpreted in a way that $FimVc_{HubP}$ is present as monomer under these conditions, since the monomeric protein can't be detected in iSCAMs as it does not fulfill the 30 kDa requirement of the machine. We therefore postulate that the oligomerization state of $FimVc_{HubP}$ changes upon binding to $GGDEF_{PdeB}$. This hypothesis is further supported by the obtained HDX-MS data: When $FimVc_{HubP}$ is in complex with its interaction partner the deuterium exchange of a large region was altered. This would be untypical for the binding of a single interaction partner but hints towards oligomerization of $FimVc_{HubP}$ when it is bound to $GGDEF_{PdeB}$.

After our first study about the GGDEF-mediated polar targeting was published (Rossmann & Rick et al., 2019), another group found that in *P. aeruginosa* an active DGC (DgcP) also interacts with the landmarkprotein FimV (Nicastro et al., 2020). In contrast to PdeB, DgcP consists of a GGDEF domain with active DGC activity, but has no EAL domain. Upstream of the GGDEF domain, a region with no homology to known domains is located. We analyzed the primary sequence of this protein but found no similarities to the binding region of $GGDEF_{PdeB}$. It seems that DgcP utilizes a different mechanism, since it is an active DGC and likely requires the I-site for end product inhibition. Apart from that, the authors of the study claim that DgcP does not interact with the C-terminal region of FimV but a cytoplasmic region in the middle of the primary sequence (Nicastro et al., 2020). These major differences might explain why DgcP and PdeB utilize different modes of action to interact with their landmark protein. Another factor may be that the sequence and client proteins of HubP orthologs vary between species (Buensuceso et al., 2016; Nicastro et al., 2020; Rossmann et al., 2015). This might also explain why $GGDEF_{PdeB}$ only interacts with the FimVc-domains of *Shewanella* species, and why we did not observe interaction with the FimVc-domains of *L. pneumophila* or *P. aeruginosa* (data not shown). However, this could be exploited for further *in silico* analysis to identify residues that are specific to $FimVc_{HubP}$ of *Shewanella* to identify residues that directly interact with $GGDEF_{PdeB}$. This could be of great interest, since the mode of action how HubP binds its interaction partners is currently unknown.

With the given results it could be possible that PdeB also interacts with another unknown factor. One indicator for that is the fact that deletion of the $FimVc_{HubP}$-domain leads to drastic reduction of polar PdeB-sfGFP fluorescence, but not full absence. However, this interaction would also be mediated by the GGDEF-domain of PdeB, since deletion of $GGDEF_{PdeB}$ results in full absence of polar fluorescence. It could be possible that $GGDEF_{PdeB}$ might also interacts with different region of HubP, but the obtained results do not support this hypothesis, since no interaction with the other cytoplasmic regions of HubP was observed in B2H assays. Another indicator for a second interaction partner would be the low diffusion

rates of PdeB-mVenus *in vivo*, which were observed during single molecule microscopy. However, this could also be explained by the extraordinary high affinity of the $GGDEF_{PdeB}$-$FimVc_{HubP}$ interaction with a K_D value in the nanomolar range.

4.5 PdeB creates phenotypic heterogeneity and asymmetric cell division

But what are the consequences of the GGDEF-mediated polar localization? The first hypotheses were that PdeB might act locally, either by creating local gradients (**fig. 4.3**) or by regulating the polar flagella system through direct protein-protein interaction.

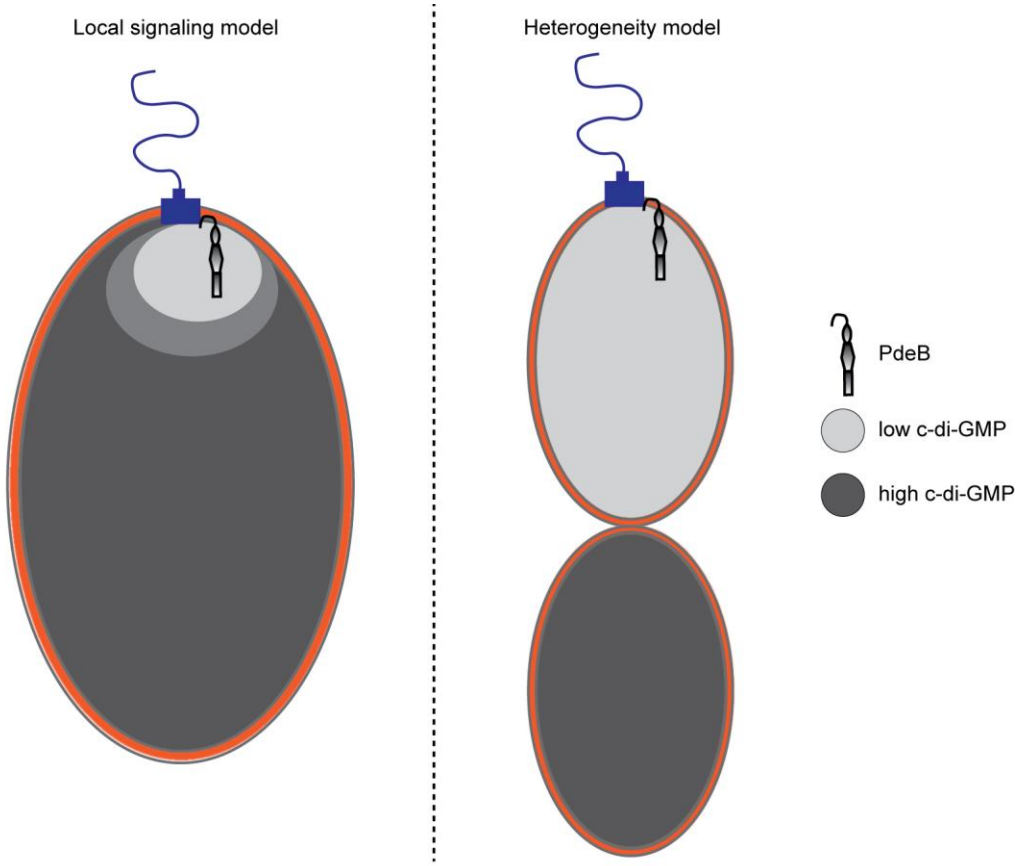

Figure 4.3) Local signaling and heterogeneity model. The polar localization of PdeB made two models possible: Either PdeB acts locally by creating local gradients (left, local signaling model), or PdeB creates heterogeneity by asymmetric cell division (right, heterogeneity model). Our results make the local model unlikely, since PdeB was found to act on global targets and not on the polar flagellum. Instead, we assume that the polar localization results in a mother cell with low c-di-GMP levels and a daughter cell with high c-di-GMP levels. A similar model was published in Nicastro et al., 2020, Kulasekara et al., 2013 and Laventje et al., 2019

However, these possibilities are quite unlikely with our obtained results. While PdeB localizes to the flagellated pole, we did not find altered transcription or activity of this system in presence or absence of *pdeB*. Instead, we found that PdeB regulates the lateral flagella system at the transcriptional and posttranslational level. Additionally, we found that PdeB regulates the MSHA- and Bpf-system which are both located subpolarly. Thus, we propose that PdeB does not regulate a local pool of c-di-GMP but instead the global level. The polar localization results in generation of two phenotypically different cells after cell division, where the mother cell inherits polarly localized PdeB, but the daughter cell does not. The extraordinary high affinity of the $GGDEF_{PdeB}$-$FimVc_{HubP}$ interaction assures that the daughter cell does not inherit PdeB molecules and the $FimVc_{HubP}$ dependent activation assures that only the mother cell has active PdeB molecules. Another factor that is important in this process is the low production rate of PdeB. Our transcriptional analysis shows that *pdeB* is weakly transcribed and we determined that cells usually only harbor around six PdeB molecules. The low production may also be the reason why HubP localizes early at the new pole but PdeB does not. Considering the signal intensity during fluorescence microscopy, HubP is produced in higher amounts than PdeB. Additionally, we observed that more HubP molecules localize at the old pole than the new pole. Therefore, when new PdeB molecules are produced before the cell division is completed; the chance that they localize at the old pole is higher than at the new pole. Another possibility why PdeB localizes late at the new pole is that the binding site of HubP could be occupied by other proteins. As previously stated, HubP interacts with a variety of client proteins such as chemotaxis compounds (F. Rossmann et al., 2015). However, this hypothesis is quite unlikely since PdeB would likely replace other client proteins due to its high affinity to HubP. However, it is likely that this process is more complex and controlled by polar identity. Polar identity can be established by numerous factors, such as peptidoglycan with specific features, lipid content, membrane curvature and proton motif force and polar determinants (Davis & Waldor, 2013). All these factors could contribute to observation that PdeB is limited to the old pole.

Taken together, the polar localization leads to asymmetric cell division, where only the mother cell obtains PdeB molecules. Thus, the PDE activity of PdeB leads to the formation of a mother cell with low c-di-GMP levels and a daughter cell with high c-di-GMP levels. This is further assured by the HubP-dependent activation of PDE activity: Even when the daughter cell inherits some PdeB molecules by chance, they remain inactive as long as they are not recruited to the cell pole.

PdeB was found to be epistatic to other tested DGCs. This means that the PDE activity of PdeB overrules the signal of other c-di-GMP producing and degrading enzymes when PdeB

is active. However, after cell division the daughter cell does not harbor active PdeB molecules. Thus, the other inherited PDEs and DGCs determine the cellular c-di-GMP level after cell division. This could serve as some kind of decision point were the other c-di-GMP-related enzymes determine the metabolic activity of the cell (**fig. 4.4**). Since c-di-GMP does not only regulate the motile to sessile transition but also anabolic and catabolic pathways (Römling et al., 2013), this decision point could be crucial to optimize the metabolic activity before the epistatic PDE activity of PdeB gets activated in the daughter cell.

To understand the benefit of this process it is necessary to focus on the population instead of on the single cell level. We investigated this process by observing the cell divisions of cells in presence and absence of active PdeB. Under these conditions, we observed that PdeB induces the production of two phenotypically different cells after cell division. The mother cell exhibits low c-di-GMP levels and high motility, while the daughter cell has high c-di-GMP levels and extends its MSHA-pili and produces adhesion factors. We also found that the GGDEF domain of PdeB binds GTP and this process is essential for full PDE activity. The GTP-level decreases during cell division and, therefore, it is likely that PdeB is inactive during cell division. When the division is completed, the GTP level raises again, which results in increased activity of PdeB and low c-di-GMP levels of the mother cell. Then, the mother cell detaches but the daughter cell remains attached to the surface. This could be an efficient colonization strategy (**fig. 4.5**).

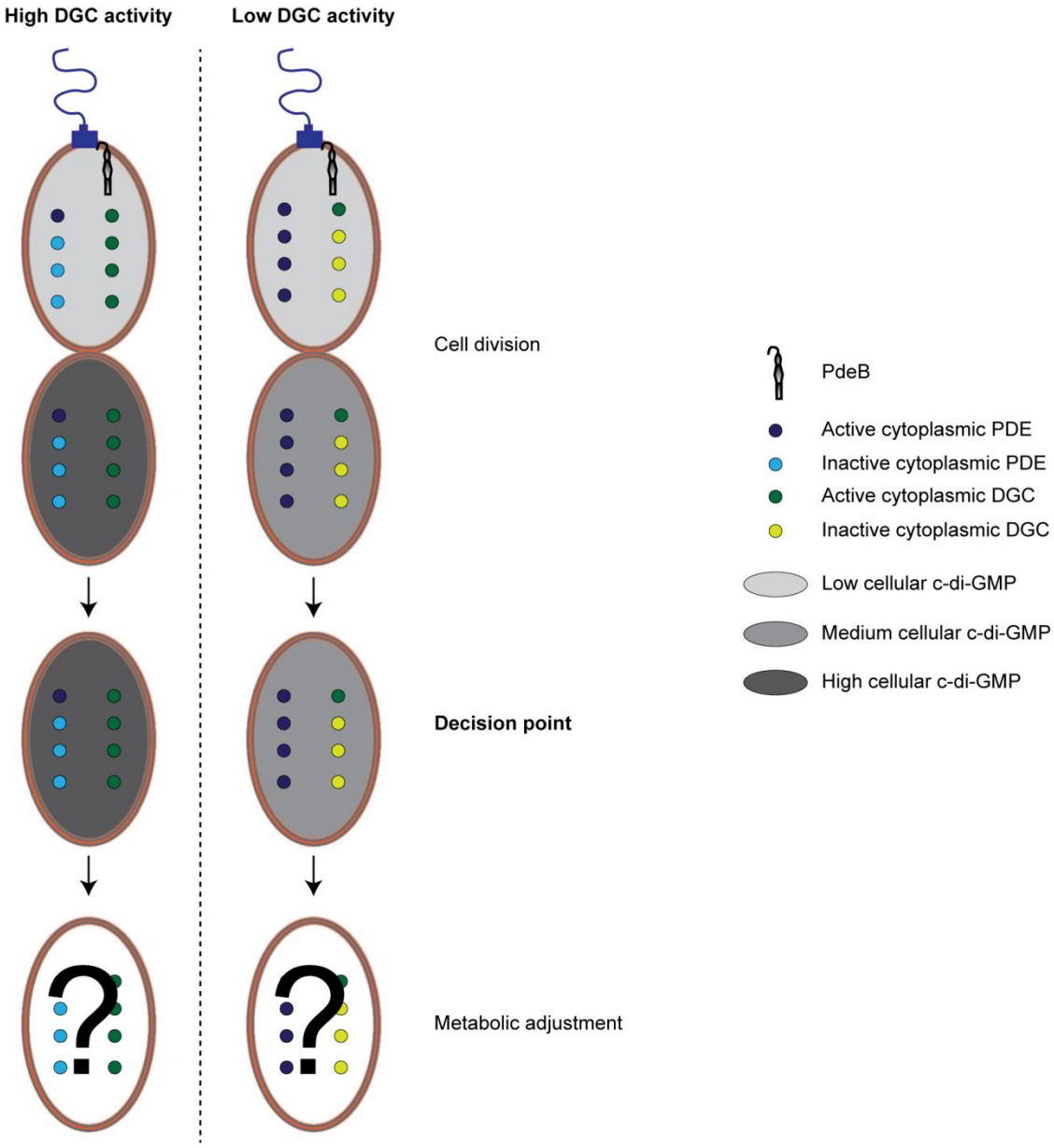

Figure 4.4) Decision point hypothesis. PdeB was found to be epistatic to other tested DGCs. After cell division, the influence of PdeB is absent in the daughter cell and the inherited cellular DGCs and PDEs determine the cellular c-di-GMP level. This could be some sort of decision point, where the cell could adjust its metabolic activity, since c-di-GMP regulates numerous processes such as the use of energy- and carbon sources (Römling et al., 2013).

We propose that the main driver for this differentiation in *Shewanella* is PdeB. Similar mechanisms were also observed in other bacteria, like *P. aeruginosa*. The group of Urs Jenal observed that in *P. aeruginosa* the c-di-GMP level rapidly increases when the cell adheres to a surface. The c-di-GMP receptor FimW localizes to the new cell pole in response to the altered c-di-GMP level. The cell then undergoes asymmetric cell division. Importantly,

P. aeruginosa harbors an active PDE called Pch which localizes at the old pole in a similar fashion as PdeB. Thus, the mother cell decreases its c-di-GMP level and switches back to a motile lifestyle, while the daughter cell remains adhered to the surface (Laventie et al., 2019, Kulasekara et al., 2013)

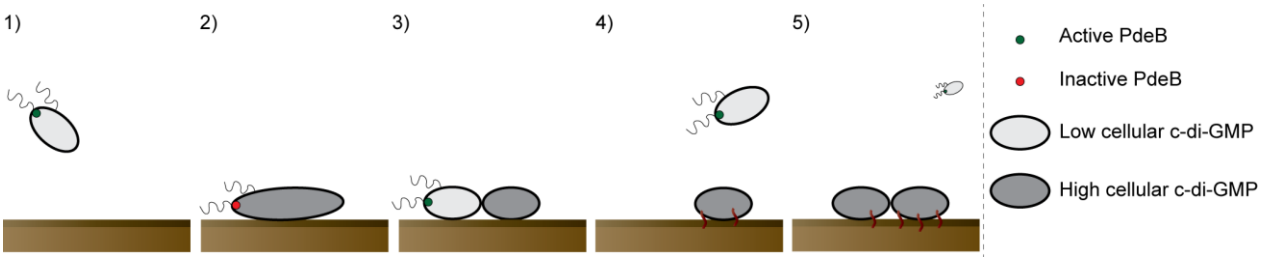

Figure 4.5) Phenotypical heterogeneity. The polar localization of PdeB was found to create a motile mother and a sessile daughter cell. When a motile cell attaches to a surface and divides (1-2) it is likely that the c-di-GMP level increases. Then, when the fission is completed (3), the daughter cell does not inherit PdeB and remains a high c-di-GMP level. The mother cell then detaches from the surface (4), while the daughter cell remains sessile and colonizes the surface (5). Similar models were published by: Jones et al., 2015; Laventie et al., 2019, Kulasekara et al., 2013

We also found that *pdeB* is constitutively expressed. Additionally, the group of Alfred Spormann found that *pdeB* not only creates a phenotype in liquid medium, but also in biofilms (Chao et al., 2013). Cells inside biofilms are phenotypically diverse, since the nutrient and oxygen availability differ strongly between surface exposed layers and the inner parts of the biofilm. In general, nutrient availability is very low in the inner part of biofilms, inducing the production of hunger signals like ppGpp. Also, the activator of PdeB may not be transported to the inner regions of biofilms. Therefore, it is likely that PdeB is inactive in the inner parts of biofilms. In contrast to that, the nutrient availability on the surface of biofilms is high and cells in the outer layers are likely to be exposed to the activator of PdeB. It is possible that the constitutive expression of *pdeB* promotes the production of new spreader cells that spontaneously detach from the surface, as outlined in **fig. 4.6**. Since the cells constitutively produce PdeB and the cells in the outer layer of cell associations are exposed to the activator of PdeB, PdeB may support the spontaneous formation of spreader cells. However, further studies are necessary to confirm this hypothesis. Attached cells would need to be observed by microscopy and the events of spontaneous detachment would need to be quantified in presence and absence of *pdeB*.

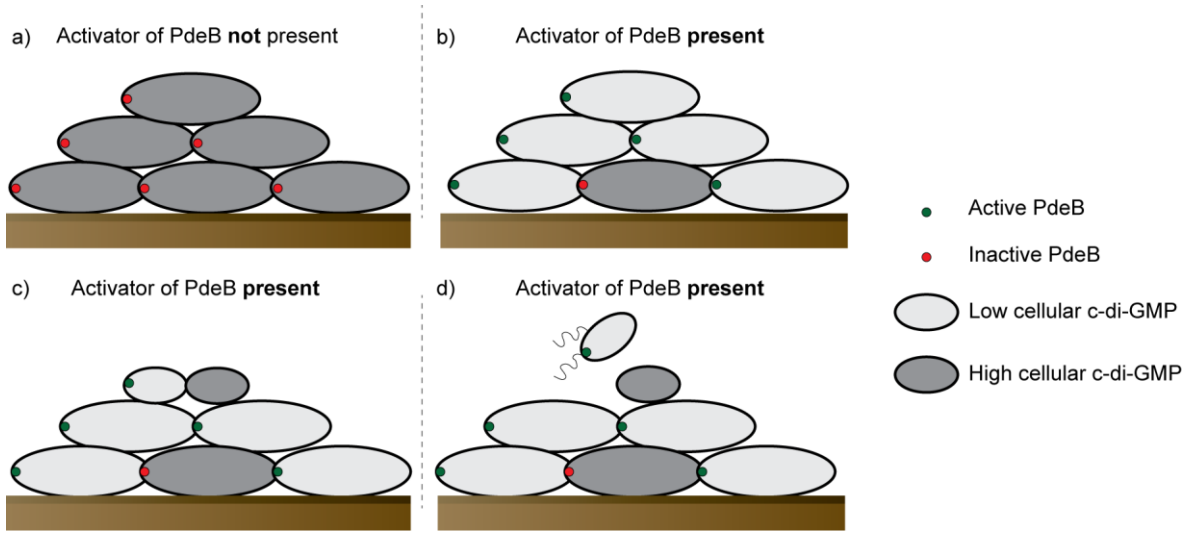

Figure 4.6) Model for spontaneous generation of spreader cells due to constitutive production of PdeB. PdeB is constitutively expressed. When the activator of PdeB is not present (1), all cells in a cell association have a high c-di-GMP level. When the activator of PdeB is present (2), cells that are exposed to it have active PdeB and, therefore, lower c-di-GMP levels than cells in the inner part of the biofilm. This low c-di-GMP level could increase the rate of spontaneously detaching cells (3-4).

The spontaneous production of spreader cells and the heterogeneity after cell division can be combined into a model of a PdeB dependent colonization strategy (**fig. 4.7**). When cells are brought into a new environment some cells will adhere to the surface while other use flagella mediated motility to spread into new regions. Our model suggests that the attached cells continue dividing and produce biofilm factors to increase the biomass on the colonized regions. The motile cells, however, spread further through the environment and leave non-motile daughter cells behind that colonize the new region (“touch-seed-and-go”). Thus, it can be concluded that the population prioritizes the increase of biomass over the quantity of spreader cells at this stage of colonization.

When the cell number increases in the colonized regions, the statistical chance to spontaneously generate spreader cells elevates. The constitutive production of PdeB might support this process, as outlined in **fig. 4.6**. This process assures the constant production of new spreader cells and assures the colonization of the new environment.

The postulated colonization strategy may be especially important in natural environments when the cells have competitors. It could be advantageous under these conditions to first focus on the increase of biomass to prevent that other bacterial species can colonize the same region. Additionally, this colonization model would be very energy efficient, since not all cells need to express motility and biofilm factors.

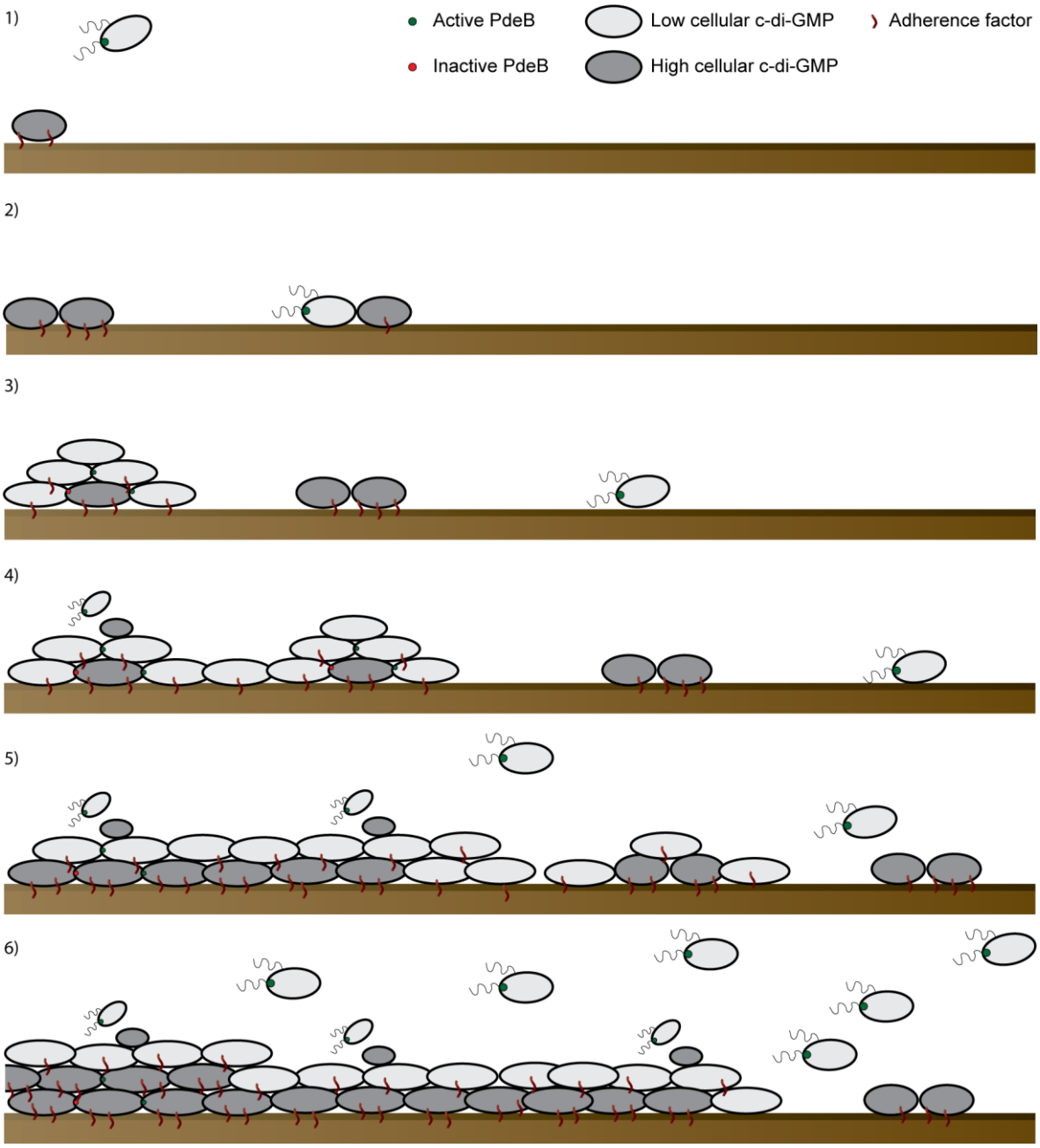

Figure 4.7) Combined colonization model. The previously shown models can be integrated into a combined model how the spatiotemporal organization of PdeB affects the colonization strategy. When cells colonize a new environment, motile cells spread in new regions while some cells remain attached and produce biofilm factors (1-2). After cell division the mother cell is still motile while the daughter cell remains attached to the surface (2-3). The attached cells increase the attached biomass and the activity of PdeB spontaneously produces new spreader cells (4-6). This results in a constant support of new motile spreader cells.

In this study we were able to unravel the structural basis of a novel function for GGDEF domains and found that this process governs the colonization behavior of *S. putrefaciens* CN-32. The results underline the importance of spatiotemporal organization and show how heterogeneity provides tremendous advantages for bacterial populations, especially during the adaption to rapidly changing environments and for the colonization of new habitats.

5. Bibliography

Ausmees, N., Mayer, R., Weinhouse, H., Volman, G., Amikam, D., Benziman, M., & Lindberg, M. (2001). Genetic data indicate that proteins containing the GGDEF domain possess diguanylate cyclase activity. *FEMS Microbiology Letters*, *204*(1), 163–167. https://doi.org/10.1111/j.1574-6968.2001.tb10880.x

Bähre, H., & Kaever, V. (2017). Identification and quantification of cyclic di-guanosine monophosphate and its linear metabolites by reversed-phase LC-MS/MS. In *Methods in Molecular Biology* (Vol. 1657, pp. 45–58). Humana Press Inc. https://doi.org/10.1007/978-1-4939-7240-1_5

Baker, A. E., Diepold, A., Kuchma, S. L., Scott, J. E., Ha, D. G., Orazi, G., Armitage, J. P., & O'Toole, G. A. (2016). PilZ domain protein FlgZ mediates cyclic di-GMP-dependent swarming motility control in pseudomonas aeruginosa. *Journal of Bacteriology*, *198*(13), 1837–1846. https://doi.org/10.1128/JB.00196-16

Bateman, A., & Khanna, A. (2014). *The Pfam Protein Families Database Enset improvement project View project Dicer-independent microRNA processing View project*. https://doi.org/10.1093/nar/gkh121

Bellini, D., Caly, D. L., Mccarthy, Y., Bumann, M., An, S. Q., Dow, J. M., Ryan, R. P., & Walsh, M. A. (2014). Crystal structure of an HD-GYP domain cyclic-di-GMP phosphodiesterase reveals an enzyme with a novel trinuclear catalytic iron centre. *Molecular Microbiology*, *91*(1), 26–38. https://doi.org/10.1111/mmi.12447

Blagotinsek, V., Schwan, M., Steinchen, W., Mrusek, D., Hook, J. C., Rossmann, F., Freibert, S. A., Kratzat, H., Murat, G., Kressler, D., Beckmann, R., Beeby, M., Thormann, K. M., & Bange, G. (2020). An ATP-dependent partner switch links flagellar C-ring assembly with gene expression. *Proceedings of the National Academy of Sciences of the United States of America*, *117*(34), 20826–20835. https://doi.org/10.1073/pnas.2006470117

Bobrov, A. G., Kirillina, O., Ryjenkov, D. A., Waters, C. M., Price, P. A., Fetherston, J. D., Mack, D., Goldman, W. E., Gomelsky, M., & Perry, R. D. (2011). Systematic analysis of cyclic di-GMP signalling enzymes and their role in biofilm formation and virulence in Yersinia pestis. *Molecular Microbiology*, *79*(2), 533–551. https://doi.org/10.1111/j.1365-2958.2010.07470.x

Briegel, A., Ortega, D. R., Tocheva, E. I., Wuichet, K., Zhuo, L., Songye, C., Müller, A., Iancu, C. V., Murphy, G. E., Dobro, M. J., Zhulin, I. B., & Jensen, G. J. (2009). Universal architecture of bacterial chemoreceptor arrays. *Proceedings of the National Academy of Sciences of the United States of America*, *106*(40), 17181–17186. https://doi.org/10.1073/pnas.0905181106

Bubendorfer, S., Held, S., Windel, N., Paulick, A., Klingl, A., & Thormann, K. M. (2012). Specificity of motor components in the dual flagellar system of Shewanella putrefaciens CN-32. *Molecular Microbiology*, *83*(2), 335–350. https://doi.org/10.1111/j.1365-2958.2011.07934.x

Bubendorfer, S., Koltai, M., Rossmann, F., Sourjik, V., & Thormann, K. M. (2014). Secondary bacterial flagellar system improves bacterial spreading by increasing the directional persistence of swimming. *Proceedings of the National Academy of Sciences of the United States of America*, *111*(31), 11485–11490. https://doi.org/10.1073/pnas.1405820111

Buensuceso, R. N. C., Nguyen, Y., Zhang, K., Daniel-Ivad, M., Sugiman-Marangos, S. N., Fleetwood, A. D., Zhulin, I. B., Junop, M. S., Howell, P. L., & Burrows, L. L. (2016). The Conserved

Tetratricopeptide Repeat-Containing C-Terminal Domain of Pseudomonas aeruginosa FimV Is Required for Its Cyclic AMP-Dependent and -Independent Functions. *Journal of Bacteriology*, *198*(16), 2263–2274. https://doi.org/10.1128/JB.00322-16

Busby, S., & Ebright, R. H. (1999). Transcription activation by catabolite activator protein (CAP). In *Journal of Molecular Biology* (Vol. 293, Issue 2, pp. 199–213). Academic Press. https://doi.org/10.1006/jmbi.1999.3161

Cai, Q., Li, Z., Ouyang, Q., Luo, C., & Gordon, V. D. (2016). Singly flagellated Pseudomonas aeruginosa chemotaxes efficiently by unbiased motor regulation. *MBio*, *7*(2). https://doi.org/10.1128/mBio.00013-16

Castro, M., Deane, S. M., Ruiz, L., Rawlings, D. E., & Guiliani, N. (2015). Diguanylate Cyclase Null Mutant Reveals That C-Di-GMP Pathway Regulates the Motility and Adherence of the Extremophile Bacterium Acidithiobacillus caldus. *PLOS ONE*, *10*(2), e0116399. https://doi.org/10.1371/journal.pone.0116399

Chan, C., Paul, R., Samoray, D., Amiot, N. C., Giese, B., Jenal, U., & Schirmer, T. (2004). Structural basis of activity and allosteric control of diguanylate cyclase. *Proceedings of the National Academy of Sciences of the United States of America*, *101*(49), 17084–17089. https://doi.org/10.1073/pnas.0406134101

Chao, L., Rakshe, S., Leff, M., & Spormann, A. M. (2013). PdeB, a cyclic Di-GMP-specific phosphodiesterase that regulates Shewanella oneidensis MR-1 motility and biofilm formation. *Journal of Bacteriology*, *195*(17), 3827–3833. https://doi.org/10.1128/JB.00498-13

Chiavelli, D. A., Marsh, J. W., & Taylor, R. K. (2001). The Mannose-Sensitive Hemagglutinin of Vibrio cholerae Promotes Adherence to Zooplankton. *Applied and Environmental Microbiology*, *67*(7), 3220–3225. https://doi.org/10.1128/AEM.67.7.3220-3225.2001

Christen, M., Kulasekara, H. D., Christen, B., Kulasekara, B. R., Hoffman, L. R., & Miller, S. I. (2010). Asymmetrical distribution of the second messenger c-di-GMP upon bacterial cell division. *Science*, *328*(5983), 1295–1297. https://doi.org/10.1126/science.1188658

Claudine, B., & Harwood, C. S. (2013). Cyclic diguanosine monophosphate represses bacterial flagella synthesis by interacting with the Walker a motif of the enhancer-binding protein FleQ. *Proceedings of the National Academy of Sciences of the United States of America*, *110*(46), 18478–18483. https://doi.org/10.1073/pnas.1318972110

Cluzel, P., Surette, M., & Leibler, S. (2000). An ultrasensitive bacterial motor revealed by monitoring signaling proteins in single cells. *Science*, *287*(5458), 1652–1655. https://doi.org/10.1126/science.287.5458.1652

Cole, S. J., & Lee, V. T. (2016). Cyclic di-GMP signaling contributes to Pseudomonas aeruginosa-mediated catheter-associated urinary tract infection. *Journal of Bacteriology*, *198*(1), 91–97. https://doi.org/10.1128/JB.00410-15

Amikam, D., Galperin, M.Y. (2006). PilZ domain is part of the bacterial c-di-GMP binding protein. *Bioinformatics (Oxford, England)*, *22*(1), 3–6. https://doi.org/10.1093/BIOINFORMATICS/BTI739

Ryjenkov, Simm, Römling, Gomelsky (2006). The PilZ domain is a receptor for the second messenger c-di-GMP: the PilZ domain protein YcgR controls motility in enterobacteria. *The Journal of Biological Chemistry*, *281*(41), 30310–30314. https://doi.org/10.1074/JBC.C600179200

Davis, B. M., & Waldor, M. K. (2013). Establishing polar identity in gram-negative rods. *Current Opinion in Microbiology*, *16*(6), 752–759. https://doi.org/10.1016/J.MIB.2013.08.006

Dundas, C. M., Graham, A. J., Romanovicz, D. K., & Keitz, B. K. (2018). Extracellular Electron Transfer by Shewanella oneidensis Controls Palladium Nanoparticle Phenotype. *ACS Synthetic Biology*, *7*(12), 2726–2736. https://doi.org/10.1021/acssynbio.8b00218

Eli, D., Randall, T. E., Almblad, H., Harrison, J. J., & Banin, E. (2017a). Measuring Cyclic Diguanylate (c-di-GMP)-Specific Phosphodiesterase Activity Using the MANT-c-di-GMP Assay. In *Methods in molecular biology (Clifton, N.J.)* (Vol. 1657, pp. 263–278). https://doi.org/10.1007/978-1-4939-7240-1_20

Feirer, N., Xu, J., Allen, K. D., Koestler, B. J., Bruger, E. L., Waters, C. M., White, R. H., & Fuqua, C. (2015). A Pterin-Dependent Signaling Pathway Regulates a Dual-Function Diguanylate Cyclase-Phosphodiesterase Controlling Surface Attachment in Agrobacterium tumefaciens. *MBio*, *6*(4), e00156. https://doi.org/10.1128/mBio.00156-15

Felgner, S., Preusse, M., Beutling, U., Stahnke, S., Pawar, V., Rohde, M., Brönstrup, M., Stradal, T., & Häussler, S. (2020). Host-induced spermidine production in motile pseudomonas aeruginosa triggers phagocytic uptake. *ELife*, *9*, 1–56. https://doi.org/10.7554/ELIFE.55744

Ferreira, J. L., Gao, F. Z., Rossmann, F. M., Nans, A., Brenzinger, S., Hosseini, R., Wilson, A., Briegel, A., Thormann, K. M., Rosenthal, P. B., & Beeby, M. (2019). γ-proteobacteria eject their polar flagella under nutrient depletion, retaining flagellar motor relic structures. *PLOS Biology*, *17*(3), e3000165. https://doi.org/10.1371/journal.pbio.3000165

Floyd, K. A., Lee, C. K., Xian, W., Nametalla, M., Valentine, A., Crair, B., Zhu, S., Hughes, H. Q., Chlebek, J. L., Wu, D. C., Hwan Park, J., Farhat, A. M., Lomba, C. J., Ellison, C. K., Brun, Y. V., Campos-Gomez, J., Dalia, A. B., Liu, J., Biais, N., … Yildiz, F. H. (2020). c-di-GMP modulates type IV MSHA pilus retraction and surface attachment in Vibrio cholerae. *Nature Communications 2020 11:1*, *11*(1), 1–16. https://doi.org/10.1038/s41467-020-15331-8

Fujiu, K., Nakayama, Y., Iida, H., Sokabe, M., & Yoshimura, K. (2011). Mechanoreception in motile flagella of Chlamydomonas. *Nature Cell Biology*, *13*(5), 630–632. https://doi.org/10.1038/ncb2214

Karimova, Pidoux, Ullmann, Ladant (1998). A bacterial two-hybrid system based on a reconstituted signal transduction pathway. *Proceedings of the National Academy of Sciences of the United States of America*, *95*(10), 5752–5756. https://doi.org/10.1073/PNAS.95.10.5752

Gibson, D. G., Young, L., Chuang, R. Y., Venter, J. C., Hutchison, C. A., & Smith, H. O. (2009). Enzymatic assembly of DNA molecules up to several hundred kilobases. *Nature Methods*, *6*(5), 343–345. https://doi.org/10.1038/nmeth.1318

Gilles-Gonzalez, M. A., & Gonzalez, G. (2004). Signal transduction by heme-containing PAS-domain proteins. In *Journal of Applied Physiology* (Vol. 96, Issue 2, pp. 774–783). J Appl Physiol (1985). https://doi.org/10.1152/japplphysiol.00941.2003

Govindarajan, S., Nevo-Dinur, K., & Amster-Choder, O. (2012). Compartmentalization and spatiotemporal organization of macromolecules in bacteria. In *FEMS Microbiology Reviews* (Vol. 36, Issue 5, pp. 1005–1022). Oxford Academic. https://doi.org/10.1111/j.1574-6976.2012.00348.x

Hajam, I. A., Dar, P. A., Shahnawaz, I., Jaume, J. C., & Lee, J. H. (2017). Bacterial flagellin-a potent

immunomodulatory agent. In *Experimental and Molecular Medicine* (Vol. 49, Issue 9, p. 373). Nature Publishing Group. https://doi.org/10.1038/emm.2017.172

Hall, C. L., & Lee, V. T. (2018). Cyclic-di-GMP regulation of virulence in bacterial pathogens. In *Wiley Interdisciplinary Reviews: RNA* (Vol. 9, Issue 1). Blackwell Publishing Ltd. https://doi.org/10.1002/wrna.1454

Hallberg, Z. F., Wang, X. C., Wright, T. A., Nan, B., Ad, O., Yeo, J., & Hammond, M. C. (2016). Hybrid promiscuous (Hypr) GGDEF enzymes produce cyclic AMP-GMP (3', 3'-cGAMP). *Proceedings of the National Academy of Sciences of the United States of America*, *113*(7), 1790–1795. https://doi.org/10.1073/pnas.1515287113

Harshey, R. M. (2003). Bacterial Motility on a Surface: Many Ways to a Common Goal. *Annual Review of Microbiology*, *57*(1), 249–273. https://doi.org/10.1146/annurev.micro.57.030502.091014

Hau, H. H., & Gralnick, J. A. (2007). Ecology and Biotechnology of the Genus Shewanella. *Http://Dx.Doi.Org/10.1146/Annurev.Micro.61.080706.093257*, *61*, 237–258. https://doi.org/10.1146/ANNUREV.MICRO.61.080706.093257

Heckler, I., Hossain, S., & Boon, E. M. (2020). Heme inhibits the activity of a c-di-GMP phosphodiesterase in Vibrio cholerae. *Biochemical and Biophysical Research Communications*, *529*(4), 1112–1116. https://doi.org/10.1016/j.bbrc.2020.06.048

Hengge, R. (2016). Trigger phosphodiesterases as a novel class of c-di-GMP effector proteins. In *Philosophical Transactions of the Royal Society B: Biological Sciences* (Vol. 371, Issue 1707). Royal Society of London. https://doi.org/10.1098/rstb.2015.0498

Hennig, S., Strauss, H. M., Vanselow, K., Yildiz, Ö., Schulze, S., Arens, J., Kramer, A., & Wolf, E. (2009). Structural and functional analyses of PAS domain interactions of the clock proteins Drosophila PERIOD and mouse period2. *PLoS Biology*, *7*(4), 0836–0853. https://doi.org/10.1371/journal.pbio.1000094

Hickman, J. W., & Harwood, C. S. (2008). Identification of FleQ from Pseudomonas aeruginosa as a c-di-GMP-responsive transcription factor. *Molecular Microbiology*, *69*(2), 376–389. https://doi.org/10.1111/j.1365-2958.2008.06281.x

Høiby, N., Bjarnsholt, T., Givskov, M., Molin, S., & Ciofu, O. (2010). Antibiotic resistance of bacterial biofilms. In *International Journal of Antimicrobial Agents* (Vol. 35, Issue 4, pp. 322–332). Int J Antimicrob Agents. https://doi.org/10.1016/j.ijantimicag.2009.12.011

Holt, H. M., Gahrn-Hansen, B., & Bruun, B. (2005). Shewanella algae and Shewanella putrefaciens: Clinical and microbiological characteristics. In *Clinical Microbiology and Infection* (Vol. 11, Issue 5, pp. 347–352). Blackwell Publishing Ltd. https://doi.org/10.1111/j.1469-0691.2005.01108.x

Spöring, Martinez ,

Hotz , Schwarz-Linek , Grady, Nava-Sedeño, Vissers, Singer, Rohde, Bourquin, Hatzikirou, Poon, Dufour, Erhardt (2018). Hook length of the bacterial flagellum is optimized for maximal stability of the flagellar bundle. *PLoS Biology*, *16*(9). https://doi.org/10.1371/JOURNAL.PBIO.2006989

Lassak, Henche, Binnenkade, Thormann (2010). ArcS, the cognate sensor kinase in an atypical Arc system of Shewanella oneidensis MR-1. *Applied and Environmental Microbiology*, *76*(10), 3263–3274. https://doi.org/10.1128/AEM.00512-10

Jarrod Smith, T., Sondermann, H., & O'Toolea, G. A. (2018). Type 1 does the two-step: Type 1

secretion substrates with a functional periplasmic intermediate. *Journal of Bacteriology*, *200*(18). https://doi.org/10.1128/JB.00168-18

Jones, C. J., Utada, A., Davis, K. R., Thongsomboon, W., Zamorano Sanchez, D., Banakar, V., Cegelski, L., Wong, G. C. L., & Yildiz, F. H. (2015). C-di-GMP Regulates Motile to Sessile Transition by Modulating MshA Pili Biogenesis and Near-Surface Motility Behavior in Vibrio cholerae. *PLOS Pathogens*, *11*(10), e1005068. https://doi.org/10.1371/journal.ppat.1005068

Josenhans, C., & Suerbaum, S. (2002). The role of motility as a virulence factor in bacteria. *International Journal of Medical Microbiology*, *291*(8), 605–614. https://doi.org/10.1078/1438-4221-00173

Schuhmacher, Rossmann, Dempwolff, Knauer, Altegoer, Steinchen, Dörrich, Klingl, Stephan, Linne, Thormann, Bange (2015). MinD-like ATPase FlhG effects location and number of bacterial flagella during C-ring assembly. *Proceedings of the National Academy of Sciences of the United States of America*, *112*(10), 3092–3097. https://doi.org/10.1073/PNAS.1419388112

Pratt , Tamayo, Tischler, Camilli (2007). PilZ domain proteins bind cyclic diguanylate and regulate diverse processes in Vibrio cholerae. *The Journal of Biological Chemistry*, *282*(17), 12860–12870. https://doi.org/10.1074/JBC.M611593200

Kelley, L. A., Mezulis, S., Yates, C. M., Wass, M. N., & Sternberg, M. J. E. (2015). The Phyre2 web portal for protein modeling, prediction and analysis. *Nature Protocols 2015 10:6*, *10*(6), 845–858. https://doi.org/10.1038/nprot.2015.053

Ko, J., Ryu, K. S., Kim, H., Shin, J. S., Lee, J. O., Cheong, C., & Choi, B. S. (2010). Structure of PP4397 Reveals the Molecular Basis for Different c-di-GMP Binding Modes by Pilz Domain Proteins. *Journal of Molecular Biology*, *398*(1), 97–110. https://doi.org/10.1016/J.JMB.2010.03.007

Kobayashi, K., Saitoh, T., Shah, D. S. H., Ohnishi, K., Goodfellow, I. G., Sockett, R. E., & Aizawa, S. I. (2003). Purification and characterization of the flagellar basal body of Rhodobacter sphaeroides. *Journal of Bacteriology*, *185*(17), 5295–5300. https://doi.org/10.1128/JB.185.17.5295-5300.2003

Krogh, A., È rn Larsson, B., von Heijne, G., & L Sonnhammer, E. L. (n.d.). *Predicting Transmembrane Protein Topology with a Hidden Markov Model: Application to Complete Genomes*. https://doi.org/10.1006/jmbi.2000.4315

Kuchma, S. L., Delalez, N. J., Filkins, L. M., Snavely, E. A., Armitage, J. P., & O'Toole, G. A. (2015). Cyclic di-GMP-mediated repression of swarming motility by Pseudomonas aeruginosa PA14 Requires the MotAB stator. *Journal of Bacteriology*, *197*(3), 420–430. https://doi.org/10.1128/JB.02130-14

Kulasekara, B. R., Kamischke, C., Kulasekara, H. D., Christen, M., Wiggins, P. A., Miller, S. I., Aldridge, P., Paul, R., Goymer, P., Rainey, P., Jenal, U., Arora, S., Ritchings, B., Almira, E., Lory, S., Ramphal, R., Baker, M., Wolanin, P., Stock, J., … Solano, C. (2013). c-di-GMP heterogeneity is generated by the chemotaxis machinery to regulate flagellar motility. *ELife*, *2*, e01402. https://doi.org/10.7554/eLife.01402

Kunz, S., Tribensky, A., Steinchen, W., Oviedo-Bocanegra, L., Bedrunka, P., & Graumann, P. L. (2020). Cyclic di-GMP signaling in bacillus subtilis is governed by direct interactions of diguanylate cyclases and cognate receptors. *MBio*, *11*(2). https://doi.org/10.1128/mBio.03122-19

Laventie, B. J., Sangermani, M., Estermann, F., Manfredi, P., Planes, R., Hug, I., Jaeger, T., Meunier, E.,

Broz, P., & Jenal, U. (2019). A Surface-Induced Asymmetric Program Promotes Tissue Colonization by Pseudomonas aeruginosa. *Cell Host and Microbe*, *25*(1), 140-152.e6. https://doi.org/10.1016/j.chom.2018.11.008

Letunic, I., Khedkar, S., & Bork, P. (2021). SMART: Recent updates, new developments and status in 2020. *Nucleic Acids Research*, *49*(D1), D458–D460. https://doi.org/10.1093/nar/gkaa937

Liu, Chong, Liew, C. W., Wong, Y. H., Tan, S. T., Poh, W. H., Manimekalai, M. S. S., Rajan, S., Xin, L., Liang, Z. X., Grüber, G., Rice, S. A., & Lescar, J. (2018). Insights into biofilm dispersal regulation from the crystal structure of the PAS-GGDEF-EAL region of RbdA from Pseudomonas aeruginosa. *Journal of Bacteriology*, *200*(3). https://doi.org/10.1128/JB.00515-17

Liu, Cong, Yang, J., Liu, L., Li, B., Yuan, H., & Liu, W. (2017). Sodium lactate negatively regulates Shewanella putrefaciens CN32 biofilm formation via a three-component regulatory system (LrbS-LrbA-LrbR). *Applied and Environmental Microbiology*, *83*(14). https://doi.org/10.1128/AEM.00712-17

Christen, Christen, Allan, Folcher, Jenö, Grzesiek, Jenal (2007). DgrA is a member of a new family of cyclic diguanosine monophosphate receptors and controls flagellar motor function in Caulobacter crescentus. *Proceedings of the National Academy of Sciences of the United States of America*, *104*(10), 4112–4117. https://doi.org/10.1073/PNAS.0607738104

Osorio-Valeriano, Altegoer, Steinchen, Urban, Ying Liu, Bange, Thanbichler (2019). ParB-type DNA Segregation Proteins Are CTP-Dependent Molecular Switches. *Cell*, *179*(7), 1512-1524.e15. https://doi.org/10.1016/J.CELL.2019.11.015

Macnab, R. M., & Aizawa, S. I. (1984). Bacterial Motility and the Bacterial Flagellar Motor. *Annual Review of Biophysics and Bioengineering*, *13*(1), 51–83. https://doi.org/10.1146/annurev.bb.13.060184.000411

Mantoni, F., Paiardini, A., Brunotti, P., D'Angelo, C., Cervoni, L., Paone, A., Cappellacci, L., Petrelli, R., Ricciutelli, M., Leoni, L., Rampioni, G., Arcovito, A., Rinaldo, S., Cutruzzolà, F., & Giardina, G. (2018). Insights into the GTP-dependent allosteric control of c-di-GMP hydrolysis from the crystal structure of PA0575 protein from *Pseudomonas aeruginosa*. *The FEBS Journal*, *285*(20), 3815–3834. https://doi.org/10.1111/febs.14634

Matsuyama, B. Y., Krasteva, P. V., Baraquet, C., Harwood, C. S., Sondermann, H., & Navarro, M. V. A. S. (2016). Mechanistic insights into c-di-GMP-dependent control of the biofilm regulator FleQ from Pseudomonas aeruginosa. *Proceedings of the National Academy of Sciences of the United States of America*, *113*(2), E209–E218. https://doi.org/10.1073/pnas.1523148113

Minamino, T. (2014). Protein export through the bacterial flagellar type III export pathway. In *Biochimica et Biophysica Acta - Molecular Cell Research* (Vol. 1843, Issue 8, pp. 1642–1648). Elsevier. https://doi.org/10.1016/j.bbamcr.2013.09.005

Kühn, Schmidt, Farthing, Rossmann, Helm, Wilson, Eckhardt, Thormann (2018). Spatial arrangement of several flagellins within bacterial flagella improves motility in different environments. *Nature Communications*, *9*(1). https://doi.org/10.1038/S41467-018-07802-W

Morgan, J. L. W., McNamara, J. T., & Zimmer, J. (2014). Mechanism of activation of bacterial cellulose synthase by cyclic di-GMP. *Nature Structural and Molecular Biology*, *21*(5), 489–496. https://doi.org/10.1038/nsmb.2803

Navarro, De, Bae, Wang, Sondermann (2009). Structural analysis of the GGDEF-EAL domain-

containing c-di-GMP receptor FimX. *Structure (London, England : 1993)*, *17*(8), 1104–1116. https://doi.org/10.1016/J.STR.2009.06.010

Nakamura, S., & Minamino, T. (2019). Flagella-Driven Motility of Bacteria. *Biomolecules*, *9*(7). https://doi.org/10.3390/BIOM9070279

Nesper, J., Hug, I., Kato, S., Hee, C. S., Habazettl, J. M., Manfredi, P., Grzesiek, S., Schirmer, T., Emonet, T., & Jenal, U. (2017). Cyclic di-GMP differentially tunes a bacterial flagellar motor through a novel class of chey-like regulators. *ELife*, *6*. https://doi.org/10.7554/eLife.28842

Newell, P. D., Monds, R. D., & O'Toole, G. A. (2009). LapD is a bis-(3',5')-cyclic dimeric GMP-binding protein that regulates surface attachment by Pseudomonas fluorescens Pf0-1. *Proceedings of the National Academy of Sciences of the United States of America*, *106*(9), 3461–3466. https://doi.org/10.1073/pnas.0808933106

Nicastro, G. G., Kaihami, G. H., Pulschen, A. A., Hernandez-Montelongo, J., Boechat, A. L., de Oliveira Pereira, T., Rosa, C. G. T., Stefanello, E., Colepicolo, P., Bordi, C., & Baldini, R. L. (2020). c-di-GMP-related phenotypes are modulated by the interaction between a diguanylate cyclase and a polar hub protein. *Scientific Reports*, *10*(1), 1–11. https://doi.org/10.1038/s41598-020-59536-9

O'Boyle, N., Houeix, B., Kilcoyne, M., Joshi, L., & Boyd, A. (2013). The MSHA pilus of Vibrio parahaemolyticus has lectin functionality and enables TTSS-mediated pathogenicity. *International Journal of Medical Microbiology*, *303*(8), 563–573. https://doi.org/10.1016/j.ijmm.2013.07.010

Paintdakhi, A., Parry, B., Campos, M., Irnov, I., Elf, J., Surovtsev, I., & Jacobs-Wagner, C. (2016). Oufti: an integrated software package for high-accuracy, high-throughput quantitative microscopy analysis. *Molecular Microbiology*, *99*(4), 767–777. https://doi.org/10.1111/MMI.13264

Paul, K., Nieto, V., Carlquist, W. C., Blair, D. F., & Harshey, R. M. (2010). The c-di-GMP Binding Protein YcgR Controls Flagellar Motor Direction and Speed to Affect Chemotaxis by a "Backstop Brake" Mechanism. *Molecular Cell*, *38*(1), 128–139. https://doi.org/10.1016/j.molcel.2010.03.001

Pecina, A., Schwan, M., Blagotinsek, V., Rick, T., Klüber, P., Leonhard, T., Bange, G., & Thormann, K. M. (2021). The Stand-Alone PilZ-Domain Protein MotL Specifically Regulates the Activity of the Secondary Lateral Flagellar System in Shewanella putrefaciens. *Frontiers in Microbiology*, *12*. https://doi.org/10.3389/fmicb.2021.668892

Pei, J., & Grishin, N. V. (2001). GGDEF domain is homologous to adenylyl cyclase. *Proteins: Structure, Function and Genetics*, *42*(2), 210–216. https://doi.org/10.1002/1097-0134(20010201)42:2<210::AID-PROT80>3.0.CO;2-8

Pongratz, I., Antonsson, C., Whitelaw, M. L., & Poellinger, L. (1998). Role of the PAS Domain in Regulation of Dimerization and DNA Binding Specificity of the Dioxin Receptor. *Molecular and Cellular Biology*, *18*(7), 4079–4088. https://doi.org/10.1128/mcb.18.7.4079

Povolotsky, T. L., & Hengge, R. (2016). Genome-based comparison of cyclic di-GMP signaling in pathogenic and commensal Escherichia coli strains. *Journal of Bacteriology*, *198*(1), 111–126. https://doi.org/10.1128/JB.00520-15

Hartmann, van Teeseling, Thanbichler, Drescher (2020). BacStalk: A comprehensive and interactive image analysis software tool for bacterial cell biology. *Molecular Microbiology*, *114*(1), 140–150. https://doi.org/10.1111/MMI.14501

Rao, F., Yang, Y., Qi, Y., & Liang, Z. X. (2008). Catalytic mechanism of cyclic di-GMP-specific

phosphodiesterase: A study of the EAL domain-containing RocR from Pseudomonas aeruginosa. *Journal of Bacteriology*, *190*(10), 3622–3631. https://doi.org/10.1128/JB.00165-08

Reinders, A., Hee, C. S., Ozaki, S., Mazur, A., Boehm, A., Schirmer, T., & Jenal, U. (2016). Expression and genetic activation of cyclic di-GMP-specific phosphodiesterases in Escherichia coli. *Journal of Bacteriology*, *198*(3), 448–462. https://doi.org/10.1128/JB.00604-15

Rodionov, D. A., Yang, C., Li, X., Rodionova, I. A., Wang, Y., Obraztsova, A. Y., Zagnitko, O. P., Overbeek, R., Romine, M. F., Reed, S., Fredrickson, J. K., Nealson, K. H., & Osterman, A. L. (2010). Genomic encyclopedia of sugar utilization pathways in the Shewanella genus. *BMC Genomics*, *11*(1), 494. https://doi.org/10.1186/1471-2164-11-494

Roelofs, K. G., Jones, C. J., Helman, S. R., Shang, X., Orr, M. W., Goodson, J. R., Galperin, M. Y., Yildiz, F. H., & Lee, V. T. (2015). Systematic Identification of Cyclic-di-GMP Binding Proteins in Vibrio cholerae Reveals a Novel Class of Cyclic-di-GMP-Binding ATPases Associated with Type II Secretion Systems. *PLoS Pathogens*, *11*(10). https://doi.org/10.1371/journal.ppat.1005232

Römling, U., Galperin, M. Y., & Gomelsky, M. (2013). Cyclic di-GMP: the first 25 years of a universal bacterial second messenger. *Microbiology and Molecular Biology Reviews : MMBR*, *77*(1), 1–52. https://doi.org/10.1128/MMBR.00043-12

Ross, P., Weinhouse, H., Aloni, Y., Michaeli, D., Weinberger-Ohana, P., Mayer, R., Braun, S., de Vroom, E., van der Marel, G. A., van Boom, J. H., & Benziman, M. (1987). Regulation of cellulose synthesis in Acetobacter xylinum by cyclic diguanylic acid. *Nature*, *325*(6101), 279–281. https://doi.org/10.1038/325279a0

Rossmann, F., Brenzinger, S., Knauer, C., Dörrich, A. K., Bubendorfer, S., Ruppert, U., Bange, G., & Thormann, K. M. (2015a). The role of FlhF and HubP as polar landmark proteins in Shewanella putrefaciens CN-32. *Molecular Microbiology*, *98*(4), 727–742. https://doi.org/10.1111/mmi.13152

Rossmann, F. M., Rick, T., Mrusek, D., Sprankel, L., Dörrich, A. K., Leonhard, T., Bubendorfer, S., Kaever, V., Bange, G., & Thormann, K. M. (2019). The GGDEF domain of the phosphodiesterase PdeB in Shewanella putrefaciens mediates recruitment by the polar landmark protein HubP. *Journal of Bacteriology*, *201*(7). https://doi.org/10.1128/JB.00534-18

Rotem, O., Nesper, J., Borovok, I., Gorovits, R., Kolot, M., Pasternak, Z., Shin, I., Glatter, T., Pietrokovski, S., Jenal, U., & Jurkevitch, E. (2016). An extended cyclic di-GMP network in the predatory bacterium Bdellovibrio bacteriovorus. *Journal of Bacteriology*, *198*(1), 127–137. https://doi.org/10.1128/JB.00422-15

Ryan, R. P., Fouhy, Y., Lucey, J. F., Crossman, L. C., Spiro, S., He, Y. W., Zhang, L. H., Heeb, S., Cámara, M., Williams, P., & Dow, J. M. (2006). Cell-cell signaling in Xanthomonas campestris involves an HD-GYP domain protein that functions in cyclic di-GMP turnover. *Proceedings of the National Academy of Sciences of the United States of America*, *103*(17), 6712–6717. https://doi.org/10.1073/pnas.0600345103

Subramanian, Gao, Dann Ill, Kearns (2017). MotI (DgrA) acts as a molecular clutch on the flagellar stator protein MotA in Bacillus subtilis. *Proceedings of the National Academy of Sciences of the United States of America*, *114*(51), 13537–13542. https://doi.org/10.1073/PNAS.1716231114

Sampedro, I., Parales, R. E., Krell, T., & Hill, J. E. (2015). Pseudomonas chemotaxis. In *FEMS Microbiology Reviews* (Vol. 39, Issue 1, pp. 17–46). Oxford University Press. https://doi.org/10.1111/1574-6976.12081

Saville, R. M., Dieckmann, N., & Spormann, A. M. (2010). Spatiotemporal activity of the mshA gene system in Shewanella oneidensis MR-1 biofilms. *FEMS Microbiology Letters*, *308*(1), 76–83. https://doi.org/10.1111/J.1574-6968.2010.01995.X

Sawai, H., Yoshioka, S., Uchida, T., Hyodo, M., Hayakawa, Y., Ishimori, K., & Aono, S. (2010). Molecular oxygen regulates the enzymatic activity of a heme-containing diguanylate cyclase (HemDGC) for the synthesis of cyclic di-GMP. *Biochimica et Biophysica Acta - Proteins and Proteomics*, *1804*(1), 166–172. https://doi.org/10.1016/j.bbapap.2009.09.028

Schindelin, J., Arganda-Carreras, I., Frise, E., Kaynig, V., Longair, M., Pietzsch, T., Preibisch, S., Rueden, C., Saalfeld, S., Schmid, B., Tinevez, J. Y., White, D. J., Hartenstein, V., Eliceiri, K., Tomancak, P., & Cardona, A. (2012). Fiji: An open-source platform for biological-image analysis. In *Nature Methods* (Vol. 9, Issue 7, pp. 676–682). Nature Publishing Group. https://doi.org/10.1038/nmeth.2019

Schirmer, T. (2016). C-di-GMP Synthesis: Structural Aspects of Evolution, Catalysis and Regulation. In *Journal of Molecular Biology* (Vol. 428, Issue 19, pp. 3683–3701). Academic Press. https://doi.org/10.1016/j.jmb.2016.07.023

Schmidt, A. J., Ryjenkov, D. A., & Gomelsky, M. (2005). The ubiquitous protein domain EAL is a cyclic diguanylate-specific phosphodiesterase: Enzymatically active and inactive EAL domains. *Journal of Bacteriology*, *187*(14), 4774–4781. https://doi.org/10.1128/JB.187.14.4774-4781.2005

Semmler, A. B. T., Whitchurch, C. B., Leech, A. J., & Mattick, J. S. (2000). Identification of a novel gene, fimV, involved in twitching motility in Pseudomonas aeruginosa. *Microbiology*, *146*(6), 1321–1332. https://doi.org/10.1099/00221287-146-6-1321

Sievers, F., Wilm, A., Dineen, D., Gibson, T. J., Karplus, K., Li, W., Lopez, R., McWilliam, H., Remmert, M., Söding, J., Thompson, J. D., & Higgins, D. G. (2011). Fast, scalable generation of high-quality protein multiple sequence alignments using Clustal Omega. *Molecular Systems Biology*, *7*(1), 539. https://doi.org/10.1038/MSB.2011.75

Sim, M., Koirala, S., Picton, D., Strahl, H., Hoskisson, P. A., Rao, C. V., Gillespie, C. S., & Aldridge, P. D. (2017). Growth rate control of flagellar assembly in Escherichia coli strain RP437. *Scientific Reports*, *7*(1), 1–11. https://doi.org/10.1038/srep41189

Geromanos, Visser, Silva, Dorschel, Li, Gorenstein, Bateman, Langridge (2009). The detection, correlation, and comparison of peptide precursor and product ions from data independent LC-MS with data dependant LC-MS/MS. *Proteomics*, *9*(6), 1683–1695. https://doi.org/10.1002/PMIC.200800562

Slater, H., Alvarez-Morales, A., Barber, C. E., Daniels, M. J., & Dow, J. M. (2002). A two-component system involving an HD-GYP domain protein links cell-cell signalling to pathogenicity gene expression in Xanthomonas campestris. *Molecular Microbiology*, *38*(5), 986–1003. https://doi.org/10.1046/j.1365-2958.2000.02196.x

Smith, T. J., Sondermann, H., & O'Toole, G. A. (2018). Co-opting the Lap System of Pseudomonas fluorescens to Reversibly Customize Bacterial Cell Surfaces. *ACS Synthetic Biology*, *7*(11), 2612–2617. https://doi.org/10.1021/acssynbio.8b00278

Son, K., Guasto, J. S., & Stocker, R. (2013). Bacteria can exploit a flagellar buckling instability to change direction. *Nature Physics 2013 9:8*, *9*(8), 494–498. https://doi.org/10.1038/nphys2676

Springer, W. R., & Koshland, D. E. (1977). Identification of a protein methyltransferase as the cheR

gene product in the bacterial sensing system. *Proceedings of the National Academy of Sciences of the United States of America*, *74*(2), 533–537. https://doi.org/10.1073/pnas.74.2.533

Srivastava, D., Harris, R. C., & Waters, C. M. (2011). Integration of cyclic di-GMP and quorum sensing in the control of vpsT and aphA in Vibrio cholerae. *Journal of Bacteriology*, *193*(22), 6331–6341. https://doi.org/10.1128/JB.05167-11

Steinchen, W., Schuhmacher, J. S., Altegoer, F., Fage, C. D., Srinivasan, V., Linne, U., Marahiel, M. A., & Bange, G. (2015). Catalytic mechanism and allosteric regulation of an oligomeric (p)ppGpp synthetase by an alarmone. *Proceedings of the National Academy of Sciences*, *112*(43), 13348–13353. https://doi.org/10.1073/PNAS.1505271112

Stelitano, V., Brandt, A., Fernicola, S., Franceschini, S., Giardina, G., Pica, A., Rinaldo, S., Sica, F., & Cutruzzolà, F. (2013). Probing the activity of diguanylate cyclases and c-di-GMP phosphodiesterases in real-time by CD spectroscopy. *Nucleic Acids Research*, *41*(7), e79–e79. https://doi.org/10.1093/nar/gkt028

Stępień-Pyśniak, D., Hauschild, T., Kosikowska, U., Dec, M., & Urban-Chmiel, R. (2019). Biofilm formation capacity and presence of virulence factors among commensal Enterococcus spp. from wild birds. *Scientific Reports*, *9*(1), 1–7. https://doi.org/10.1038/s41598-019-47602-w

Sultan, S. Z., Manne, A., Stewart, P. E., Bestor, A., Rosa, P. A., Charon, N. W., & Motaleba, M. A. (2013). Motility is crucial for the infectious life cycle of borrelia burgdorferi. *Infection and Immunity*, *81*(6), 2012–2021. https://doi.org/10.1128/IAI.01228-12

Sultan, S. Z., Pitzer, J. E., Boquoi, T., Hobbs, G., Miller, M. R., & Motaleb, M. A. (2011). Analysis of the HD-GYP domain cyclic dimeric gmp phosphodiesterase reveals a role in motility and the enzootic life cycle of Borrelia burgdorferi. *Infection and Immunity*, *79*(8), 3273–3283. https://doi.org/10.1128/IAI.05153-11

Thomsen, M. C. F., & Nielsen, M. (2012). Seq2Logo: a method for construction and visualization of amino acid binding motifs and sequence profiles including sequence weighting, pseudo counts and two-sided representation of amino acid enrichment and depletion. *Nucleic Acids Research*, *40*(Web Server issue), W281. https://doi.org/10.1093/NAR/GKS469

Tischler, A. D., & Camilli, A. (2004). Cyclic diguanylate (c-di-GMP) regulates Vibrio cholerae biofilm formation. *Molecular Microbiology*, *53*(3), 857–869. https://doi.org/10.1111/j.1365-2958.2004.04155.x

Tischler, A. D., & Camilli, A. (2005). Cyclic diguanylate regulates Vibrio cholerae virulence gene expression. *Infection and Immunity*, *73*(9), 5873–5882. https://doi.org/10.1128/IAI.73.9.5873-5882.2005

Trampari, E., Stevenson, C. E. M., Little, R. H., Wilhelm, T., Lawson, D. M., & Malone, J. G. (2015). Bacterial Rotary Export ATPases Are Allosterically Regulated by the Nucleotide Second Messenger Cyclic-di-GMP. *The Journal of Biological Chemistry*, *290*(40), 24470. https://doi.org/10.1074/JBC.M115.661439

Traxler, M. F., Summers, S. M., Nguyen, H. T., Zacharia, V. M., Hightower, G. A., Smith, J. T., & Conway, T. (2008). The global, ppGpp-mediated stringent response to amino acid starvation in Escherichia coli. *Molecular Microbiology*, *68*(5), 1128–1148. https://doi.org/10.1111/j.1365-2958.2008.06229.x

Mattick, J. S. (2015). *Type IV Pili and Twitching Motility*.

https://doi.org/10.1146/annurev.micro.56.012302.160938

Veening, J. W., Smits, W. K., & Kuipers, O. P. (2008). Bistability, epigenetics, and bet-hedging in bacteria. In *Annual Review of Microbiology* (Vol. 62, pp. 193–210). Annu Rev Microbiol. https://doi.org/10.1146/annurev.micro.62.081307.163002

Vorobiev, S. M., Neely, H., Yu, B., Seetharaman, J., Xiao, R., Acton, T. B., Montelione, G. T., & Hunt, J. F. (2012). Crystal structure of a catalytically active GG(D/E)EF diguanylate cyclase domain from Marinobacter aquaeolei with bound c-di-GMP product. *Journal of Structural and Functional Genomics*, *13*(3), 177–183. https://doi.org/10.1007/s10969-012-9136-4

Wang, Y. C., Chin, K. H., Tu, Z. Le, He, J., Jones, C. J., Sanchez, D. Z., Yildiz, F. H., Galperin, M. Y., & Chou, S. H. (2016a). Nucleotide binding by the widespread high-affinity cyclic di-GMP receptor MshEN domain. *Nature Communications*, *7*(1), 1–12. https://doi.org/10.1038/ncomms12481

Wang, Y. C., Chin, K. H., Tu, Z. Le, He, J., Jones, C. J., Sanchez, D. Z., Yildiz, F. H., Galperin, M. Y., & Chou, S. H. (2016b). Nucleotide binding by the widespread high-affinity cyclic di-GMP receptor MshEN domain. *Nature Communications*, *7*(1), 1–12. https://doi.org/10.1038/ncomms12481

Wassmann, P., Chan, C., Paul, R., Beck, A., Heerklotz, H., Jenal, U., & Schirmer, T. (2007). Structure of BeF3--Modified Response Regulator PleD: Implications for Diguanylate Cyclase Activation, Catalysis, and Feedback Inhibition. *Structure*, *15*(8), 915–927. https://doi.org/10.1016/j.str.2007.06.016

Waterhouse, A., Bertoni, M., Bienert, S., Studer, G., Tauriello, G., Gumienny, R., Heer, F. T., de Beer, T. A. P., Rempfer, C., Bordoli, L., Lepore, R., & Schwede, T. (2018). SWISS-MODEL: homology modelling of protein structures and complexes. *Nucleic Acids Research*, *46*(W1), W296–W303. https://doi.org/10.1093/NAR/GKY427

Waterhouse, A. M., Procter, J. B., Martin, D. M. A., Clamp, M., & Barton, G. J. (2009). Jalview Version 2—a multiple sequence alignment editor and analysis workbench. *Bioinformatics*, *25*(9), 1189–1191. https://doi.org/10.1093/BIOINFORMATICS/BTP033

Whitney, J. C., Whitfield, G. B., Marmont, L. S., Yip, P., Neculai, A. M., Lobsanov, Y. D., Robinson, H., Ohman, D. E., & Howell, P. L. (2015). Dimeric c-di-GMP is required for post-translational regulation of alginate production in pseudomonas aeruginosa. *Journal of Biological Chemistry*, *290*(20), 12451–12462. https://doi.org/10.1074/jbc.M115.645051

Wood, T. K. (2013). Precedence for the structural role of flagella in biofilms. In *mBio* (Vol. 4, Issue 2). https://doi.org/10.1128/mBio.00225-13

Wu, C., Cheng, Y. Y., Yin, H., Song, X. N., Li, W. W., Zhou, X. X., Zhao, L. P., Tian, L. J., Han, J. C., & Yu, H. Q. (2013a). Oxygen promotes biofilm formation of Shewanella putrefaciensCN32through a diguanylate cyclase and an adhesin. *Scientific Reports*, *3*. https://doi.org/10.1038/srep01945

Wu, C., Cheng, Y. Y., Yin, H., Song, X. N., Li, W. W., Zhou, X. X., Zhao, L. P., Tian, L. J., Han, J. C., & Yu, H. Q. (2013b). Oxygen promotes biofilm formation of Shewanella putrefaciensCN32through a diguanylate cyclase and an adhesin. *Scientific Reports*, *3*. https://doi.org/10.1038/srep01945

Xie, L., Altindal, T., Chattopadhyay, S., & Wu, X.-L. (2011). From the Cover: Bacterial flagellum as a propeller and as a rudder for efficient chemotaxis. *Proceedings of the National Academy of Sciences of the United States of America*, *108*(6), 2246. https://doi.org/10.1073/PNAS.1011953108

Xin, L., Zeng, Y., Sheng, S., Chea, R. A., Liu, Q., Li, H. Y., Yang, L., Xu, L., Chiam, K.-H., & Liang, Z.-X.

(2019). Regulation of flagellar motor switching by c-di-GMP phosphodiesterases in Pseudomonas aeruginosa. *The Journal of Biological Chemistry*, *294*(37), 13789. https://doi.org/10.1074/JBC.RA119.009009

Yamaichi, Y., Bruckner, R., Ringgaard, S., Möll, A., Cameron, D. E., Briegel, A., Jensen, G. J., Davis, B. M., & Waldor, M. K. (2012). A multidomain hub anchors the chromosome segregation and chemotactic machinery to the bacterial pole. *Genes & Development*, *26*(20), 2348–2360. https://doi.org/10.1101/gad.199869.112

Young, T. D., Liau, W. T., Lee, C. K., Mellody, M., Wong, G. C. L., Kasko, A. M., & Weiss, P. S. (2020). Selective Promotion of Adhesion of Shewanella oneidensis on Mannose-Decorated Glycopolymer Surfaces. *ACS Applied Materials & Interfaces*, *12*(32), 35767–35781. https://doi.org/10.1021/ACSAMI.0C04329

Zähringer, F., Lacanna, E., Jenal, U., Schirmer, T., & Boehm, A. (2013). Structure and signaling mechanism of a zinc-sensory diguanylate cyclase. *Structure*, *21*(7), 1149–1157. https://doi.org/10.1016/j.str.2013.04.026

Zhou, G., Yuan, J., & Gao, H. (2015). Regulation of biofilm formation by BpfA, BpfD, and BpfG in Shewanella oneidensis. *Frontiers in Microbiology*, *6*(AUG). https://doi.org/10.3389/fmicb.2015.00790

Zhou, H., Zheng, C., Su, J., Chen, B., Fu, Y., Xie, Y., Tang, Q., Chou, S. H., & He, J. (2016). Characterization of a natural triple-tandem c-di-GMP riboswitch and application of the riboswitch-based dual-fluorescence reporter. *Scientific Reports*, *6*(1), 1–13. https://doi.org/10.1038/srep20871

Zhu, S., Nishikino, T., Hu, B., Kojima, S., Homma, M., & Liu, J. (2017). Molecular architecture of the sheathed polar flagellum in Vibrio alginolyticus. *Proceedings of the National Academy of Sciences of the United States of America*, *114*(41), 10966–10971. https://doi.org/10.1073/pnas.1712489114

Zhu, Yuan, & Gu. (2017). Structural basis for the regulation of chemotaxis by MapZ in the presence of c-di-GMP. *Acta Crystallographica. Section D, Structural Biology*, *73*(Pt 8), 683–691. https://doi.org/10.1107/S2059798317009998

In revision

Tim Rick, Vanessa Kreiling, Alexander Höing, Svenja Fiedler, Timo Glatter, Wieland Steinchen, Georg Hochberg, Heike Bähre, Roland Seifert, Gert Bange, Shirley K. Knauer, Peter L. Graumann, Kai M. Thormann. (2021). A GGDEF domain serves as a spatial on-switch for a phosphodiesterase by direct interaction with a polar landmark protein. *NPJ Biofilms and Microbiomes* (submitted)

Doi (biorxiv): https://doi.org/10.1101/2021.08.12.456111

6. Supplement

6.1 Supplemental tables

Supplemental table 1) Escherichia coli strains that were used in this study. The individual tables are available in Rossmann & Rick et al., 2019 and Rick & Kreiling et al., 2021

Strain	Genotype	Purpose	Reference
Escherichia coli			
DH5α λpir	ϕ80d*lacZ* ΔM15 Δ(*lacZYA-argF*)U169 *recA1 hsdR17 deoR thi-l supE44 gyrA96 relA1*/λpir	cloning strain	Miller VL et al., 1988
WM3064	*thrB1004 pro thi rpsL hsdS lacZ* ΔM15 RP4-1360 Δ(*araBAD*) 567Δ*dapA* 1341::[*erm pir*(wt)]	conjugation strain for *Shewanella*	W. Metcalf, University of Illinois, Urbana-Champaign
BTH101	*F⁻, cya-99, araD139, galE15, galK16, rpsL1 (Strr), hsdR2, mcrA1,mcrB1*	host for bacterial two-hybrid analysis	Euromedex, France
BL21(DE3)	***fhuA2 [lon] ompT gal (λ DE3) [dcm] ΔhsdS λ DE3 = λ sBamHIo ΔEcoRI-B int::(lacI::PlacUV5::T7 gene1) i21 Δnin5***	**protein overproduction strain**	NEB

Supplemental table 2) *Shewanella putrefaciens* CN-32 strains that were used in this study. The individual tables are available in Rossmann & Rick et al., 2019 and Rick & Kreiling et al., 2021

Strain	Genotype	Purpose	Reference
***S. putrefaciens* CN-32**			
S798	CN32	wild-type strain	Fredrickson *et al., 1988*
S2025	Δcluster I	strain where all polar flagella and chemotaxis genes were deleted (sputcn32_2551 – sputcn32_2602)	Bubendorfer et al., 2012
S2241	*fliM*1 -mCherry	functional, markerless in-frame tag of mCherry to the C-terminus of the polar motor switch protein FliM1 (Sputcn32_2569)	Bubendorfer et al., 2012
S2575	Δ*flaAB1*	markerless in-frame deletion of the polar flagellins	Bubendorfer et al., 2012
S2576	Δ*flaAB2*	markerless in-frame deletion of the lateral flagellins	Bubendorfer et al., 2012
S2800	*flaB1*::lux	transcriptional fusion of *flaB1*-RBS-luxCDABE	Rossmann & Rick et al., 2019
S2801	*flaA2* :: lux	transcriptional fusion of *flaA2*-RBS-luxCDABE	Rossmann & Rick et al., 2019
S3145	Δ*hubP*	markerless in-frame deletion	Rossmann & Rick et al.,

		of the gene *hubP* (*sputcn32_2442*)	2019
S3297	Δ*pdeB*	markerless in-frame deletion of the gene *sputcn32_3405 (pdeB*)	Rossmann & Rick et al., 2019
S3419	*flgE2*-T242C	markerless in-frame substitution of Thr242 to Cys in the lateral hook protein FlgE2 (Sputcn32_3465), fully functional and suitable for maleimide staining	Rossmann et al., 2015
S3778	*hubP*-mCherry	functional, markerless in-frame tag of mCherry to the C-terminus of the polar landmarkprotein HubP (Sputcn32_2442)	Rossmann et al., 2015
S3915	*ΔpdeB* flaB1:: lux	markerless in-frame deletion of the gene *sputcn32_3405* (*pdeB*) in the transcriptional fusion flaB1-RBS-luxCDABE	Rossmann & Rick et al., 2019
S3916	ΔpdeB flaA2 :: lux	markerless in-frame deletion of the gene sputcn32_3405 (pdeB) in the transcriptional fusion of flaA2-RBS-luxCDABE	Rossmann & Rick et al., 2019
S4003	ΔflgE1	markerless in-frame deletion of the the polar hook protein FlgE1 (Sputcn32_3465)	Rossmann & Rick et al., 2019
S4063	flgE1-T183C	markerless in-frame substitution of Thr183 to Cys in the polar hook protein FlgE1 (Sputcn32_3465), fully functional and suitable for maleimide staining	Rossmann & Rick et al., 2019
S4091	ΔpdeB pdeB+	ΔpdeB complemented with full length pdeB	Rossmann & Rick et al., 2019
S4234	PdeB-sfGFP	functional markerless in-frame tag of sfGFP to the C-terminus of PdeB via a flexible GS-linker	Rossmann & Rick et al., 2019
S4235	PdeB-sfGFP ΔhubP	functional, markerless in-frame tag of GFP to the C-terminus of PdeB (Sputcn32_3405) in the ΔhubP background	Rossmann & Rick et al., 2019
S4236	*pdeB*-E637A	Δ*pdeB* complemented with full length *pdeB* variant where Glu 637 in the active center (EIL-motif to AIL) of the EAL domain was mutated to Ala	Rossmann & Rick et al., 2019
S4237	*pdeB*-E637A-gfp	markerless substitution of the EIL motif to AIL (residue 637) in the background of *PdeB-sfGFP*	Rossmann & Rick et al., 2019
S4237	*pdeb*-ΔEAL-gfp	markerless in-frame deletion of the EAL-domain of PdeB (residues 598 - 847) in the background of *PdeB-sfGFP*	Rossmann & Rick et al., 2019
S4238	*pdeb*-ΔPAS-gfp	markerless in-frame deletion of the PAS-domain of PdeB (residues 317 - 416) in the background of *PdeB-sfGFP*	Rossmann & Rick et al., 2019
S4239	*pdeb*-ΔPeriplasmic-region-gfp	markerless in-frame deletion of the periplasmic region of PdeB (residues 51 - 214) in the background of *PdeB-sfGFP*	Rossmann & Rick et al., 2019
S4240	*pdeb-D508A-E509A-gfp*	markerless substitution of the GGDEF motif to GGAAF (residues 508 and 509) in the background of PdeB-sfGFP	Rossmann & Rick et al., 2019
S4241	*PdeB-sfGFP hubP*-mCherry	functional, markerless in-frame tag of GFP to the C-terminus of PdeB	Rossmann & Rick et al., 2019

		(Sputcn32_3405) in the *hubP*-mCherry background	
S4325	*pdeb*-ΔGGDEF-Δ EAL	markerless in-frame deletion of the EAL- and GGDEF-domain of PdeB (residues 420 - 847) in the background of *PdeB-sfGFP*	Rossmann & Rick et al., 2019
S4326	*pdeb*-ΔPAS-ΔGGDEF-ΔEAL-gfp	markerless in-frame deletion of the EAL-, PAS- and GGDEF-domain of PdeB (residues 317 - 847) in the background of *PdeB-sfGFP*	Rossmann & Rick et al., 2019
S4327	*pdeb*-ΔHAMP-ΔPAS-ΔGGDEF-ΔEAL-gfp	markerless in-frame deletion of the EAL-, PAS- HAMP- and GGDEF-domain of PdeB (residues 255 - 847) in the background of *PdeB-sfGFP*	Rossmann & Rick et al., 2019
S4357	Δ*pdeB* Δ*flaAB1*	markerless in-frame deletion of the gene *pdeB (sputcn32_3405)* in a background with deleted polar flagellins	Rossmann & Rick et al., 2019
S4358	Δ*pdeB* Δ*flaAB2*	markerless in-frame deletion of the gene *pdeB (sputcn32_3405)* in a background with deleted lateral flagellins	Rossmann & Rick et al., 2019
S4360	*pdeB*-ΔGGDEF-gfp	markerless in-frame deletion of PdeB GGDEF-domain (residues 421 - 588)	Rossmann & Rick et al., 2019
S4362	*PdeB-sfGFP fliM1*-mCherry	functional, markerless in-frame tag of GFP to the C-terminus of PdeB (Sputcn32_3405) in the *fliM1-mCherry* background	Rossmann & Rick et al., 2019
S4370	*PdeB-sfGFP* Δcluster I	functional markerless in-frame tag of sfGFP to the C-terminus of PdeB via a flexible GS-linker in a strain where all polar flagella and chemotaxis genes were deleted (Sputcn32_2551 – Sputcn32_2602)	Rossmann & Rick et al., 2019
S4938	*flgE2*-T242C *ΔpdeB*	markerless in-frame substitution of Thr242 to Cys in the lateral hook protein FlgE2 (Sputcn32_3465) in the *ΔpdeB* background, fully functional and suitable for maleimide staining	Rossmann & Rick et al., 2019
S4939	*flgE2*-T242C *ΔhubP ΔpdeB*	markerless in-frame substitution of Thr242 to Cys inthe lateral hook protein FlgE2 (Sputcn32_3465) in the *ΔhubP ΔpdeB* background, fully functional and suitable for maleimide staining	Rossmann & Rick et al., 2019
S4940	*flgE2*-T242C *ΔhubP*	markerless in-frame substitution of Thr242 to Cys in the lateral hook protein FlgE2 (Sputcn32_3465) in the *ΔhubP* background, fully functional and suitable for maleimide staining	Rossmann & Rick et al., 2019
S5756	*flgE1*-T183C *ΔpdeB*	markerless in-frame substitution of Thr183 to Cys in the polar hook protein FlgE1 (Sputcn32_3465) in the *ΔpdeB* background, fully functional and suitable for maleimide staining	Rossmann & Rick et al., 2019
S6452	*PdeB-sfGFP* V522G V523G Q524G	markerless in-frame fusion of *pdeB* with sf*gfp* substitution	Rick & Kreiling et al., 2021

		of Q524G	
S6453	*PdeB-sfGFP* K490G V491G M492G Q593G	markerless in-frame fusion of *pdeB* with sf*gfp* substitution of M492G Q593G	Rick & Kreiling et al., 2021
S6454	*PdeB-sfGFP* R557G A558G P559G Y560G	markerless in-frame fusion of *pdeB* with *sfgfp* substitution of A558G P559G Y560G	Rick & Kreiling et al., 2021
S6496	Δ*flaAB*$_2$ Δ*mshE*	markerless in-frame deletion of the gene *mshE (sputcn32_0563)* in a background with deleted lateral flagellins	Rick & Kreiling et al., 2021
S6497	Δ*flaAB*$_2$ Δ*pdeB* Δ*mshE*	markerless in-frame deletion of the gene *mshE (sputcn32_0563)* in a background with deleted lateral flagellins and deletion of the gene *pdeB* (*sputcn32_3405*)	Rick & Kreiling et al., 2021
S6527	*PdeB-sfGFP* K490D Q493A	markerless in-frame fusion of *pdeB* with sf*gfp* substitution of K490D Q493A	Rick & Kreiling et al., 2021
S6528	*PdeB-sfGFP* Q524A K527D Q528A	markerless in-frame fusion of *pdeB* with sf*gfp* substitution of Q524A K527D Q528A	Rick & Kreiling et al., 2021
S6683	Δ*flaAB*$_2$ *mshA* S68C	functional substitution of *mshA* S68C in a background with deleted lateral flagellins	Rick & Kreiling et al., 2021
S6684	Δ*flaAB*$_2$ Δ*pdeB mshA* S68C	functional substitution of *mshA* S68C in a background with deleted lateral flagellins and deletion of the gene *pdeB* (*sputcn32_3405*)	Rick & Kreiling et al., 2021
S6688	Δ*flaAB*$_2$ Δ*aggA*	markerless in-frame deletion of the gene *aggA (sputcn32_3594)* in a background with deleted lateral flagellins	Rick & Kreiling et al., 2021
S6689	Δ*flaAB*$_2$ Δ*pdeB* Δ*aggA*	markerless in-frame deletion of the gene *aggA (sputcn32_3594)* in a background with deleted lateral flagellins and deletion of the gene *pdeB (sputcn32_3405)*	Rick & Kreiling et al., 2021
S6690	Δ*flaAB*$_2$ Δ*pdeB* Δ*mshE* Δ*aggA*	markerless in-frame deletion of the gene *aggA (sputcn32_3594)* in a background with deleted lateral flagellins, and deletion of the genes *pdeB (sputcn32_3405)* and *mshE (sputcn32_0563)*	Rick & Kreiling et al., 2021
S6691	Δ*flaAB*$_2$ Δ*pilB*	markerless in-frame deletion of the gene *pilB (sputcn32_3423)* in a background with deleted lateral flagellins	Rick & Kreiling et al., 2021
S6692	Δ*flaAB*$_2$ Δ*pdeB* Δ*pilB*	markerless in-frame deletion of the gene *pilB (sputcn32_3423)* in a background with deleted lateral flagellins and deletion of the gene *pdeB (sputcn32_3405)*	Rick & Kreiling et al., 2021
S6693	Δ*flaAB*$_2$ Δ*pdeB* Δ*mshE* Δ*pilB*	markerless in-frame deletion of the gene *pilB (sputcn32_3423)* in a background with deleted lateral flagellins, and deletion of the genes *pdeB (sputcn32_3405)* and *mshE (sputcn32_0563)*	Rick & Kreiling et al., 2021
S6729	*PdeB-sfGFP* K527E Q528S	markerless in-frame fusion of *pdeB* with sf*gfp* substitution	Rick & Kreiling et al., 2021

		of K527E Q528S	
S7024	*pdeB-mvenus*	markerless in-frame fusion of *pdeB* with *mvenus*	Rick & Kreiling et al., 2021
S7025	*pdeB-mvenus* D508A E509A	markerless in-frame fusion of *pdeB* D508A E509A with *mvenus*	Rick & Kreiling et al., 2021
S7026	*pdeB-mvenus* E637A	markerless in-frame fusion of *pdeB* E637A with *mvenus*	Rick & Kreiling et al., 2021
S7243	*PdeB-sfGFP* K527S Q528S	markerless in-frame fusion of *pdeB* with sf*gfp* substitution of K527S Q528S	Rick & Kreiling et al., 2021
S7243	*PdeB-sfGFP* Q524S Q528S	markerless in-frame fusion of *pdeB* with sf*gfp* substitution of Q524S Q528S	Rick & Kreiling et al., 2021
S7244	*PdeB-sfGFP* K527S	markerless in-frame fusion of *pdeB* with *sfgfp* substitution of K527S	Rick & Kreiling et al., 2021
S7245	*PdeB-sfGFP* G497A	markerless in-frame fusion of *pdeB* with *sfgfp* substitution of G497A	Rick & Kreiling et al., 2021
S7246	*PdeB-sfGFP Q499S*	markerless in-frame fusion of *pdeB* with *sfgfp* substitution of Q499S	Rick & Kreiling et al., 2021
S7247	*PdeB-sfGFP* E500S	markerless in-frame fusion of *pdeB* with *sfgfp* substitution of E500S	Rick & Kreiling et al., 2021
S7444	Δ*flaAB*$_2$ Δ*mshE* Δ*aggA*	markerless in-frame deletion of the gene *aggA (sputcn32_3594)* in a background with deleted lateral flagellins and deletion of the gene *mshE (sputcn32_0563)*	Rick & Kreiling et al., 2021
S7445	Δ*flaAB*$_2$ Δ*mshE* Δ*pilB*	markerless in-frame deletion of the gene *pilB (sputcn32_3423)* in a background with deleted lateral flagellins and deletion of the gene *mshE (sputcn32_0563)*	Rick & Kreiling et al., 2021
S7504	*pdeB* K527E Q528S	markerless in-frame substitution of *pdeB* K527E Q528S	Rick & Kreiling et al., 2021
S7505	*pdeB* G497A	markerless in-frame substitution of *pdeB* G497A	Rick & Kreiling et al., 2021
S7506	*pdeB* K578S	markerless in-frame substitution of *pdeB* K578S	Rick & Kreiling et al., 2021
S7507	*pdeB-mvenus* K527E Q528S	markerless in-frame fusion of *pdeB*-K527E Q528S with *mvenus*	Rick & Kreiling et al., 2021
S7508	*pdeB* K580S	markerless in-frame substitution of *pdeB* K580S	Rick & Kreiling et al., 2021
S7562	*PdeB-sfGFP* K578S	markerless in-frame fusion of *pdeB* with *sfgfp* substitution of K578S	Rick & Kreiling et al., 2021
S7564	*PdeB-sfGFP* K580S	markerless in-frame fusion of *pdeB* with *sfgfp* substitution of K580S	Rick & Kreiling et al., 2021
S7614	pMMB-Gm-Bc3-5 AAV (hok-sok)	wildtype strain containing the c-di-GMP biosensor plasmid	Rick & Kreiling et al., 2021
S7616	Δ*pdeB* pMMB-Gm-Bc3-5 AAV (hok-sok)	c-di-GMP biosensor plasmid in the background of deleted *pdeB* (*sputcn32_3405*)	Rick & Kreiling et al., 2021
S7653	*pdeB* K527E Q528S pMMB-Gm-Bc3-5 AAV (hok-sok)	c-di-GMP biosensor plasmid in the background of *pdeB* K527E Q528S substitution	Rick & Kreiling et al., 2021
S7654	*pdeB* G497A pMMB-Gm-Bc3-5 AAV (hok-sok)	c-di-GMP biosensor plasmid in the background of *pdeB* G497A substitution	Rick & Kreiling et al., 2021
S7655	*pdeB* K578S pMMB-Gm-Bc3-5 AAV (hok-sok)	c-di-GMP biosensor plasmid in the background of *pdeB* K578S substitution	Rick & Kreiling et al., 2021
S7691	*lapA*-GS-3xFLAG	functional markerless in-frame tag of 3xFLAG to the C-terminus of *lapA* via a	Rick & Kreiling et al., 2021

		flexible GS-linker	
S7692	Δ*pdeB lapA*-GS-3xFLAG	functional markerless in-frame tag of 3xFLAG to the C-terminus of *lapA* via a flexible GS-linker in the background of deleted *pdeB (sputcn32_3405)*	Rick & Kreiling et al., 2021
S7703	*lapB*-GS-3xFLAG	functional markerless in-frame tag of 3xFLAG to the C-terminus of *lapB* via a flexible GS-linker	Rick & Kreiling et al., 2021
S7704	Δ*pdeB lapB*-GS-3xFLAG	functional markerless in-frame tag of 3xFLAG to the C-terminus of *lapB* via a flexible GS-linker in the background of deleted *pdeB (sputcn32_3405)*	Rick & Kreiling et al., 2021

Supplemental table 3) Shewanella oneidensis MR1 strains that were used in this study. The individual tables are available in Rossmann & Rick et al., 2019 and Rick & Kreiling et al., 2021

Strain	Genotype	Purpose	Reference
***S. oneidensis* MR-1**			
S7296	Δ*pdeB*	Markerless in-frame deletion of *pdeB* of *S. oneidensis* MR-1	this study
S7294	*PdeB-sfGFP*	Markerless in-frame fusion of *pdeB* with *sfgfp* in *S. oneidensis* MR-1	this study
S7423	pMMB-Gm-Bc3-5 AAV (hok-sok)	MR-1 wildtype strain containing the c-di-GMP biosensor plasmid	this study
S7425	Δ*pdeB* pMMB-HS-Bc-3-5-AAV (hok-sok)	c-di-GMP biosensor plasmid in the background of deleted *pdeB* (*SO_0437*)	this study

Supplemental table 4) Plasmids that were used in this study. The individual tables are available in Rossmann & Rick et al., 2019 and Rick & Kreiling et al., 2021

Plasmid	Relevant genotype or phenotype	Source or reference
pNPTS-138-R6KT	*mob*RP4+ *ori*-R6K *sacB* β-galactosidase fragment alpha, suicide plasmid for in frame deletions/insertions in *Shewanella*, Km^r	Lassak et al., 2010
pET-24c	overproduction vector for His-tagged proteins	EMD Biosciences
pBTOK	pBBR1-MCS2 backbone (pBBR origin, Km^r); TetR, Promoter and multiple cloning site of pASK-IBA3plus and *E. coli* rrnB1 T1 and lambda phage T0 terminator. Overproduction plasmid, inducible with anhydrotetracycline	Rossmann et al., 2015
pMMB-Gm-Bc3-5 AAV (hok-sok)	pMMB67EH (Gm) backbone containing the c-di-GMP biosensor (turboRFP with an AAV tag) and the hok/sok region from pXB300. Used as c-di-GMP reporter.	Fitnat Yildiz, UCSC Santa Cruz, CA

Supplemental table 5) overexpression vectors that were used in this study. The individual tables are available in Rossmann & Rick et al., 2019 and Rick & Kreiling et al., 2021

Plasmid	Relevant genotype or phenotype	Source or reference
Overexpression vectors		
pBTOK *dgcA*-6xHis	Vector for ectopical expression of *dgcA* (*E. coli*) in *S. putrefaciens* CN-32 with C-terminal 6xHis	Rick & Kreiling et al., 2021
pBTOK *dgcA*-6xHis D216E	Vector for ectopical expression of *dgcA* (*E. coli*) in *S. putrefaciens* CN-32 with C-terminal 6xHis and D216E	Rick & Kreiling et al., 2021
pBTOK *dgcA*-6xHis E276K	Vector for ectopical expression of *dgcA* (*E. coli*) in *S. putrefaciens* CN-32 with C-terminal 6xHis and E276K	Rick & Kreiling et al., 2021
pBTOK GGDEF(PdeB)-gfp	Overproduction vector for GFP-tagged GGDEF-domain of SpPdeB	Rossmann & Rick et al., 2019
pET24c	overproduction vector for His-tagged proteins	EMD Biosciences
pET24c (MR-1) FimV-Cdomain-6xHis	Vector used to express the C-terminal domain of MR-1 FimV (residues 1000 - 1110) with C-terminal 6xHis translational fusion	Rick & Kreiling et al., 2021
pET24c 3xFLAG-(CN-32) HubP-FimV-Cdomain-6xHis	Vector used to express the C-terminal domain of MR-1 FimV (residues 1000 - 1110) with C-terminal 6xHis translational fusion	Rick & Kreiling et al., 2021
pET24c FimVc-FLAG	Overproduction vector for FLAG- and his-tagged FimVc-domain of *Sp*HubP	Rossmann & Rick et al., 2019
pET24c MBP	Overproduction vector for his-tagged maltose binding protein	Rossmann & Rick et al., 2019
pET24c MBP-Cyto	Overproduction vector for MBP- and his-tagged cytoplasmic part of SpPdeB	Rossmann & Rick et al., 2019
pET24c MBP-GGDEF	Overproduction vector for MBP- and his-tagged GGDEF-domain of SpPdeB	Rossmann & Rick et al., 2019
pET24c MBP-PdeB (MR-1) GGDEF-6xHis	Vector used to express the GGDEF-domain of MR-1 PdeB (residues 417 - 585) with N-terminal MBP and C-terminal 6xHis translational fusion	Rick & Kreiling et al., 2021
pET24c MBP-PdeB (MR-1) GGDEF-6xHis E497S	Vector used to express the GGDEF-domain of MR-1 PdeB (residues 417 - 585) with N-terminal MBP and C-terminal 6xHis translational fusion	Rick & Kreiling et al., 2021
pET24c MBP-PdeB (MR-1) GGDEF-6xHis G494A	Vector used to express the GGDEF-domain of MR-1 PdeB (residues 417 - 585) with N-terminal MBP and C-terminal 6xHis translational fusion	Rick & Kreiling et al., 2021
pET24c MBP-PdeB (MR-1) GGDEF-6xHis K524E Q525S	Vector used to express the GGDEF-domain of MR-1 PdeB (residues 417 - 585) with N-terminal MBP and C-terminal 6xHis translational fusion	Rick & Kreiling et al., 2021
pET24c MBP-PdeB (MR-1) GGDEF-6xHis K524S	Vector used to express the GGDEF-domain of MR-1 PdeB (residues 417 - 585) with N-terminal MBP and C-terminal 6xHis translational fusion	Rick & Kreiling et al., 2021
pET24c MBP-PdeB (MR-1) GGDEF-6xHis Q525S	Vector used to express the GGDEF-domain of MR-1 PdeB (residues 417 - 585) with N-terminal MBP and C-terminal 6xHis translational fusion	Rick & Kreiling et al., 2021
pET24c MBP-PdeB (MR-1) PAS-GGDEF-6xHis	Vector used to express the PAS- and GGDEF-domain of MR-1 PdeB (residues 304 - 585) with N-terminal MBP and C-terminal 6xHis translational fusion	Rick & Kreiling et al., 2021
pET24c MBP-PdeB (MR-1) PAS-GGDEF-6xHis K524E Q525S	Vector used to express the PAS- and GGDEF-domain of MR-1 PdeB (residues 304 - 585) with N-terminal MBP and C-terminal 6xHis translational fusion	Rick & Kreiling et al., 2021
pET24c *mshE*_Ndomain-6xHis	Vector used to express the N-terminal domain of CN-32 MshE (residues 2 - 145) with C-terminal 6xHis translational fusion	Rick & Kreiling et al., 2021
pET24c *mshE*-6xHis	Vector used to express MshE of CN-32 with C-terminal 6xHis translational fusion	Rick & Kreiling et al., 2021
pET24c *pilB*_Ndomain-6xHis	Vector used to express the N-terminal domain of CN-32 PilB (residues 2 - 145)	Rick & Kreiling et al., 2021

with C-terminal 6xHis translational fusion	

Supplemental table 6) In-frame insertion vectors that were used in this study. The individual tables are available in Rossmann & Rick et al., 2019 and Rick & Kreiling et al., 2021

Plasmid	Relevant genotype or phenotype	Source or reference
In-frame insertion vectors		
pNPTS CN-32 *pdeB* G497A	Suicide vector for markerless in-frame insertion of *pdeB* of *S. putrefaciens* CN-32 with G497A	Rick & Kreiling et al., 2021
pNPTS CN-32 *pdeB* K527E Q528S	Suicide vector for markerless in-frame insertion of *pdeB* of *S. putrefaciens* CN-32 with K527E Q528S	Rick & Kreiling et al., 2021
pNPTS CN-32 *pdeB* K578S	Suicide vector for markerless in-frame insertion of *pdeB* of *S. putrefaciens* CN-32 with K578S	Rick & Kreiling et al., 2021
pNPTS CN-32 *pdeB* K580S	Suicide vector for markerless in-frame insertion of *pdeB* of *S. putrefaciens* CN-32 with K580S	Rick & Kreiling et al., 2021
pNPTS CN-32 *PdeB-sfGFP* E500S	Suicide vector for markerless in-frame insertion of *PdeB-sfGFP* of *S. putrefaciens* CN-32 with E500S	Rick & Kreiling et al., 2021
pNPTS CN-32 *PdeB-sfGFP* G497A	Suicide vector for markerless in-frame insertion of *PdeB-sfGFP* of *S. putrefaciens* CN-32 with G497A	Rick & Kreiling et al., 2021
pNPTS CN-32 *PdeB-sfGFP* K490D Q493A	Suicide vector for markerless in-frame insertion of *PdeB-sfGFP* of *S. putrefaciens* CN-32 with K490D Q493A	Rick & Kreiling et al., 2021
pNPTS CN-32 *PdeB-sfGFP* K490G V491G M492G Q593G	Suicide vector for markerless in-frame insertion of *PdeB-sfGFP* of *S. putrefaciens* CN-32 with K490G V491G M492G Q593G	Rick & Kreiling et al., 2021
pNPTS CN-32 *PdeB-sfGFP* K527D	Suicide vector for markerless in-frame insertion of *PdeB-sfGFP* of *S. putrefaciens* CN-32 with K527D	Rick & Kreiling et al., 2021
pNPTS CN-32 *PdeB-sfGFP* K527D Q528S	Suicide vector for markerless in-frame insertion of *PdeB-sfGFP* of *S. putrefaciens* CN-32 with K527D Q528S	Rick & Kreiling et al., 2021
pNPTS CN-32 *PdeB-sfGFP* K527E Q528S	Suicide vector for markerless in-frame insertion of *PdeB-sfGFP* of *S. putrefaciens* CN-32 with K527E Q528S	Rick & Kreiling et al., 2021
pNPTS CN-32 *PdeB-sfGFP* K527S	Suicide vector for markerless in-frame insertion of *PdeB-sfGFP* of *S. putrefaciens* CN-32 with K527S	Rick & Kreiling et al., 2021
pNPTS CN-32 *PdeB-sfGFP* K527S Q528S	Suicide vector for markerless in-frame insertion of *PdeB-sfGFP* of *S. putrefaciens* CN-32 with K527S Q528S	Rick & Kreiling et al., 2021
pNPTS CN-32 *PdeB-sfGFP* K578S	Suicide vector for markerless in-frame insertion of *PdeB-sfGFP* of *S. putrefaciens* CN-32 with K578S	Rick & Kreiling et al., 2021
pNPTS CN-32 *PdeB-sfGFP* K580S	Suicide vector for markerless in-frame insertion of *PdeB-sfGFP* of *S. putrefaciens* CN-32 with K580S	Rick & Kreiling et al., 2021
pNPTS CN-32 *PdeB-sfGFP* Q499S	Suicide vector for markerless in-frame insertion of *PdeB-sfGFP* of *S. putrefaciens* CN-32 with Q499S	Rick & Kreiling et al., 2021
pNPTS CN-32 *PdeB-sfGFP* Q524A K527D Q528A	Suicide vector for markerless in-frame insertion of *PdeB-sfGFP* of *S. putrefaciens* CN-32 with Q524A K527D Q528A	Rick & Kreiling et al., 2021
pNPTS CN-32 *PdeB-sfGFP* Q524S	Suicide vector for markerless in-frame insertion of *PdeB-sfGFP* of *S. putrefaciens* CN-32 with Q524S	Rick & Kreiling et al., 2021
pNPTS CN-32 *PdeB-sfGFP* Q524S Q528S	Suicide vector for markerless in-frame insertion of *PdeB-sfGFP* of *S. putrefaciens* CN-32 with Q524S Q528S	Rick & Kreiling et al., 2021
pNPTS CN-32 *PdeB-sfGFP* Q528S	Suicide vector for markerless in-frame insertion of *PdeB-sfGFP* of *S. putrefaciens* CN-32 with Q528S	Rick & Kreiling et al., 2021
pNPTS CN-32 *PdeB-sfGFP* R557G	Suicide vector for markerless in-frame	Rick & Kreiling et al., 2021

A558G P559G Y560G	insertion of *PdeB-sfGFP* of *S. putrefaciens* CN-32 with R557G A558G P559G Y560G	
pNPTS CN-32 *PdeB-sfGFP* V522G V523G Q524G	Suicide vector for markerless in-frame insertion of *PdeB-sfGFP* of *S. putrefaciens* CN-32 with V522G V523G Q524G	Rick & Kreiling et al., 2021
pNPTS CN-32 *pdeB-venus*	Suicide vector for markerless in-frame insertion of *pdeB-mvenus* of *S. putrefaciens* CN-32	Rick & Kreiling et al., 2021
pNPTS CN-32 *pdeB-venus* D508A E509A	Suicide vector for markerless in-frame insertion of *pdeB-mvenus* of *S. putrefaciens* CN-32 with 508A E509A	Rick & Kreiling et al., 2021
pNPTS CN-32 *pdeB-venus* E637A	Suicide vector for markerless in-frame insertion of *pdeB-mvenus* of *S. putrefaciens* CN-32 with E637A	Rick & Kreiling et al., 2021
pNPTS CN-32 *aggC*-GS-3xFLAG	Suicide vector for markerless in-frame insertion of 3xFLAG to the C-terminus of *aggC* via a flexible GS-linker	Rick & Kreiling et al., 2021
pNPTS CN-32 *lapA*-GS-3xFLAG	Suicide vector for markerless in-frame insertion of 3xFLAG to the C-terminus of *lapA* via a flexible GS-linker	Rick & Kreiling et al., 2021
pNPTS CN-32 *mshA* S68C	Suicide vector for markerless in-frame insertion of *mshA* of *S. putrefaciens* CN-32 with S68C	Rick & Kreiling et al., 2021
pNPTS MR-1 *PdeB-sfGFP*	Suicide vector for markerless in-frame insertion of *PdeB-sfGFP* of *S. oneidensis* MR-1	Rick & Kreiling et al., 2021
pNPTS138-R6KT *flaA2*:: lux	in-frame insertion suicide vector for the lux-system to *flaA2*	Rossmann & Rick et al., 2019
pNPTS138-R6KT *flaB1*:: lux	in-frame insertion suicide vector for the lux-system to *flaB1*	Rossmann & Rick et al., 2019
pNPTS138-R6KT *flgE1*-T183C	in-frame insertion suicide vector for the polar hook protein FlgE1 (Sputcn32_3465) with the substitution of Thr183 to Cys	Rossmann & Rick et al., 2019
pNPTS138-R6KT *pdeB*	in-frame insertion suicide vector for complementation of *pdeB* (*sputcn32_3405*)	Rossmann & Rick et al., 2019
pNPTS138-R6KT *pdeB* D508A E509A GFP	in-frame insertion suicide vector for *PdeB-sfGFP* with a mutated GGDEF-motif	Rossmann & Rick et al., 2019
pNPTS138-R6KT *pdeB* E637A GFP	in-frame insertion suicide vector for *PdeB-sfGFP* with a mutated EAL-motif	Rossmann & Rick et al., 2019
pNPTS138-R6KT *pdeB*-E637A	in-frame insertion suicide vector for *pdeB* (*sputcn32_3405*) with a mutated EAL-motif	Rossmann & Rick et al., 2019
pNPTS138-R6KT PdeB-sfGFP	in-frame insertion suicide vector for C-terminal GFP-tag of pdeB	Rossmann & Rick et al., 2019

Supplemental table 7) In-frame deletion vectors that were used in this study. The individual tables are available in Rossmann & Rick et al., 2019 and Rick & Kreiling et al., 2021

Plasmid	Relevant genotype or phenotype	Source or reference
In-frame deletion vectors		
pNPTS CN-32 Δ*aggA*	Suicide vector for markerless in-frame deletion of *aggA* of *S. putrefaciens* CN-32	Rick & Kreiling et al., 2021
pNPTS CN-32 Δ*mshE*	Suicide vector for markerless in-frame deletion of *mshE* of *S. putrefaciens* CN-32	Rick & Kreiling et al., 2021
pNPTS CN-32 Δ*pilB*	Suicide vector for markerless in-frame deletion of *pilB* of *S. putrefaciens* CN-32	Rick & Kreiling et al., 2021
pNPTS MR-1 Δ*pdeB*	Suicide vector for markerless in-frame deletion of *pdeB* of *S. oneidensis* MR-1	Rick & Kreiling et al., 2021
pNPTS138-R6KT pdeB-ΔEAL-gfp	Suicide vector for deletion of the EAL-domain of PdeB (Sputcn32_3405)	Rossmann & Rick et al., 2019
***pNPTS138-R6KT pdeB*-ΔGGDEF-gfp**	Suicide vector for deletion of the GGDEF-domain of PdeB (Sputcn32_3405)	Rossmann & Rick et al., 2019
pNPTS138-R6KT *pdeB*–ΔGGDEF-ΔEAL-gfp	Suicide vector for deletion of the GGDEF- and EAL-domain of PdeB (Sputcn32_3405)	Rossmann & Rick et al., 2019
pNPTS138-R6KT *pdeB*–ΔHAMP-ΔPAS-ΔGGDEF-ΔEAL-gfp	Suicide vector for deletion of the HAMP-, PAS-, GGDEF- and EAL-domain of PdeB (Sputcn32_3405)	Rossmann & Rick et al., 2019

pNPTS138-R6KT *pdeB*-ΔPAS-gfp	Suicide vector for deletion of the PAS-domain of PdeB (Sputcn32_3405)	Rossmann & Rick et al., 2019
pNPTS138-R6KT *pdeB*–ΔPAS-ΔGGDEF-ΔEAL-gfp	Suicide vector for deletion of the PAS-, GGDEF- and EAL-domain of PdeB (Sputcn32_3405)	Rossmann & Rick et al., 2019
pNPTS138-R6KT *pdeB*-Δperiplasmic region-GFP	Suicide vector for deletion of the periplasmic region of PdeB (Sputcn32_3405)	Rossmann & Rick et al., 2019
pNPTS138-R6KT *ΔflgE1*	*flge1* (*Sputcn32_3465*) deletion suicide vector	Rossmann & Rick et al., 2019
pNPTS138-R6KT *ΔpdeB*	*pdeB* (*sputcn32_3405*) in frame deletion suicide vector	Rossmann & Rick et al., 2019

Supplemental table 8) Primer that were used in this study. The individual tables are available in Rossmann & Rick et al., 2019 and Rick & Kreiling et al., 2021

For construct	Identifier	Sequence
pET24c MBP-PdeB (MR-1) GGDEF-6xHis	TR258 MBP fw	TTAACTTTAAGAAGGAGATATACAATGAAAATAGAAGAAGGTAAACTGGTAATCTGG
	TR259 MBP rv	GCTGCCCCCGAGGTTGTTGTTATTGTTATTGT
	TR260	AATAACAACAACCTCGGGGGCAGCGAAGAACTTCTTAAGCATCAGCTAC
	TR257	GTGGTGGTGGTGGTGGTGCTCAATGGTGATGGTGATGGTGGTAAATGTGGATTTGGTTGGTGC
pET24c MBP-PdeB (MR-1) GGDEF-6xHis K524S	TR510 MBP ol plas fw	TTAACTTTAAGAAGGAGATATACAATGAAAATAGAAGAAGGTAAACTGGTAATCTGG
	TR511 So KtoS fw	CAATAATTTGGCTCAGCAACTGCGCCACAGC
	TR512 So KtoS rv	GTTGCTGAGCCAAATTATTGCTCAAGTATCGCTGC
	TR513 soGGDEF ol plas rv	GTGGTGGTGGTGGTGGTGCTCAATGGTGATGGTGATGGTGGTAAATGTGGATTTGGTTGGTGC
pET24c MBP-PdeB (MR-1) GGDEF-6xHis Q525S	TR510 MBP ol plas fw	TTAACTTTAAGAAGGAGATATACAATGAAAATAGAAGAAGGTAAACTGGTAATCTGG
	TR514 So QtoS fw	GAGCAATAATGCTCTTCAGCAACTGCGCCACAGC
	TR515 So QtoS rv	GCTGAAGAGCATTATTGCTCAAGTATCGCTGC
	TR513 soGGDEF ol plas rv	GTGGTGGTGGTGGTGGTGCTCAATGGTGATGGTGATGGTGGTAAATGTGGATTTGGTTGGTGC
pET24c MBP-PdeB (MR-1) GGDEF-6xHis K524E Q525S	TR510 MBP ol plas fw	TTAACTTTAAGAAGGAGATATACAATGAAAATAGAAGAAGGTAAACTGGTAATCTGG
	TR593 SO KQ to ES rv	TAATGCTTTCCAGCAACTGCGCCACAGCTAA
	TR594 SO KQ to ES fw	GCAGTTGCTGGAAAGCATTATTGCTCAAGTATCGCTGCAAGTG
	TR513 soGGDEF ol plas rv	GTGGTGGTGGTGGTGGTGCTCAATGGTGATGGTGATGGTGGTAAATGTGGATTTGGTTGGTGC
pET24c MBP-PdeB (MR-1) GGDEF-6xHis G494A	TR510 MBP ol plas fw	TTAACTTTAAGAAGGAGATATACAATGAAAATAGAAGAAGGTAAACTGGTAATCTGG
	TR544 G494A fw	ATTCCTGTGGCGCAAGACATGACTGAATCGCCCTAG
	TR555 G494A rv	ATGTCTTGCGCCACAGGAATTATTAGCCCGCA
	TR513 soGGDEF ol plas rv	GTGGTGGTGGTGGTGGTGCTCAATGGTGATGGTGATGGTGGTAAATGTGGATTTGGTTGGTGC
pET24c MBP-PdeB (MR-1) GGDEF-6xHis E497S	TR510 MBP ol plas fw	TTAACTTTAAGAAGGAGATATACAATGAAAATAGAAGAAGGTAAACTGGTAATCTGG
	TR558 E497S fw	GGGCTAATAACGACTGTGGCCCAAGACATGACT

	TR559 E497S rv	GCCACAGTCGTTATTAGCCCGCATAGGAGGTG
	TR513 soGGDEF ol plas rv	GTGGTGGTGGTGGTGGTGCTCAATGGTGATGGTGATGGTGGTAAATGTGGATTTGGTTGGTGC
pET24c MBP-PdeB (MR-1) PAS-GGDEF-6xHis	TR588 MBP fw SO	TTAACTTTAAGAAGGAGATATACAATGAAAATAGAAGAAGGTAAACTGGTAATCTGG
	TR589 MBP rv OL SO	TACCGCGCTCCCCGAGGTTGTTGTTATTGTTATTGT
	TR590 pet SO PAS fw	CAACCTCGGGGAGCGCGGTAAAATAACCTTAGA
	TR591 pet rv	GTGGTGGTGGTGGTGGTGCTCAATGGTGATGGTGATGGTGGTAAATGTGGATTTGGTTGGTGC
pET24c mshE-6xHis	TR258 MshE OW fw	TTAACTTTAAGAAGGAGATATACAATGAAACCCAGATTAAAGATGCGTTT
	TR259 MshE OW rv	GTGGTGGTGGTGGTGGTGCTCAATGGTGATGGTGATGGTGCGCCTCAACGCCTTGTTGG
pET24c mshE_Ndomain-6xHis	TR372	TTAACTTTAAGAAGGAGATATACAATGCACCATCACCATCACCATAAACCCAGATTAAAGATGCGTTTGG
	TR383	GTGGTGGTGGTGGTGGTGCCTAACGACGATAAAGATTATCAAAGGCC
pET24c pilB_Ndomain-6xHis	TR374	TTAACTTTAAGAAGGAGATATACAATGCACCATCACCATCACCATATGCCAACCACTGGTCTTCATTTA
	TR384	GTGGTGGTGGTGGTGGTGCCTATTCAAGGATTTTTTCAAGGGCTTTAG
pNPTS CN-32 Δ*aggA*	TR377	GCGAATTCGTGGATCCAGATTGAAATCAGCCCTAGACGAAGC
	TR378	TGTTAGTTCCTACTAAAGTATTCATTGCAAACCTCC
	TR379	TACTTTAGTAGGAACTAACAAATGAAAACCGTAATC
	TR380	GCCAAGCTTCTCTGCAGGATGGAGTTTGTTCTAATACTATTGGGC
pNPTS CN-32 Δ*pilB*	TR320 PilB KO1	GAATTCGTGGATCCAGATATGTATAAGCTGGAGATAAATATGAAAGG
	TR321 PilB KO2	TCGTCACCCGACCAGTGGTTGGCATAGATTCTTAA
	TR322 PilB KO3	AACCACTGGTCGGGTGACGAGTTTTTAACAGC
	TR323 PilB KO4	CAAGCTTCTCTGCAGGATCTTTTGGGCTCAATCTTCTTTGG
pNPTS CN-32 Δ*mshE*	AP241 EcoRV 0563 up fw	GAATTCGTGGATCCAGATGCTTACGCCAAGCCAGCTC
	AP242 OL_0563_up_rv	CCTCAACGCCCATCTTTAATCTGGGTTTCATTGGC
	AP243 OL_0563_down_fw	ATTAAAGATGGGCGTTGAGGCGTAATTATGC
	AP244 EcoRV_0563_down_rv	CAAGCTTCTCTGCAGGATCAAGGCAAATCGGCACCAAAG
pNPTS CN-32 *mshA* S68C	TR353	GCGAATTCGTGGATCCAGATAAATGTAACCGACGACGCACAG
	TR357	ATACATCCTTACACTCCACACCCTGAATAGCCG
	TR358	GGGTGTGGAGTGTAAGGATGTATCTAGCATTATTATCGATG
	TR356	GCCAAGCTTCTCTGCAGGATGCTAGGCAGGCCTTTTCTAGTA
pNPTS CN-32 *lapA*-GS-3x-FLAG	VK239 EcoRV OL up 3591 fw 2	GCGAATTCGTGGATCCAGATGGTGGTAGCCACAACGATGC
	VK240 up 3591 OL FLAG rv	AATATCATGATCTTTATAATCGCCATCATGATCTTTATAATCACTGCCAGGGATCATAGTGCCATTGTTATGAG
	VK241 OL FLAG 3591 down fw	GGCGATTATAAAGATCATGATATTGATTATAAAGATGATGATGATAAATAAATAAAATCGTTTTGATGGCCTATAGAAATATAGG
	VK233 EcoRV 3591-down rv	GCCAAGCTTCTCTGCAGGATGGCTTCTAGTGACTCAATATTGAGTGTC
pNPTS CN-32 *lapB*-GS-3x-FLAG	VK222 EcoRV OL up 3592 fw	GCGAATTCGTGGATCCAGATCCCTAGCGATCTACGCCG
	VK223 up 3592 OL FLAG rv	AATATCATGATCTTTATAATCGCCATCATGATCTTTATAATCACTGCCTTTTTTACTGCCCCCATTGAACAG
	VK224 OL	GATTATAAAGATCATGATATTGATTATAAAGATGATGATGATAAATAGGTTCAA

	FLAG 3592 down fw	TGGGGGCAGTAAAAAATG
	VK225 EcoRV 3592 down rv	GCCAAGCTTCTCTGCAGGATCTCCGCCGCCACTATACTATC
pNPTS CN-32 *PdeB-sfGFP* K527S	TR564 pdeb OL plas fw	GCCAAGCTTCTCTGCAGGATGCAAGGCAATATGGATCCATCC
	TR568 K to S rv	TGATCTGGCTTAACAACTGCACCACAGATAAAGC
	TR579 K to S fw	GCAGTTGTTAAGCCAGATCAGTGCTCAAGTCTCATTACAAG
	TR567 pdeB OL plas rv	GCGAATTCGTGGATCCAGATGCCAAAGACGCGACTACAACTA
pNPTS CN-32 *PdeB-sfGFP* K527S Q528S	TR564 pdeb OL plas fw	GCCAAGCTTCTCTGCAGGATGCAAGGCAATATGGATCCATCC
	TR565	TGATGCTGCTTAACAACTGCACCACAGATAAAGC
	TR566	GCAGTTGTTAAGCAGCATCAGTGCTCAAGTCTCATTACAAG
	TR567 pdeB OL plas rv	GCGAATTCGTGGATCCAGATGCCAAAGACGCGACTACAACTA
pNPTS CN-32 *PdeB-sfGFP* K527D	TR244 ol pdeB up	GCCAAGCTTCTCTGCAGGATGCAAGGCAATATGGATCCATCC
	TR399	TGATCTGGTCTAACAACTGCACCACAGATAAAGC
	TR400	GGTGCAGTTGTTAGACCAGATCAGTGCTCAAGTCTCATTA
	TR247 rv PdeB down	GCGAATTCGTGGATCCAGATGCCAAAGACGCGACTACAACTA
pNPTS CN-32 *PdeB-sfGFP* K527D Q528S	TR244 ol pdeB up	GCCAAGCTTCTCTGCAGGATGCAAGGCAATATGGATCCATCC
	TR344 KQ to ES rv	TGATCGAGTCTAACAACTGCACCACAGATAAAGCACTGCGAT
	TR345 KQ to ES fw	GCAGTTGTTAGACTCGATCAGTGCTCAAGTCTCATTACAAG
	TR247 rv PdeB down	GCGAATTCGTGGATCCAGATGCCAAAGACGCGACTACAACTA
pNPTS CN-32 *PdeB-sfGFP* Q524A K527D Q528A	TR244 ol pdeB up	GCCAAGCTTCTCTGCAGGATGCAAGGCAATATGGATCCATCC
	TR281	TGCGTCTAACAATGCCACCACAGATAAAGCACTGCGA
	TR282	GCATTGTTAGACGCAATCAGTGCTCAAGTCTCATTACAAG
	TR247 rv PdeB down	GCGAATTCGTGGATCCAGATGCCAAAGACGCGACTACAACTA
pNPTS CN-32 *PdeB-sfGFP* G497A	TR564 pdeb OL plas fw	GCCAAGCTTCTCTGCAGGATGCAAGGCAATATGGATCCATCC
	TR570 G rv	CCTGTGGAGCAAGGCAGGCTTGCATCACTTTAG
	TR571 G fw	AGCCTGCCTTGCTCCACAGGAGTTATTGGGGCGGATTGGTGG
	TR567 pdeB OL plas rv	GCGAATTCGTGGATCCAGATGCCAAAGACGCGACTACAACTA
pNPTS CN-32 *PdeB-sfGFP* Q499S	TR564 pdeb OL plas fw	GCCAAGCTTCTCTGCAGGATGCAAGGCAATATGGATCCATCC
	TR572 Q rxxd rv	CGCTTGGACCAAGGCAGGCTTGCATCACTTTAG
	TR573 Q rxxd rv	AGCCTGCCTTGGTCCAAGCGAGTTATTGGGGCGGATTGGTGG
	TR567 pdeB OL plas rv	GCGAATTCGTGGATCCAGATGCCAAAGACGCGACTACAACTA
pNPTS CN-32 *PdeB-sfGFP* E500S	TR564 pdeb OL plas fw	GCCAAGCTTCTCTGCAGGATGCAAGGCAATATGGATCCATCC
	TR574 E rxxd rv	TCTGTGGACCAAGGCAGGCTTGCATCACTTTAG
	TR575 E rxxd rv	AGCCTGCCTTGGTCCACAGAGCTTATTGGGGCGGATTGGTGG
	TR567 pdeB OL plas rv	GCGAATTCGTGGATCCAGATGCCAAAGACGCGACTACAACTA
pNPTS CN-32 *PdeB-sfGFP* Q524S Q528S	TR244 ol pdeB up	GCCAAGCTTCTCTGCAGGATGCAAGGCAATATGGATCCATCC
	TR347 SLLKS rv	TTAACAAACTCACCACAGATAAAGCACTGCGAT
	TR348 SLLKS fw	ATCTGTGGTGAGTTTGTTAAAGTCGATCAGTGCTCAAGTCTCATTACAAG
	TR247 rv PdeB down	GCGAATTCGTGGATCCAGATGCCAAAGACGCGACTACAACTA

pNPTS CN-32 *PdeB-sfGFP* K527E Q528S	TR564 pdeb OL plas fw	GCCAAGCTTCTCTGCAGGATGCAAGGCAATATGGATCCATCC
	TR395* ES rv	TGATCGATTCTAACAACTGCACCACAGATAAAGC
	TR396* ES fw	GCAGTTGTTAGAATCGATCAGTGCTCAAGTCTCATTACAAG
	TR567 pdeB OL plas rv	GCGAATTCGTGGATCCAGATGCCAAAGACGCGACTACAACTA
pNPTS CN-32 *PdeB-sfGFP* K490D Q493A	TR244 ol pdeB up	GCCAAGCTTCTCTGCAGGATGCAAGGCAATATGGATCCATCC
	TR279	TGCCATCACGTCAGCAACCATGGCCAACATGC
	TR280	GACGTGATGGCAGCCTGCCTTGGTCCACAG
	TR247 rv PdeB down	GCGAATTCGTGGATCCAGATGCCAAAGACGCGACTACAACTA
pNPTS CN-32 *PdeB-sfGFP* R557G A558G P559G Y560G	TR244 ol pdeB up	GCCAAGCTTCTCTGCAGGATGCAAGGCAATATGGATCCATCC
	TR252	GCCACCCCCTCCACCAAAGGCGACACCGATACTT
	TR253	GGAGGGGGTGGCATCAATGCCCAAGAGTTGTTGAA
	TR247 rv PdeB down	GCGAATTCGTGGATCCAGATGCCAAAGACGCGACTACAACTA
pNPTS CN-32 *PdeB-sfGFP* V522G V523G Q524G	TR244 ol pdeB up	GCCAAGCTTCTCTGCAGGATGCAAGGCAATATGGATCCATCC
	TR248	AACCCCCTCCAGATAAAGCACTGCGATTACAAATCA
	TR249	GGAGGGGGTTTGTTAAAGCAGATCAGTGCTCAAG
	TR247 rv PdeB down	GCGAATTCGTGGATCCAGATGCCAAAGACGCGACTACAACTA
pNPTS CN-32 *PdeB-sfGFP* K490G V491G M492G Q593G	TR244 ol pdeB up	GCCAAGCTTCTCTGCAGGATGCAAGGCAATATGGATCCATCC
	TR279	TGCCATCACGTCAGCAACCATGGCCAACATGC
	TR280	GACGTGATGGCAGCCTGCCTTGGTCCACAG
	TR247 rv PdeB down	GCGAATTCGTGGATCCAGATGCCAAAGACGCGACTACAACTA
pNPTS CN-32 *PdeB-sfGFP* K578S	TR564 pdeb OL plas fw	GCCAAGCTTCTCTGCAGGATGCAAGGCAATATGGATCCATCC
	TR600 cn32 Ksalt to S rv	CGCCCCCTTCGCGCTAGCAGCAAGACAGGCAATATCAG
	TR601 cn32 Ksalt to S fw	GCCTGTCTTGCTGCTAGCGCGAAGGGGGCGAATCAAAT
	TR567 pdeB OL plas rv	GCGAATTCGTGGATCCAGATGCCAAAGACGCGACTACAACTA
pNPTS CN-32 *PdeB-sfGFP* K580S	TR564 pdeb OL plas fw	GCCAAGCTTCTCTGCAGGATGCAAGGCAATATGGATCCATCC
	TR602 cn32 Kc to S rv	TTGATTCGCCCCGCTCGCTTTAGCAGCAAGACAGG
	TR603 cn32 Kc to S fw	CTTGCTGCTAAAGCGAGCGGGGCGAATCAAATCCATATTTATG
	TR567 pdeB OL plas rv	GCGAATTCGTGGATCCAGATGCCAAAGACGCGACTACAACTA
pNPTS CN-32 *pdeB* G497A	TR564 pdeb OL plas fw	GCCAAGCTTCTCTGCAGGATGCAAGGCAATATGGATCCATCC
	TR570 G rv	CCTGTGGAGCAAGGCAGGCTTGCATCACTTTAG
	TR571 G fw	AGCCTGCCTTGCTCCACAGGAGTTATTGGGGCGGATTGGTGG
	TR567 pdeB OL plas rv	GCGAATTCGTGGATCCAGATGCCAAAGACGCGACTACAACTA
pNPTS CN-32 *pdeB* K578S	TR564 pdeb OL plas fw	GCCAAGCTTCTCTGCAGGATGCAAGGCAATATGGATCCATCC
	TR600 cn32 Ksalt to S rv	CGCCCCCTTCGCGCTAGCAGCAAGACAGGCAATATCAG
	TR601 cn32 Ksalt to S fw	GCCTGTCTTGCTGCTAGCGCGAAGGGGGCGAATCAAAT
	TR567 pdeB OL plas rv	GCGAATTCGTGGATCCAGATGCCAAAGACGCGACTACAACTA
pNPTS CN-32 *pdeB* K580S	TR564 pdeb OL plas fw	GCCAAGCTTCTCTGCAGGATGCAAGGCAATATGGATCCATCC
	TR602 cn32 Kc to S rv	TTGATTCGCCCCGCTCGCTTTAGCAGCAAGACAGG

	TR603 cn32 Kc to S fw	CTTGCTGCTAAAGCGAGCGGGGCGAATCAAATCCATATTTATG
	TR567 pdeB OL plas rv	GCGAATTCGTGGATCCAGATGCCAAAGACGCGACTACAACTA
pNPTS CN-32 *pdeB-mvenus*	TR244 ol pdeB up	GCCAAGCTTCTCTGCAGGATGCAAGGCAATATGGATCCATCC
	TR456 PdeB-Venus up rv	CTCGCCCTTGCTCACTGCGCGTTGTGCTAAACCCATCTCA
	TR457 Venus OL PdeB fw	TTAGCACAACGCGCAGTGAGCAAGGGCGAGGAGCTGTTCA
	TR458 Venus OL PdeB fw	AGCGCAAATTCATCACTTGTACAGCTCGTCCATGCCGAGA
	TR459 PdeB-Venus dn fw	GACGAGCTGTACAAGTGATGAATTTGCGCTTTTAGTCCGA
	TR247 rv PdeB down	GCGAATTCGTGGATCCAGATGCCAAAGACGCGACTACAACTA
pNPTS CN-32 *pdeB-venus* D508A E509A	TR244 ol pdeB up	GCCAAGCTTCTCTGCAGGATGCAAGGCAATATGGATCCATCC
	TR456 PdeB-Venus up rv	CTCGCCCTTGCTCACTGCGCGTTGTGCTAAACCCATCTCA
	TR457 Venus OL PdeB fw	TTAGCACAACGCGCAGTGAGCAAGGGCGAGGAGCTGTTCA
	TR458 Venus OL PdeB fw	AGCGCAAATTCATCACTTGTACAGCTCGTCCATGCCGAGA
	TR459 PdeB-Venus dn fw	GACGAGCTGTACAAGTGATGAATTTGCGCTTTTAGTCCGA
	TR247 rv PdeB down	GCGAATTCGTGGATCCAGATGCCAAAGACGCGACTACAACTA
pNPTS CN-32 *pdeB-venus* E637A	TR244 ol pdeB up	GCCAAGCTTCTCTGCAGGATGCAAGGCAATATGGATCCATCC
	TR456 PdeB-Venus up rv	CTCGCCCTTGCTCACTGCGCGTTGTGCTAAACCCATCTCA
	TR457 Venus OL PdeB fw	TTAGCACAACGCGCAGTGAGCAAGGGCGAGGAGCTGTTCA
	TR458 Venus OL PdeB fw	AGCGCAAATTCATCACTTGTACAGCTCGTCCATGCCGAGA
	TR459 PdeB-Venus dn fw	GACGAGCTGTACAAGTGATGAATTTGCGCTTTTAGTCCGA
	TR247 rv PdeB down	GCGAATTCGTGGATCCAGATGCCAAAGACGCGACTACAACTA
pNPTS MR-1 Δ*pdeB*	TR582 SO pdeB KO cterm500	GCCAAGCTTCTCTGCAGGATGCCAAGCCATAATCTTATGCTTTAGG
	TR583 SO pdeB KO start	GTTGTGCTAAGTTGCCTATGCGCATCTTTTACC
	TR584 SO pdeB KO stop	CATAGGCAACTTAGCACAACGCGCATAGGG
	TR581 SO pdeB nterm500	GCGAATTCGTGGATCCAGATTAACAGCATGTTTAGACGCCGC
pNPTS MR-1 *PdeB-sfGFP*	TR576 SO up fw	GCCAAGCTTCTCTGCAGGATCCGCAGCAGAGCGTTTTAAGC
	TR577 SO pdeb nterm rv	TGCTGCTGCCTGCGCGTTGTGCTAAGCGC
	TR578 SO PdeB-sfGFP fw	ACAACGCGCAGGCAGCAGCAAAGGAGAAGAACTTTTC
	TR579 SO PdeB-sfGFP rv	CAATCCCCTAGGATCCTTTGTAGAGCTCATCC
	TR580 SO pdeb nterm fw	CAAAGGATCCTAGGGGATTGCGCTTTTAAGGTG
	TR581 SO pdeB nterm500	GCGAATTCGTGGATCCAGATTAACAGCATGTTTAGACGCCGC
pNPTS MR-1 *PdeB-sfGFP* K524E Q525S	TR582 SO pdeB KO cterm500	GCCAAGCTTCTCTGCAGGATGCCAAGCCATAATCTTATGCTTTAGG
	TR593 SO KQ to ES rv	TAATGCTTTCCAGCAACTGCGCCACAGCTAA
	TR594 SO KQ to ES fw	GCAGTTGCTGGAAAGCATTATTGCTCAAGTATCGCTGCAAGTG
	TR581 SO pdeB nterm500	GCGAATTCGTGGATCCAGATTAACAGCATGTTTAGACGCCGC

pNPTS MR-1 *PdeB-sfGFP* G494A	TR582 SO pdeB KO cterm500	GCCAAGCTTCTCTGCAGGATGCCAAGCCATAATCTTATGCTTTAGG
	TR544 G494A fw	ATTCCTGTGGCGCAAGACATGACTGAATCGCCCTAG
	TR555 G494A rv	ATGTCTTGCGCCACAGGAATTATTAGCCCGCA
	TR581 SO pdeB nterm500	GCGAATTCGTGGATCCAGATTAACAGCATGTTTAGACGCCGC
pNPTS MR-1 *PdeB-sfGFP* K575S	TR582 SO pdeB KO cterm500	GCCAAGCTTCTCTGCAGGATGCCAAGCCATAATCTTATGCTTTAGG
	TR598 aSak rv	GGTGCCCTTGGCACTAGCGGCAATACAGGCGATATCT
	TR599 aSak fw	GCCTGTATTGCCGCTAGTGCCAAGGGCACCAACCAAAT
	TR581 SO pdeB nterm500	GCGAATTCGTGGATCCAGATTAACAGCATGTTTAGACGCCGC
pNPTS MR-1 *PdeB-sfGFP* K577S	TR582 SO pdeB KO cterm500	GCCAAGCTTCTCTGCAGGATGCCAAGCCATAATCTTATGCTTTAGG
	TR596 akaS rv	TTGGTTGGTGCCACTGGCTTTAGCGGCAATACAGG
	TR597 akaS fw	ATTGCCGCTAAAGCCAGTGGCACCAACCAAATCCACATTTA
	TR581 SO pdeB nterm500	GCGAATTCGTGGATCCAGATTAACAGCATGTTTAGACGCCGC
pNPTS138-R6KT *ΔPdeB*	FR52	GTAGAATTCGATCCATCCATGTTATATGCGCC
	FR53	AACTAATCTCGCCAATGTGCATCTTTTACCACG
	FR54	GCACATTGGCGAGATTAGTTAATCTCGATTAACCGA
	FR55	TCCGGGCCCATTACCGTGATAATGGCTTACACC
pNPTS138-R6KT PdeB	FR52	GTAGAATTCGATCCATCCATGTTATATGCGCC
	FR55	TCCGGGCCCATTACCGTGATAATGGCTTACACC
pNPTS138-R6KT pdeB E637A	FR415	GAATTCGTGGATCCAGATGATCCATCCATGTTATATGCGCC
	FR416	GAATTCGTGGATCCAGATGATCCATCCATGTTATATGCGCC
	FR416	CAGTAGGATGGCCATCCGTTGCCGTTGTGG
	FR417	CAACGGATGGCCATCCTACTGCGAATACAGG
pNPTS138-R6KT *ΔflgE1*	AD97	GCGAATTCGTGGATCCAGATGCGTAATGACATCGAGCCAAG
	AD98	GGATCTGCAGGTTAAACGACATAATTCACCTCTAC
	AD99	GTCGTTTAACCTGCAGATCCGCTAGTTTTGACA
	AD100	CCAAGCTTCTCTGCAGGATCATCACCGGATTACCTCGGTC
pNPTS138-R6KT *flgE1*-T183C	AD97	GCGAATTCGTGGATCCAGATGCGTAATGACATCGAGCCAAG
	AD101	GGTATACGTTTTAGGATCGCACGGATCGAACGC
	AD102	GCTGCGTTCGATCCGTGCGATCCTAAAACG
	AD100	CCAAGCTTCTCTGCAGGATCATCACCGGATTACCTCGGTC
pNPTS138-R6KT *pdeB* 1xGS sfGFP	FR410	GAATTCGTGGATCCAGATTTTACATCCAGTCCTGTGGCC
	FR411	GAAAAGTTCTTCTCCTTTGCTGCTGCCTGCGCGTTGTGCTAAACCCAT
	FR393	AGCAAAGGAGAAGAACTTTTC
	FR412	GGATCCTTTGTAGAGCTCATCC
	FR413	GGATGAGCTCTACAAAGGATCCTGATGAATTTGCGCTTTTAGTCCG
	FR414	CAAGCTTCTCTGCAGGATCCGTCAAACCAGCCAAAGAC
pNPTS138-R6KT	FR520	GCGAATTCGTGGATCCAGATTTTATTGTTGGTTTAGGTTATATCTGGTTA

***pdeB*-ΔGGDEF-gfp**		
	FR533	CTTTATCATCTTCTTGAGTAATATCGCGTAATATCACTA
	FR534	TACTCAAGAAGATGATAAAGATAAAGAGCTCACCTA
	FR535	GCCAAGCTTCTCTGCAGGATCAAAACCACTACCAAAGTCATCCA
pNPTS138-R6KT *flaB1*::lux	B394	GGAATTCGCGAGCGGTTTGGCCACT
	B395	TCCGGGCCCACTTGAGGTAATTGGTTAGCTTGG
pNPTS138-R6KT *flaA2*:: lux	B397	GGAATTCGCTTCAATCGTTGCACAGGG
	B398	TCCGGGCCCACGCGTCATATTGGCTGATTCAAC
pNPTS138-R6KT *pdeB*-Δperiplasmic region	FR415	GAATTCGTGGATCCAGATGATCCATCCATGTTATATGCGCC
	FR419	GAACTTGCAGCTGCTGGATATTAGCAAGTTCACG
	FR420	TATCCAGCAGCTGCAAGTTCAATTTTCCGATGG
	FR421	CAAGCTTCTCTGCAGGATGCCTGACGGTTAAGCAGTAAAG
pNPTS138-R6KT *pdeB*-ΔPAS	FR415	GAATTCGTGGATCCAGATGATCCATCCATGTTATATGCGCC
	FR440	CTTGAGTAATCGATTCTAAAGTGATTTTAGCTCGTTC
	FR441	TTTAGAATCGATTACTCAAGAAGAGTTACTGAAGCG
	FR418	CAAGCTTCTCTGCAGGATTAACCG CTACGAGTGGGAACG
pNPTS138-R6KT *pdeB* D508A-E509A	FR415	GAATTCGTGGATCCAGATGATCCATCCATGTTATATGCGCC
	FR422	ACCGAAGGCGGCCCCACCAATCCGCCCCAATAACTCC
	FR423	ATTGGTGGGGCCGCCTTCGGTTTAGTGATTTGTAATCGC
	FR418	CAAGCTTCTCTGCAGGATTAACCGCTACGAGTGGGAACG
pNPTS138-R6KT *pdeB*-ΔEAL-GFP	FR516	GCGAATTCGTGGATCCAGATACTGAAGCGCCAGTTACAAAAAAGA
	FR517	CTCATATTGCTCACGATATTGGTAGGTGAGCTCTTTATCTTTATC
	FR518	TATCGTGAGCAATATGAGATGGGTTT
	FR519	GCCAAGCTTCTCTGCAGGATGATTCCATTCTTTTGTTTGTCTGCC
pNPTS138-R6KT *pdeB*-ΔHAMP-ΔGGDEF-ΔEAL-ΔPAS-gfp	FR524	GCGAATTCGTGGATCCAGATTCTCGAATCCTCTTGGCACG
	FR525	CTCATATTGCTCACGATATCTTCGTAACCAGATATAACCTAAAC
	FR518	TATCGTGAGCAATATGAGATGGGTTT
	FR519	GCCAAGCTTCTCTGCAGGATGATTCCATTCTTTTGTTTGTCTGCC
pNPTS138-R6KT *pdeB*-ΔGGDEF-ΔEAL-ΔPAS-gfp	FR522	GCGAATTCGTGGATCCAGATCAAAGAGTCGAAGGGGCATATTTAA
	FR523	CTCATATTGCTCACGATATTCTTTTTGCTGATAAATCCTCGCTAAT
	FR518	TATCGTGAGCAATATGAGATGGGTTT
	FR519	GCCAAGCTTCTCTGCAGGATGATTCCATTCTTTTGTTTGTCTGCC
pNPTS138-R6KT *pdeB*-ΔGGDEF-ΔEAL-ΔPAS-gfp	FR522	GCGAATTCGTGGATCCAGATCAAAGAGTCGAAGGGGCATATTTAA
	FR523	CTCATATTGCTCACGATATTCTTTTTGCTGATAAATCCTCGCTAAT
	FR518	TATCGTGAGCAATATGAGATGGGTTT
	FR519	GCCAAGCTTCTCTGCAGGATGATTCCATTCTTTTGTTTGTCTGCC
pNPTS138-R6KT *pdeB*-ΔGGDEF-ΔEAL-gfp	FR520	GCGAATTCGTGGATCCAGATTTTATTGTTGGTTTAGGTTATATCTGGTTA
	FR521	CTCATATTGCTCACGATATTCTTGAGTAATATCGCGTAATATCACTA
	FR518	TATCGTGAGCAATATGAGATGGGTTT
	FR519	GCCAAGCTTCTCTGCAGGATGATTCCATTCTTTTGTTTGTCTGCC

pBTOK p*deB*-GGDEF-gfp	FR558	AATGAATAGTTCGACAAAAATAGGAGGGCAAATATGATTACTCAAGAAGAGTTACTGAAGCG
	FR554	GGAGTCCAAGCTCAGCTAATGTTAGGATCCTTTGTAGAGCTCATCC
pET24c FLAG-FimVc-His	LS77	TTAACTTTAAGAAGGAGATATACAATGCACCATCACCATCACCATGATGAAGCCTTAGCCGCATTGGAT
	LS78	GTGGTGGTGGTGGTGGTGCTCATTTATCATCATCATCTTTATAATCAATATCATGATCTTTATAATCGCCATCATGATCTTTATAATCGCTGCCACTAATCTCTTTTAGTAAACGTCCGG
pET24c MBP-His	FR555	TTAACTTTAAGAAGGAGATATACAATGAAAATAGAAGAAGGTAAACTGGTAATCTGG
	FR563	GTGGTGGTGGTGGTGGTGCTCAATGGTGATGGTGATGGTGCCCGAGGTTGTTGTTATTGTTATTGT
pET24c MBP-GGDEF-His	FR555	TTAACTTTAAGAAGGAGATATACAATGAAAATAGAAGAAGGTAAACTGGTAATCTGG
	FR556	GCTGCCCCCGAGGTTGTTGTTATTGTTATTGT
	TR19	AACAACCTCGGGGGCAGCATTACTCAAGAAGAGTTACTGAAGCG
	TR20	GTGGTGGTGGTGGTGGTGCTCAATGGTGATGGTGATGGTGTGCGCGTTGTGCTAAACCCAT
pET24c MBP-PdeB(Cyto)-His	FR555	TTAACTTTAAGAAGGAGATATACAATGAAAATAGAAGAAGGTAAACTGGTAATCTGG
	FR556	GCTGCCCCCGAGGTTGTTGTTATTGTTATTGT
	TR68	AACAACCTCGGGGGCAGCAGAGGTTTGCTCAAACCTTTTAAGAAT
	TR69	GTGGTGGTGGTGGTGGTGCTCAATGGTGATGGTGATGGTGTGCGCGTTGTGCTAAACCCAT
pKNT25, pUT18, pUT18C FimVc(HubP)	LS41	CAGGGTCGACTCTAGAGTTGTCAGCCACCGATGATGATCTC
	LS42	TTAGTTACTTAGGTACCCGGGGACTAATCTCTTTTAGTAAACGTCCGGCC
pKT25 FimVc(HubP)	LS39	CTGCAGGTCGACTCTAGAGTTGTCAGCCACCGATGATGATCTC
	LS40	GAGCTCGGTACCCGGGGACTAATCTCTTTTAGTAAACGTCCGGCC
pKNT25, pUT18, pUT18C repeats_1-10(HubP)	LS35	CTGCAGGTCGACTCTAGAGGATGAGGATGACCTCCATGATATGG
	LS36	GAGCTCGGTACCCGGGGAAGTAATTTATCGATATCAATAAAACCATTTTCATTCTGG
pKT25 repeats_1-10(HubP)	LS37	CAGGGTCGACTCTAGAGGATGAGGATGACCTCCATGATATGG
	LS38	TTAGTTACTTAGGTACCCGGGGAAGTAATTTATCGATATCAATAAAACCATTTTCATTCTGG
pKNT25, pUT18, pUT18C GGDEF(PdeB)	TR05	CTGCAGGTCGACTCTAGAGATTACTCAAGAAGAGTTACTGAAGCG
	TR06	GAGCTCGGTACCCGGGGTGCGCGTTGTGCTAAACCCAT
pKT25 GGDEF(PdeB)	TR07	CAGGGTCGACTCTAGAGATTACTCAAGAAGAGTTACTGAAGCG
	TR08	TTAGTTACTTAGGTACCCGGGGTGCGCGTTGTGCTAAACCCAT

Supplemental table 9) Overview of all GGDEF- and EAL-proteins of *S. putrefaciens* CN-32.

Protein	Type	Domain architecture
Sputcn32_0305	EAL	REC, EAL
Sputcn32_0601	EAL	EAL
Sputcn32_0814	EAL	TM, CSS-motif, TM, EAL
Sputcn32_2106	EAL	EAL
Sputcn32_0099	EAL, GGDEF	5x(TM), PAS, GGDEF, EAL
Sputcn32_0133	EAL, GGDEF	TM, Low complexity region, TM, HAMP, PAS, PAC, GGDEF, EAL
Sputcn32_0327	EAL, GGDEF	Low complexity region, PAS, GGDEF, EAL

Sputcn32_0555	EAL, GGDEF	TM, TM, GGDEF, EAL
Sputcn32_0654	EAL, GGDEF	GAF, GGDEF, EAL
Sputcn32_1253	EAL, GGDEF	3x(PAS, PAC), GGDEF, EAL
Sputcn32_1800	EAL, GGDEF	GAF, PAC, GGDEF, EAL
Sputcn32_1851	EAL, GGDEF	Signal peptide, TM, GGDEF, EAL
Sputcn32_1858	EAL, GGDEF	GAF, PAS, PAC, GGDEF, EAL
Sputcn32_1917	EAL, GGDEF	5x(TM),3x (PAS, PAC), GGDEF, EAL
Sputcn32_2456	EAL, GGDEF	2CS-domain, repeats, PAC, PAS, PAC, GGDEF, EAL
Sputcn32_2800	EAL, GGDEF	TM, GGDEF, EAL
Sputcn32_2830	EAL, GGDEF	TM, Low complexity region, HAMP, GGDEF, EAL
Sputcn32_3319	EAL, GGDEF	EAL, ~~GGDEF~~, low complexity region
Sputcn32_3328	EAL, GGDEF	REC, GGDEF, EAL
Sputcn32_3405	EAL, GGDEF	TM, CHASE, TM, HAMP, PAS, GGDEF, EAL
Sputcn32_3597	EAL, GGDEF	TM, LapD-domain, HAMP, GGDEF, EAL
Sputcn32_3598	EAL, GGDEF	GAF, GAF, GGDEF, EAL
Sputcn32_3648	EAL, GGDEF	3x(TCs), Low complexity region, PAC, PAS, PAC, GGDEF, EAL
Sputcn32_3856	EAL, GGDEF	MASE, CHASE, 2x(PAS, PAC), GGDEF, EAL
Sputcn32_3917	EAL, GGDEF	TM, TM, PAS, PAC, GGDEF, EAL
Sputcn32_0384	GGDEF	TM, low complexity region, GGDEF
Sputcn32_0414	GGDEF	SNOAL, GGDEF
Sputcn32_0470	GGDEF	signal peptide, 3x(TPR), TPS, TPR_8, TM, GGDEF
Sputcn32_0498	GGDEF	7TMR-DISMED2, 7TMR-DISM_7TM. GGDEF
Sputcn32_1039	GGDEF	TM, TM; GAF, GGDEF
Sputcn32_1235	GGDEF	TPR, TPR, GGDEF
Sputcn32_1291	GGDEF	coiled coil, GGDEF
Sputcn32_1365	GGDEF	low complexity, low complexity, GGDEF
Sputcn32_1412	GGDEF	PAS, GGDEF
Sputcn32_1523	GGDEF	GGDEF
Sputcn32_1741	GGDEF	GGDEF
Sputcn32_1934	GGDEF	signal peptide, 3x(PBPb), TM, GGDEF
Sputcn32_2096	GGDEF	GGDEF
Sputcn32_2671	GGDEF	TM, coiled coil, TM, HAMP, GGDEF
Sputcn32_3018	GGDEF	PAS, PAC, GAF, GGDEF
Sputcn32_3085	GGDEF	GGDEF
Sputcn32_3168	GGDEF	low complexity, 4x(TM), GGDEF
Sputcn32_3244	GGDEF	Protoglobin, GGDEF

Sputcn32_3269	GGDEF	7TM-Histidinkinasefamily, PAS, GGDEF
Sputcn32_3306	GGDEF	PAS, GGDEF
Sputcn32_3390	GGDEF	low complexity, PAS, PAC, GGDEF

6.2 Supplemental figures

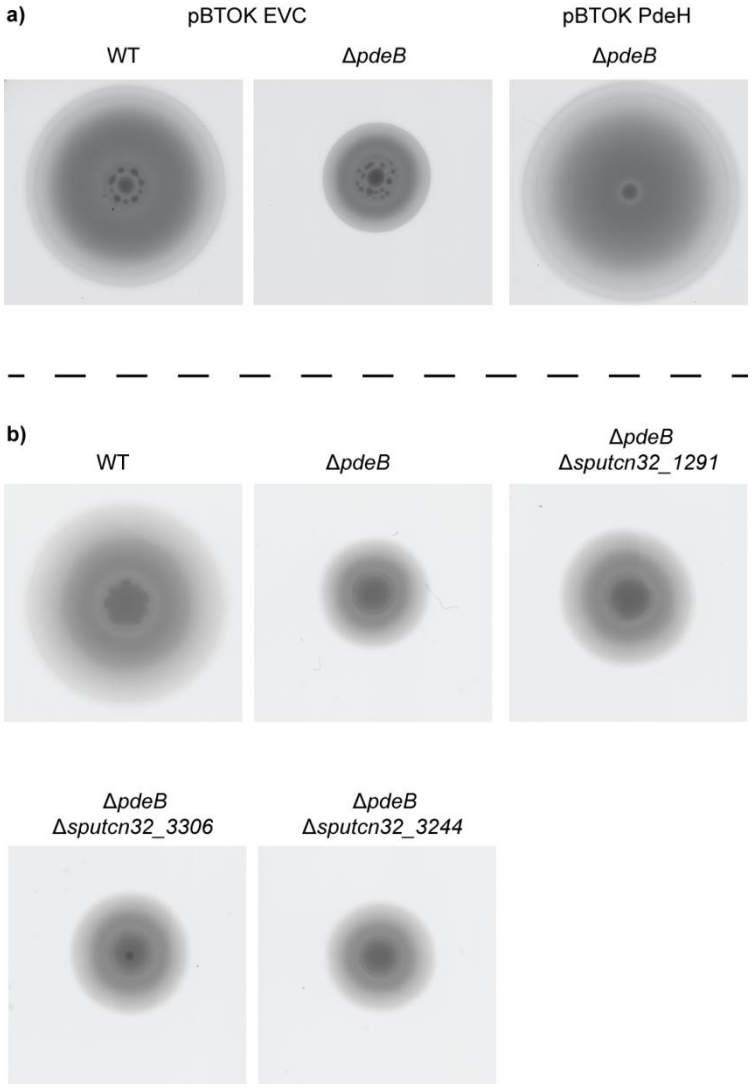

Supplemental figure 1) a) Overexpression of PdeH fully complements the spreading phenotype on motility plates of the Δ*pdeB* mutation. **b)** PdeB is epistatic to other DGCs. The spreading radius of mutants that lack *pdeB* and a gene for a DGC was observed by motility assays. Deletion of these DGCs did not fully complement the spreading phenotype of the Δ*pdeB* mutant.

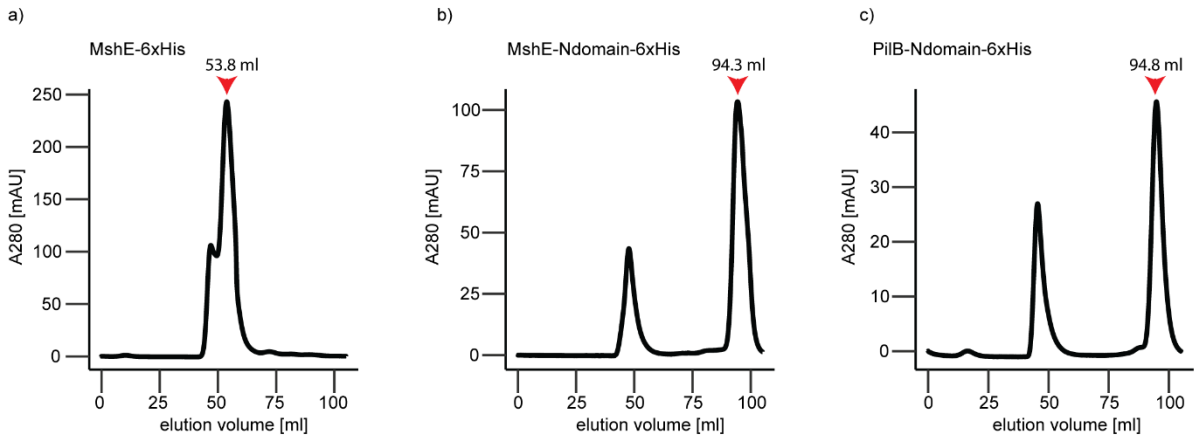

Supplemental figure 2) a-b) The extension ATPase MshE (a) and its N-terminal domain (b) were heterologously produced and purified. The SEC chromatogram indicates that MshE elutes es penta- or hexamer while the N-terminal domain elutes as monomer. **c)** The N-terminal domain of PilB was purified by SEC and eluted as monomer. (Rick & Kreiling et al., 2021, modified)

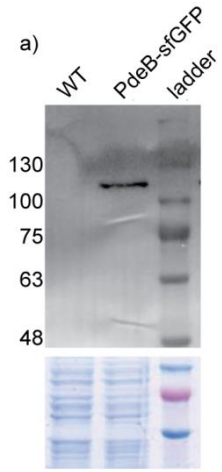

Supplemental figure 3) The stability and expression of PdeB-sfGFP was verified by immunoblot analysis. (Rossmann & Rick et al., 2019, modified)

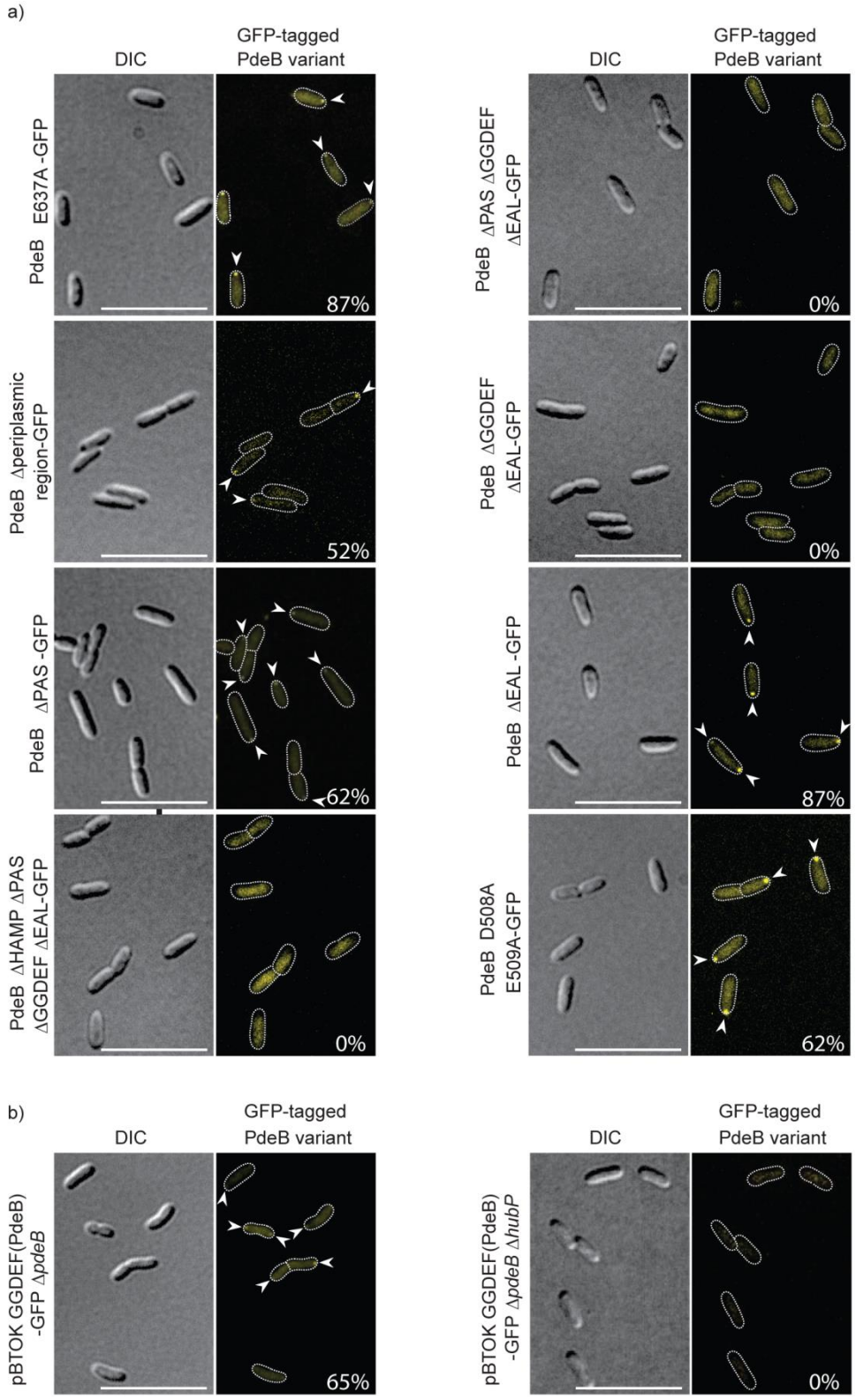

Supplemental figure 4) Micrographs of PdeB-sfGFP truncations. a) The localization of truncated PdeB-sfGFP versions was tested by fluorescence microscopy to identify domains that are essential for polar localization. Additionally the A-sites of the GGDEF and EAL domains were mutated. **b)** The localization of the GGDEF-domain of PdeB was tested in presence and absence of *hubP*. scale bar = 10 µm. (Rossmann & Rick et al., 2019, modified)

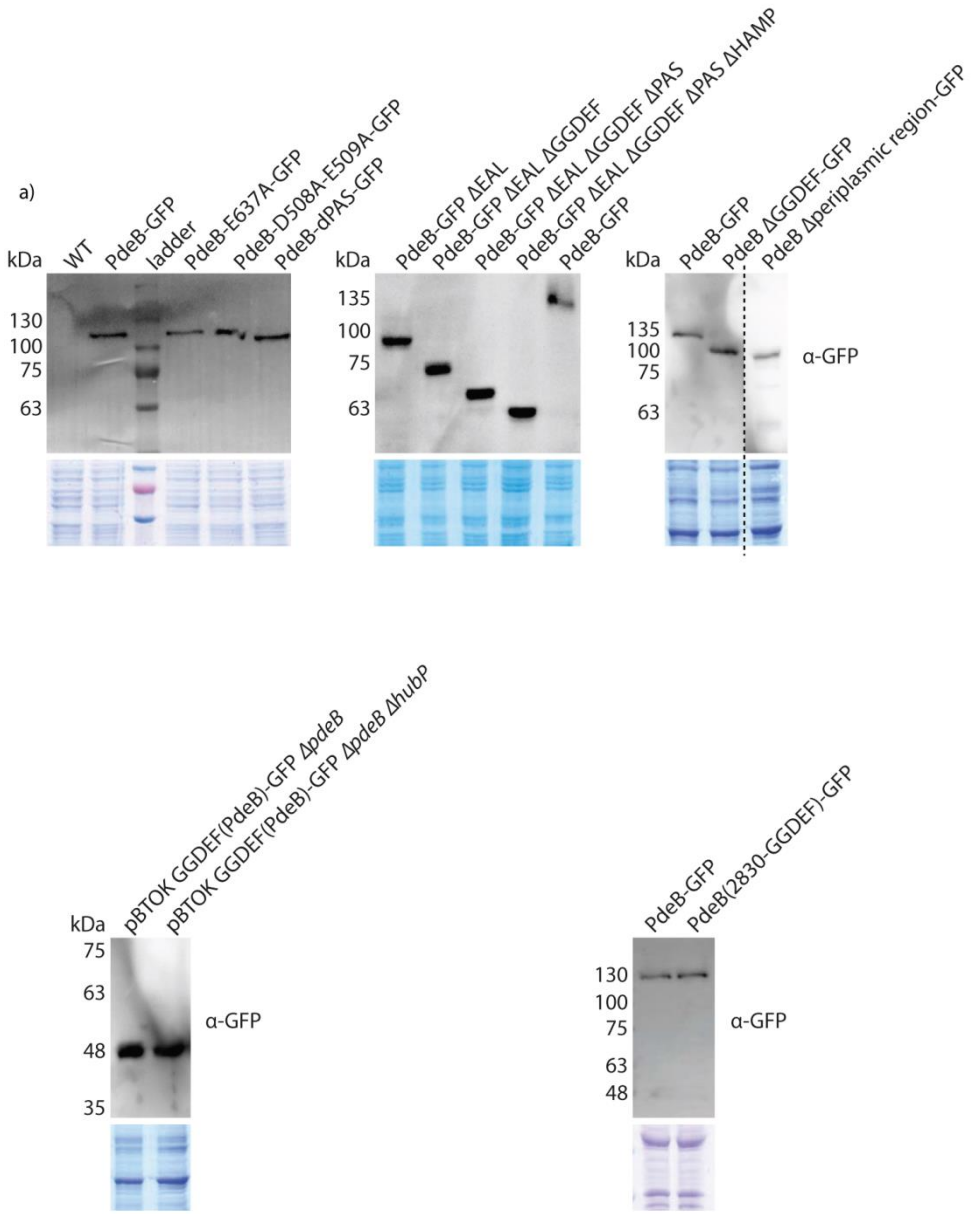

Supplemental figure 5) a) The stability and expression of truncated PdeB-sfGFP versions was verified by immunoblot analysis. **b)** The The stability and expression of the ectopically produced GGDEF-sfGFP protein was verified by immunoblot analysis. **c)** The The stability and expression of PdeB-sfGFP with the an exchange of its GGDEF domain against the GGDEF domain of Sputcn32_2830 was verified by immunoblot analysis. (Rossmann & Rick et al., 2019, modified)

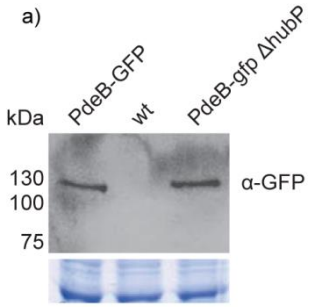

Supplemental figure 6) a) The stability and expression of PdeB-sfGFP in Δ*hubP* was verified by immunoblot analysis. (Rossmann & Rick et al., 2019, modified)

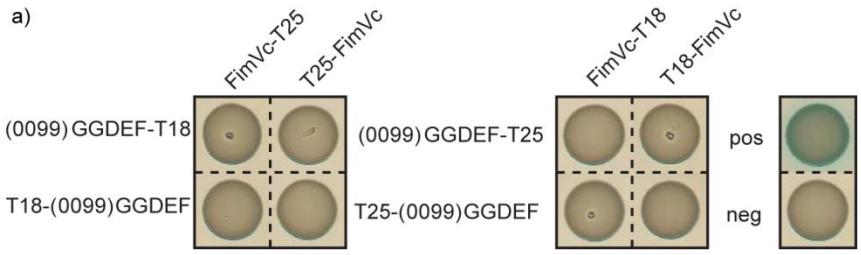

Supplemental figure 7) The interaction of the GGDEF-domain of Sputcn32_0099 with FimVc$_{HubP}$ was tested by B2H assays. No interaction for these proteins was found. A leucine zipper was used as positive control and empty plasmids as negative control. (Rossmann & Rick et al., 2019, modified)

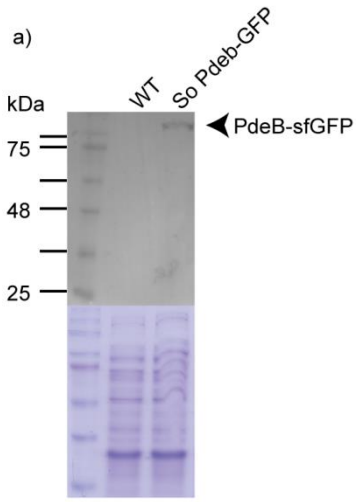

Supplemental figure 8) a) The stability and expression of *So*PdeB-sfGFP was verified by immunoblot analysis. (Rick & Kreiling et al., 2021, modified)

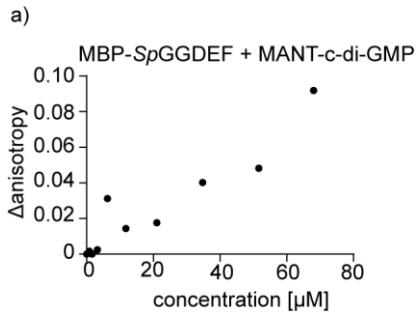

Supplemental figure 9) FP assay with GGDEF-domain and MANT-c-di-GMP. a) The binding of MANT-c-di-GMP to the GGDEF domain of *Sp*PdeB was tested by FP assays. No binding curve was observed but only unspecific binding in unphysiologically high concentrations. (Rick & Kreiling et al., 2021, modified)

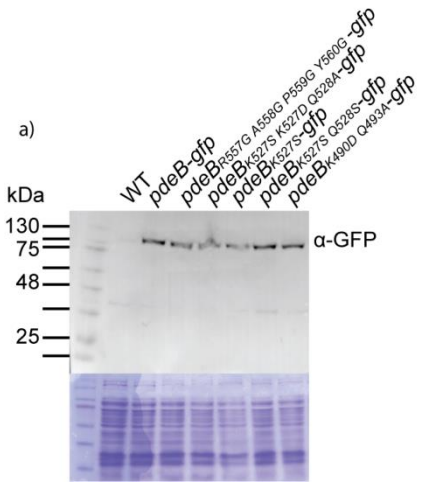

Supplemental figure 10) The stability and expression of PdeB-sfGFP with mutations in different regions of the GGDEF-domain was verified by immunoblot analysis. (Rick & Kreiling et al., 2021, modified)

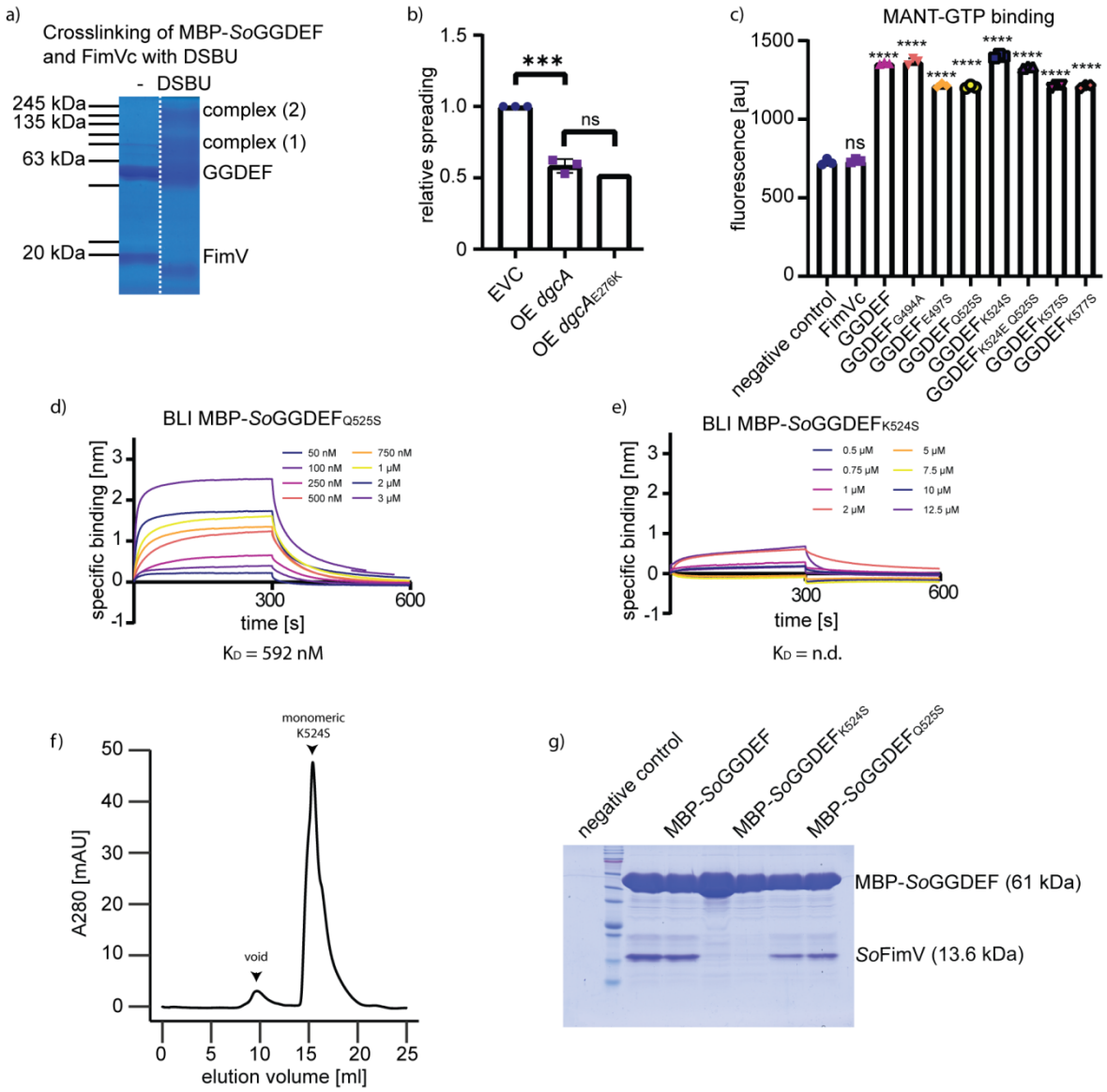

Supplemental figure 11) a) The crosslinking of *So*GGDEF with *So*FimVc was verified by SDS-PAGE. **b)** Mutating the aspartic acid of the ER-motif of the i-site of GGDEF-domains does not inhibit the DGC activity. This was tested by overproducing the active DGC VdcA and using the spreading on motility plates as read-out. **c)** The mutated GGDEF$_{PdeB}$ that show reduced affinity to FimVc$_{HubP}$ still bind GTP with roughly the same affinity. **d)** The affinity of *So*GGDEF$_{Q525S}$ to *So*FimVc$_{HubP}$ was tested using BLI assays. Mutating Q525 resulted in an around 3-times increased K_D value compared to the wild type vewrsion. **e-g)** The affinity of affinity of *So*GGDEF$_{K524S}$ to *So*FimVc$_{HubP}$ was tested using BLI assays (e). However, the measurement was disturbed by unspecific binding; likely due to aggregation of the protein. Thus we verified that the aggregation is low and the protein can be used for other assays by storing it for three days at 4°C and analyzing the protein with SEC (f). The protein only showed mild aggregation and was therefore suitable for pull-down assays (g). The *So*GGDEF$_{K524S}$ protein was not able to bind *So*FimV$_{HubP}$ in pull-down assays, as shown by SDS-page (g). The wild type and *So*GGDEF$_{Q525S}$ proteins served as controls. (Rick & Kreiling et al., 2021, modified)

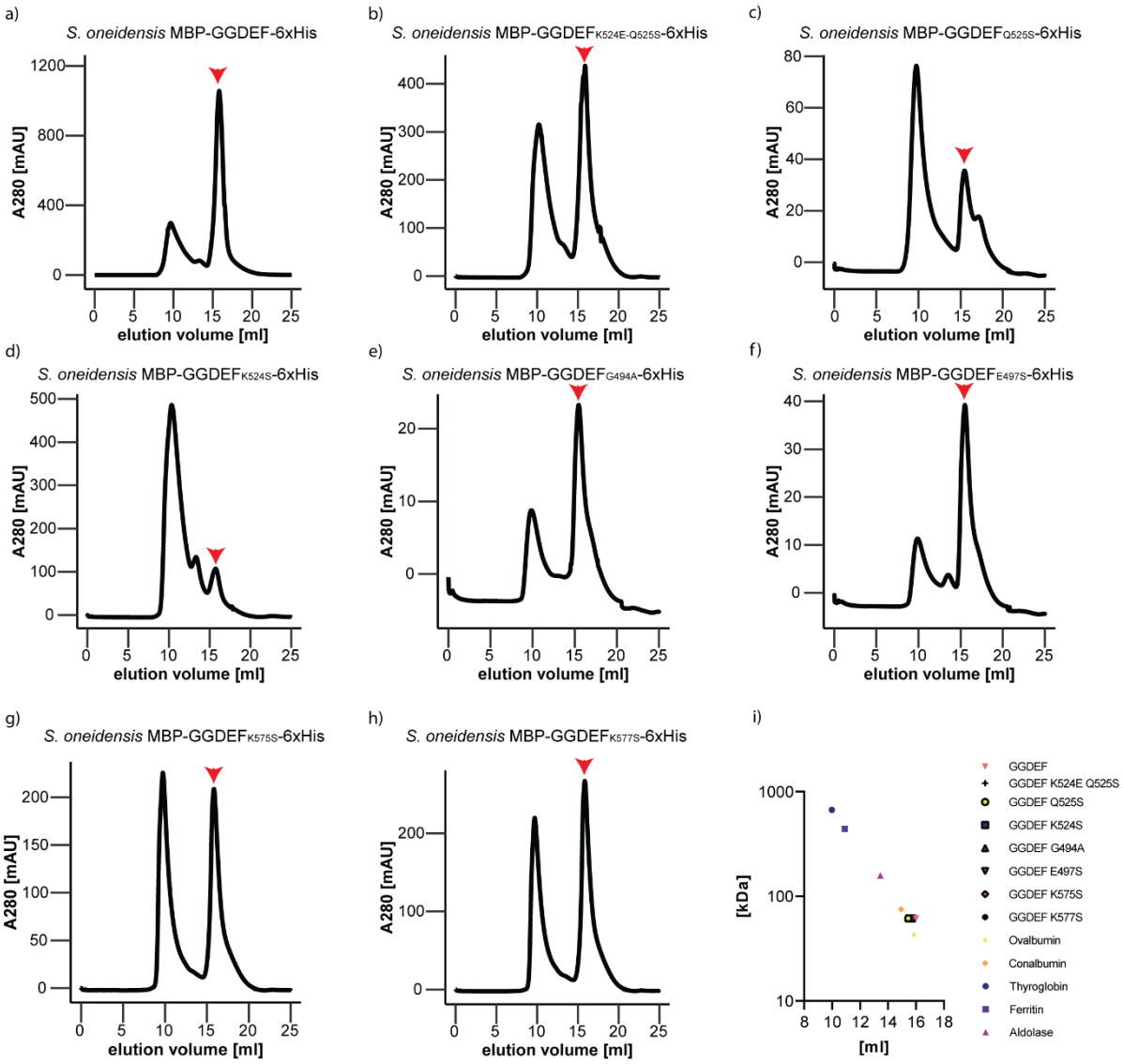

Supplemental figure 12) SEC chromogramms of mutated MBP-GGDEF-6xHis proteins. a-h) The SEC chromatograms are shown by plotting the elution volume against the asorbace at 280 nm. All proteins eluted as monomers. TI) The elution volume of the different GGDEF-proteins was plotted together with calibration proteins against their molecular weight. All GGDEF proteins elute roughly at the same volume. (Rick & Kreiling et al., 2021, modified)

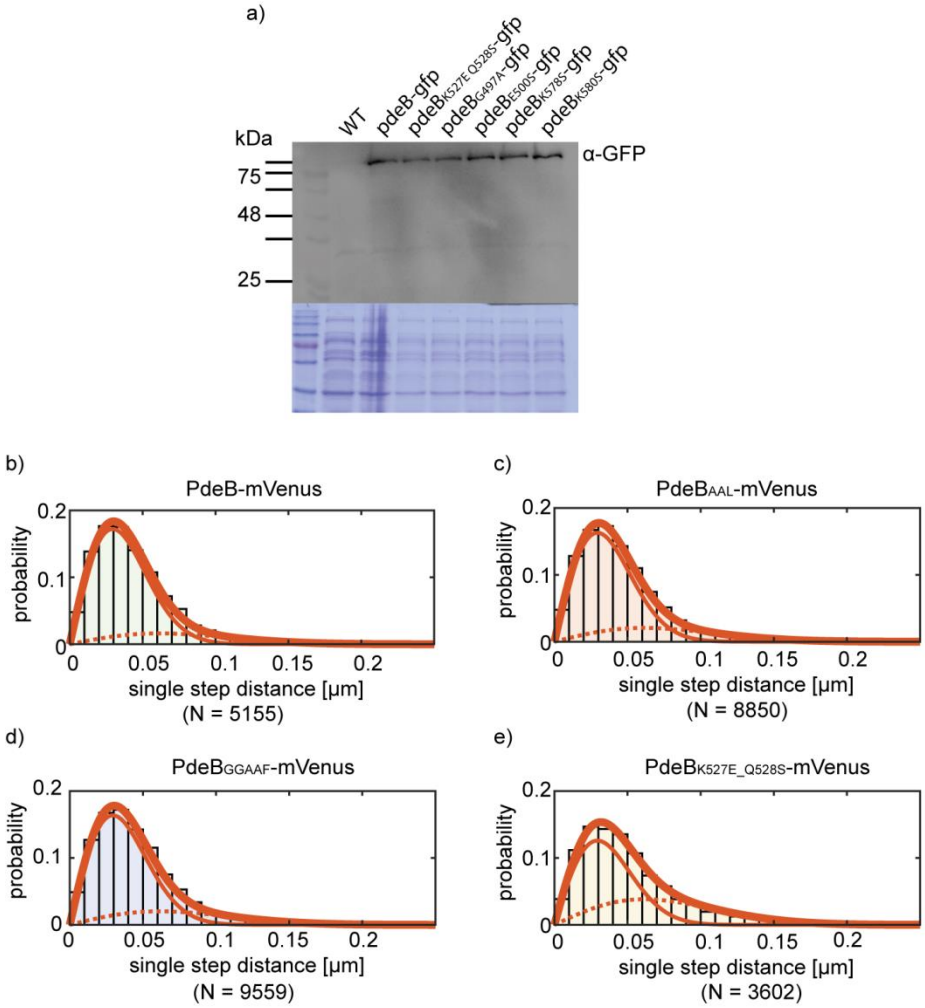

Supplemental figure 13) a) The stability and expression of PdeB-sfGFP mutants with reduced affinity to FimVc$_{HubP}$ was verified by immunoblot analysis. **b-e**) **Controlls of single molecule microscopy**. The graphs show fits for the jump distance analysis that was used for the diffusion rate analysis. A Rayleigh fit was used for the population with low diffusion rates and is shown as solid thin line. The dotted line shows the fit for the fast population, while the thick solid line shows the fit for both populations together. $R^2 > 0.999$. (Rick & Kreiling et al., 2021, modified)

Danksagung

An dieser Stelle möchte ich meinem Doktorvater Kai Thormann danken, der mir die Arbeit an diesem Projekt ermöglicht hat. Vielen Dank für die unglaubliche Unterstützung und Hilfe! Danke auch für die vielen Freiheiten die du mir gegeben hast; ich weiß es zu schätzen dass ich so viel ausprobieren durfte und die Möglichkeit hatte meinen Interessen und Nebenprojekten nachzugehen.

Desweiteren gillt man Dank Ulrike Ruppert, die duch ihre tolle und gewissenhafte Arbeit einen riesen Teil zu diesem Projekt beigetragen hat. Nicht nur die Arbeit mit dir war toll sondern du bist auch menschlich einfach Gold! Danke für die nette Zeit zusammen im Labor.

Danke auch an Vanessa Kreiling die an diesem Projekt mitgearbeitet hat und meine Nachfolge antritt. Ich wünsche dir noch viel Erfolg mit dem Projekt. An dieser Stelle möchte ich auch Alexander Höing danken, der mit seiner Expertise in Biochemie das Projekt nach vorne getrieben hat und mir noch etwas Nachhilfe in diesem Projekt gegeben hat! Bro, ich find es immer noch mega nice dass du bei uns eingestiegen bist! Richtige nice „Schnappsidee“! …Äh… Ich meine… gutes Networking!

Vielen Dank auch an meine liebe Anna, mit der ich mir jahrelang den Laborplatz teilen durfte und die mir beim Korrigieren geholfen hat! Wir waren schon ein gutes Team =) Die Arbeit zusammen hat echt Spaß gemacht und auf dich konnte man immer zählen wenn man was anzünden wollte =D

Danke auch an den süßen Luki, dafür dass er so blond und süß ist und meine Einleitung korrigiert hat! Mit dir konnte ich immer alle möglichen Sachen besprechen und du warst sowohl in wissenschaftlicher, als auch in menschlicher Hinsicht eine Bereicherung! Danke auch für die tolle Zeit im Studium! Alex und du waren immer ein Bischen meine Vorbilder muss ich zugeben <3

Danke auch an Cari und Julian, die mir beim Korrigieren geholfen haben! Die Zeit mit euch im Institut, Studium und Privatleben war echt schön! Viel Erfolg weiterhin, bei euch läuft es ja echt nice =) Vielen Dank auch an Daniel der spontan über meine Arbeit gelesen hat, mega vielen Dank! Ich wünsche dir viel Spaß und Erfolg in der AG Thormann!

Vielen Dank auch an John für die schöne Zeit im Büro! Das hat echt sehr gut harmoniert und super viel Spaß gemacht! Wir haben echt viel Quatsch zusammen gemacht, das war nice! Ich würde ja ein paar Beispiele nennen, aber vielleicht sollen die besser nicht mit veröffentlicht werden =D

Danke auch an die restlichen Mitglieder der AG Thormann, namentlich Nicole, Meike und Svenja! Die AG ist echt ein gutes Team! Besonders Svenja möchte ich an dieser Stelle noch weiterhin viel Erfolg wünschen. Du warst eine tolle Masterstudentin und es hat sehr viel Spaß gemacht mit dir zusammen zu arbeiten! An dieser Stelle auch noch Danke an die tollen Alumnis Marco, Max und Suse!

Weiterhin möchte ich den restlichen Mitgliedern des Instituts für die schöne Zeit bei der Arbeit und im Privatleben danken! Leider kann ich hier nicht alle namentlich erwähnen, deswegen beschränke ich mich auf Jannek, Robina, Saina und Henry! Die Zeit mit euch war echt nice!

Last but not least möchte ich meinem ehemaligen Betreuer Florian Rossmann danken. Du hattest einen prägenden Einfluss auf mich und ich bin sehr froh dass du mich durch meine Bachelor- Hiwi- und Masterzeit begleitet hast! Von dir habe ich viel gelernt und mit dir zu arbeiten war toll! Behalte deine entspannte Art bei =) Danke auch an meinen lieben Brudi Kevin, der mich auf persönlicher Ebene immer sehr unterstützt hat und meine Mutter die mir einige Male aufgeholfen hat.